Micromechanics of progressive failure in carbon fibre-reinforced composites using finite element method.

Sirivedin, Suparerk

Micromechanics of Progressive Failure

in

Carbon Fibre-Reinforced Composites

Using Finite Element Method

by

Suparerk Sirivedin

A thesis is submitted for the degree of

Doctor of Philosophy

in the University of London

King's College London

Department of Mechanical Engineering

June 2001

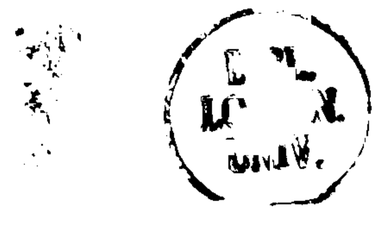

ABSTRACT

The role of the interphase in the failure of carbon fibre/epoxy composites has been investigated using elasto-plastic finite element (FE) analysis. It has been found that the interphase has little effect on the fibre stresses but a significant effect on matrix strains. Plastic strains in the matrix material were found to decrease when an interphase was included in the model.

Failure in a short fibre composite was investigated using the Rice and Tracey void-growth model and slow crack growth was assumed. A crack initiation criterion was developed to predict the initiation angle for the matrix crack and the applied strain at failure. In a long fibre composite, a high strain rate near the fibre fracture location induced by the fibre recoil makes catastrophic failure involving rapid crack-growth in the matrix material more likely. The semi-cone angle of a matrix crack was predicted to be about twice the value for a short fibre system using the minimum strain energy criterion. It was also found that the fibre stress profiles are characteristic of the matrix crack geometries.

The effects of the inter-fibre spacing and the presence of a matrix crack on the stress redistribution in a planar array and hexagonal array of fibres composite have been investigated using 3-D elasto-plastic FE analysis. Matrix cracks were found to have a significant effect in determining the stress amplification factor (SAF) in planar array composites but have less effect in hexagonal array composites. The presence of a matrix crack was also found to increase the positively affected length (PAL) and better agreement for the fibre stress profiles with the LRS results was obtained.

Publication Arising From The Research

- Sirivedin S., Fenner, D. N., Nath, R. B., and Galiotis, C. (2000), Matrix Crack Propagation Criteria for Model Short-Carbon Fibre/Epoxy Composites, *Composite Science and Technology*, **60**, 2835-2847.

- Sirivedin S., Fenner, D. N., Nath, R. B., and Galiotis, C., Rate Dependent Matrix Cracking for Model Carbon Fibre/Epoxy Composites, *To be submitted.*

- Sirivedin S., Fenner, D. N., Nath, R. B., and Galiotis, C., Effect of The Inter-fibre Spacing on The Stress Redistribution in Planar Array and Hexagonal Array Composites, *To be submitted.*

Acknowledgements

I gratefully would like to thank Dr David N. Fenner, my supervisor, for his guidance, support, and useful advice throughout the course of this research and the preparation of this thesis.

I wish to thank Prof. Costas Galiotis for providing useful data and discussions on the collaboration instituted between the Mechanical Engineering Department at King's College London and Institute of Chemical Engineering and High Temperature Processes-Foundation for Research and Technology-Hellas (ICE/HT-FORTH), Patras, Greece. Thanks are heartily extended to Dr R. B. Nath, Dr. N. P. O'Dowd, Dr G. Papadakis and Mr Peter di Cara for their help and useful discussions.

I am also grateful to The Royal Thai Government Scholarship and King Mongkut's Institute of Technology North Bangkok (KMITNB) for financial support throughout the course of my study.

I wish to give special thanks to my parents, Mr Prasom and Mrs Jarunee Sirivedin, my fiancé, Ms Nutsuda Ruangsriroj, and my brother, Mr Kumpanat Sirivedin, for their encouragement and support throughout the course of my study. To my friends, Dr Bruno G. Lara, Ms Olga Duran, Mr Yahya Zweiry, Mr. M. Pauzi, Mr G. Papalexopoulous, Dr B.W. Bekit, Mr N. Orfanos, Mr D. Castiglia, Mr P. Asadamongkon, Mr Yas Abbas, Mr Paresh Desai, and other people in department of Mechanical Engineering for their help.

CONTENTS

Nomenclature and Abbreviations

Symbol

D_p	critical void size
E_f	elastic modulus of fibre
E_m	elastic modulus of matrix
E_i^{avg}	average modulus of interphase
E_{avg}	average elastic modulus
G	shear modulus of elasticity
$\mathcal{G}$	strain energy release rate
H	strength coefficient
K	constant
L, l	length
L_f	stress transfer length
R, Θ, Z	polar coordinate
R	radius, inter-fibre spacing
R_m	matrix radius
R_c	composite radius
U_i	internal energy
U_s	recoverable elastic strain energy
U_p	energy dissipated by plasticity
U_{net}	total strain energy

U_c	energy dissipated by time dependent deformation
U_{avai}	energy available
$U_f^{thermal}$, $U_m^{thermal}$	strain energy stored in the curing process in fibre and matrix
$U_f^{thermal}$, $U_m^{thermal}$	strain energy in fibre and matrix before the fibre break
U_f^{break} , U_m^{break}	recoverable strain energy in fibre and matrix after the fibre break
$U_m^{plas.dis.}$	energy dissipated by matrix plasticity
V	volume
W	strain energy
a	crack length
d	diameter
d_p	critical void spacing
hv	photon or quantum energy
l_c	composite length
l_f	fibre length
l_m	matrix length
m	strain-rate sensitivity exponent
n	strain hardening exponent
r	radius
r_f	fibre radius
r_i	interphase radius
r_a	outer radius of interphase portion

r_b	inner radius of interphase portion
r_c	critical radius
$\mathbf{r}^2$	coefficient of determination
t	time
v	velocity
x, y, z	Cartesian coordinate
ΔT	temperature change
δ	Displacement
ε	Strain
$\varepsilon_1^p, \varepsilon_2^p, \varepsilon_3^p$	principal plastic strains
$\varepsilon_{appl.}$	applied strain
ε_{nom}	nominal strain
$\varepsilon_{elastic}$	elastic strain
ε_{eng}	engineering strain
ε_f^*	critical fracture strain
ε_{ft}	tensile fracture strain
ε_{pl}	plastic strain tensor
$\varepsilon_{plastic}$	plastic strain
ε_{rr}	radial strain
$\varepsilon_{r\theta}$	shear strain
ε_{zz}	axial strain

$\varepsilon_{\theta\theta}$	hoop strain
$\bar{\varepsilon}_p$	effective or equivalent plastic strain
$\dot{\varepsilon}$	strain rate
$\dot{\bar{\varepsilon}}^{pl}$	plastic strain rate
$\dot{\varepsilon}_{rr}$	radial strain rate
$\dot{\varepsilon}_{r\theta}$	shear strain rate
$\dot{\varepsilon}_{zz}$	axial strain rate
$\dot{\varepsilon}_{\theta\theta}$	hoop strain rate
η^*	exponent
θ	angle
θ_c	predicted angle
ν	Poisson's ratio
σ	normal stress
σ_{peak}	peak value of axial stress
σ_{far}	far field stress
$\sigma_{\theta\theta}$	hoop stress
σ_{rr}	radial stress
$\sigma_{r\theta}$	shear stress
σ_{zz}	axial stress
σ_m	mean stress
σ_{true}	true stress

σ_{eng}	engineering stress
$\bar{\sigma}$	von Mises stress
τ	shear stress

Abbreviation

ASTM	American society for testing and materials
BEM	boundary element method
BMA	butadiene-maleic anhydride
CCD	charged coupled devices
DSC	differential scanning calorimetry
EAA	ethylene-acrylic acid
FE	finite element
FT-IR	Fourier transform infrared spectroscopy
GPC	gel permeation chromatography
ICE/HT-FORTH	Institute of chemical engineering and high temperature processes, foundation for Research and Technology -Hellas, Patras, Greece
ISS	interfacial shear stress
LRS	laser Raman spectroscopy
PAL	positively affected length
PVAL	polyvinyl alcohol
RT	Rice and Tracey
RVE	representative volume element

SAF	stress amplification factor
SAM	scanning Auger microprobe
SEM	scanning electron microscopy
SIMS	secondary ion mass spectrometry
SME	simplified micromechanics equations
XPS	X-ray photoelectron spectroscopy

List of Finite Element Models

Name	Description	Chapter
INPLONG	long fibre, interphase model	2
INPSHRT	short fibre, interphase model	2
VOIDSHRT	short-fibre, void growth model	3
VISCOSNE	viscoplastic model	5
CRKPROPG	crack propagation model	6

List of Tables

List of Figures

CHAPTER 1

Introduction

1.1 Micromechanics of Composites

Based on Griffith's idea [1], a composite consists of a stronger material in fibre form reinforcing a weaker matrix. Since a composite consists of two or more distinct materials, its global physical properties must be different from the constituent properties. As the stronger material is in fibre-form the strength of a composite must rely on the fibre strength and on the bonding integrity between the fibre and the matrix. The study of the strength of composites has become a favourite topic challenging engineers and material scientists for several decades. Most of the early composite studies have focused on determining the effective strength and elastic behaviour of a composite. Some remarkable progress was achieved [2-4], but no account was taken of failure mechanisms. Subsequently, there has been a growing interest in studying failure mechanisms in composites [5-7].

A micromechanical analysis is a means of understanding the complicated behaviour of composites. Gibson [8] mentioned that micromechanical models should be able to answer quickly 'What if' questions regarding the effects of various fibre/matrix combinations without the need to actually fabricate and test the composite in question. This commentary is definitely true due to the fact that failure in a composite generally originates from the small defects in the fibre and/or the matrix, e.g. fibre breakage,

micro-cracks or micro-voids in the matrix material and fibre/matrix interface debonding. These defects may play an important role in the failure of composites depending on loading conditions and constituent materials.

Various test methods have been used (see Fig. 1.1) to assess the interfacial bond strength of composite, e.g. the fragmentation test, single-fibre pull-out/push-out tests, micro-indentation test and the micro-compression test [9]. However, these test methods can only be used to examine the global behaviour of the composite. Fortunately, the stress transferred to the fibre can be measured experimentally using laser Raman spectroscopy (LRS) in the fragmentation test [10] (see Fig. 1.2). The advantage of using this technique is that the complete fibre stress state history can be monitored throughout the fibre length to within a very small spatial resolution of the order of 1 μm [11]. However, LRS is incapable of measuring the stresses in the matrix material, and is unable to capture very fast changes in fibre stress (e.g. during fibre fracture). Inspite of these limitations, LRS measurements provide useful data for modelling and validating the results of a finite element (FE) analysis of the micromechanical mechanisms of failure.

1.2 Micromechanics of Progressive Failure in Composites

Micromechanical failure in unidirectional composites can be classified into three main classes: fibre fracture, matrix cracking, and fibre/matrix interface debonding. The various failure modes in composites generally initiate from the fibre fracture, resulting in the development of matrix cracks or interface cracks depending on several factors.

It is widely accepted that a matrix crack is likely to occur in a strong interface system [12]. The presence of a thin layer between the fibre and the matrix in a sized system, called the *interphase*, has been found to improve adhesion between the fibre and the matrix. The mechanical properties of the interphase are not well understood due to the limitations of currently available measurement techniques.

Interface debonding, or cracking is another type of micromechanical failure induced by the presence of initial defects in the composite. In polymer composites, micro-voids usually form in the region adjacent to the fibre/matrix interface during fabrication. These defects are probably formed due to imperfect bonding of the matrix and the rough surface of the untreated fibre and will lead to interface cracking when the composite is subject to a mechanical loading [9].

Initial micro-voids in the polymer matrix are also defects from the fabrication process, which can develop to become observable matrix cracks. In a slow crack growth process, such as in a short, sized-fibre composite under a tensile loading, matrix cracking is likely to be governed by the development of micro-voids formed in the region near the crack tip [13].

Another form of defect is micro-void formation in a region of matrix crazing [14]. Crazes have usually been observed to have the appearance of small cracks in glassy polymers under a high strain condition. However, a key to failure in polymer composites must be a fibre fracture accompanied by the development of other initial

defects forming different patterns of crack. Just after the fibre fractures, the interfacial strength becomes a significant factor governing the inducement of interface or matrix cracks in a composite. This sequential fracture process can be classified as the micromechanics of progressive failure in composites.

Initial defects in the fibres, resulting from imperfect manufacturing introducing flaws into the fibre, will lead to fibre breaks at low strain. The fibre flaws can be assessed by the Weibull modulus distribution function [15]. Interface debonding has been found to improve the toughness of a composite and to relax the local stresses, as a result of the movement at the interface promoting stress transfer by frictional sliding [16]. By contrast, matrix cracks may result in serious damage to composite structures such as pressure vessels [17].

The fracture process in a short fibre composite can be divided into three distinctive modes [18]. The first mode occurs when localised yielding in the matrix material near the fibre-end corner leads to the fibre ends debonding, and to the formation of a penny-shaped fibre crack (*Mode* α). Once the penny-shaped fibre crack has been formed the next failure will be either interface debonding (*Mode* β) or a matrix crack (*Mode* γ), depending on the strength of the bond between the fibre and the matrix (see Fig. 1.3). Failure in a composite is a progression. In the case of a long fibre composite, fibre fractures at high strain lead to the fibre recoil, which induces a higher strain rate in the matrix material near the fracture location. Since the mechanical

properties of polymer matrix depend on the strain rate, the geometry of matrix cracks is different from that in a short fibre composites.

According to experimental observations [19-28], matrix cracks in polymer composites were found to have different shapes, which include a disc-shaped crack, conical shaped crack, star-shaped crack and an interface crack. The conditions inducing the different matrix crack geometries will be investigated in this research.

In a unidirectional multi-fibre system, the strength of the composite depends on the number of fibres used, i.e. the fibre volume fraction in the composite. Hence, the fibre packing arrangement is a factor determining the composite strength, as long as no fibre fracture occurs. Micromechanical modelling of multi-fibre composite can be implemented in the same manner as micromechanical modelling of a single-fibre composite. The inter-fibre spacing plays an important role in determining the stress redistribution near the fibre fracture location. Fracture in a fibre may induce fracture in the neighbouring intact fibres. A suitable inter-fibre spacing, which will prevent a domino effect of fibre fracture, can be established using a micromechanical analysis of the multi-fibre composite.

1.3 Literature Survey & Review of Micromechanical Analysis of Composites

Cox [2] proposed his pioneering model in the micromechanical analysis of composites in 1952. Cox's model, known as the shear lag model, describes stress transfer in a short fibre composite. This work has been widely referred to and used as the basis for

the more sophisticated micromechanical analysis of composites. However, this model can describe only the linear elastic behaviour of a composite and does not include any type of failure mechanisms. Recent studies [29-33] have attempted to include failure mechanisms in the model. It is necessary to know the exact nature of failure in order to avoid critical loading conditions and to assist in the design of composites. Fundamentally, the micromechanical analysis of composites is separated into experimental and analytical work. The former work involves using measurement techniques to investigate mechanical behaviour and failure in composites, e.g. LRS measurement, scanning electron microscopy (SEM) and photo-elastic modelling. Mathematical methods include analytical methods and numerical techniques such as FE analysis, boundary element method (BEM) and finite difference analysis.

Matrix cracking in a boron fibre embedded in an epoxy matrix was first reported by Mullin *et al.* [19] in 1968. Mullin *et al.* classified failure resulting from fibre fracture into three cases. The first case is the occurrence of a disc-shaped crack, two conical-shaped cracks, both, or neither, as a result of fibre fracture in the case of strong interface (see Fig. 1.4 and Fig. 1.5). The second case is failure by debonding along the interface. The last case is the initiation of a conical-shaped matrix crack at the fibre ends. In the present work, an attempt is made to estimate the angle of such cracks.

Chamis [22] also observed a similar crack pattern in a boron fibre/epoxy composite. Selvadurai and Busschen [20-21] have investigated conical-shaped matrix cracks in an E-glass fibre/polyester composite by correlating the images of several crack

geometries obtained from the charge coupled devices (CCD) microscope with the results obtained from boundary element analysis. The crack geometry obtained from boundary element analysis agreed reasonably well with the images. However, since they performed only the fragmentation test, without using any special measurement technique, they were unable to predict the critical conditions inducing conical cracks and the angle of crack propagation. Song *et al.* [25] reported that conical cracks were also found in glass fibre/nylon 6 thermoplastic injection-moulded composites. Paipetis *et al.* [27-28] have also found conical-shaped matrix cracks in carbon fibre/epoxy composites, and have used the LRS technique to measure the fibre stress history during the fragmentation test. Nath *et al.* [34] have performed linear elastic FE analysis for a short fibre composite and the results were compared with LRS measurements. By matching the stress profiles from FE analysis and LRS measurements, they predicted that the semi-cone angle of crack propagation is about 20° with a 100 μm crack length. This prediction was achieved using the hypothesis that the fibre stress profile would be a geometrical characteristic of the matrix cracks present in the composite. However, linear elastic FE analysis is unable to describe the matrix plasticity and the other forms of non-linear behaviour in the composite.

Galiotis [35] found that the conical-shaped matrix cracks in a continuous fibre composite in the fragmentation test had larger cone angles than in a single fibre composite. This discrepancy has sparked the idea of investigating the details of the fracture mechanism. Nath [36] mentioned that the larger cone angle for matrix cracks in a continuous fibre composite was possibly due to recoil in the fibre after fracture.

Curtin [37] described the fibre stress build-up in the zone of retracting fibres near the fracture location, using an analytical model, which takes account of the Weibull modulus. The results were compared with experiment and size effects were also investigated. The absence of load transfer over the debonded or slip length located near the fibre fracture location was reported. Liu *et al*. [38] have studied the effect of matrix cracking and interface debonding upon stress transfer in carbon fibre/epoxy composites. Their results have shown that matrix cracks substantially reduce the efficiency of stress transfer from the matrix to the fibre while the interface debonding has less effect. Most of the experimental, analytical and numerical work [29,30,39-42] concerned with the micromechanics of composites has focused on interface debonding rather than on matrix cracking. Nevertheless, in the field of composite laminates matrix cracking has been taken into account [17,43-47].

Early studies of the effects of matrix viscoelasticity and viscoplasticity were confined to metal matrix composites. The viscoelastic behaviour of a fibre-reinforced plastic was first studied by Lou *et al.* [48]. Wang *et al*. [49] performed FE analysis and experimental measurements to characterise the viscoplastic behaviour of a composite. The variation of polymer composite compliance as a function of loading time has been proposed by Zaoutsos *et al.* [50] in order to predict the long-term behaviour of a composite at high applied stress levels. The first attempt at using a viscoplastic model to evaluate matrix cracking was by Gao *et al.* [51]. They used the principle of minimum complementary energy and a unified viscoplasticity model to analyse cross-ply laminates containing matrix cracks and validated their model with FE results.

However, the effect of the viscoplastic behaviour of polymer composites, as a result of fibre breaks inducing high strain rate in the matrix material, has not yet been investigated.

All the micromechanical models mentioned so far contain only a single fibre. In fact, actual composite structures contain many fibres. A study of the micromechanics of multi-fibre composites can be accomplished using experimental measurement and FE analysis in the same manner as for a single fibre composite. Chamis and Caruso [52] have investigated the elastic constants of planar array fibres using the so-called 'simplified micromechanics equations' (SME), which were validated by three-dimensional FE analysis. In their model round fibres are converted to square fibres which give the same fibre volume fraction. This model describes well the elastic behaviour at different fibre volume fractions of the planar array of multi-fibre composites. Furthermore, the stress redistribution, as a result of fibre fractures, would also have an effect on amplifying the local stress in the neighbouring intact fibres near the fibre fracture location. This phenomenon was first reported by Hedgepeth and van Dyke [53]. They used 2-D and 3-D shear lag models to determine the stress concentration factor in the neighbouring intact fibres with different fibre packing arrangements. They found that the value of the stress concentration factor obtained using a 3-D shear lag analysis was lower than that obtained with 2-D analysis and the fibre volume fraction and matrix elastic modulus have no effect. Wagner and Eitan [54] used a modified shear lag model that can take account of volume fraction and matrix modulus to estimate the stress concentration factor. Their models predicted

values of stress concentration lower than Hedgepeth and van Dyke's'model at larger fibre inter-spacing. Wagner *et al.* [55] performed LRS measurement and found fair agreement with their modified shear lag models. Chohan and Galiotis [56] used LRS to measure the stress in the fibres for planar array and semi-hexagonal array of fibres. However, they were unable to measure the stress in a broken fibre located at the centre of a hexagonal array due to the reflection of Raman wave by surrounding fibres. Van den Heuvel *et al.* [57] measured the fibre stress in planar array of fibres and performed 3-dimensional linear elastic and elasto-plastic FE analyses to verify the experimental results. The stress concentration factors calculated by both types of FE analyses predicted lower values than the values obtained by LRS measurement. Lane *et al.* [58] performed 3-dimensional FE analysis to study the strain concentration in a planar array with a high fibre volume fraction. They simulated only the fibre fractures and neglected any type of related failure in the FE model, such as matrix cracking or interface debonding. This would lead to an inaccurate estimation of the stress concentration factors. Chohan and Galiotis [56] observed conical-shaped matrix cracking and interface debonding immediately after the fibre fractured in their composite system. Therefore, 3-dimensional micromechanical FE models with a simulation of matrix cracking after fibre fractures for planar array and hexagonal array of fibres will be employed to investigate the effect of matrix cracking on stress concentration factors in this work.

1.4 Aims and Objectives

The main aim of this research is to investigate and classify progressive failure mechanisms in the unidirectional long fibre and short fibre/epoxy composites. FE analysis will be used to investigate the micromechanics of progressive failure in carbon fibre-reinforced epoxy composites. The results from LRS measurement, obtained by Galiotis *et al*. [27,28,33,56] will be used to validate the FE results.

The main objectives of this research are:

(I) To investigate the effect of interphase on failure in the short and long fibre composites.

(II) To investigate the matrix cracking in a short fibre composite by the influence of micro-voids growth, nucleation and coalescence in the matrix material near the crack tip.

(III) To investigate the effect of matrix viscoplasticity on the inducement of micromechanical failure in carbon fibre-reinforced epoxy composites.

(IV) To investigate the effects of inter-fibre spacing and the presence of a matrix crack on stress redistribution in planar array of fibres composite, and to validate the materials modelling of this model for later use in the hexagonal array models.

(V) To investigate the stress redistribution in a hexagonal array of fibres composite using 3-dimensional elasto-plastic FE analysis. In this case LRS measurement cannot be used to validate the model.

1.5 Thesis Structure

- **Chapter 2** The effect of interphase is investigated using FE analysis. A comparison between the effect of interphase in the short fibre and long fibre composites is made.
- **Chapter 3** This chapter discusses the influence of micro-void growth and coalescence on induced matrix cracks in carbon fibre-reinforced epoxy composites. The results obtained from linear elastic and elasto-plastic FE analyses are compared and discussed. A criterion to predict matrix cracking is proposed and discussed.
- **Chapter 4** This chapter contains an experimental study of the viscoplastic behaviour of epoxy matrix. Rate dependent tensile testing was performed to obtain rate-sensitive stress/strain curves for later use in viscoplastic FE models. The fracture characteristics of epoxy are also discussed.
- **Chapter 5** Viscoplastic FE analysis was performed with the implementation of 'Progressional Approach'. The minimum strain energy density criterion was applied to the FE results in order to estimate the semi-cone angle of matrix crack.
- **Chapter 6** Matrix crack length is predicted using the elasto-plastic and viscoplastic FE analyses. The FE results were compared with the experimental results obtained by LRS measurement. An energy balance model was introduced to describe the fracture mechanisms of matrix cracks.
- **Chapter 7** Three-dimensional elasto-plastic FE analysis for the planar array of fibres was performed to investigate the effect of matrix cracking on the stress redistribution. The FE results were validated by the experimental results obtained

by LRS measurement. The stress concentration obtained by LRS measurement and FE analysis were compared and discussed.

- **Chapter 8** This chapter presents the prediction of the stress concentration factors for the hexagonal array of fibres using the 3-dimensional elasto-plastic FE analysis.

- **Chapter 9** Concludes the thesis with a summary of the achievement of this work. Suggestions for future research in the micromechanics of composites are also discussed.

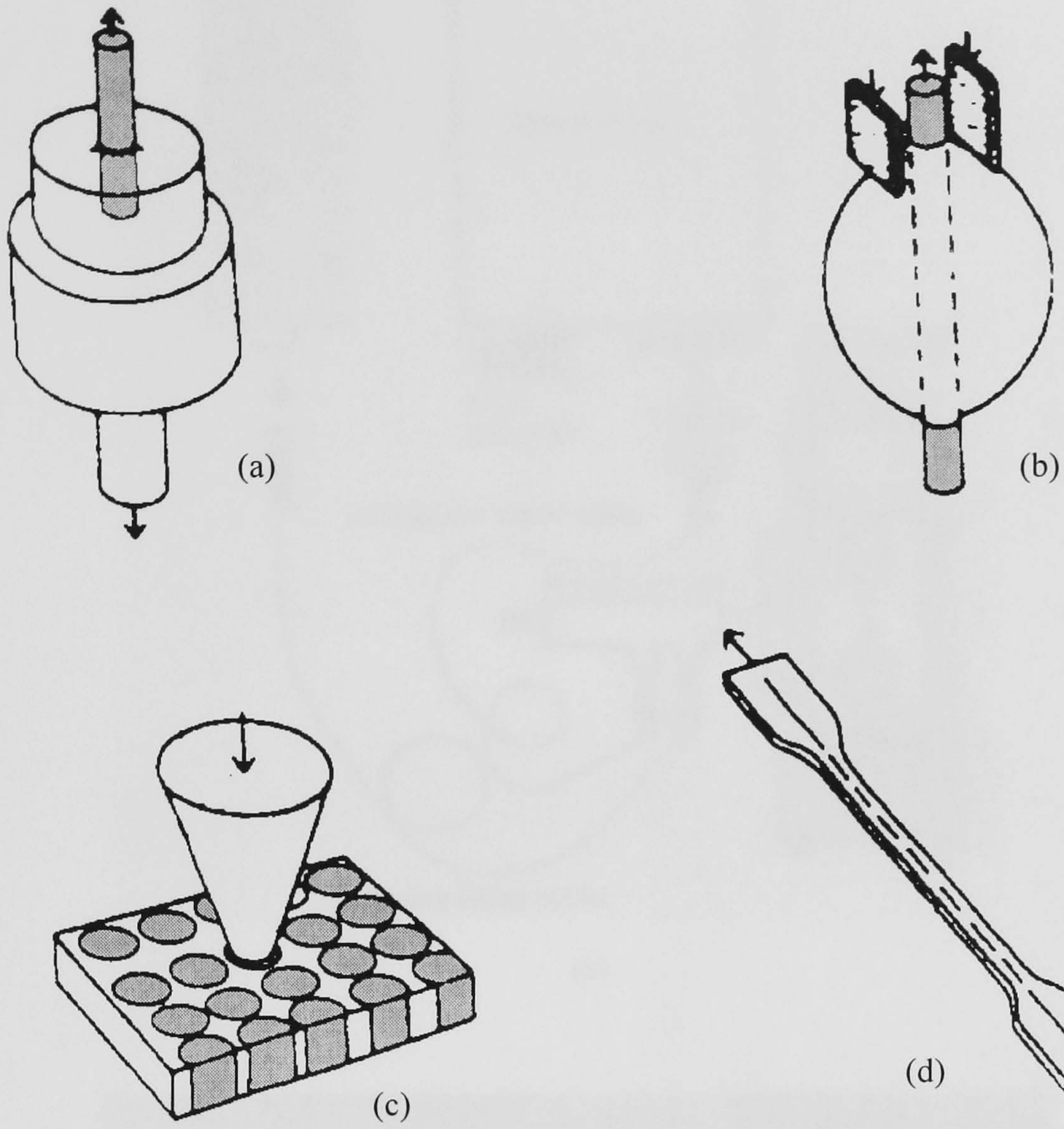

Figure 1.1 Test methods for composites (a) fibre pull-out test (b) microtension test (c) microcompression test, and (d) fragmentation test.

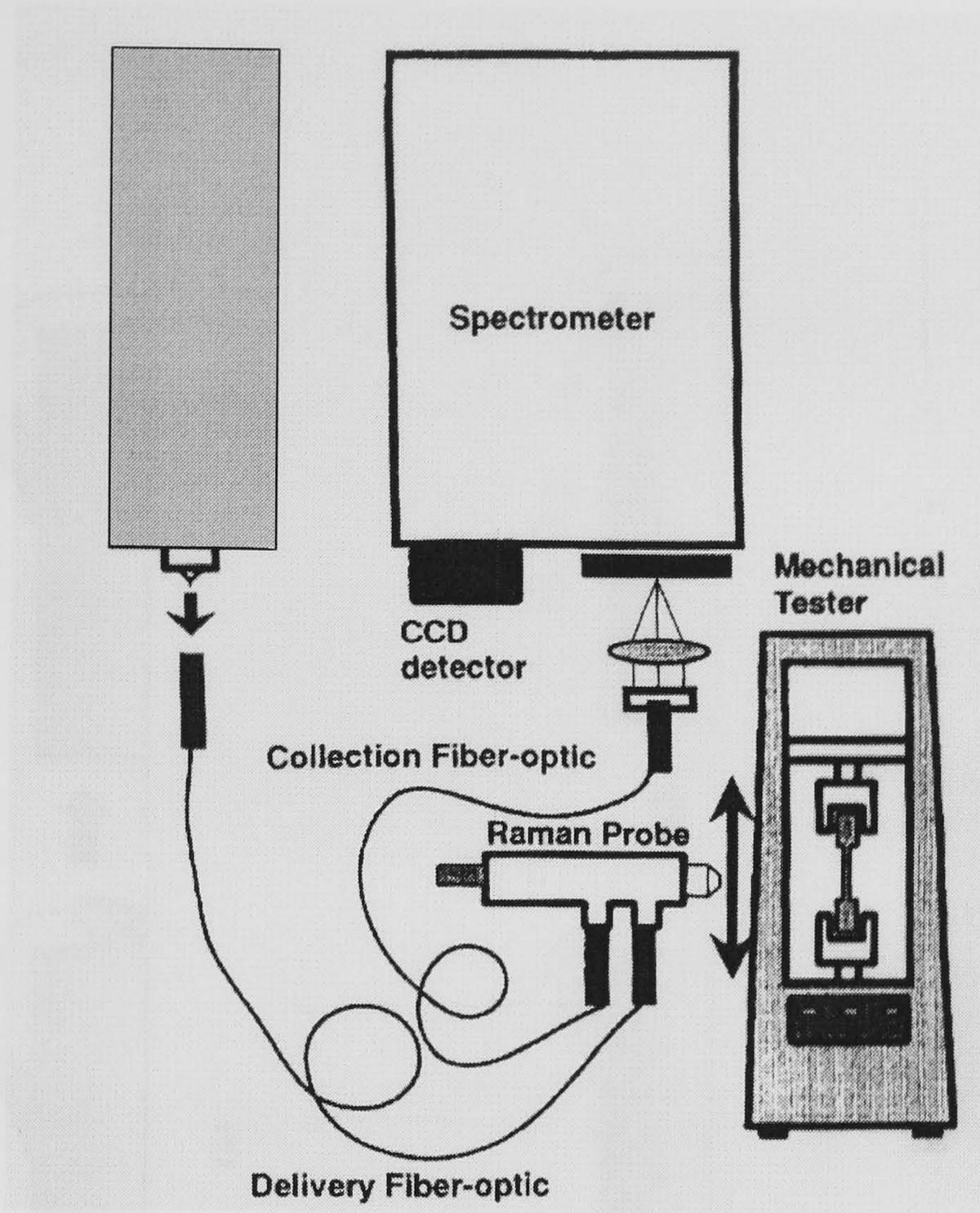

(a)

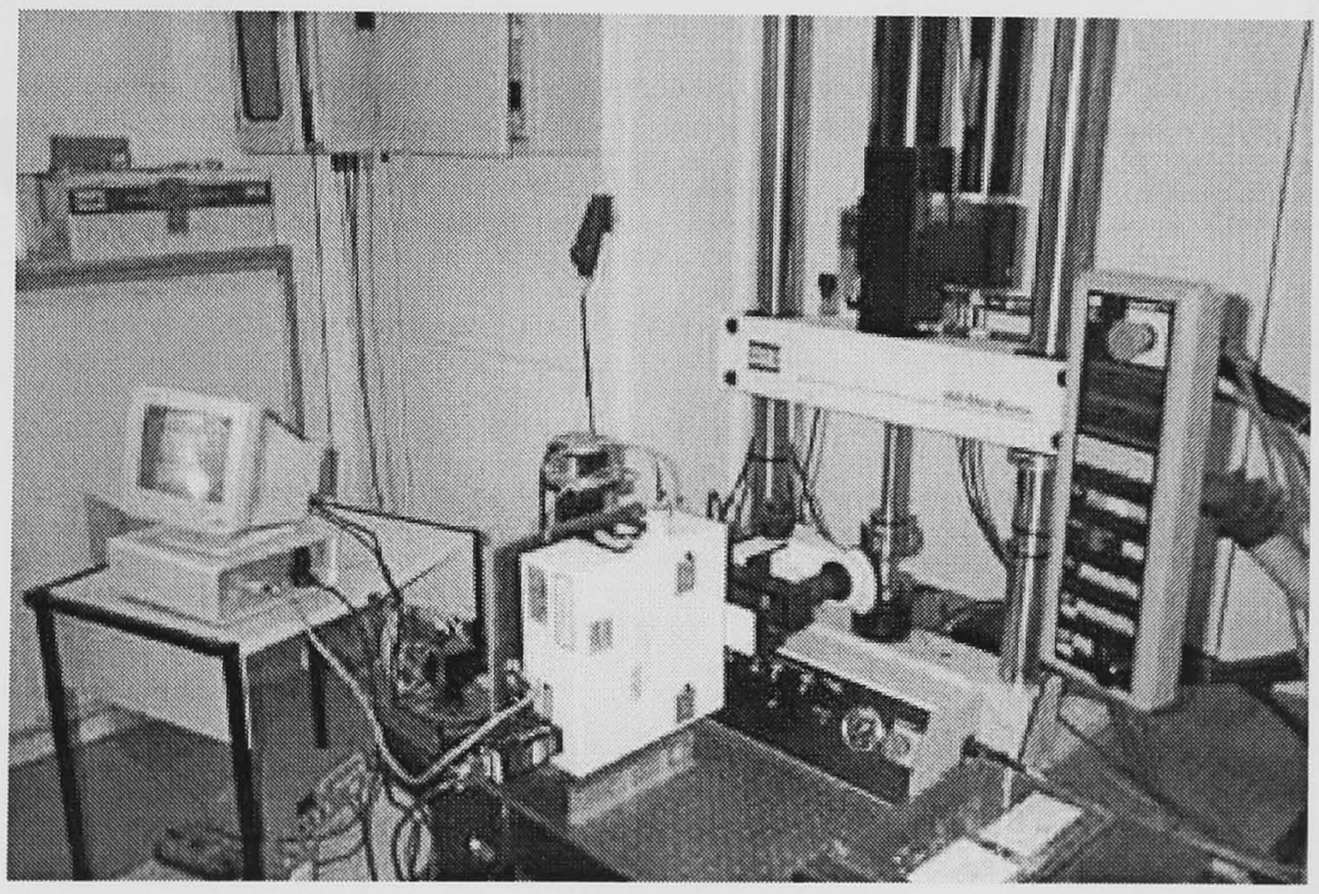

(b)

Figure 1.2 Laser Raman spectroscopy (LRS) (a) schematic of LRS system (b) actual LRS system at ICE/HT FORTH [59]

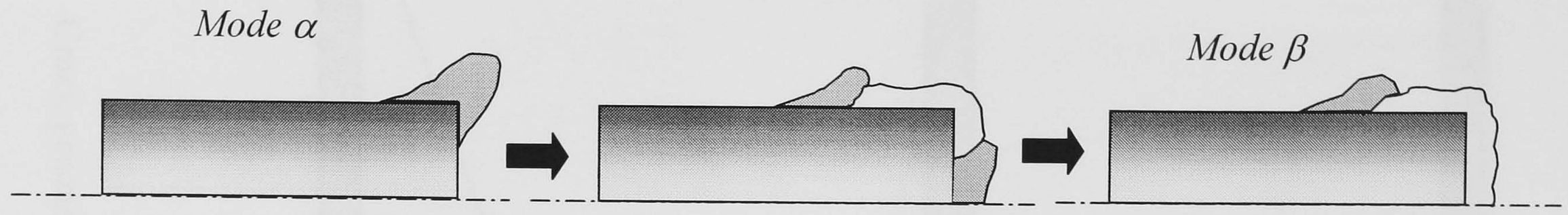

(a)

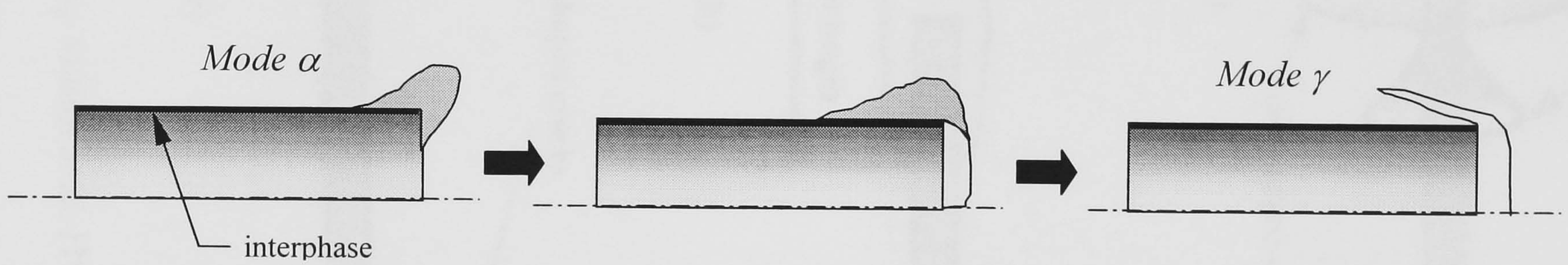

(b)

Figure 1.3 Progressive failure in a composite (a) development of *Mode β* from *Mode α* in an unsized system (b) development of *Mode γ* from *Mode α* in a sized system

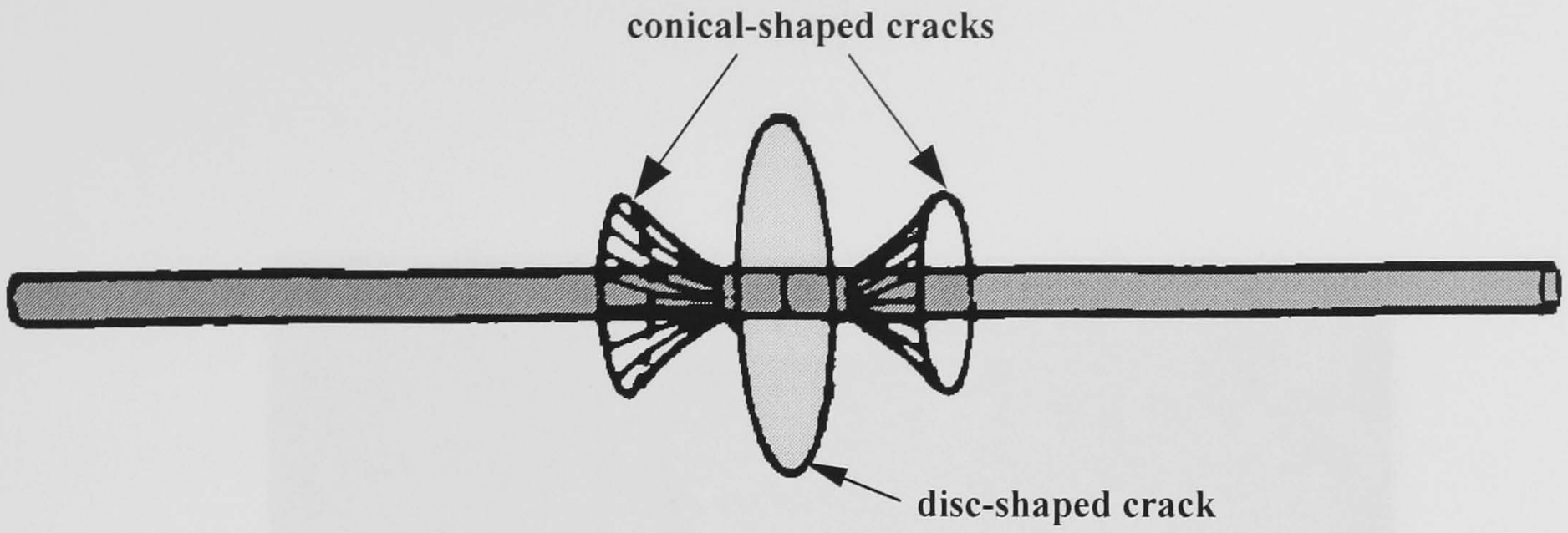

(a)

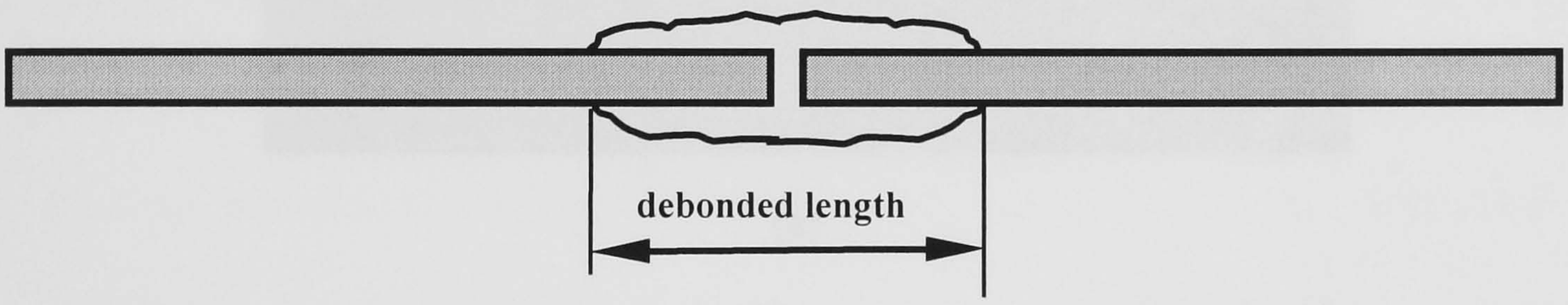

(b)

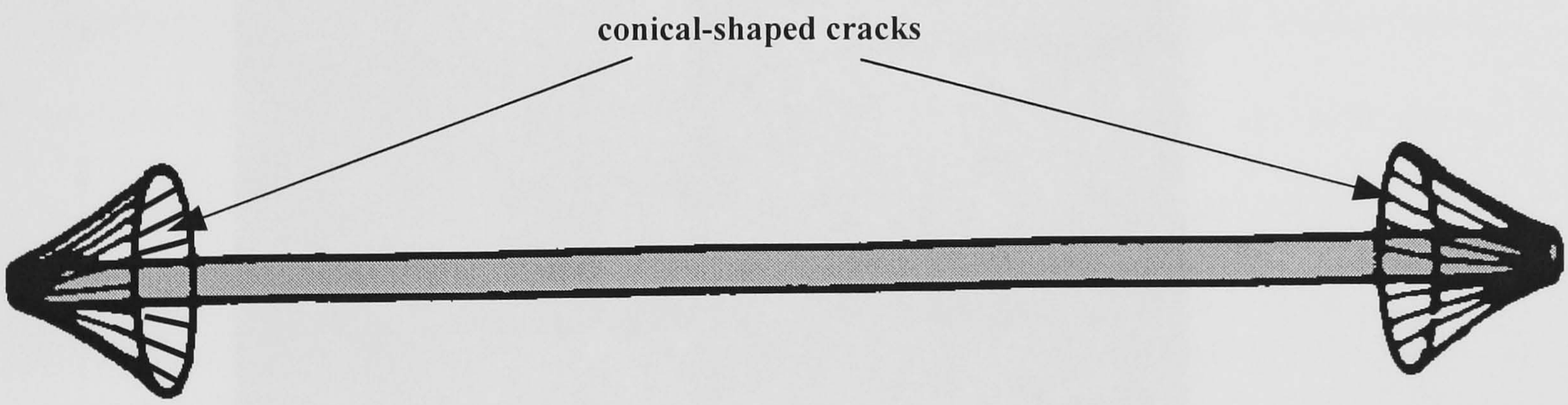

(c)

Figure 1.4 Crack geometries observed by Mullin *et al*. [19] (a) disc-shaped and conical-shaped cracks at the fibre fracture location, (b) debonding along the interface near fibre fracture location, and (c) conical-shaped cracks at both ends of fibre in a short fibre system.

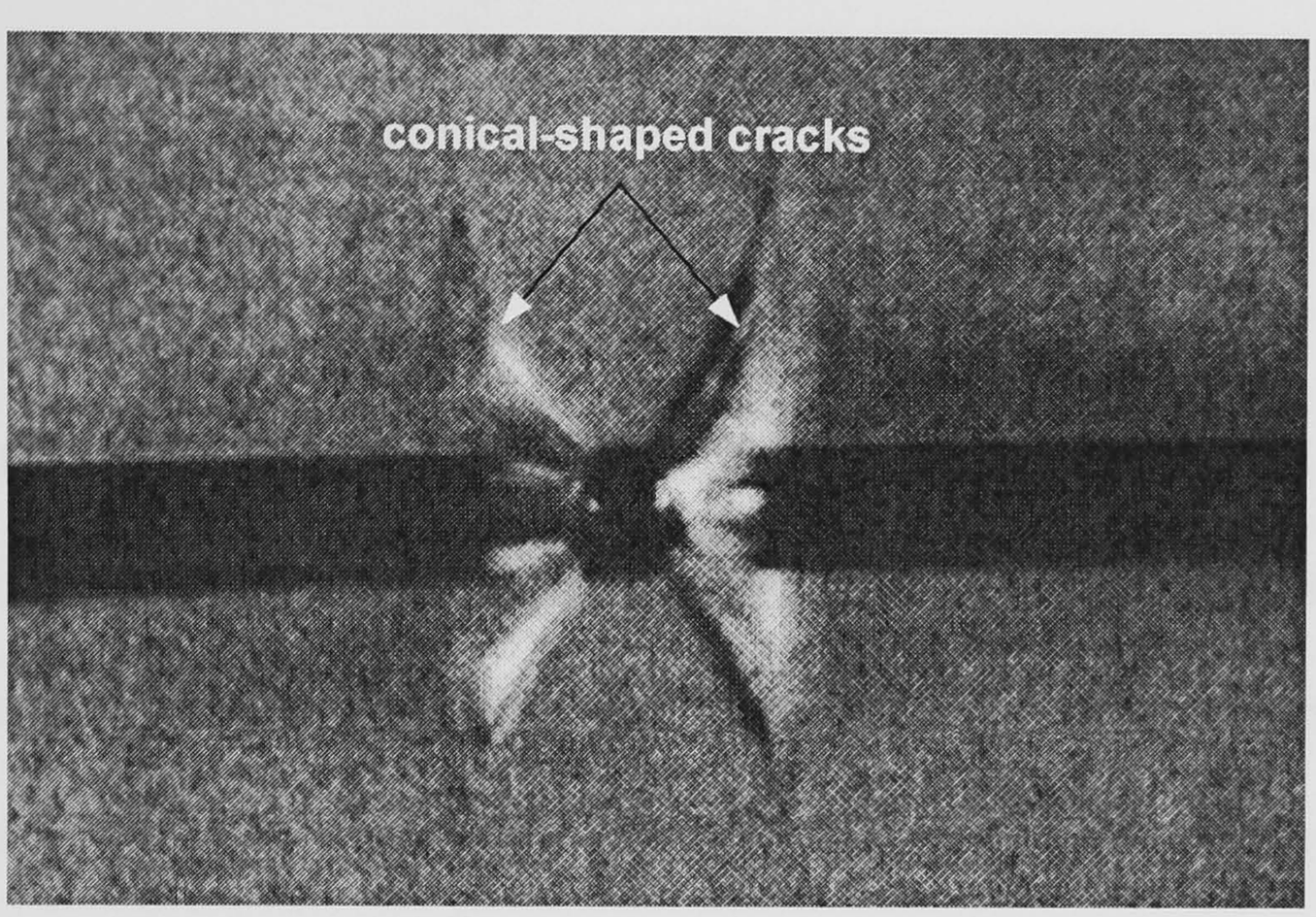

(a)

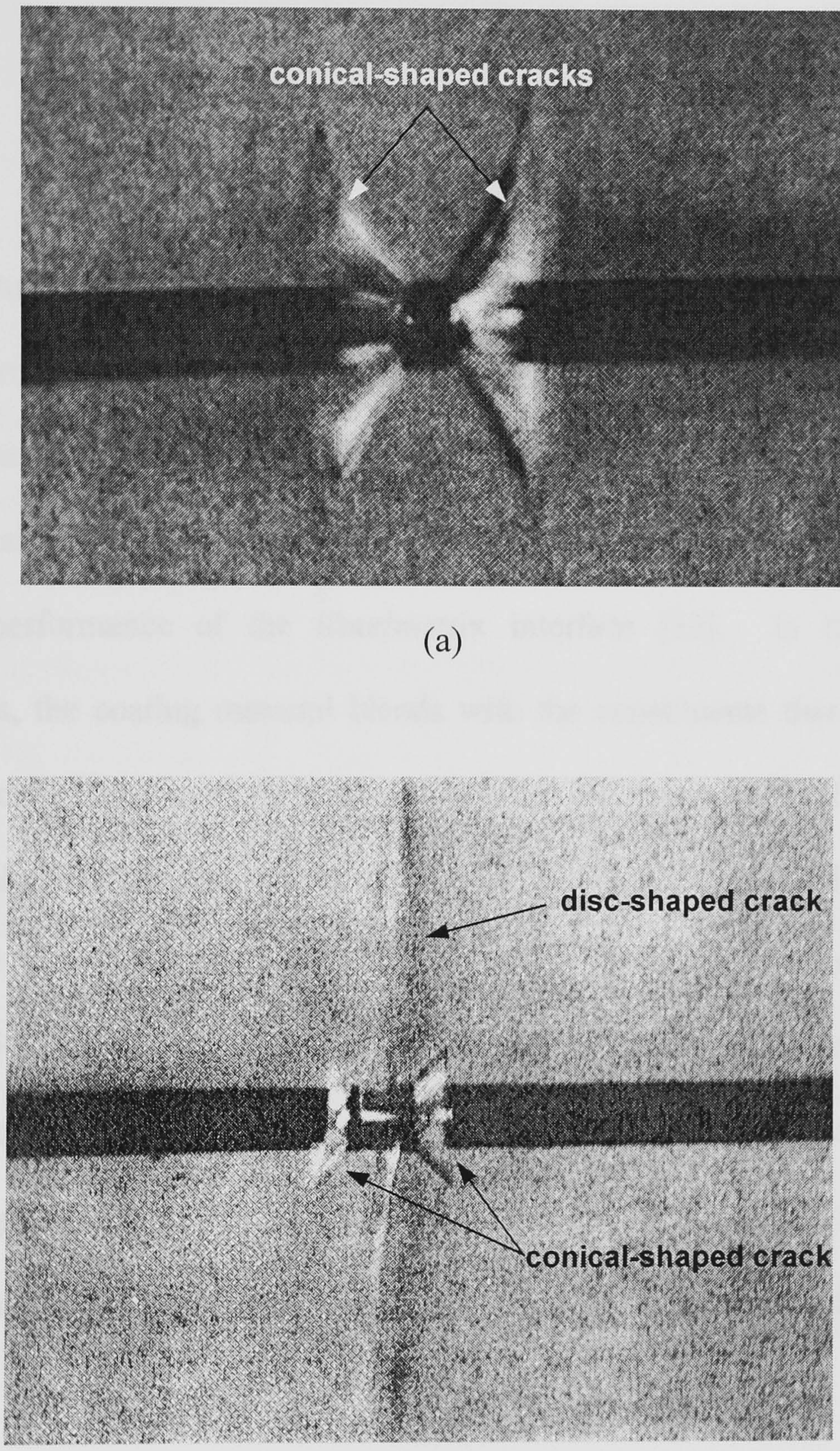

(b)

Figure 1.5 Several forms of matrix cracks in boron and tungsten fibre/epoxy composite (58x) [19] (a) conical-shaped cracks (b) conical-shaped and disc-shaped cracks

CHAPTER 2

Effect of an Interphase

2.1 Introduction

The performance of fibre-reinforced composites is highly dependent on the bond strength between the fibre and the matrix. Coating materials, such as silicone, polyvinyl alcohol (PVAL), are normally applied on the fibre surface to improve the bonding performance of the fibre/matrix interface [32]. In the fabrication of composites, the coating material blends with the constituents thereby developing a thin layer called an interphase between the fibre and matrix [60]. This thin layer has mechanical properties which vary through its thickness [61-65]. Many measurement techniques [66] have been used to investigate the properties of the interphase, including Fourier transform infrared spectroscopy (FT-IR), LRS, secondary ion mass spectrometry (SIMS) with ion scattering spectrometry, X-ray photoelectron spectroscopy (XPS or ESCA), the use of Scanning Auger Microprobe (SAM) analysis, atomic force microscope, and gel permeation chromatography (GPC).

The development of the interphase was studied by Peacock, Fife, Nield and Crick [67]. An etching technique was used to examine AS-4/PEEK composites. They found a certain amount of discrete spherulites emerged from the fibre surface and

grew into the matrix. Crasto, Own and Subramanian [61] investigated the role of the interphase on the interlaminar shear strength in graphite fibre/epoxy composites using electron microprobe analysis and SEM. The graphite fibres used in their study were electro-coated by ethylene-acrylic acid (EAA), butadiene-maleic anhydride (BMA) copolymers, and commercially surface treated. They found that the electro-coating technique with EAA coating material improved the interfacial shear strength about 20% compared to the commercially surface treatment. The electron microprobe line scan showed a smooth radial variation of interphase properties in the composite system using EAA coating material.

Analytical methods to describe the mechanical properties of the interphase have been developed by several authors. Piggott [30] introduced theoretical models, which are based on the shear lag model, to describe the effect of the interphase on stress transfer characteristics. Several interphase models, including elastic, slipping, yielding, and brittle interphase, were used to describe failure modes in several testing methods. Theocaris [62] has developed unfolding models, which are based on the fact that the interphase forms a transition zone between fibres, as a result of thermodynamic phenomena occurring at the glass transition temperature of the composite. Theocaris, Sideridis and Papanicolaou [63] have improved the original unfolding models by applying linear, parabolic, hyperbolic and logarithmic functions to express the variations of the mechanical properties of the interphase. They also have validated their models with results obtained from the differential scanning calorimetry (DSC)

thermal analyser measurements. Theocaris and Philippidis [64] have modified the unfold models to evaluate the thickness of the interphase.

Since the mechanical properties of the interphase are so complex, there is a growing interest in using numerical techniques to investigate its effect. Most of the early work was limited to the linear elastic region [68-73]. Ho and Drzal [74,75] performed elasto-plastic FE analysis to investigate the effect of the interphase thickness on stress transfer characteristics in a fragmentation test. They also have included such failure as debonding along the fibre/matrix interface in their models. However, this analysis has not simulated a continuous process of progressive failure in the composite. Nath, Fenner, and Galiotis [36] have performed the more realistic FE analysis, which takes account of the matrix plasticity and progressive failure in the composite. However, the interphase was not included in their model.

The aim of this work is to investigate the effects of interphase on the stress transfer characteristics and the interfacial shear strength in short carbon fibre and continuous carbon fibre composites in the fragmentation test.

2.2 Interphase Model

2.2.1 Theoretical model of the interphase

The mechanical properties of the interphase were modelled using the unfolding model proposed by Theocaris *et al.* [64]. Variation of the interphase moduli along the interphase radius is given by:

$$E_i(r) = E_f\left(\frac{r_f}{r}\right)^{\eta^*}\left(\frac{r_i - r}{r_i - r_f}\right) + E_m\left(\frac{r_i(r - r_f)}{r(r_i - r_f)}\right) \tag{2.1}$$

where E_i is a radial function of the interphase modulus, and E_f and E_m are the elastic modulus of fibre and matrix, respectively. The radii, r_f, r_i and r refer to the fibre radius, the interphase radius and an arbitrarily defined radius at each point in the model, respectively. The exponent η^* is defined as:

$$\eta^* = 1 + \frac{\ln\left(\frac{E_m}{E_f}\right)}{\ln\left(\frac{r_f}{r_i}\right)} \tag{2.2}$$

The radial variation of the interphase moduli for this composite system is shown in Fig. 2.1.

2.2.2 FE model of the interphase

As the interphase modulus is varying radially, modelling this kind of material behaviour in a FE analysis is very difficult. In order to implement this variation in FE model, several thin layers of elements were created to approximate a radial function of the interphase moduli (see Fig. 2.2). The mean value theorem was applied to estimate the effective modulus for each layer of elements, which is defined as:

$$E_i^{avg} = \frac{1}{r_a - r_b} \int_{r_b}^{r_a} E_i(r).dr \tag{2.3}$$

where r_a and r_b refer to the outer and inner radii of the interphase portion, respectively (see Fig. 2.2). Solving eq. (2.3) yields:

$$E_i^{avg} = \frac{\left(E_m(\eta^* - 2)(\eta^* - 1) r_f r_i \ln\left(\frac{r_a}{r_b}\right)\right)}{\left((\eta^* - 2)(\eta^* - 1)(r_a - r_b)(r_f - r_i)\right)} + \frac{E_f r_b \left(\frac{r_f}{r_b}\right)^{\eta^*} \left(r_b(\eta^* - 1) - r_i(\eta^* - 2)\right)}{\left((\eta^* - 2)(\eta^* - 1)(r_a - r_b)(r_f - r_i)\right)}$$

$$- \frac{E_f r_a \left(\frac{r_f}{r_a}\right)^{\eta^*} \left(r_a(\eta^* - 1) - r_i(\eta^* - 2)\right)}{\left((\eta^* - 2)(\eta^* - 1)(r_a - r_b)(r_f - r_i)\right)} - \frac{E_m(\eta^* - 2)(\eta^* - 1)(r_a - r_b) r_i}{\left((\eta^* - 2)(\eta^* - 1)(r_a - r_b)(r_f - r_i)\right)} \tag{2.4}$$

2.3 FE models

The short fibre and long fibre composites were modelled based on the concept of the RVE model for the axisymmetric FE analysis (see Fig. 2.3). The fibre radius r_f used in this work was 3.3 μm. The half fibre length l_f used for the long fibre and the short fibre models were 300 μm and 250 μm, respectively (see Fig. 2.3). The composite radius R_c and length l_c used were 50 μm and 300 μm. The material properties of M40B-40B carbon fibre supplied by Soficar were used to model the fibre in this analysis (see Table 2.1). MY750/HY951 epoxy matrix provided by Ciba-Geigy was used to model the matrix material. The stress/strain relationship for matrix material is shown in Fig. 2.4. The full details of mechanical properties of this epoxy are shown

in Appendix B. The interphase was assumed to be linearly elastic. The FE mesh for a long fibre composite contains 4,612 8-node quadratic elements (see Fig. 2.5). In order to avoid high stress concentration at the fibre end corner in a short fibre system a small radius of 0.1 μm was used (see Fig. 2.6). The FE mesh for a short fibre composite contains 10,243 8-node quadratic elements (see Fig. 2.6). The interphase thickness for this composite system was found to lie in the range 0.15-0.6 μm [35]. In order to examine the maximum effect, the interphase thickness of 0.3 μm and 0.6 μm were used in this work. Four layers of elements were used to represent the interphase thickness of 0.6 μm and two layers of elements were used to represent the interphase thickness of 0.3 μm for continuous fibre models. In the short fibre models, eight and four layers of elements were used to represent the interphase thickness of 0.6 μm and 0.3 μm, respectively. In order to avoid a mesh distortion problem that would occur in the interphase layer, the aspect ratio of all elements was not allowed to exceed 10. The progressional approach, which was proposed by Nath *et al.* [76], was implemented in elasto-plastic FE analysis to simulate thermal residual stresses induced by curing process and the fibre fracture for the long fibre composite models. According to the progressional approach concept, there are 3 load steps in the FE analysis (see Fig. 2.7):

(i) *Curing process*: A uniform temperature drop of 50°C was applied to simulate a curing process in this type of composite. At this stage, matrix contraction induces compressive stresses in the fibre as a result of the mismatch between the coefficients of thermal expansion of the fibre and the matrix.

(ii) *Mechanical applied strain of 1.3 %*: a uniform displacement δ was applied at one side of the composite end face to produce mechanical strain of 1.3 %, at which the first fibre fracture was found in the experiment [27,28].

(iii) *Fibre fracture*: fibre fracture was simulated in this step by removing all previously applied boundary conditions from one side of fibre end face.

For short-fibre composite models, only the load step *(i)* and *(ii)* were used in the analysis. The mechanical strain of 0.4 %, in which the matrix cracks were found in experiment [27,28], was also applied and the results compared with the models with the mechanical strain of 1.3 %.

2.4 Results Summary

2.4.1 Long fibre composite

The fibre thermal residual axial stresses in the FE models with and without the interphase were compared in Fig. 2.8. The interphase was found to relieve the fibre compressive stress by about 2% and 4 % at the thickness of 0.3 μm and 0.6 μm, respectively. The interphase is likely to confine stress fields within the fibre. However, those residual stresses are lying within the range of 0.27± 0.40 GPa, which were measured by LRS [27,28]. When the interphase thickness of 0.3 μm and 0.6 μm were included, the axial fibre stress was found to increase by about 1.8 % and 2.5 %, respectively (see Fig. 2.9). The magnitudes of fibre axial stress obtained from FE analysis are of the same order as those values measured by LRS [27,28], except the stress profiles from FE analysis are much steeper (see Fig. 2.9). This discrepancy

may result from omitting failure in the FE models. The interfacial shear stress in the model without the interphase was compared with the interfacial shear stresses obtained from the models containing the interphase in Fig. 2.10. The interphase is likely to help the composite to absorb the shear stress, and it can be seen in Fig. 2.10 that the regions of high shear stresses are reduced. The strain energy density was used to examine the ability to transfer strain energy to the interphase. A reduction of strain energy in the matrix material of about 12.7 % was found when the interphase was included in the models (see Fig. 2.11). The strain energy density in the fibre was found to increase of about 3.6 % by the effect of the interphase. A very high value of an equivalent plastic strain of about 0.875 was found in a vicinity of the crack tip for the model without the interphase. When the interphase was included in the models, the equivalent plastic strain was decreased to 0.141 and 0.0963 for the interphase thickness of 0.3 μm and 0.6 μm, respectively.

2.4.2 Short fibre composite

It has been found that the first fracture in the short carbon fibre/epoxy composite occurs at a mechanical applied strain of about 0.4 % [27,28]. In order to distinguish between the mechanical behaviour of the short fibre and long fibre composites, a mechanical applied strain of 1.3 % was used first for a comparative study. The thermal residual stresses in the short fibre system were found to be a little lower than those in the long fibre system. As a result of gross yielding in the matrix material, the shapes of the fibre stress profiles become steeper than those for the long fibre system (see Fig. 2.13). The maximum values of the axial fibre stress in the short-fibre

composite model are about half of those values in the long-fibre composite model at the same applied mechanical strain level (see Fig. 2.13). This may result from the lower fibre volume fraction and shorter stress-transfer length in the short fibre system. The maximum values of the equivalent plastic strains in matrix material for the short fibre system are much higher than those values found in the long-fibre systems. The maximum values of the equivalent plastic strain without the interphase, and with an interphase thickness of 0.3 μm and 0.6 μm are 11.4, 11 and 7.95, respectively. Those values are much higher than the fracture strain of the matrix, implying that matrix cracking would have taken place at this applied strain level. The shear stress profiles implied very high gross yielding in the matrix material, as can be observed from the shear stress transfer lengths of about 70% of the half fibre length (see Fig. 2.14).

At a mechanical applied strain of 0.4 %, the fibre axial stress and the shear stress profiles for the models with or without the interphase are slightly different (see Fig. 2.15). The fibre axial stress was about half of that found in the models with the applied mechanical strain of 1.3 %. The fibre axial stress profile obtained from LRS measurement is slightly different from the FE results and the maximum value is a little higher (see Fig. 2.15). This may be due to ignoring failure such as interface debonding or matrix crack in the FE models. The shear stress transfer lengths were reduced to about 30 % of the half fibre length. The strain energy was also used to determine the effect of interphase in this case. At the applied strain of 1.3 %, a highest reduction of strain energy in matrix material, approximately, 11.3% was

found in the model with interphase thickness of 0.6 μm, compared to the model without the interphase (see Fig. 2.17). At the applied strain of 0.4 %, the interphase has almost no effect on the strain energy in the constituents (see Fig. 2.18). The maximum value of the equivalent plastic strain was found to be in the region near the fibre corner in the matrix material. Those values are 1.71, 1.46 and 0.469, for the models without the interphase, with the interphase thickness of 0.3 μm and 0.6 μm, respectively.

2.5 Discussion

The FE results have shown the effect on the fibre stresses to be less than 3% when the interphase is included in the FE models. On the limited results available, the function of the interphase is to improve the bond strength of the fibre/matrix interface. Since the interphase has the lowest volume fraction in the RVE model, it must have a small load-carrying capacity than the other constituents in the composite. Based on the fact that the strength of the interphase is lying between the strength of the fibre and the matrix, the interphase may act as a transition zone to relieve the stresses transferred from the fibre to the matrix. This presumption is evidenced by the reductions of the strain energy in the matrix material shown in Fig. 2.11 and Fig. 2.17. The interphase also relieves plastic strains from the matrix material up to the highest reduction of about 89% in a long fibre system and of about 72 % in a short fibre system. Unfortunately, the exact mechanical properties of the interphase are not yet available to be used in a realistic FE analysis.

Material Properties	Carbon fibre	Matrix MY-750/HY-951 (relaxed properties)
Axial Tensile Modulus, GPa	392	2.6
Transverse Modulus, GPa	20	2.6
Axial Tensile Strength, GPa	3.2 *(fracture)*	41×10^{-3} *(yield)*
Axial Fracture Strain, %	0.8	6.13
Transverse Poisson's ratio, $\nu_{R\Theta}$	0.27	0.34
Poisson's ratio in R-Z direction, ν_{RZ}	0.03	0.34
Axial Coefficient of Thermal Expansion, K^{-1}	-0.25×10^{-6}	58×10^{-6}
Transverse Coefficient of Thermal Expansion, K^{-1}	25×10^{-6}	58×10^{-6}

Table 2.1 Material properties of carbon fibre and epoxy matrix

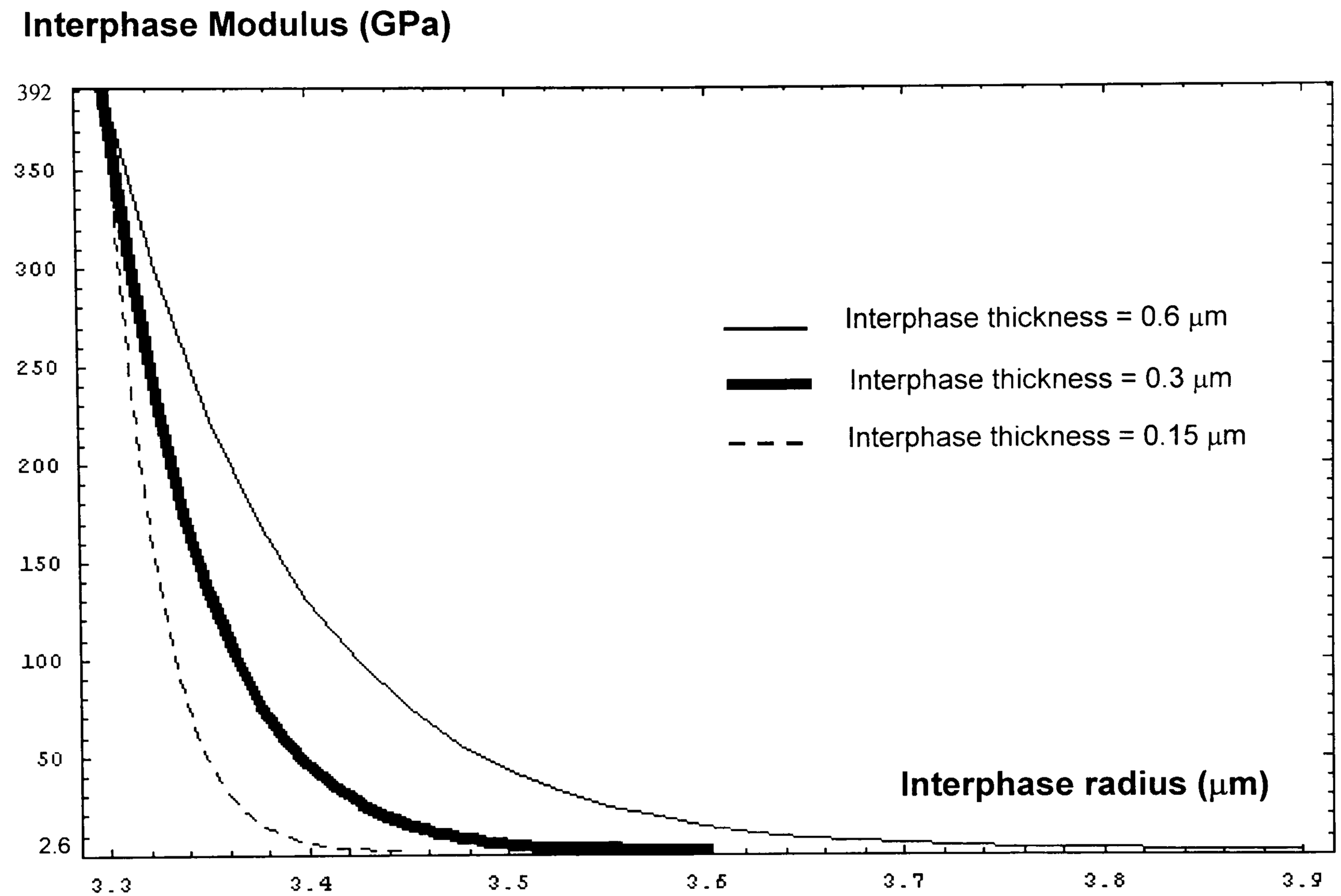

Figure 2.1 Variation of interphase moduli at different thicknesses, based on Theocaris unfolding model [65]

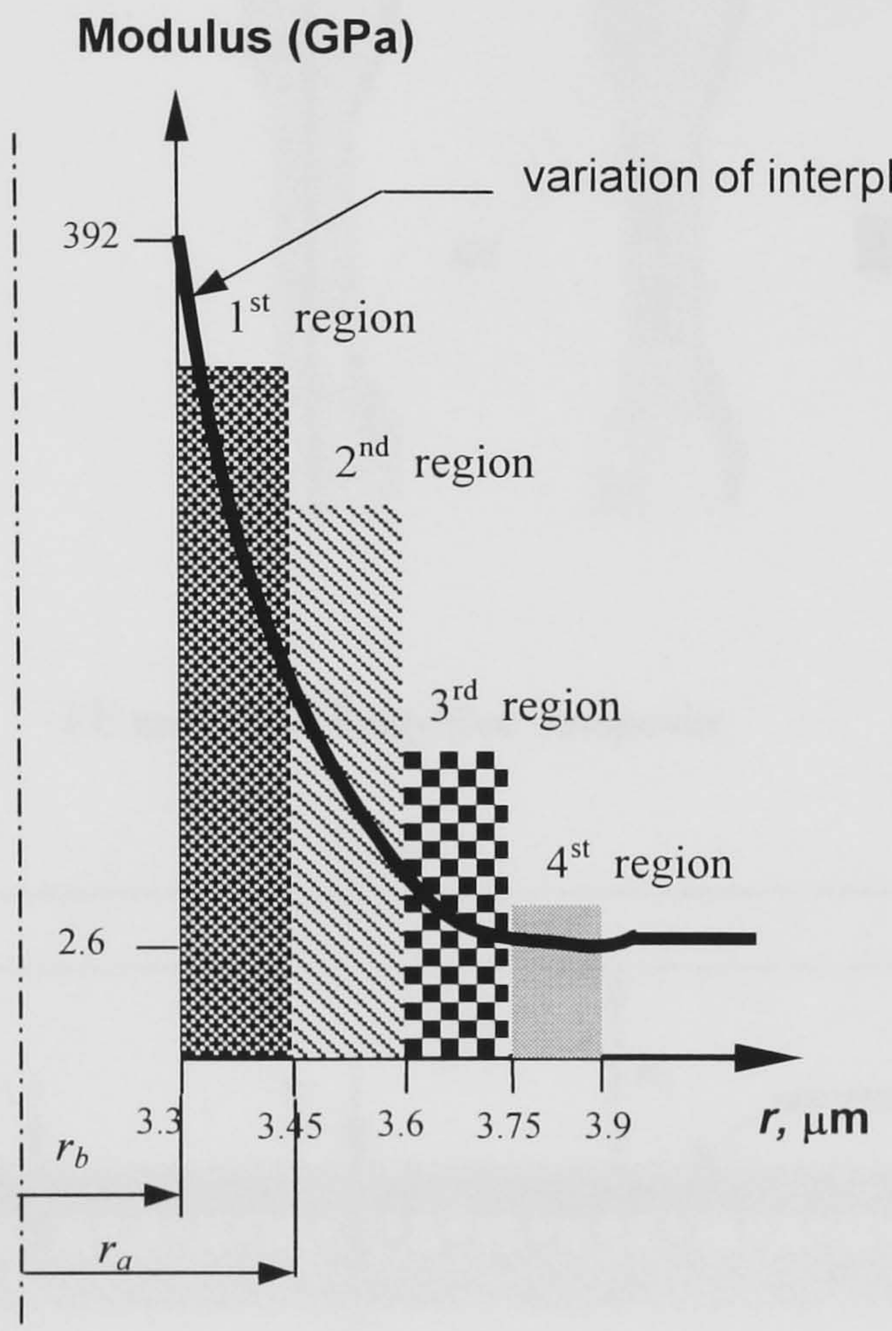

Interphase region	Modulus (GPa) Thickness 0.6 μm	Modulus (GPa) Thickness 0.3 μm
1	191.444	117.815
2	36.628	5.624
3	7.687	N/A
4	2.958	N/A

Figure 2.2 Interphase models and their moduli in FE analysis

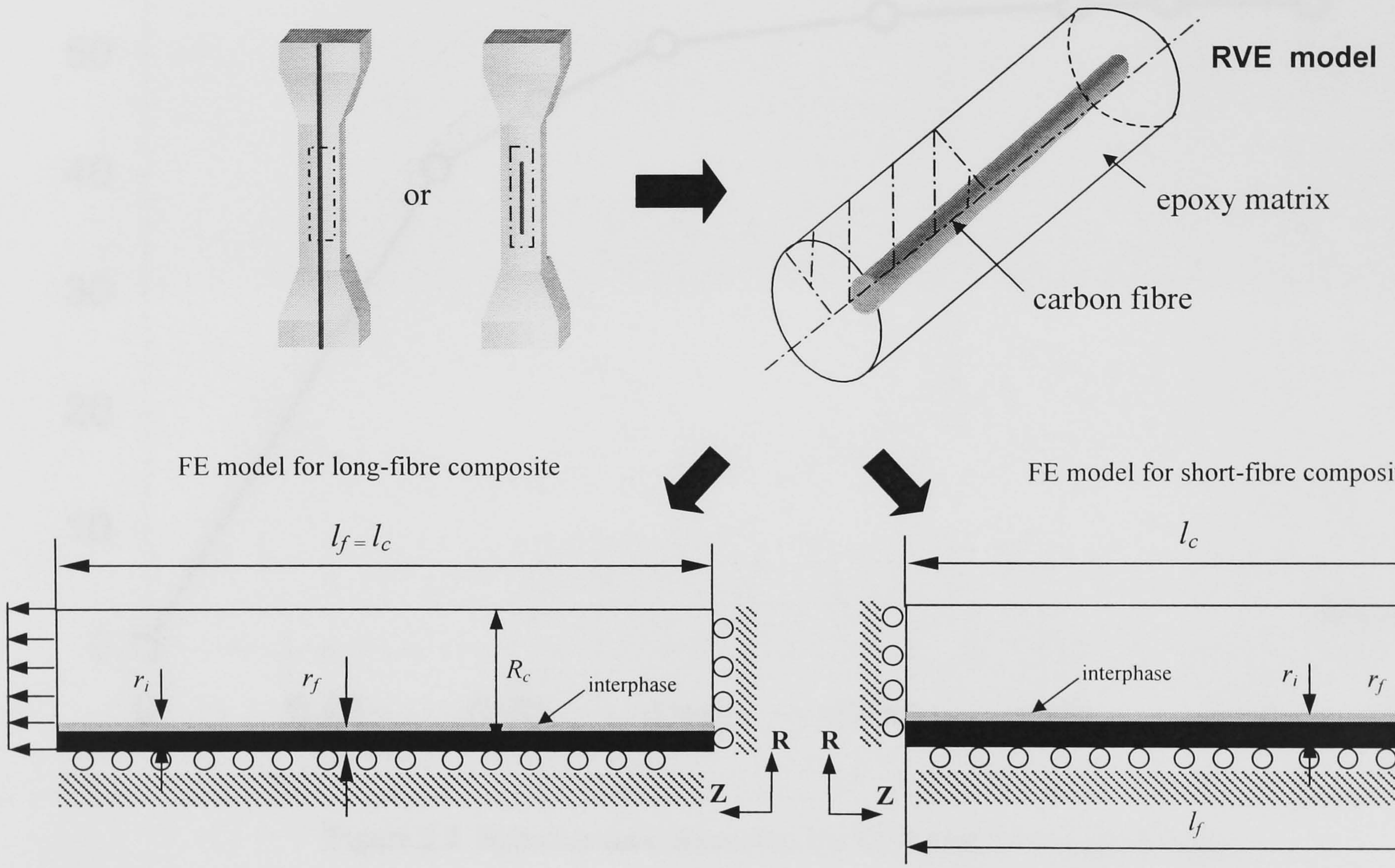

Figure 2.3 Axisymmetric FE models for short and long fibre systems based on RVE models

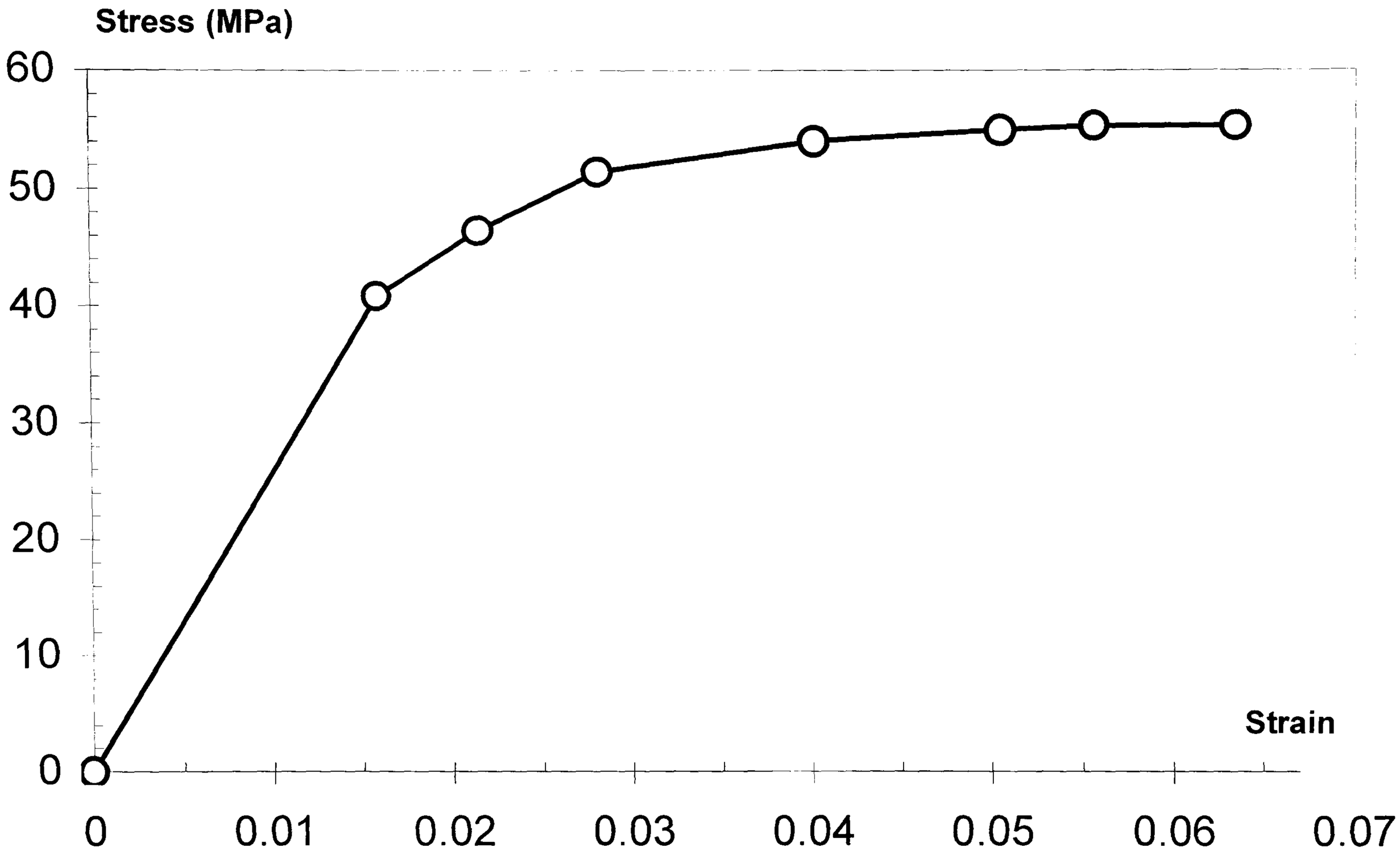

Figure 2.4 Stress/strain relationship for MY750/HY951 epoxy matrix

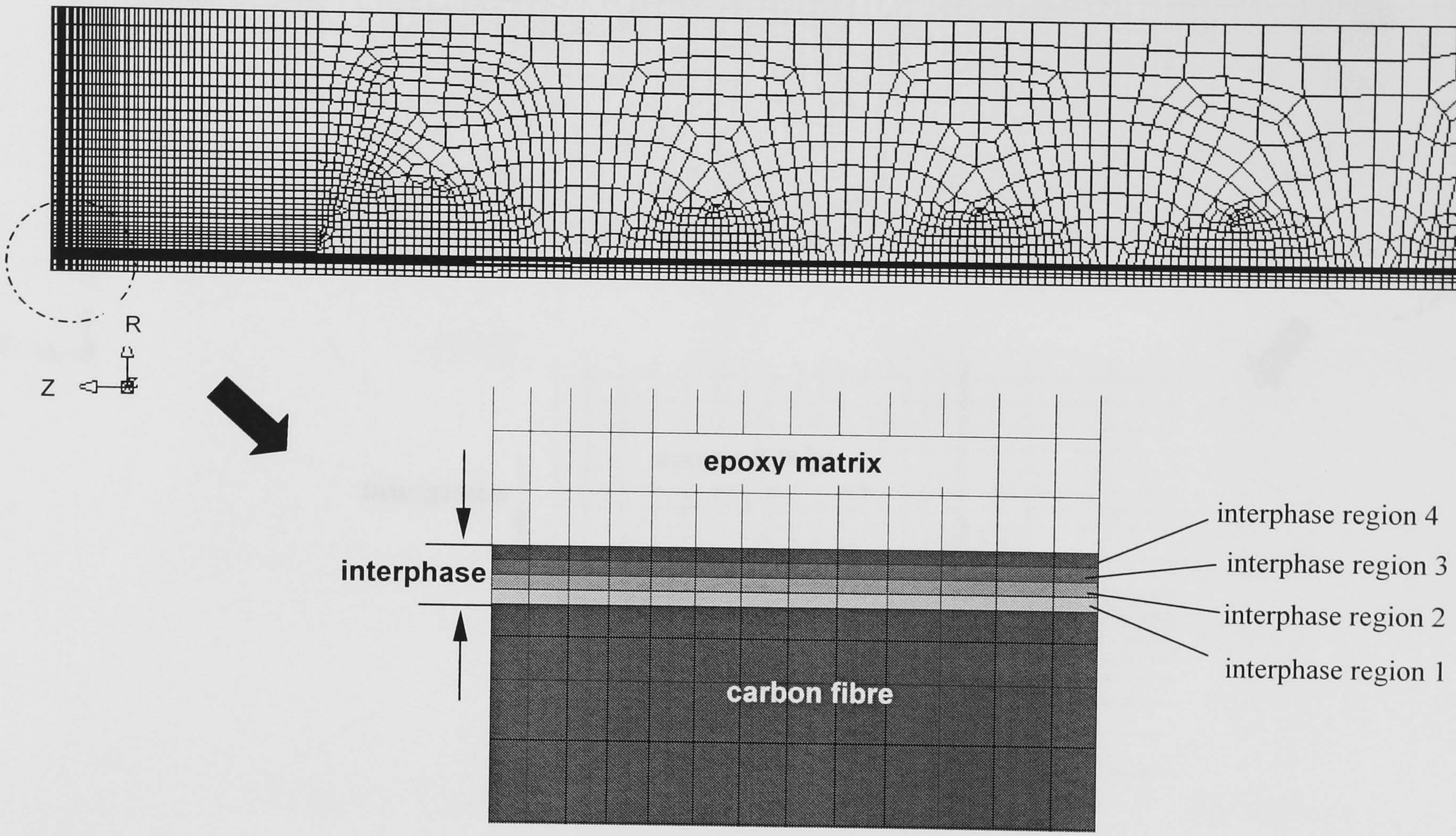

Figure 2.5 FE mesh for long-fibre composite

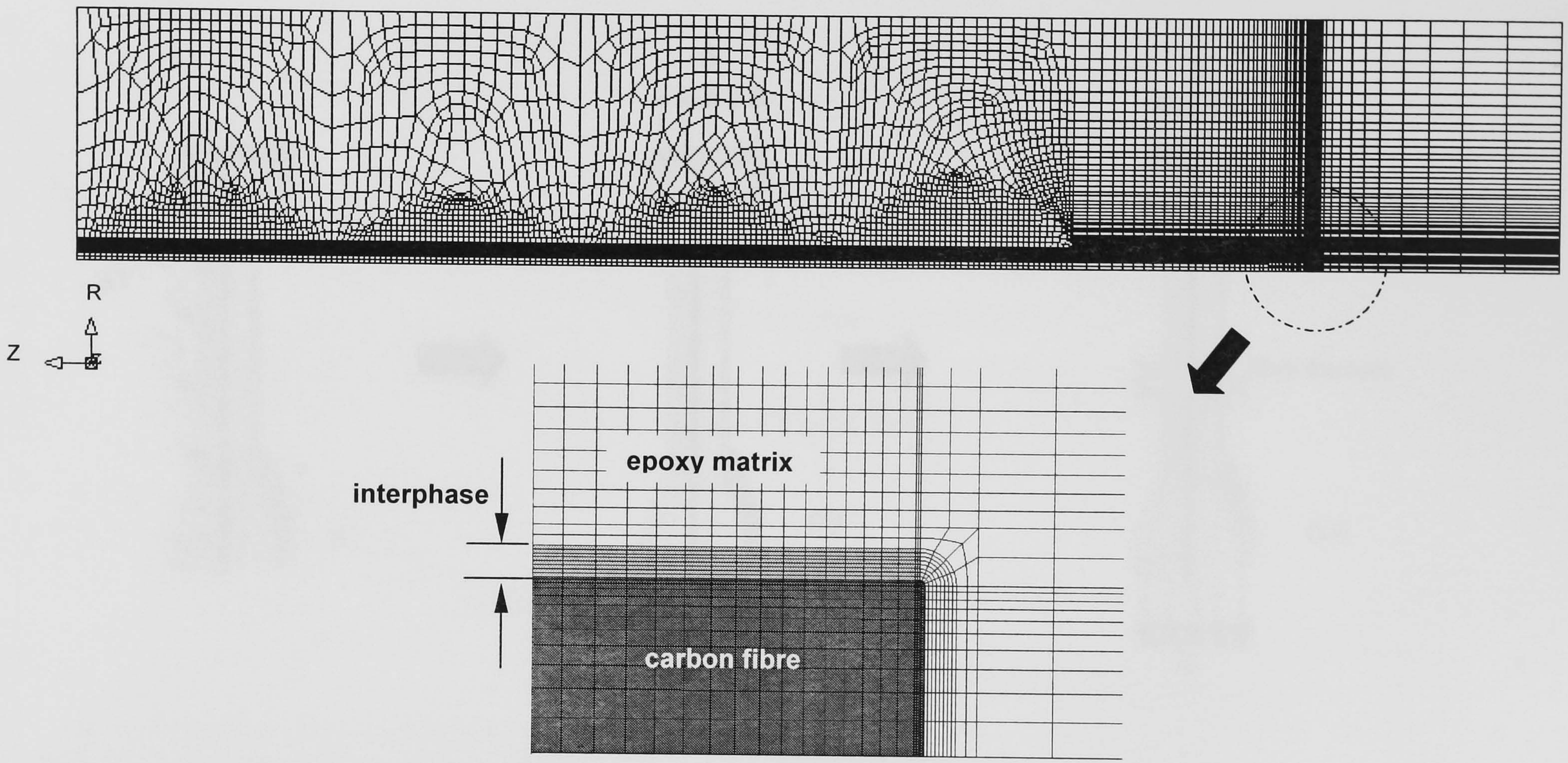

Figure 2.6 FE mesh for short-fibre composite

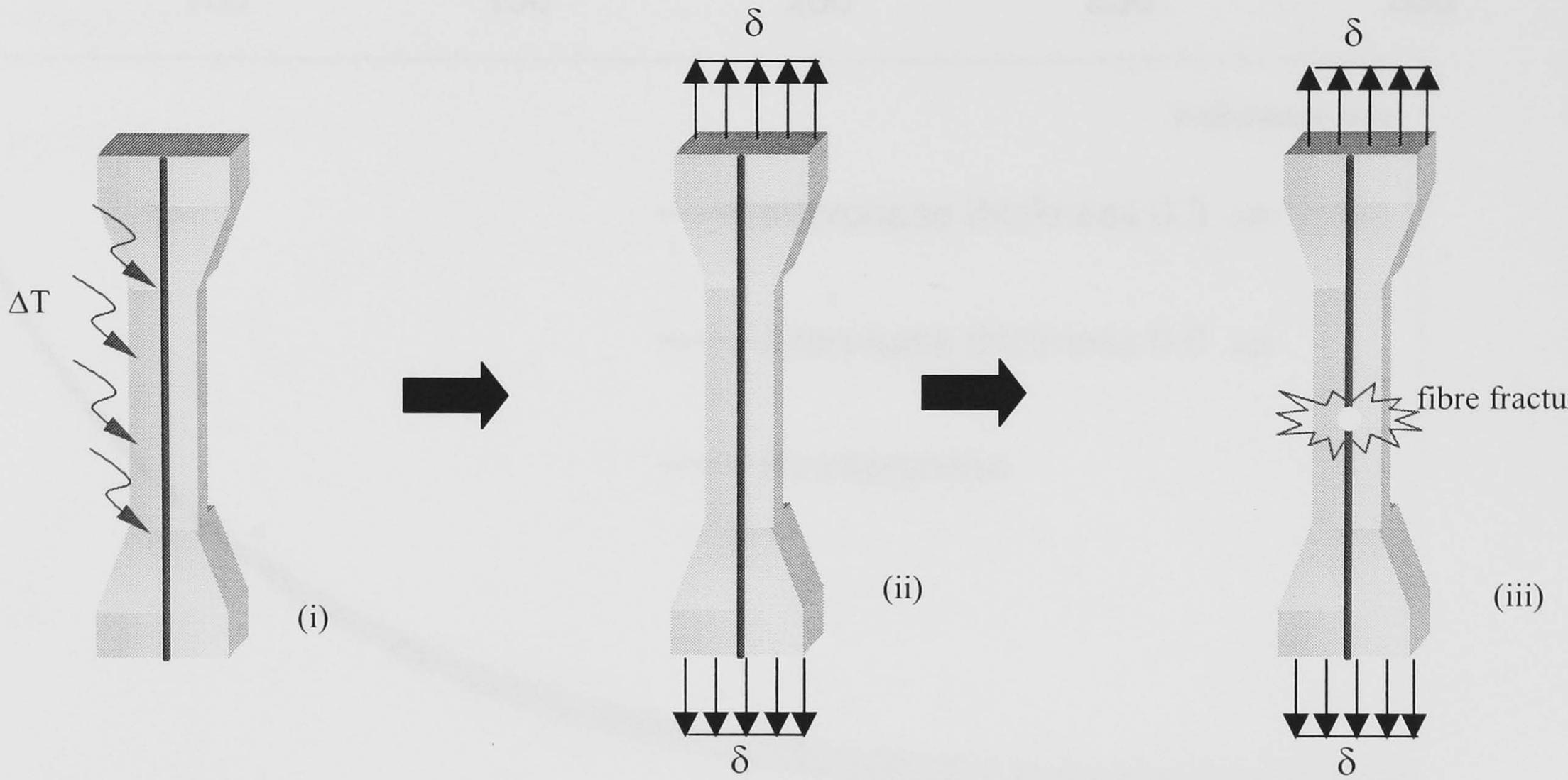

Figure 2.7 Progressional Approach implemented in axisymmetric FE analysis

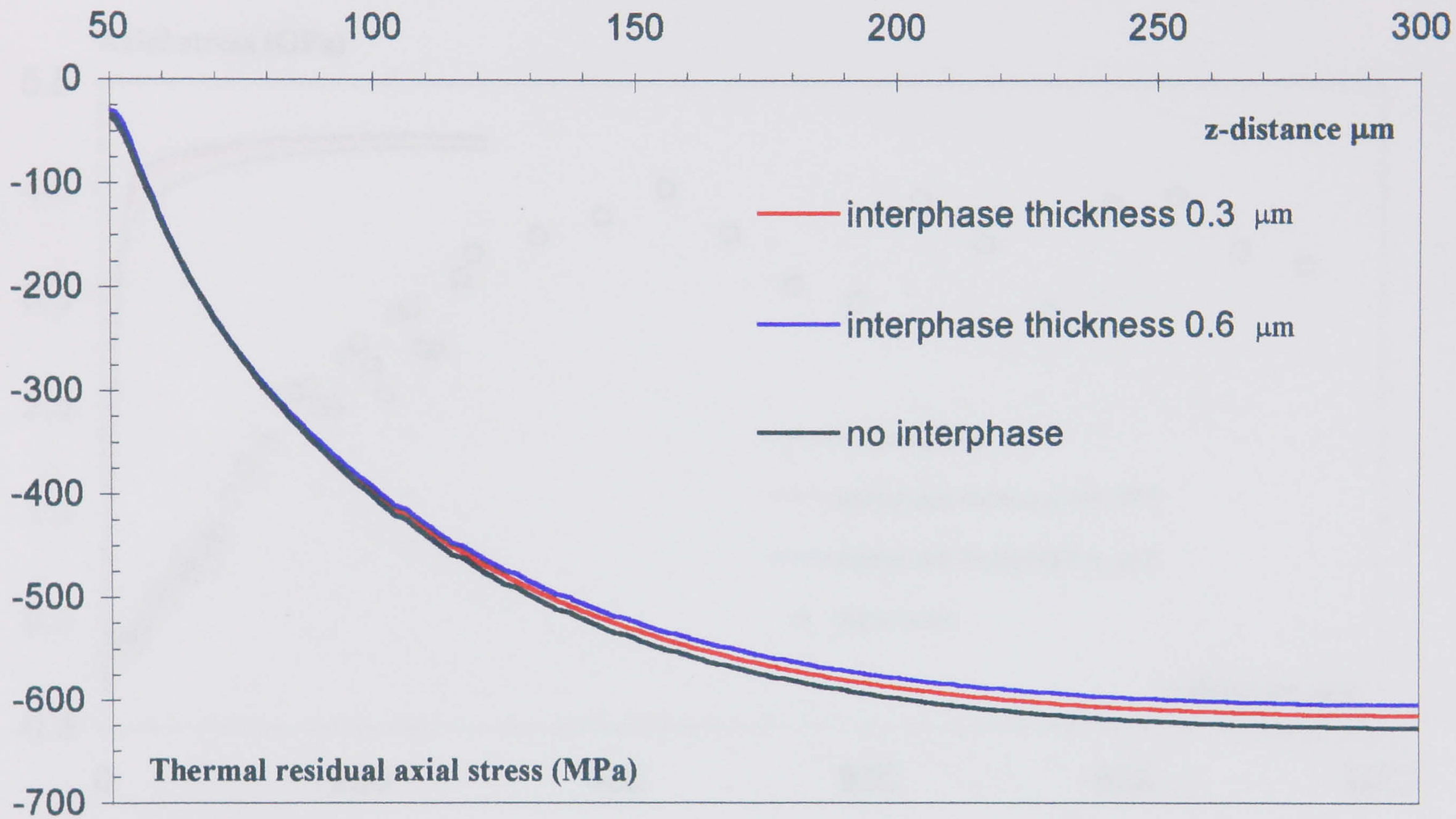

Figure 2.8 Axial variation of thermal residual stresses in long-fibre composites predicted by FE analysis

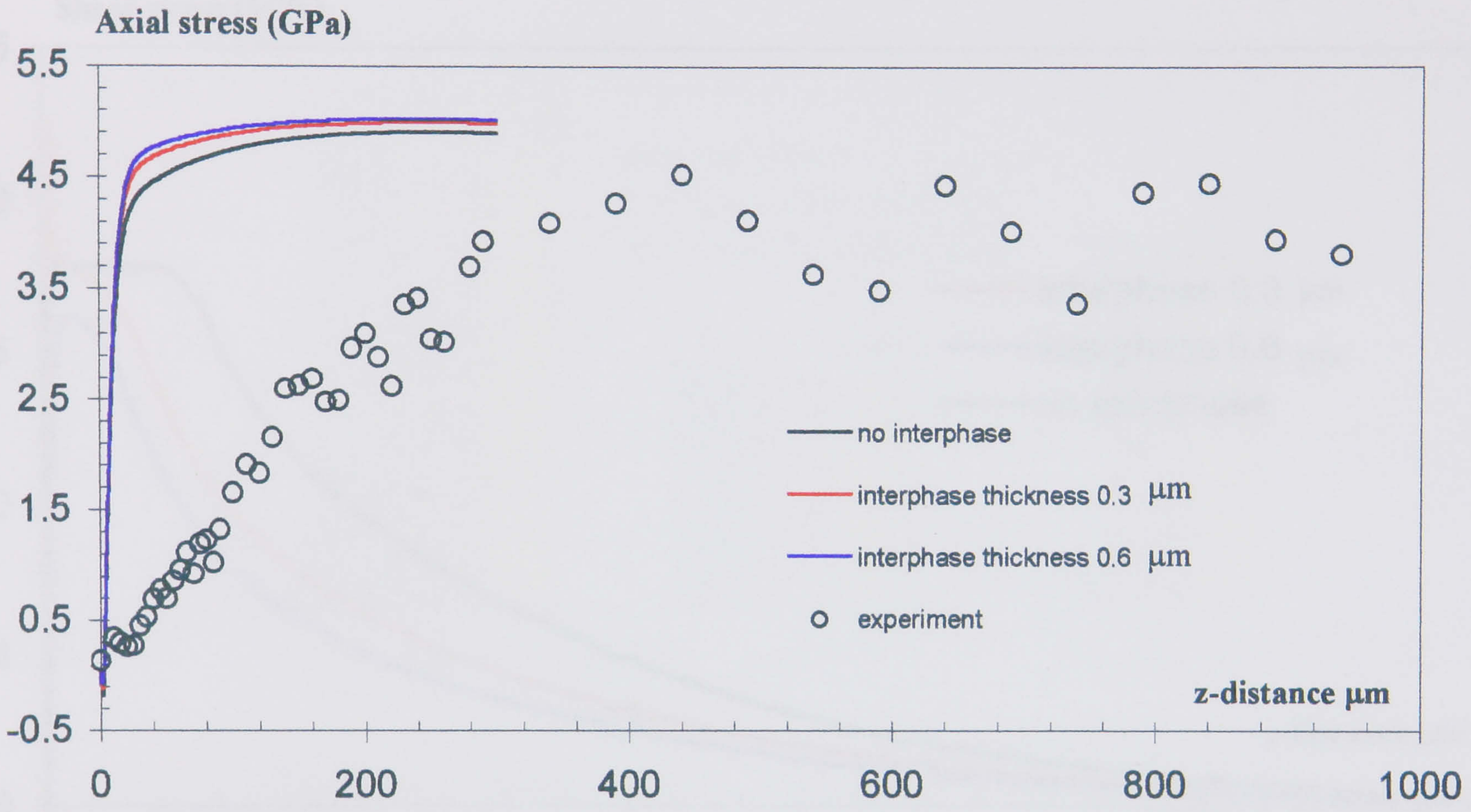

Figure 2.9 Axial variation of thermal residual stresses in long-fibre composites predicted by FE analysis

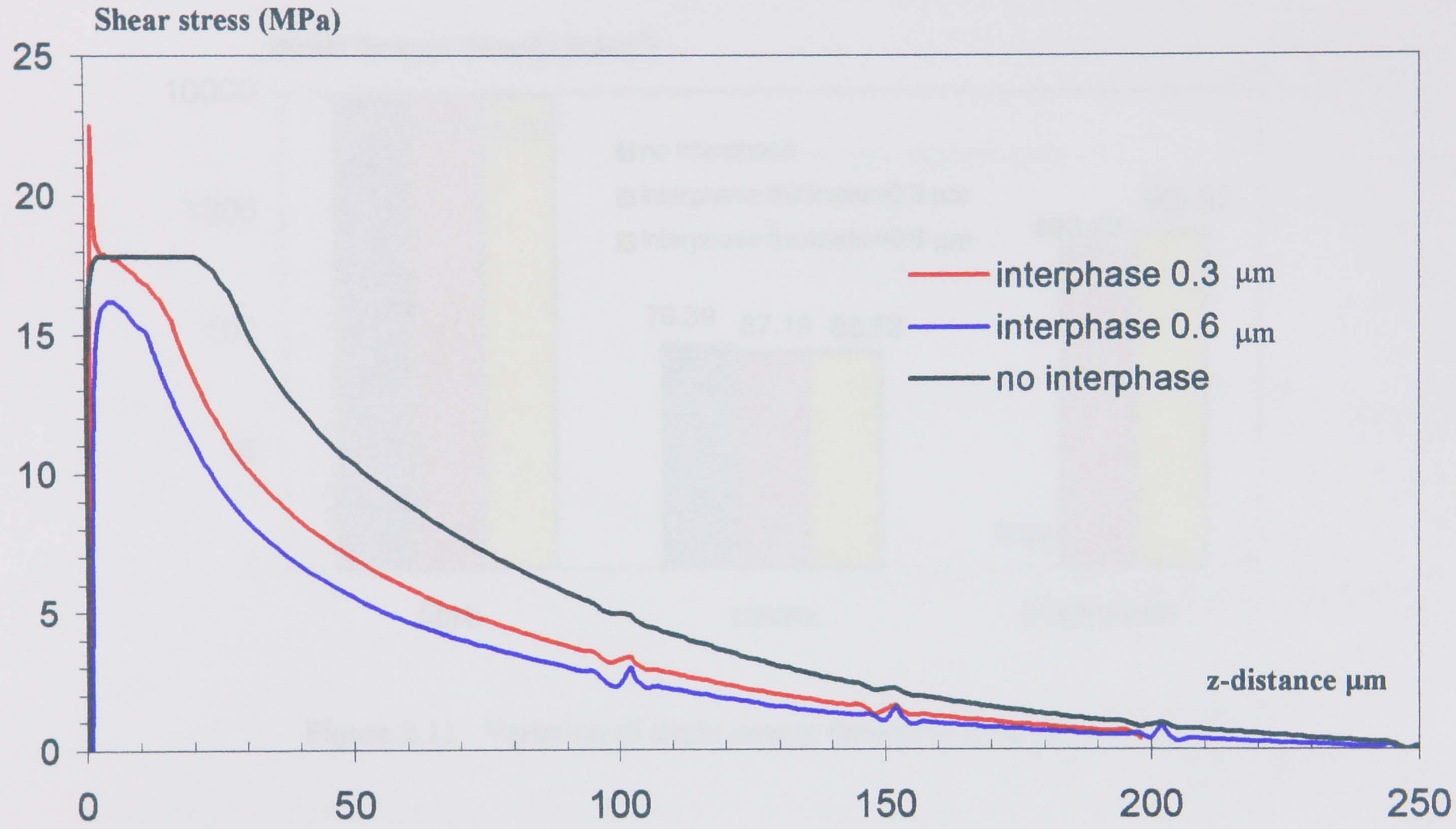

Figure 2.10 Variation of interfacial shear stresses in long-fibre composites predicted by FE analysis

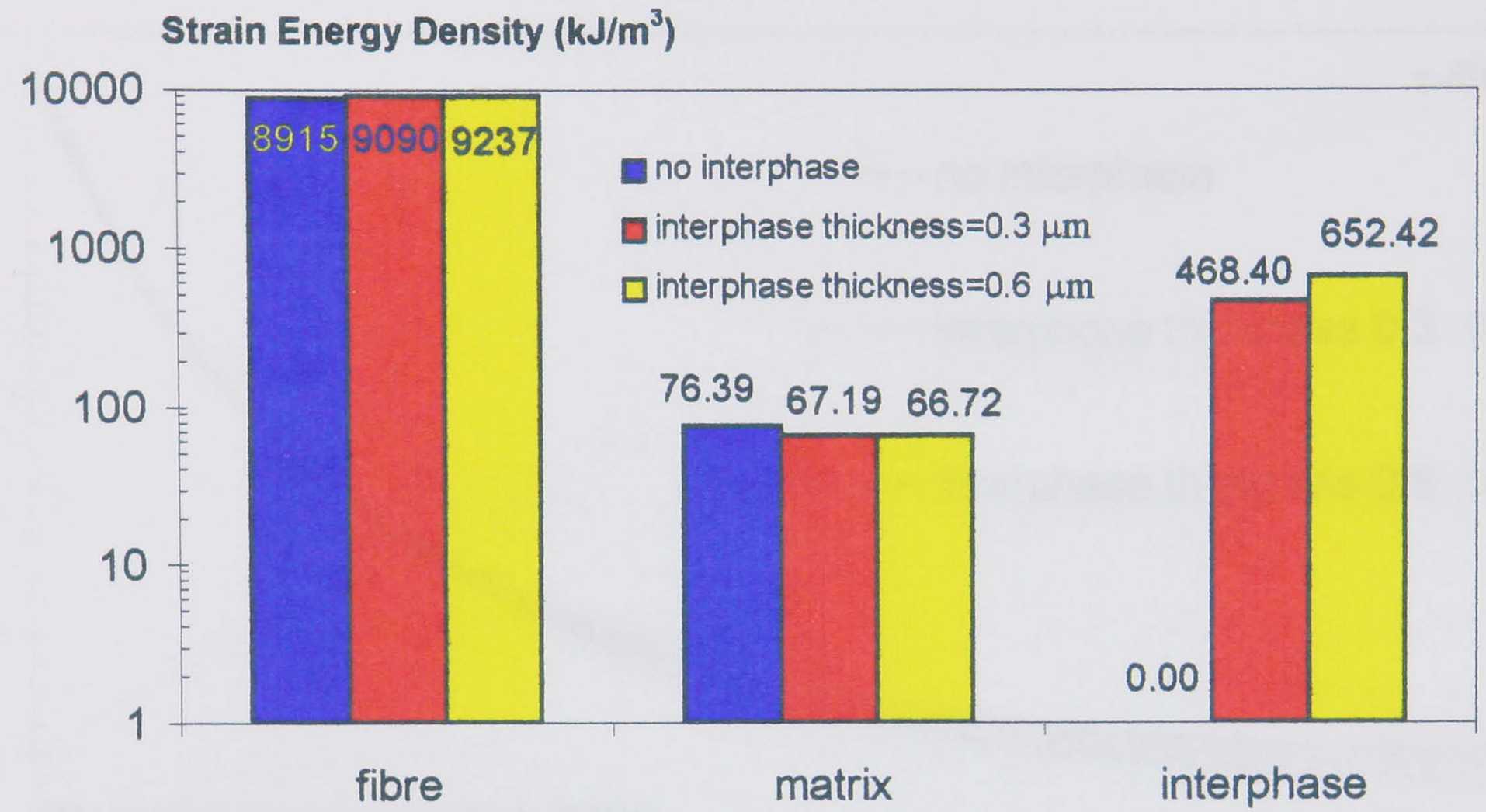

Figure 2.11 Variation of strain energy density in long-fibre composites

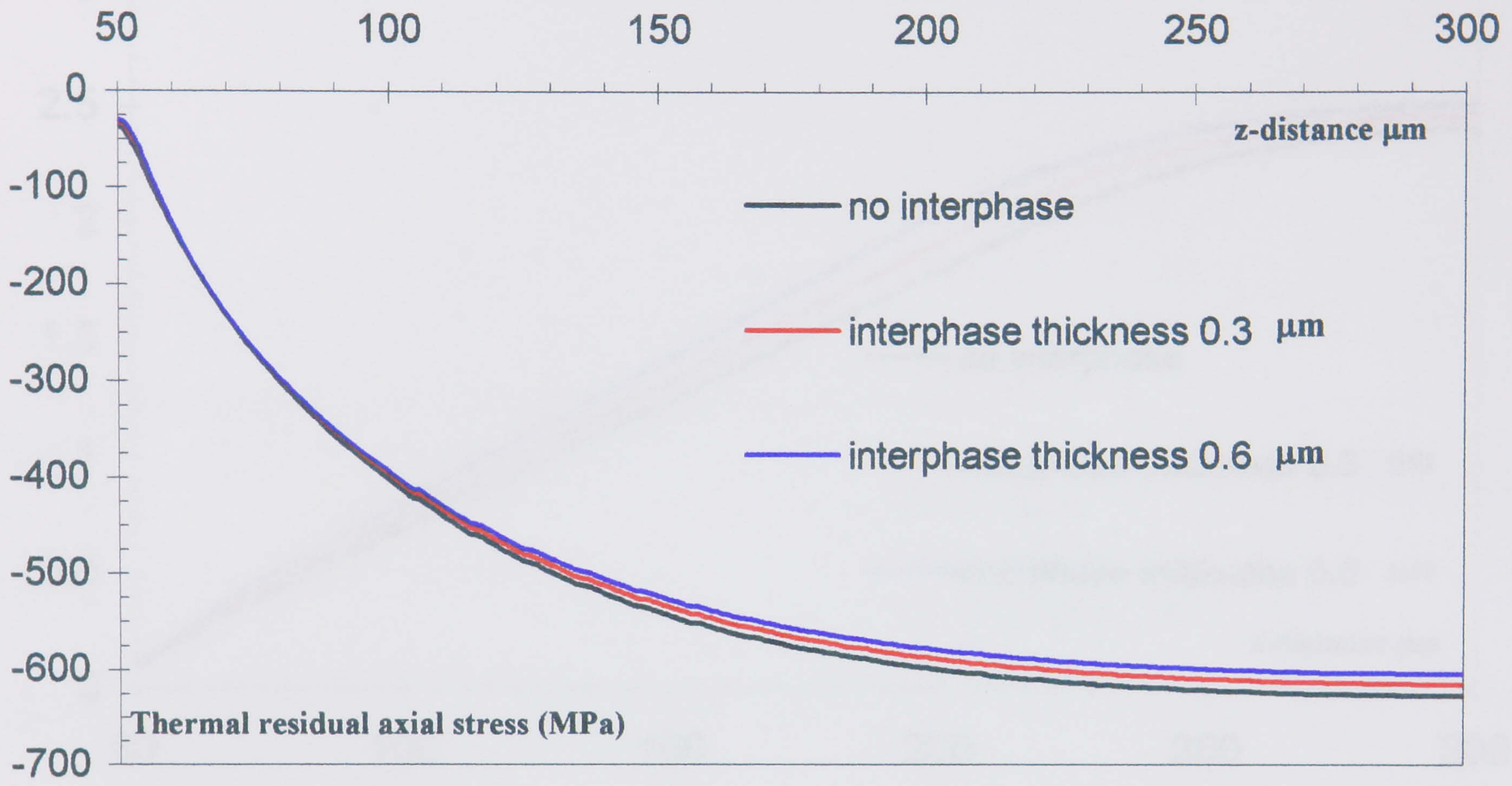

Figure 2.12 Axial variation of thermal residual stresses in short-fibre composites predicted by FE analysis

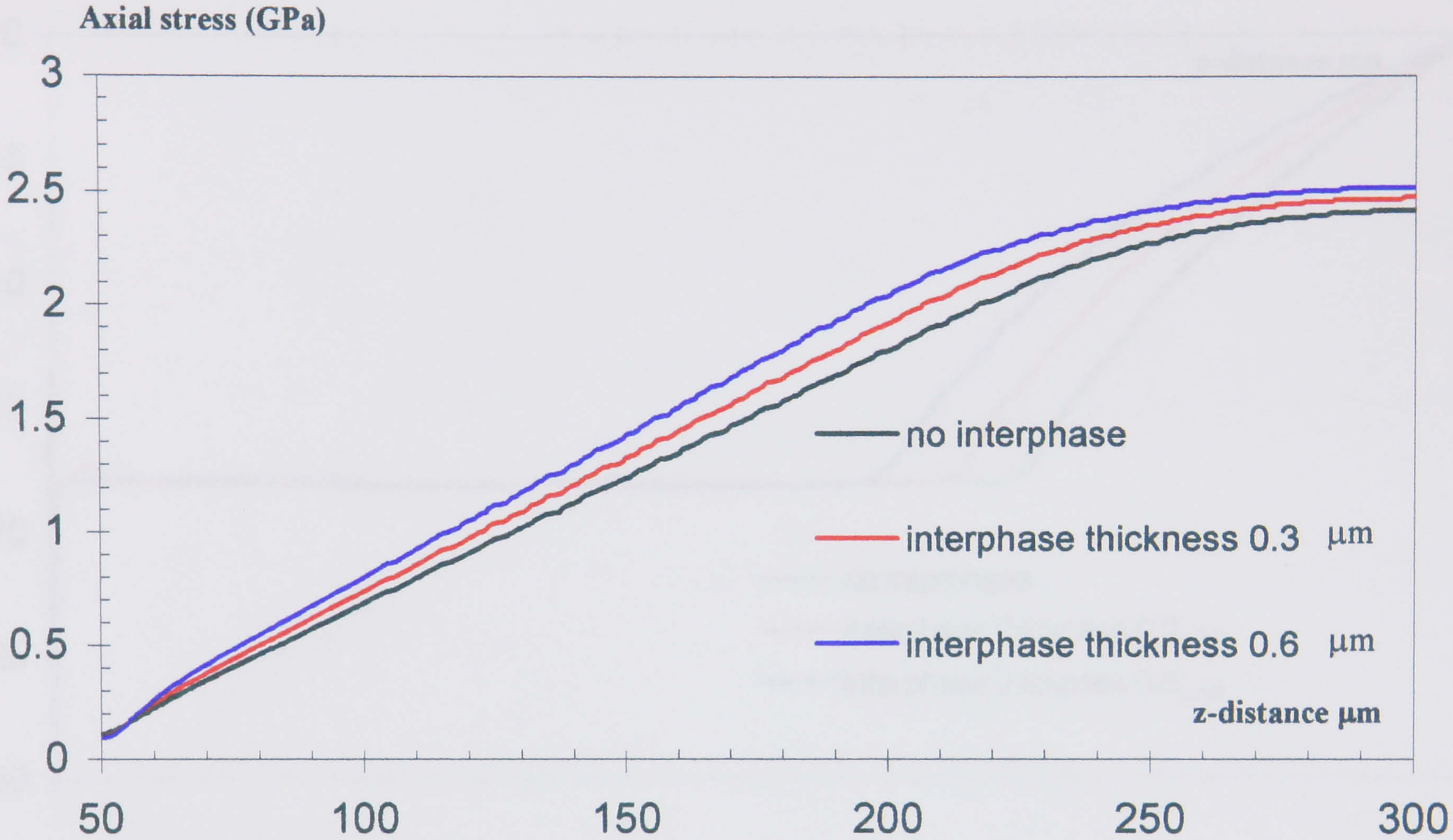

Figure 2.13 Axial variation of fibre stresses in short-fibre composites predicted by FE analysis , at a mechanical applied strain of 1.3 %

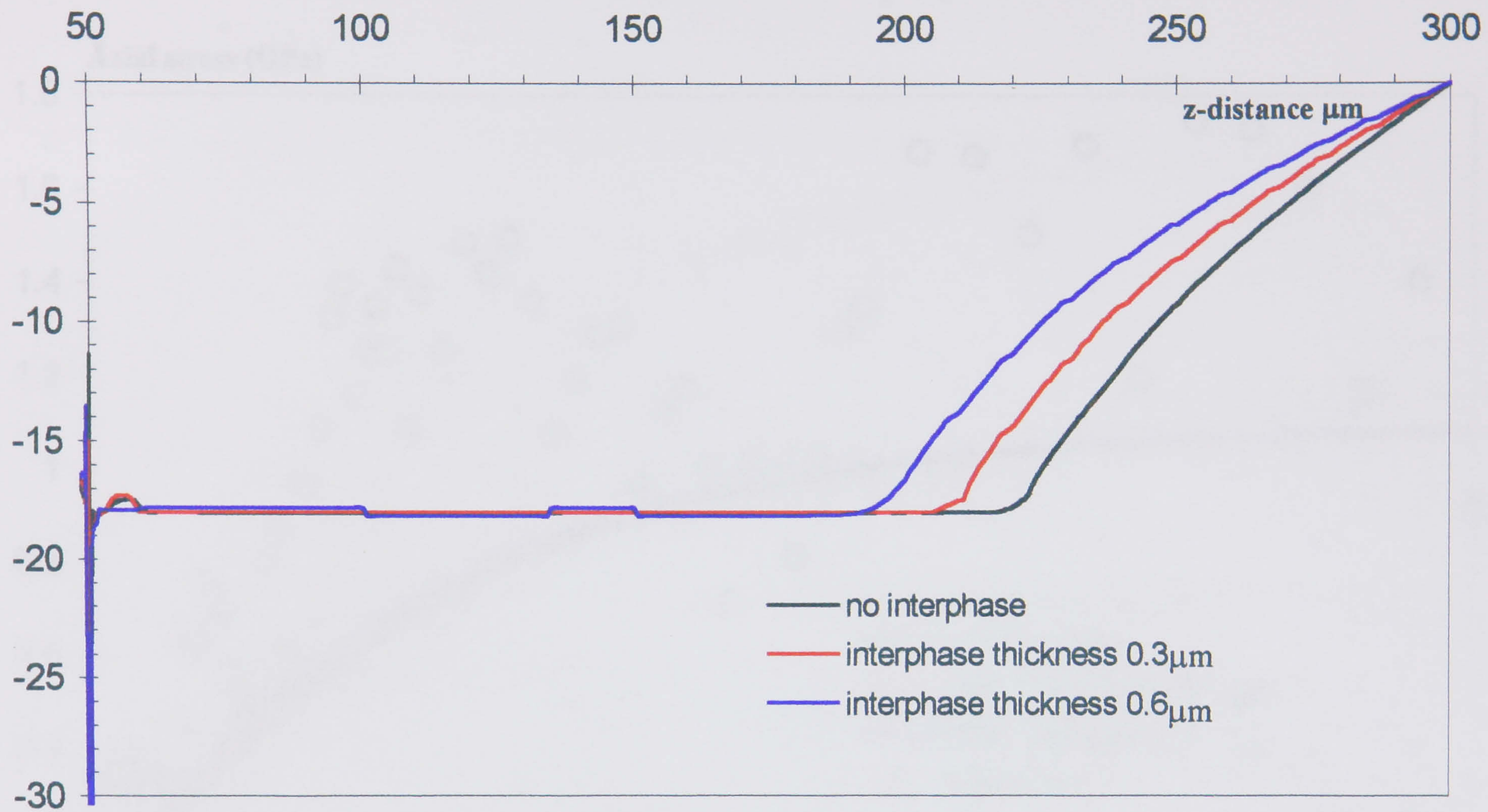

Figure 2.14 Variation of interfacial shear stresses in short-fibre composites predicted by FE analysis, at a mechanical applied strain of 1.3 %

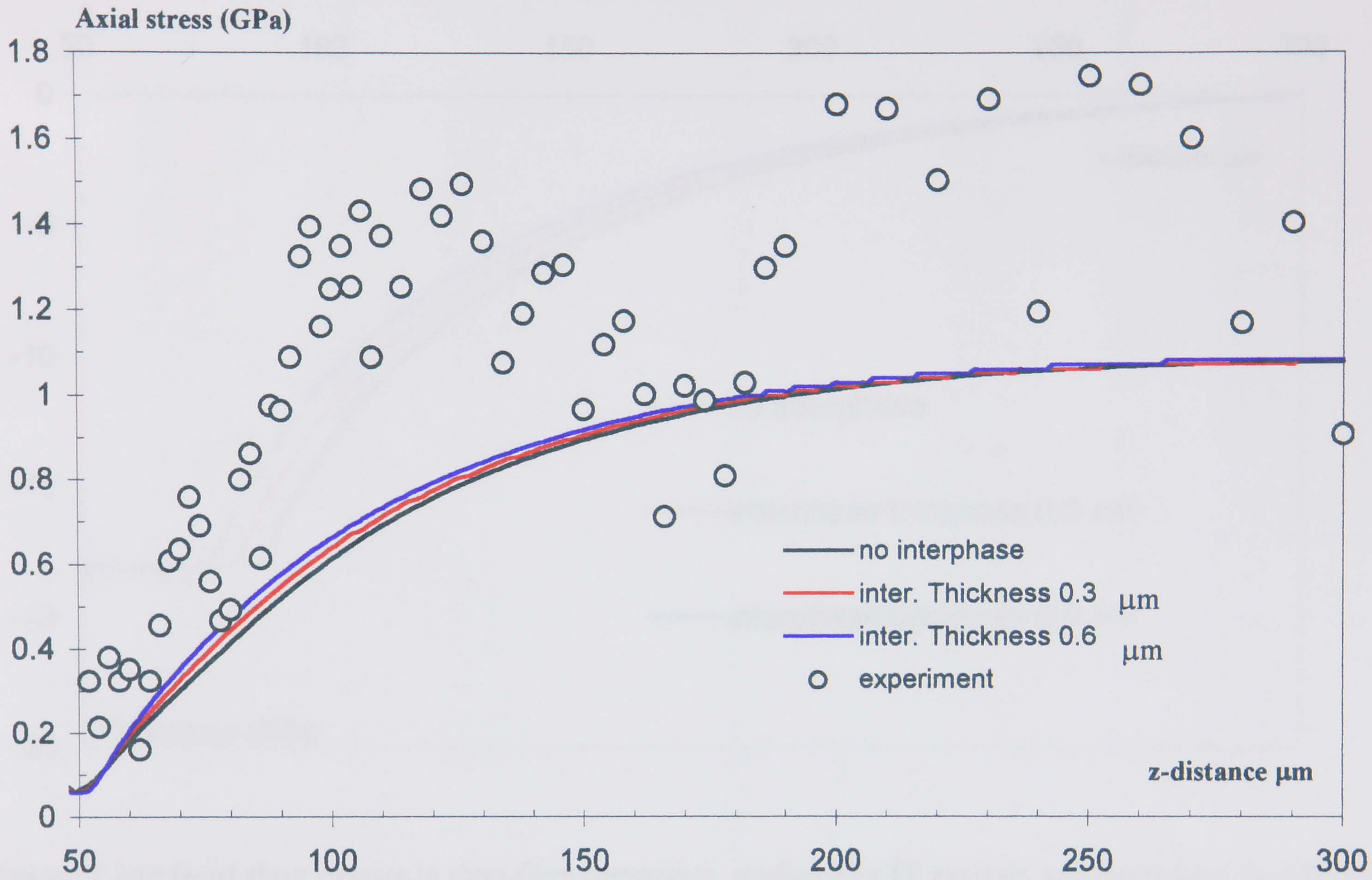

Figure 2.15 Axial variation of fibre stresses in short-fibre composites predicted by FE analysis , at a mechanical applied strain of 0.4 %

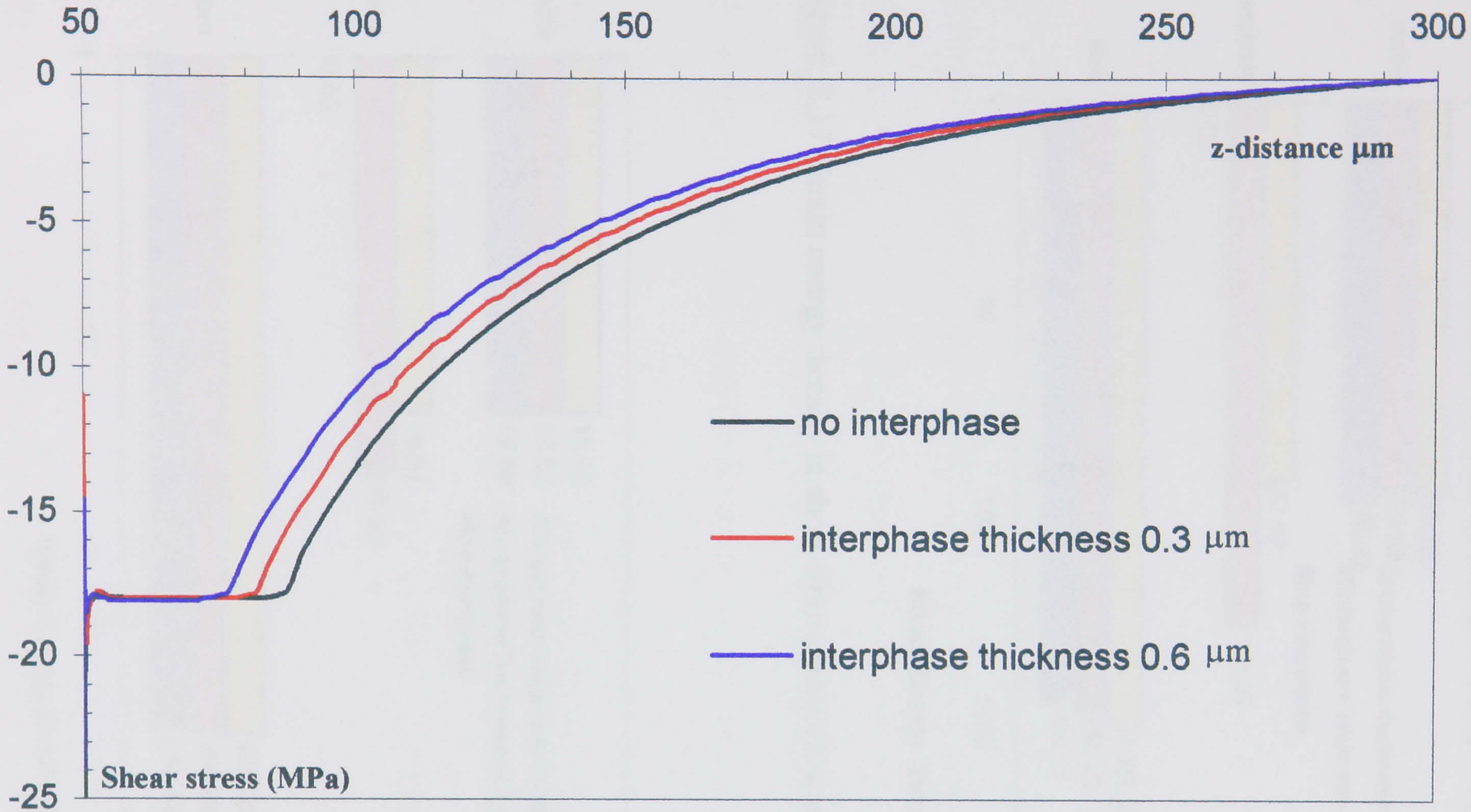

Figure 2.16 Variation of interfacial shear stresses in short-fibre composites predicted by FE analysis, at a mechanical applied strain of 0.4 %

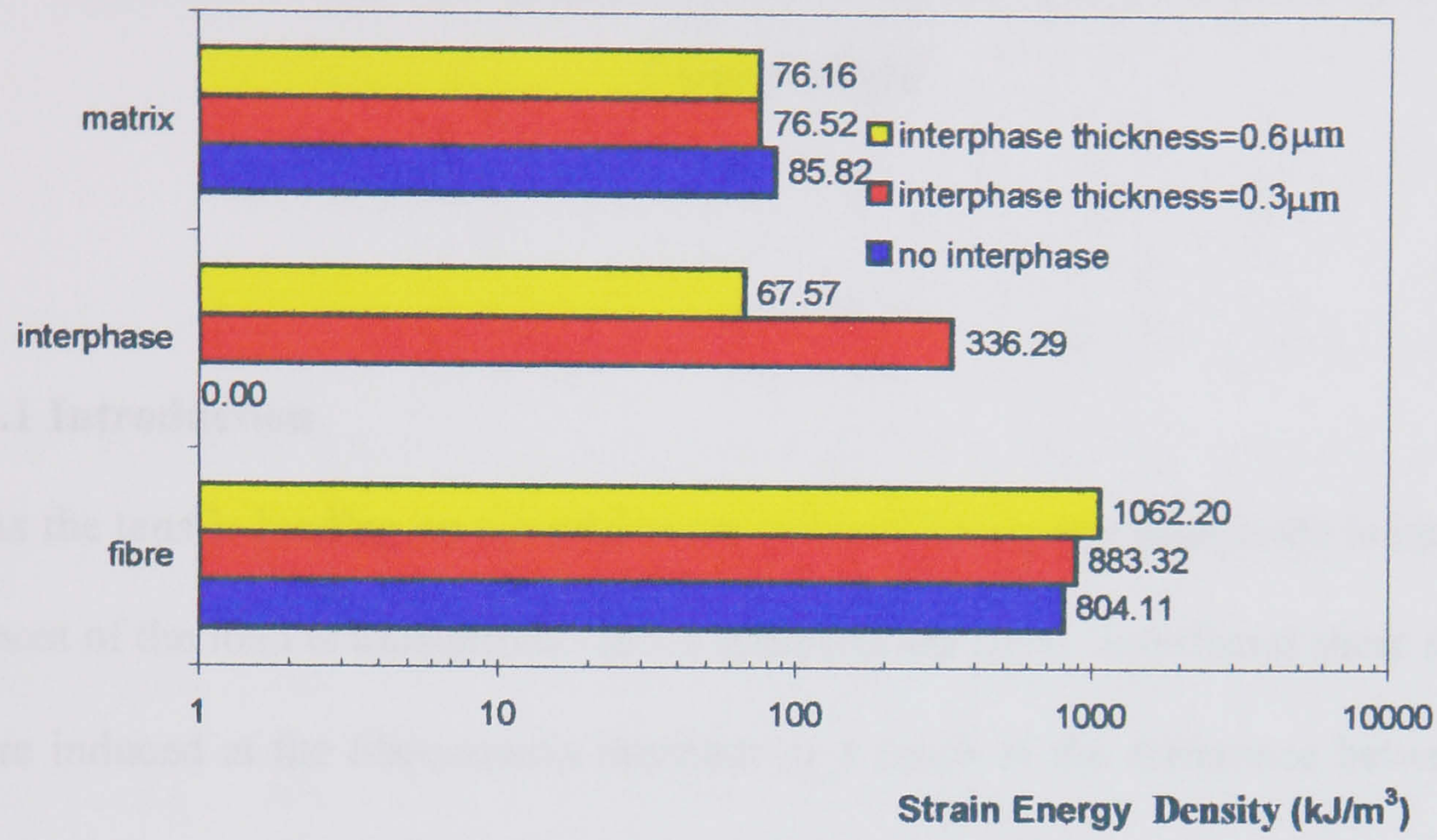

Figure 2.17 Strain energy density in short-fibre composites, applied strain = 1.3 %

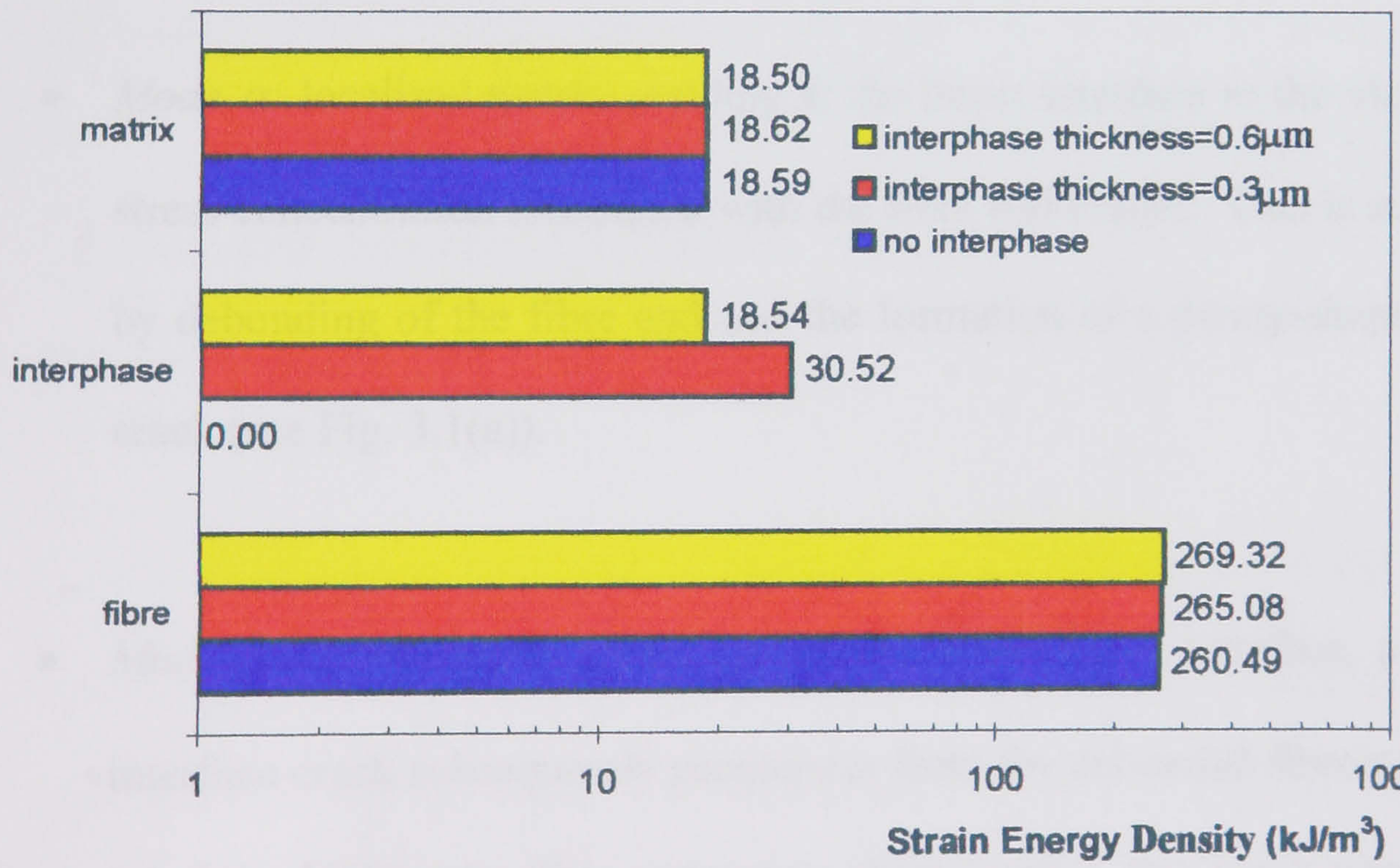

Figure 2.18 Strain energy density in short-fibre composites, applied strain = 0.4 %

CHAPTER 3

Matrix Crack Propagation Criteria for Short Fibre/Epoxy Composites

3.1 Introduction

As the tensile loading on a model short carbon fibre-epoxy composite is increased most of the load is transferred via the matrix to the fibre. Interfacial shear stresses are induced at the fibre-matrix interface as a result of the difference between the material properties of the matrix and fibre. Eventually these stresses reach a critical value, the interfacial shear strength, beyond which point one or more of the following mechanisms of interfacial failure [34] are observed experimentally:

- *Mode* α*:* localised matrix yielding at the intact interface in the vicinity of the stress concentration associated with the fibre end corner. This is accompanied by debonding of the fibre end and the formation of a penny-shaped interface crack (see Fig. 3.1(a)).

- *Mode* β*:* in the case of a relatively weak fibre-matrix interface, a cylindrical interface crack subsequently propagates from the debonded fibre end (see Fig. 3.1 (b)). Unlike the fibre end penny-shaped crack, this crack remains closed as tensile loading on the composite increases, and load transfer across its contacting faces is maintained by a mechanism of frictional stress transfer.

- *Mode γ:* in the case of a strong interface, a conical matrix crack subsequently propagates from the debonded fibre end (see Fig. 3.1(c)) at an angle θ_c to the fibre axis. This matrix crack opens with increasing applied load thereby suppressing load transfer across the crack faces.

In practice, the interfacial bond strength is increased by treating the fibres with a size. In a sized system, there is an increased likelihood of a matrix crack (*Mode* γ), as opposed to an interface crack (*Mode* β), forming part of the progressive failure mechanism of the composite. A *Mode γ* matrix crack initiated at a fibre end during loading of the composite has been observed in a single sized carbon short-fibre embedded in an epoxy matrix system [24, 27, 28, 33], in a boron fibre-epoxy system [19, 20, 21] and in a glass fibre-polyester system [20-22]. Finite element (FE) and boundary element analyses have been used to investigate this phenomenon [34, 77]. In each case the angle of the conical crack used in the model was adjusted to give the best correlation between the predicted and experimentally measured fibre stresses. No attempt was made to predict *a priori* the angle of the conical matrix crack.

A number of criteria have been proposed for the general crack kinking problem, involving brittle fracture of a homogeneous material. These include the maximum normal stress and the maximum hoop stress criteria [78], the maximum elastic strain energy release rate criterion [1], the minimum strain energy density criterion [79] and the maximum strain criterion [80]. In the case of elasto-plastic fracture

Rice's J-integral [81] is often employed, but is unsuitable for the present system because of the presence of unloading, i.e. shear strain reversal.

For bi-material elastic systems, several authors [82-89] have made theoretical and numerical predictions of crack propagation paths. These approaches are not appropriate for the current task of predicting the direction of a conical matrix crack due to the existence of matrix plasticity. Epoxy resin exhibits some ductility [90] and therefore it is reasonable to assume conditions of ductile fracture at the matrix crack tip. One possible approach is to apply a maximum hoop strain criterion to the results obtained using elasto-plastic FE analysis.

At the micro-mechanical level, the mechanism of ductile fracture includes micro-void nucleation, growth, and coalescence. A model [91] that contains a single spherical void in a perfectly plastic von Mises material was developed by Rice and Tracey (RT). In this model, the void growth rate depends exponentially on the ratio of the mean stress to the von Mises stress. The assumption is that fracture occurs when the ratio between the void size and the void spacing exceeds a critical value. The critical fracture strain ε_f^* can be obtained from this model which has been modified and used as a fracture criterion by McClintock [92], Ritchie *et al* [93], and McMeeking [94].

In this chapter the local stress/strain fields around the corner of a debonded fibre end in a short carbon fibre-epoxy composite, obtained using elastic and elasto-plastic FE analyses, are compared. Predictions for the direction of propagation of a *Mode* γ crack, based on the maximum hoop strain criterion and the RT void-

growth criterion, are compared. Using the latter criterion, the applied strain at failure for the composite is also predicted. The effects of thermal residual stresses, developed during the fabrication process, are also investigated.

3.2 Ductile fracture

Several types of voids may be present in the epoxy matrix, depending on the fabrication process employed. Small voids often form in the region adjacent to the fibres, especially in the interfacial area, and also in the matrix-rich pockets or the fibre-free regions between laminae [9].

In ductile fracture, the local plastic strains play a very important role in determining the mechanism of failure involving micro-void nucleation, growth, and coalescence. The development of plastic strains near the fibre end must be taken into consideration. The equivalent or effective plastic strain $\bar{\varepsilon}_p$ [95] is given by:

$$\bar{\varepsilon}_p = \sqrt{\frac{2}{9}\left[\left(d\varepsilon_1^p - d\varepsilon_2^p\right)^2 + \left(d\varepsilon_2^p - d\varepsilon_3^p\right)^2 + \left(d\varepsilon_3^p - d\varepsilon_1^p\right)^2\right]} \qquad (3.1)$$

where $d\varepsilon_1^p$, $d\varepsilon_2^p$, $d\varepsilon_3^p$ are the principal components of an increment of plastic strain and dt is the time increment. If this equivalent plastic strain exceeds the critical fracture strain of the material, the crack will propagate. The growth rate of micro-voids ahead of the crack tip is sensitive to the mean stress in this region. If the mean stress is negative, void closure leads to an increase in the effective fracture strength of the material. Using the approach of Rice and Tracey [91] the

critical fracture strain in a high triaxial stress field ahead of the crack tip can be expressed as:

$$\varepsilon_f^* = \frac{\ln\left(\frac{d_p}{D_p}\right)}{0.283\exp\left(1.5\sigma_m/\bar{\sigma}\right)} \tag{3.2}$$

where d_p is the critical void spacing, D_p is the critical void size (see Fig. 3.2). σ_m is the mean stress, $\bar{\sigma}$ is the von Mises stress, and the constant value 0.283 approximated from the case of highest triaxiality [91]. The micro-voids ahead of the crack tip within the epoxy matrix nucleate, grow and coalesce due to the high mean stresses induced near the fibre corner (see Fig. 3.3). The crack propagates when the plastic strain in the ligaments between voids reaches a critical value. In practice, the critical void size and void spacing are difficult parameters to measure and in order to evaluate their ratio, reference is made to the tensile test. If failure occurs in the tensile test, where $\bar{\sigma} = \sigma$ and $\sigma_m = \sigma/3$, when $\varepsilon_f^* = \varepsilon_{ft}$ [96] the ratio of the critical void spacing to void size in eq. (3.2) is then given by:

$$\ln\left(\frac{d_p}{D_p}\right) = 0.283\,\varepsilon_{ft}\exp\left(0.5\right) \tag{3.3}$$

Substitution of equation (3.3) into (3.2) gives the critical fracture strain as

$$\varepsilon_f^* = \frac{1.648\varepsilon_{ft}}{\exp\left(1.5\sigma_m/\bar{\sigma}\right)} \qquad \text{provided } \sigma_m \rangle 0 \tag{3.4}$$

The critical fracture strain in eq. (3.4) is valid provided the value of the mean stress is positive. Hence, ductile fracture will occur when:

$$\bar{\varepsilon}_p = \varepsilon_f^* \tag{3.5}$$

where $\bar{\varepsilon}_p$ is the equivalent plastic strain which is obtained from equation (1) and ε_f^* is the critical plastic strain obtained from eq. (3.4). In order to define the scale of the damage, the critical radius in the FE mesh has to be specified and needs to be very small compared to the crack length [92, 93]. Fracture is then predicted to occur when the value of the equivalent plastic strain ahead of the crack tip reaches the value of the critical plastic strain at the same point. This criterion has been employed by Ritchie *et al.* [93], Harlin *et al.* [97] and Hanxing *et al.* [98].

3.3 FE model

A FE study of the conical-shaped matrix crack in a model carbon fibre-epoxy composite system was performed by Nath *et al.* [34]. Linear-elastic FE analysis with a pre-defined matrix crack path was used and the results obtained for the fibre stress were correlated with experimental measurements obtained by Paipetis *et al* [27,28]. The angle of the conical crack in the FE model which gave the best correlation between the predicted and experimentally measured fibre stresses was found to be $\theta_c = 20^\circ$.

In the work described in this chapter, a penny-shaped crack resulting from fibre end debonding is assumed to exist. Contact elements were defined between the fibre end face and the matrix to enable load transfer to occur across the crack faces during crack closure. In the FE model, the outer matrix radius R_m, matrix length l_m, fibre radius r_f and the fibre length l_f are 50, 300, 3.25 and 260μm, respectively (see Fig. 3.4) and the mesh consists of 3,865 axisymmetric eight-node elements (see Fig. 3.5(a)). A highly refined mesh was used in the vicinity of the crack tip and collapsed eight-node axisymmetric triangular crack tip elements [98-100] were employed around the crack tip (Fig. 3.5 (b)). The presence of an interphase is neglected in this model based on the fact that its thickness in this composite system is very thin (in the range 0.1- 0.4 μm) and its mechanical properties are not well understood [35].

The incremental tensile test for a model short fibre-epoxy composite, in which the fibre stress is measured using laser Raman spectroscopy (LRS), was performed at a low strain rate. For this reason the relaxed elasto-plastic stress-strain relationship for the matrix material (MY-750/HY-951 epoxy), measured at a strain rate of 0.25×10^{-2} min^{-1}, was used in the FE model (see Fig. 3.6). In this FE analysis, the epoxy matrix is an isotropic material and the von Mises yield surface was used to determine the epoxy yield stress. The carbon fibre is a transversely isotropic material with linearly elastic behaviour (see Fig. 3.7) and the material properties for both materials are shown in Table 3.1.

Using ABAQUS [100-101], results were obtained for both linear elastic and elasto-plastic FE analyses. The effects of the thermal residual stresses induced

during manufacture were simulated by applying a temperature drop in the initial load step. In the case of elasto-plastic analysis, a series of incremental uniform displacements, δ, were applied to the model until the fracture criterion given by eq. (3.5) was satisfied in the vicinity of the crack tip.

3.4 Results Summary

3.4.1 Without thermal residual stresses

The stress and strain components in the FE model, obtained in terms of a global Cartesian co-ordinate system, were converted to components for a local polar co-ordinate system (r, θ) which has its origin at the debonded fibre end crack tip (see Fig. 3.4). In order to evaluate the critical crack propagation conditions, a critical radius from the crack tip, r_c, equal to 0.2μm was chosen which is about 32 times smaller than the crack length. The critical radius corresponds to the third ring of nodes around the crack tip thereby avoiding the inaccuracies associated with the collapsed crack-tip elements within the first ring (see Fig 3.5(c)). The angular variation of the stress and strain components at a critical radius $r_c = 0.2$ μm for an applied strain of 0.14 %, obtained using linear elastic FE analysis, are shown in Fig. 3.8 and 3.9, respectively. The corresponding results obtained using elasto-plastic FE analysis are shown in Fig. 3.10 - 3.11.

By comparing the stress results in Fig. 3.8 and Fig. 3.10, it can be seen that for the elasto-plastic results the shear stress $\sigma_{r\theta}$ in the plastic zone near the interface is reduced to about half the value obtained from linear elastic analysis. The radial stress σ_{rr} increases from a negative to positive value and has a maximum value at

about θ =140° which is only about half the maximum value obtained using linear elastic analysis. The hoop stress $\sigma_{\theta\theta}$, which is likely to play an important role in opening the crack, has its maximum value at about θ = 77° for both analyses. The maximum hoop stress predicted using elasto-plastic analysis is somewhat lower than the value obtained using linear elastic analysis due to the plastic behaviour of the matrix. The shear strain $\varepsilon_{r\theta}$ near the interface obtained using elasto-plastic analysis (see Fig. 3.11) is about 6 times greater than the value obtained using linear elastic analysis (see Fig. 3.9). The other strain components are also higher and have their turning points at about θ = 20°, which is about half the angle calculated using linear elastic analysis. To determine the mode of fracture, the elasto-plastic results were compared with the experimental results [27]. The interfacial shear strain obtained from linear elastic FE analysis is about 2 times higher than the value calculated using elasto-plastic FE analysis (see Fig 3.8, 3.10). The crack may therefore prefer to propagate into the matrix rather than along the fibre-matrix interface for a sized system.

The maximum hoop stress criterion predicts a crack angle which is much higher than that suggested by Nath *et al.* [34] and is, in any case, inappropriate for ductile fracture. The maximum hoop strain criterion predicts a crack angle of about 23°.

To use the RT void-growth model to predict fracture, the envelope of the critical fracture strain can be obtained from eq. (3.4) by computing the local values at every nodal point at the critical radius. The curve representing the angular variation of the equivalent plastic strain is then compared with the curve for the

angular variation of the critical fracture strains for every incremental load case. The failure criterion is satisfied when the two curves just touch, as shown in Fig. 3.12. It was found that the critical crack propagation conditions were satisfied at θ =16°, on the critical radius r_c=0.2 μm, when the applied strain on the composite reaches 0.14 %. The matrix crack angles predicted by the maximum hoop strain criterion are slightly higher than the RT void-growth model but only the latter is capable of predicting the applied strain at failure.

3.4.2 Effect of thermal residual stress

Fabrication of the composite specimen induces thermal residual stresses. During fabrication, the matrix is initially a viscous fluid, which subsequently cools and crystallises. Due to the coefficient of thermal expansion mismatch between the fibre and matrix materials, the larger contraction of the matrix puts the fibre into compression and also induces localised yielding at the fibre end [36]. In the elasto-plastic FE model used to investigate the effect of thermal stresses, it is assumed that the fibre end is initially bonded. A series of uniform temperature drops ΔT in the range 30-50°C (see Fig. 3.13) were applied to the FE models in order to obtain the values of the maximum residual fibre stress to compare with the experimental results [27,28]. The maximum residual fibre stress obtained for a 50°C temperature drop is predicted to be -0.78 MPa which agrees well with the experimentally measured value -0.75 MPa [27,28]. The angular variation of thermal stress/strain components around the fibre corner for ΔT = -50°C are shown in Fig. 3.14 and Fig. 3.15, respectively. At this stage, the hoop stress $\sigma_{\theta\theta}$ is negative due to the contraction of the matrix around the stiffer fibre.

In reality, there is some relieving of the residual stresses in the matrix material during cooling [74]. The hoop strain $\varepsilon_{\theta\theta}$ at the fibre corner near the interface is negative and could not lead to crack initiation in the matrix since the micro-voids would be closed. In uniaxial compression, the matrix material exhibits a higher ductility than in tension.

3.4.3 Combined effect of thermal and mechanical loading

The thermal residual stresses and strains due to fabrication are believed to affect the overall strength of the composite. As the matrix cools during fabrication of the composite, it contracts around the fibre end leading to compression in this region. The initial condition is now that the mean stress in the matrix in this region is compressive. When a uniform displacement is subsequently applied to the composite, the mean stress becomes tensile. The angular variation of stress and strain around the fibre end corner are shown in Fig. 3.16 and Fig. 3.17, respectively. At the applied strain of 0.3 %, the maximum fibre stress of 300 MPa was found to occur at the middle of fibre length. The maximum interfacial shear stress of the order of 22 MPa was found to occur at the fibre end. Those values agree well with experimental results [27,28].

The maximum hoop strain criterion predicts the angle of the crack propagation to be about 18°. The equivalent plastic strain calculated by ABAQUS is now accumulating from a state of compression. The RT void-growth model, which is based an increasing void size and a decreasing void spacing, does not take the compressive plastic strains into account. The equivalent plastic strain magnitude,

which is a current positive measure of equivalent plastic strain, was used to determine failure in the matrix material. The definition of the plastic strain magnitude is a scalar product of the two plastic strain tensor ε_{pl} [100]. It was found that the critical crack propagation conditions were satisfied at θ =16°, when the applied strain on the composite reached 0.3 % (see Fig. 3.18).

The axially elongated shape of the plastic zone for the critical condition is shown in Fig. 3.19. When the applied strain was increased beyond 0.3 % the plastic zone was observed to grow further in the axial direction with little change in the radial direction.

3.5 Discussion

The maximum hoop stress criterion has not given a realistic result due to the dominating effect of the plastic strain field in the matrix. The maximum hoop strain criterion predicts a crack angle close to that predicted using the RT micro-void growth model but is incapable of predicting the applied strain on the composite at failure.

The fracture criterion that is most appropriate to this type of analysis is the RT micro-void growth model. This criterion takes account of the effects of void nucleation, growth, and coalescence. In the macroscopic system, the effect of voids can be ignored. Nevertheless, at micro-mechanical level, ignoring this effect results in erroneous predictions of composite strength. The critical crack propagation conditions at a critical radius are obtained when the curve for the variation of the equivalent plastic strain around the crack tip touches the critical

fracture strain envelope. The applied failure strain obtained by experiment is a little higher than the applied failure strain calculated by RT void-growth model, due to debonding at the fibre end being assumed.

The thermal residual stresses and strains have a very strong influence on the failure mechanism at the fibre/matrix interface. The presence of a strong interphase is possibly preventing the interface from debonding. By assuming the existence of a strong interface, the thermal residual stresses have a strong impact on the critical applied strain. The significant difference is that the maximum value of equivalent plastic strain adjacent to the fibre/matrix interface has changed the peek location from 0° to 16° due to the action of thermal pre-loading, as a result of increasing the applied strain at failure due to the shear strain reversal. The inclusion of thermal residual stresses increases the failure strain on the composite from 0.14 % to 0.3 %.

Material Properties	Carbon fibre	Matrix MY-750/HY-951 (relaxed properties)
Axial Tensile Modulus, GPa	392	2.6
Transverse Modulus, GPa	20	2.6
Axial Tensile Strength, GPa	3.2 *(fracture)*	41×10^{-3} *(yield)*
Axial Fracture Strain, %	0.8	6.13
Transverse Poisson's ratio, $\nu_{R\Theta}$	0.27	0.34
Poisson's ratio in R-Z direction, ν_{RZ}	0.03	0.34
Axial Coefficient of Thermal Expansion, K^{-1}	-0.25×10^{-6}	58×10^{-6}
Transverse Coefficient of Thermal Expansion, K^{-1}	25×10^{-6}	58×10^{-6}

Table 3.1 Material properties of carbon fibre and epoxy matrix

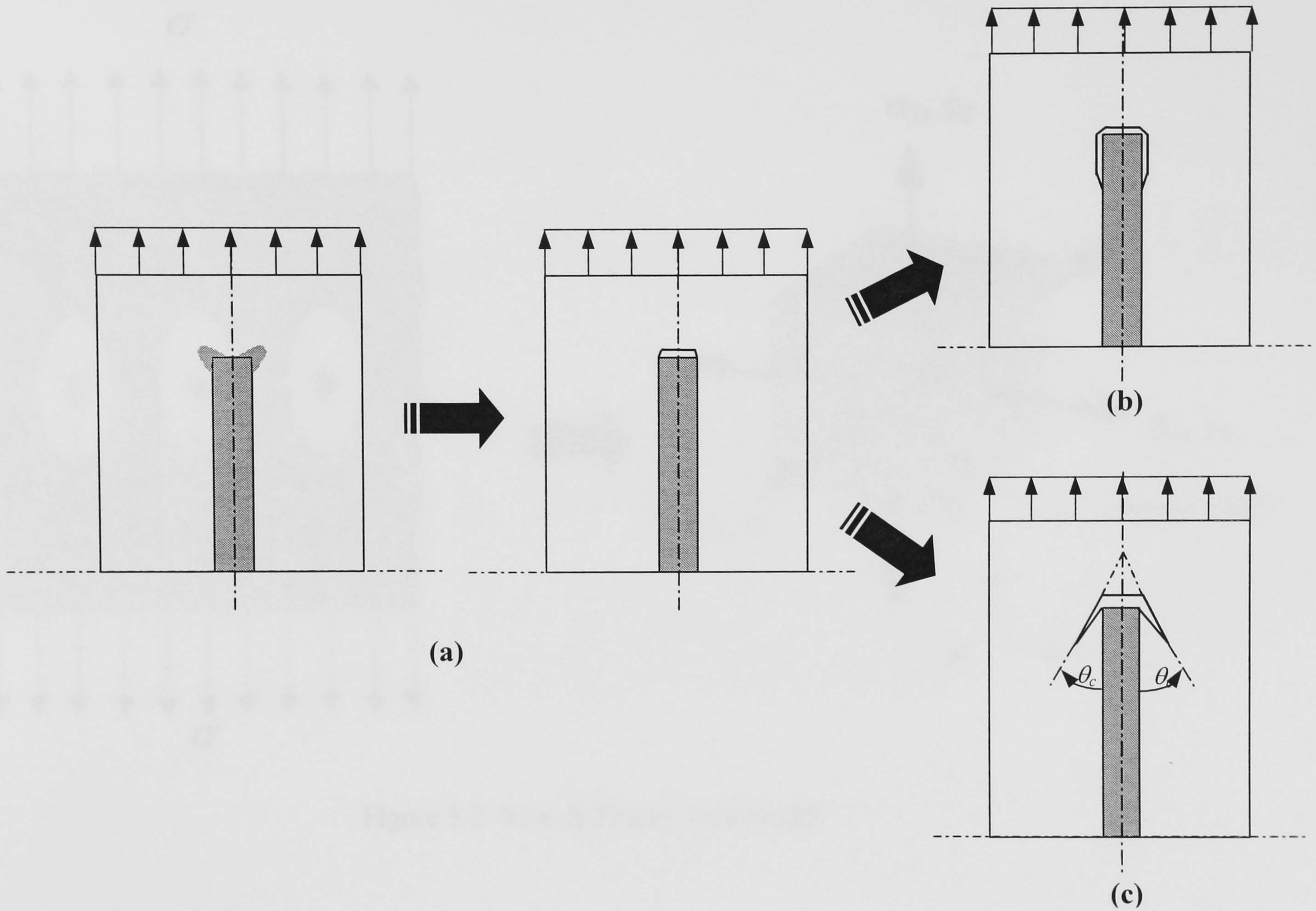

Figure 3.1 Failure mechanisms: (a) *Mode* α (b) *Mode* β (c) *Mode* γ

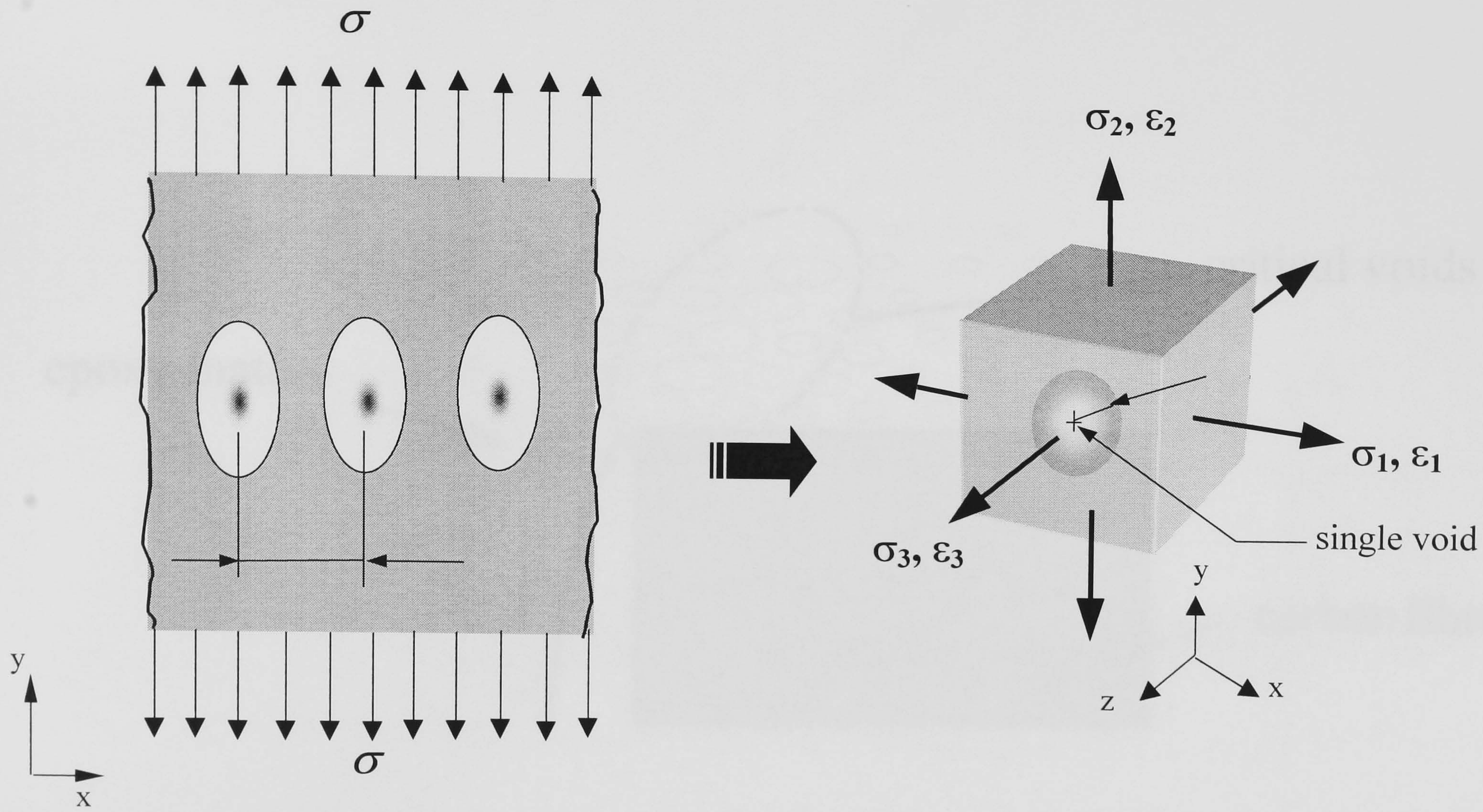

Figure 3.2 Rice & Tracey void model

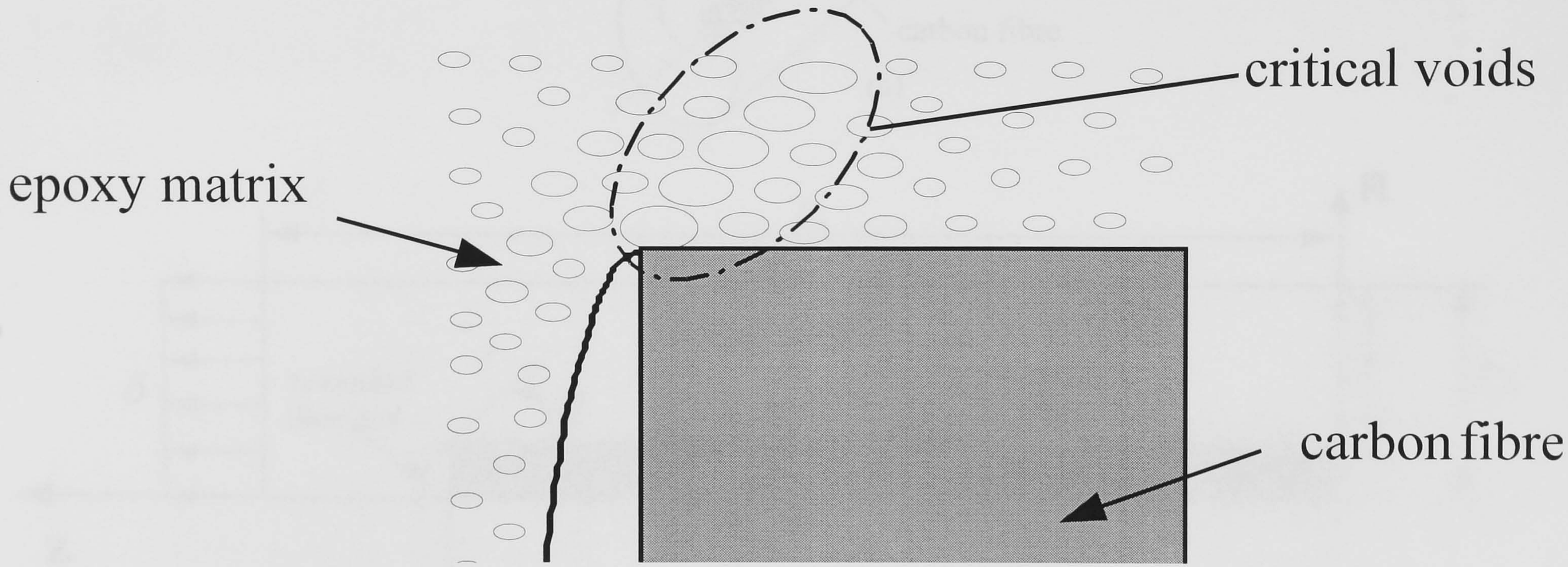

Figure 3.3 Micro-void concentration at the crack tip

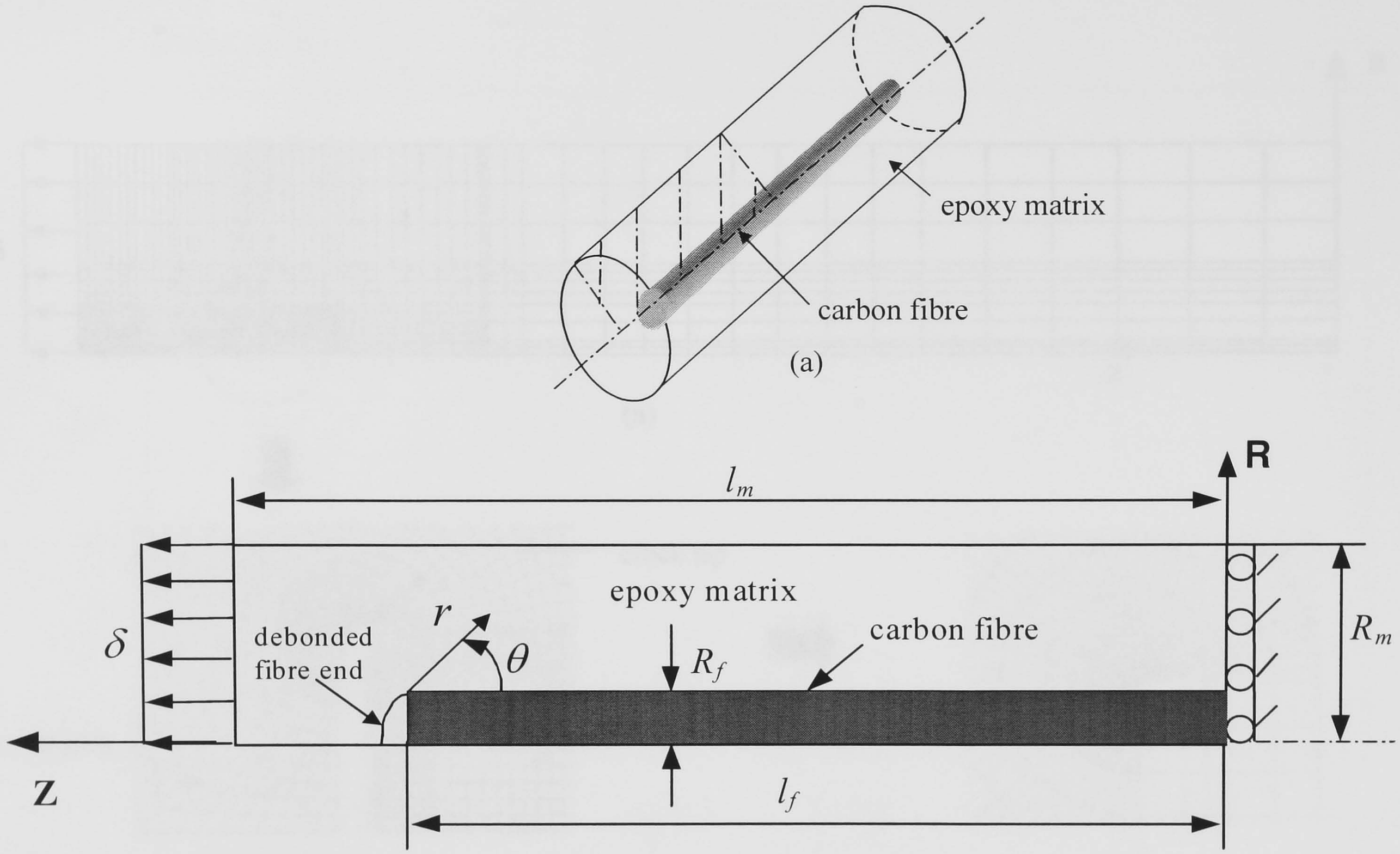

Figure 3.4 (a) Carbon fibre-epoxy composite specimen (b) axisymmetric FE model

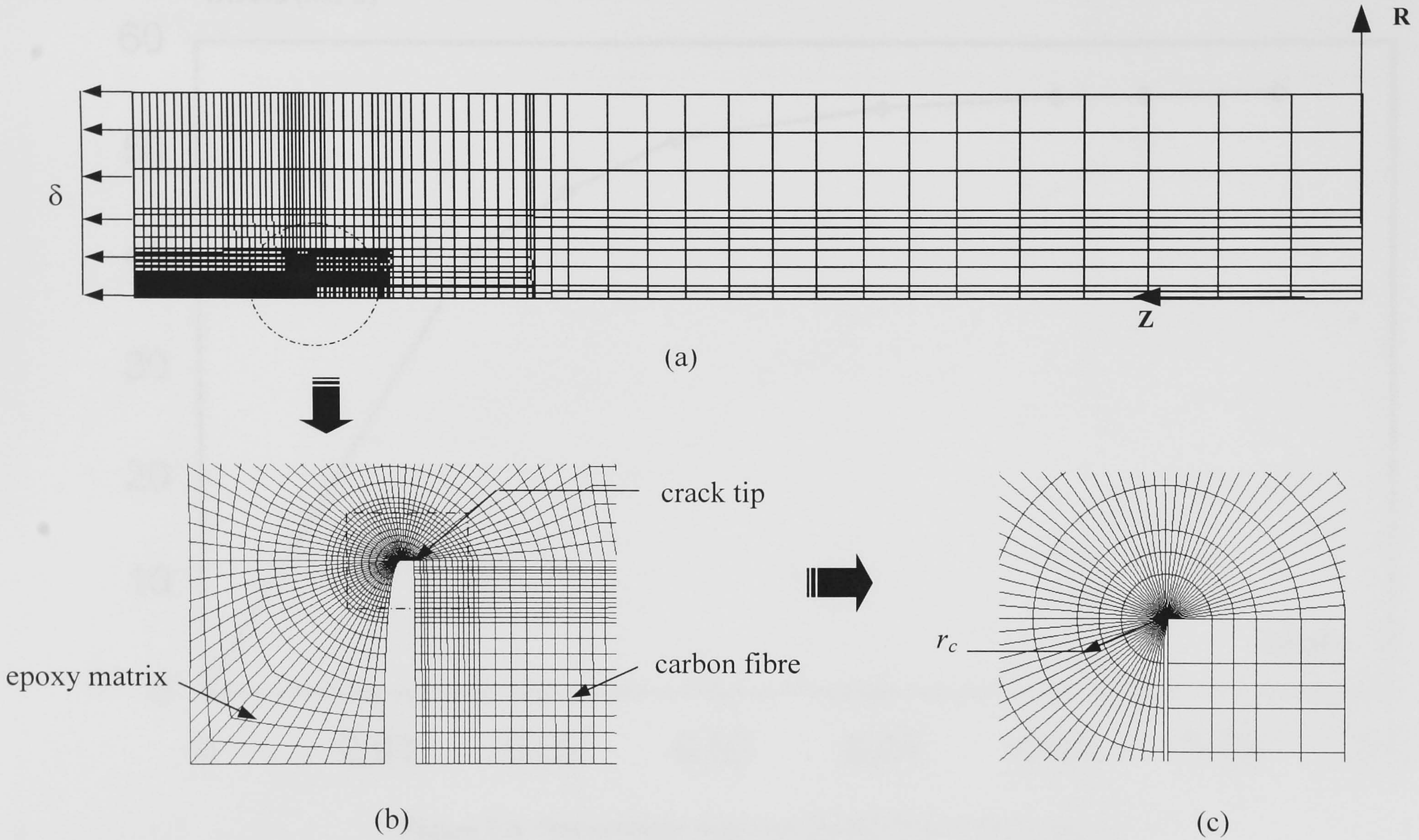

Figure 3.5 (a) Axisymmetric FE mesh (b) Detail of FE mesh around the fibre end (c) Detail of a critical radius, r_c

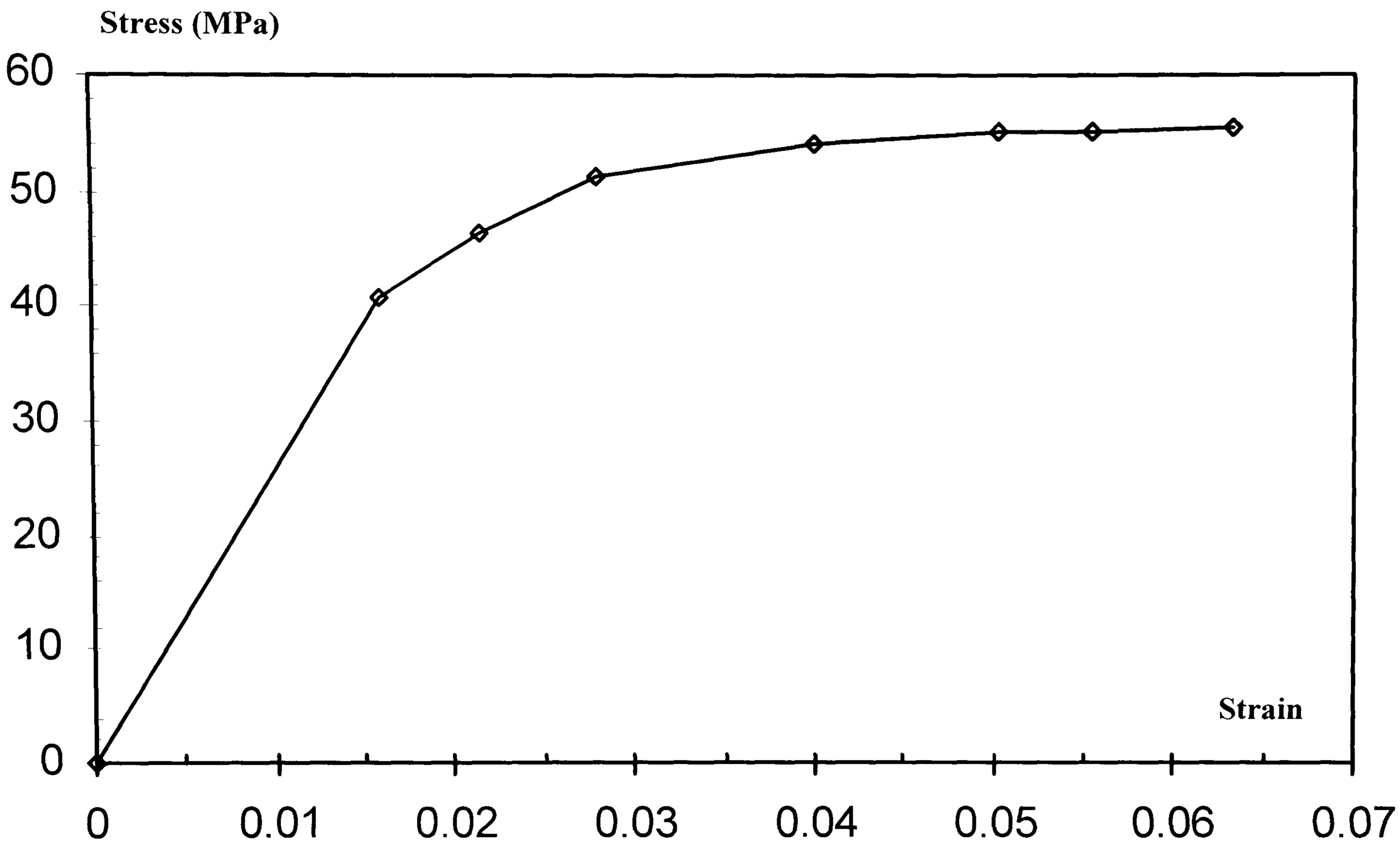

Figure 3.6 Stress-strain diagram for MY750/HY951 epoxy

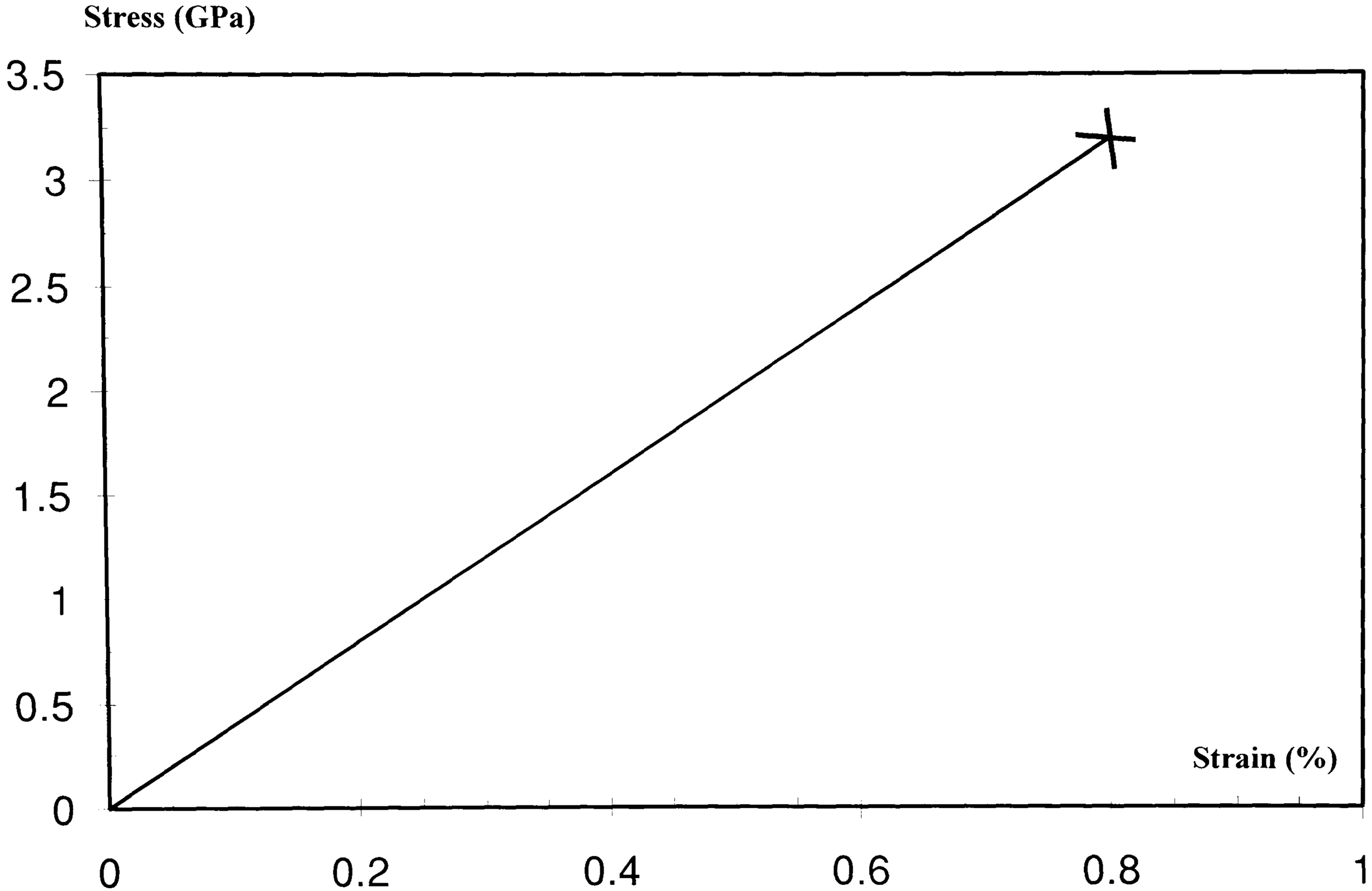

Figure 3.7 Stress-strain diagram for carbon fibre

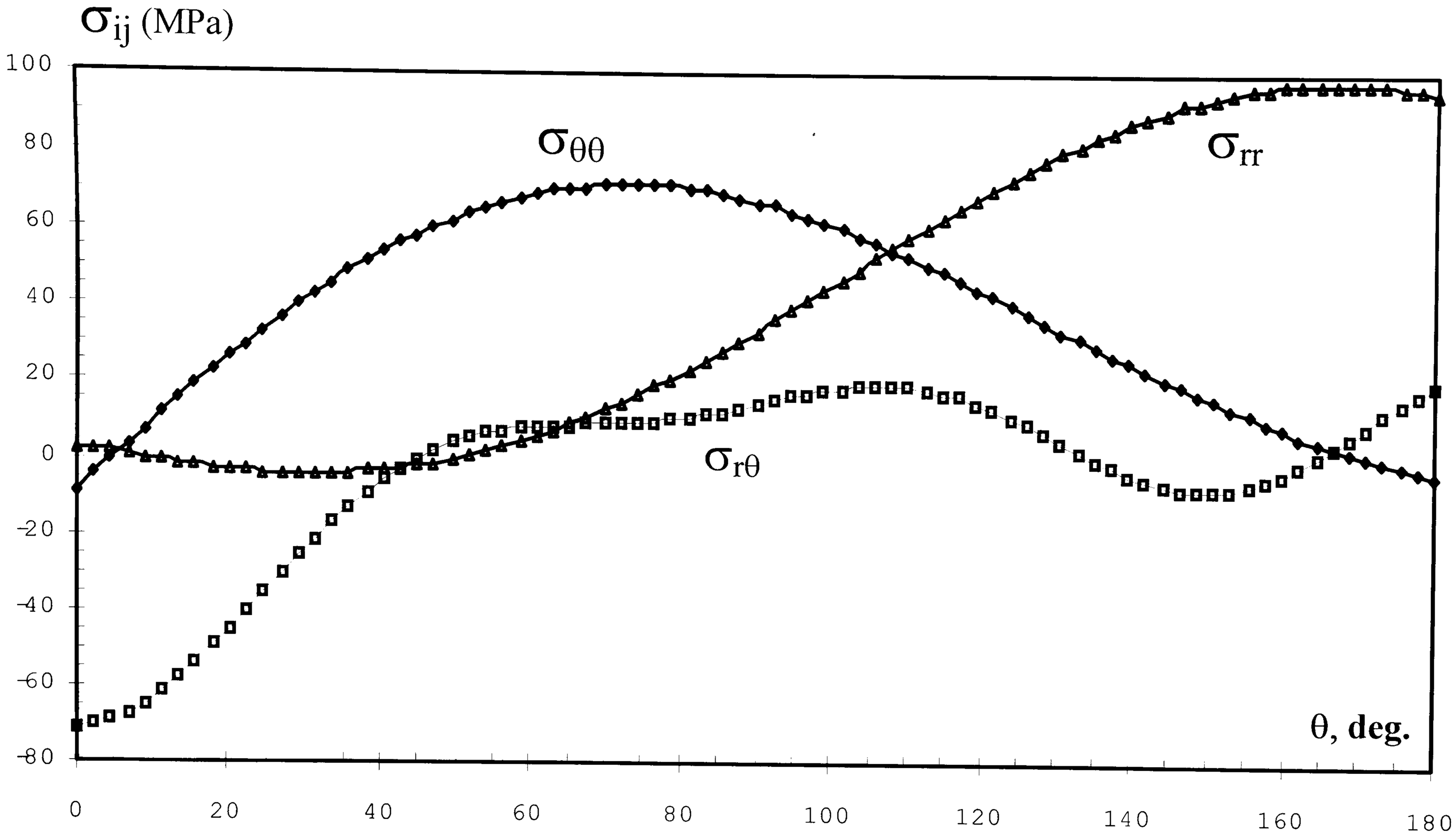

Figure 3.8 Angular variation of stresses, obtained from linear elastic FE analysis for $\varepsilon_{appl.}$=0.14%.

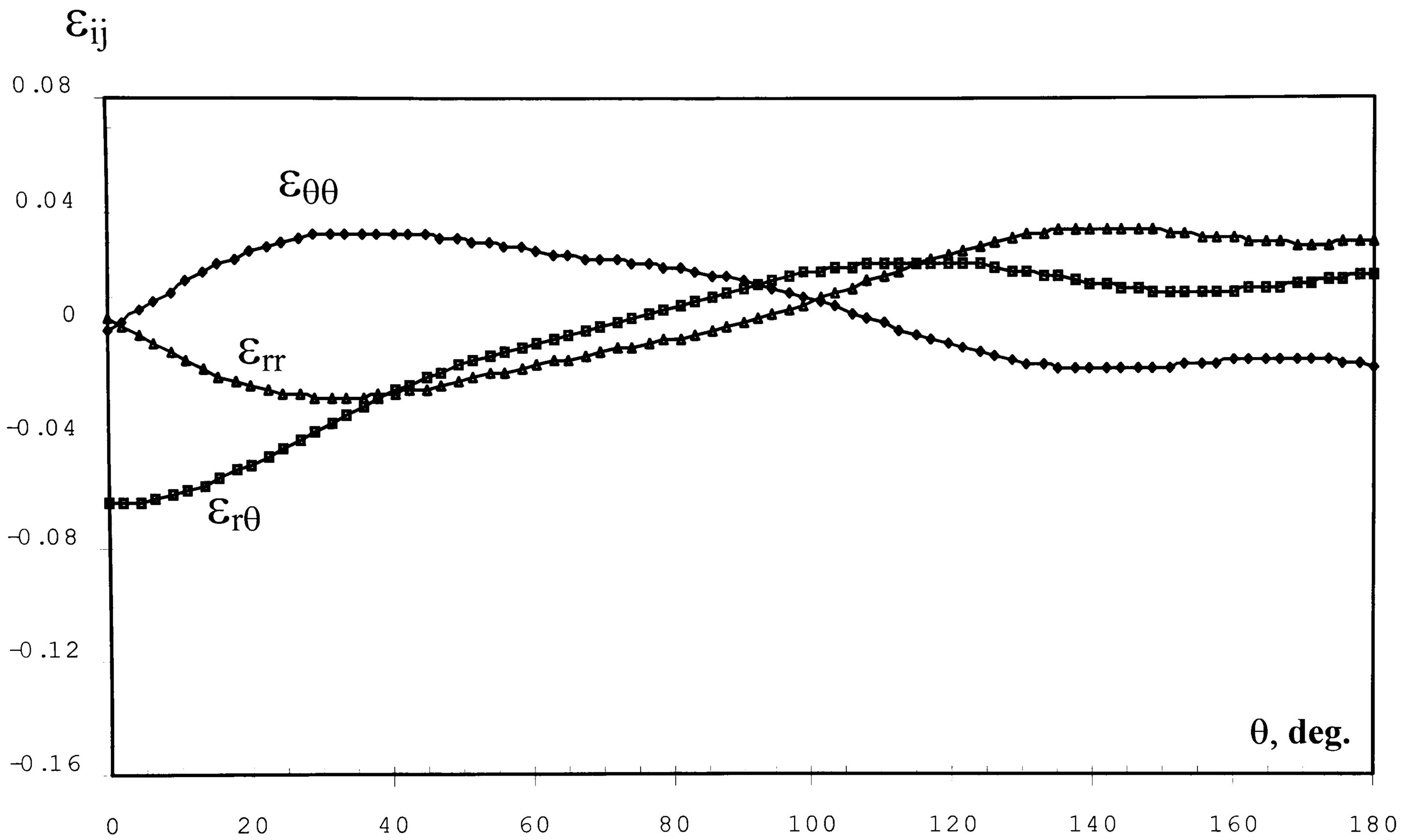

Figure 3.9 Angular variation of strains, obtained from linear elastic FE analysis for $\varepsilon_{appl.}$=0.14%

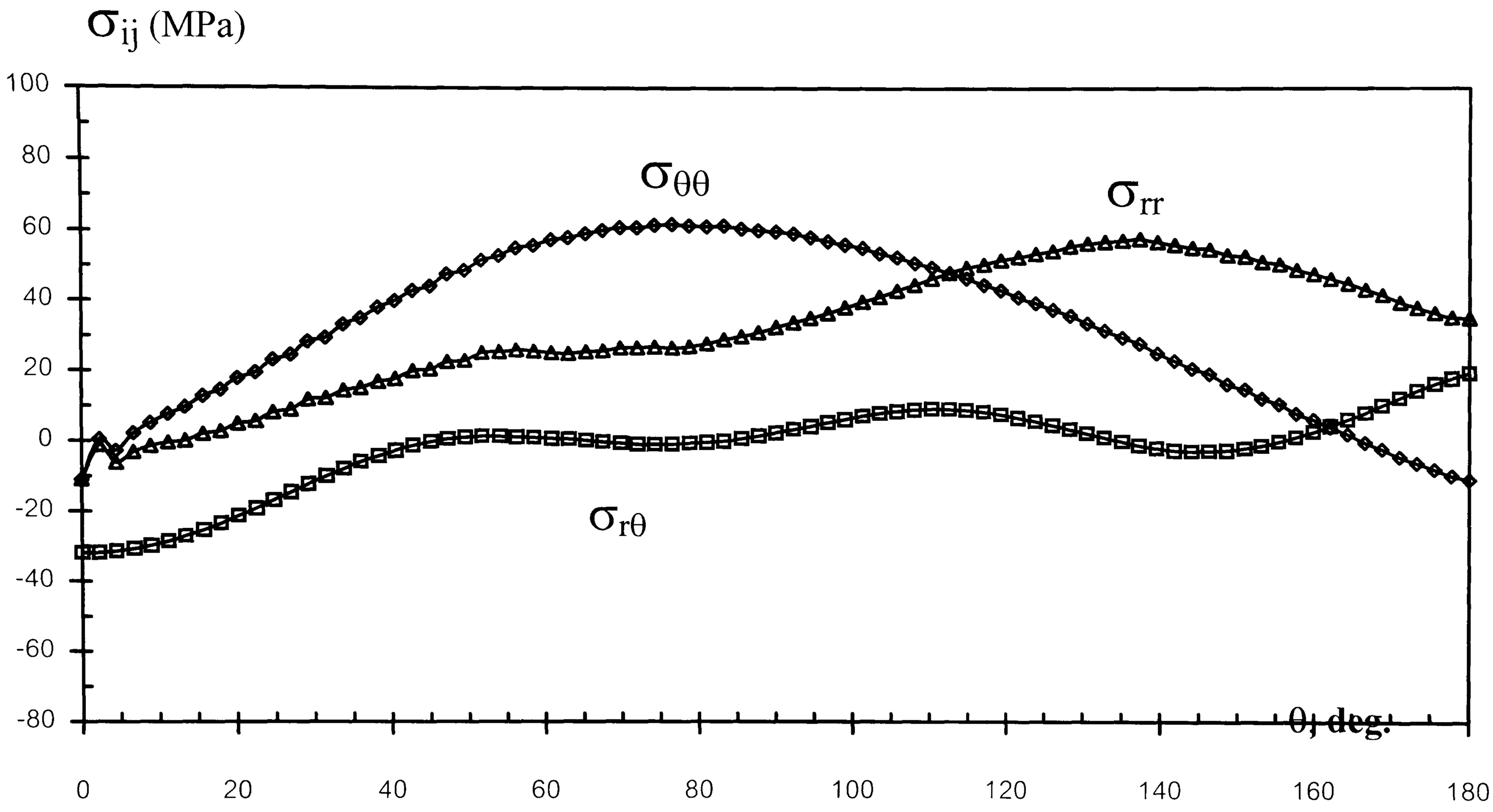

Figure 3.10 Angular variation of stresses, obtained from elasto-plastic FE analysis for $\varepsilon_{appl.}$=0.14%

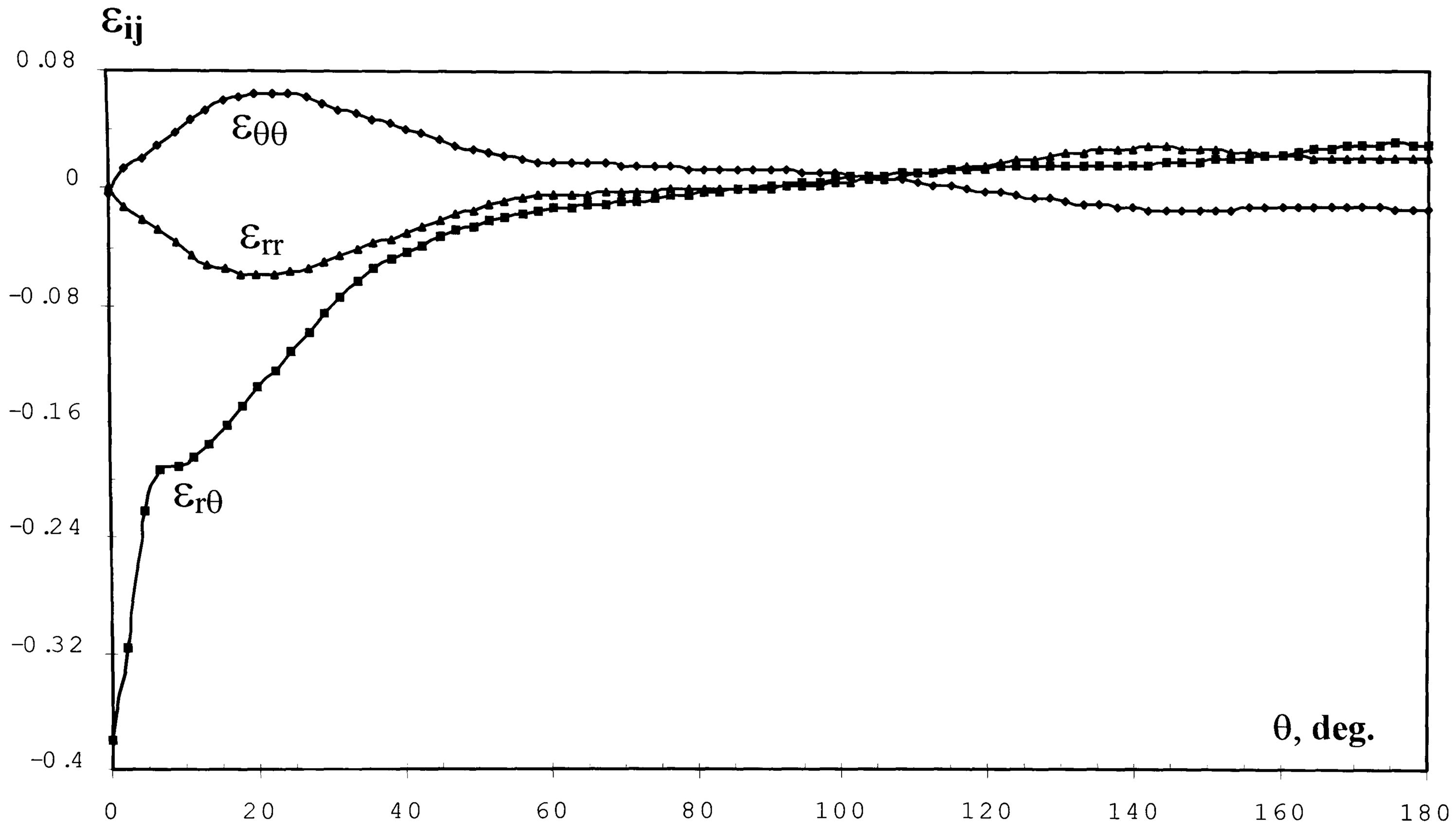

Figure 3.11 Angular variation of strains, obtained from elasto-plastic FE analysis for $\varepsilon_{appl.}$=0.14%.

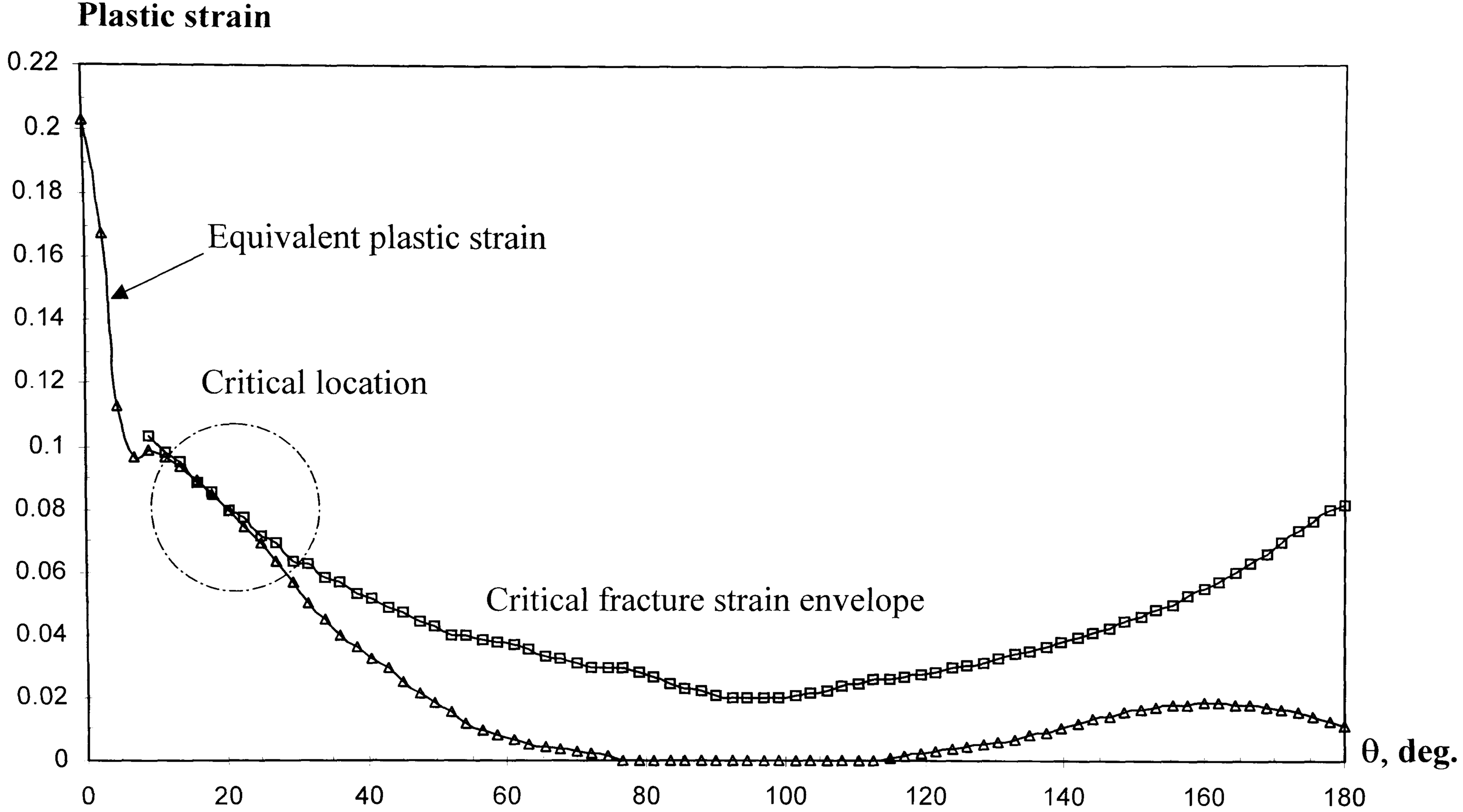

Figure 3.12 Crack initiation condition at r_c =0.2 μm for $\varepsilon_{appl.}$=0.14%

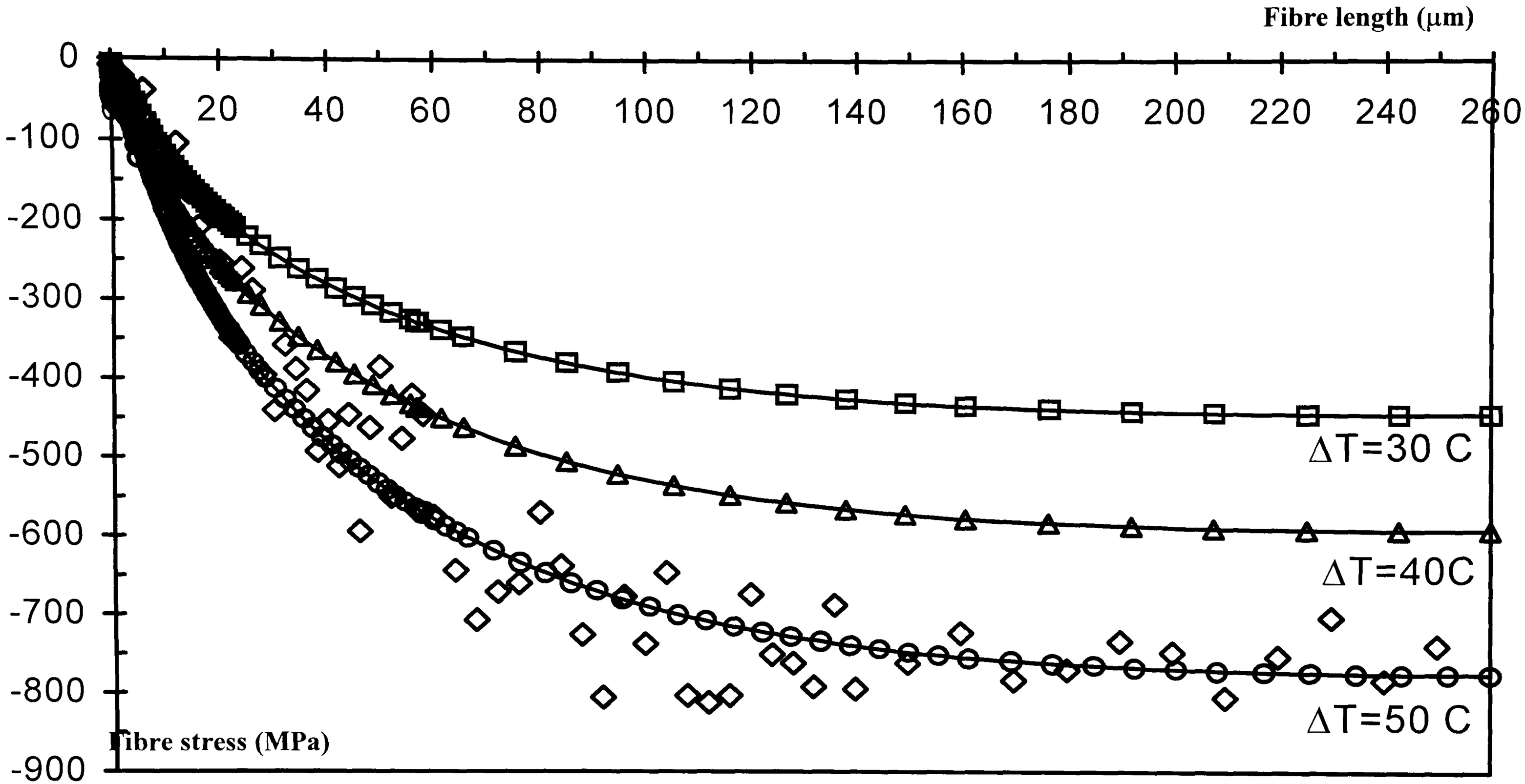

Figure 3.13 Axial variation of fibres stress for elasto-plastic analysis with various temperature drops ΔT

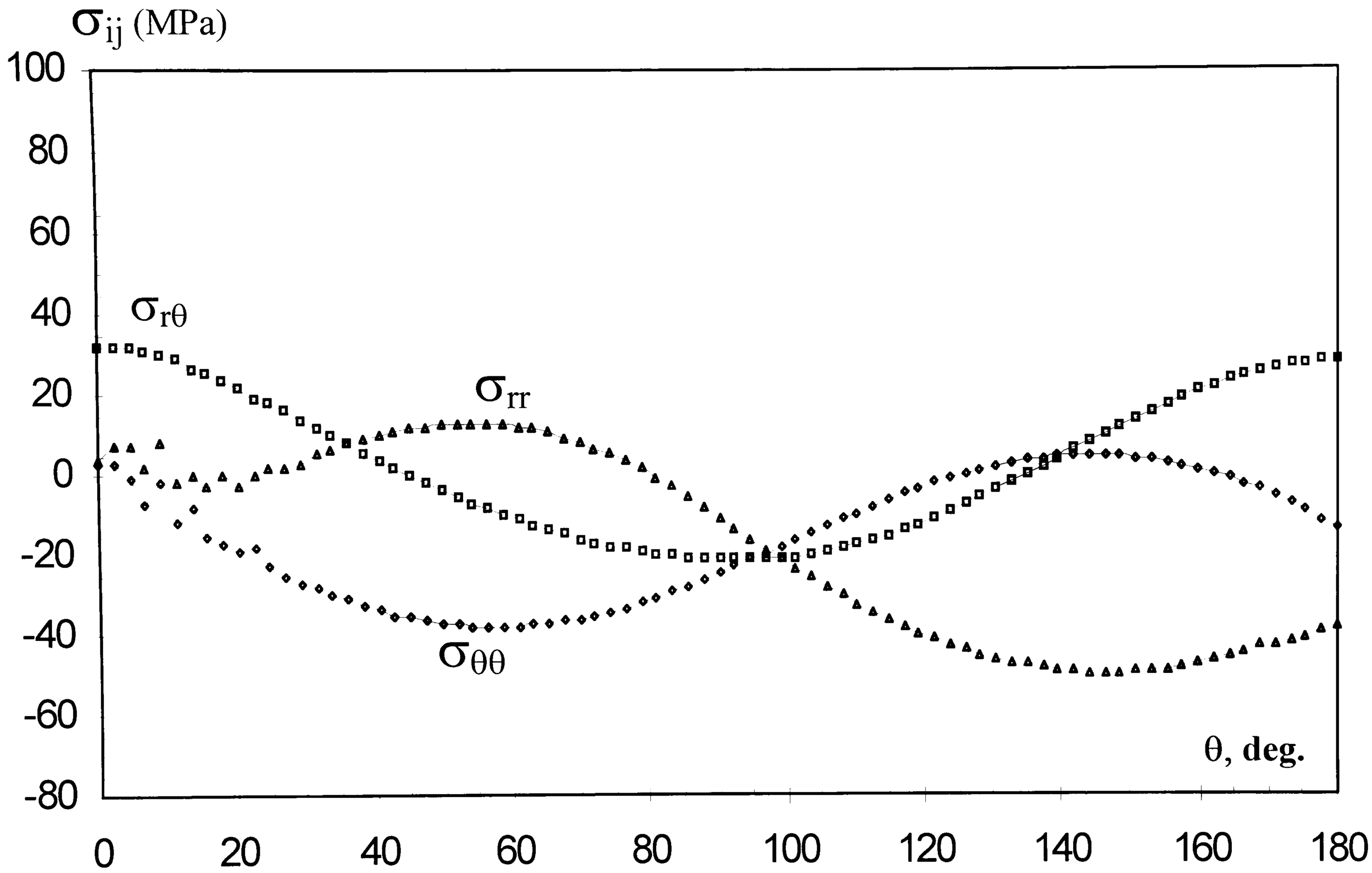

Figure 3.14 Angular variation of stresses, obtained from elasto-plastic analysis under thermal load, for $\Delta T=50°C$

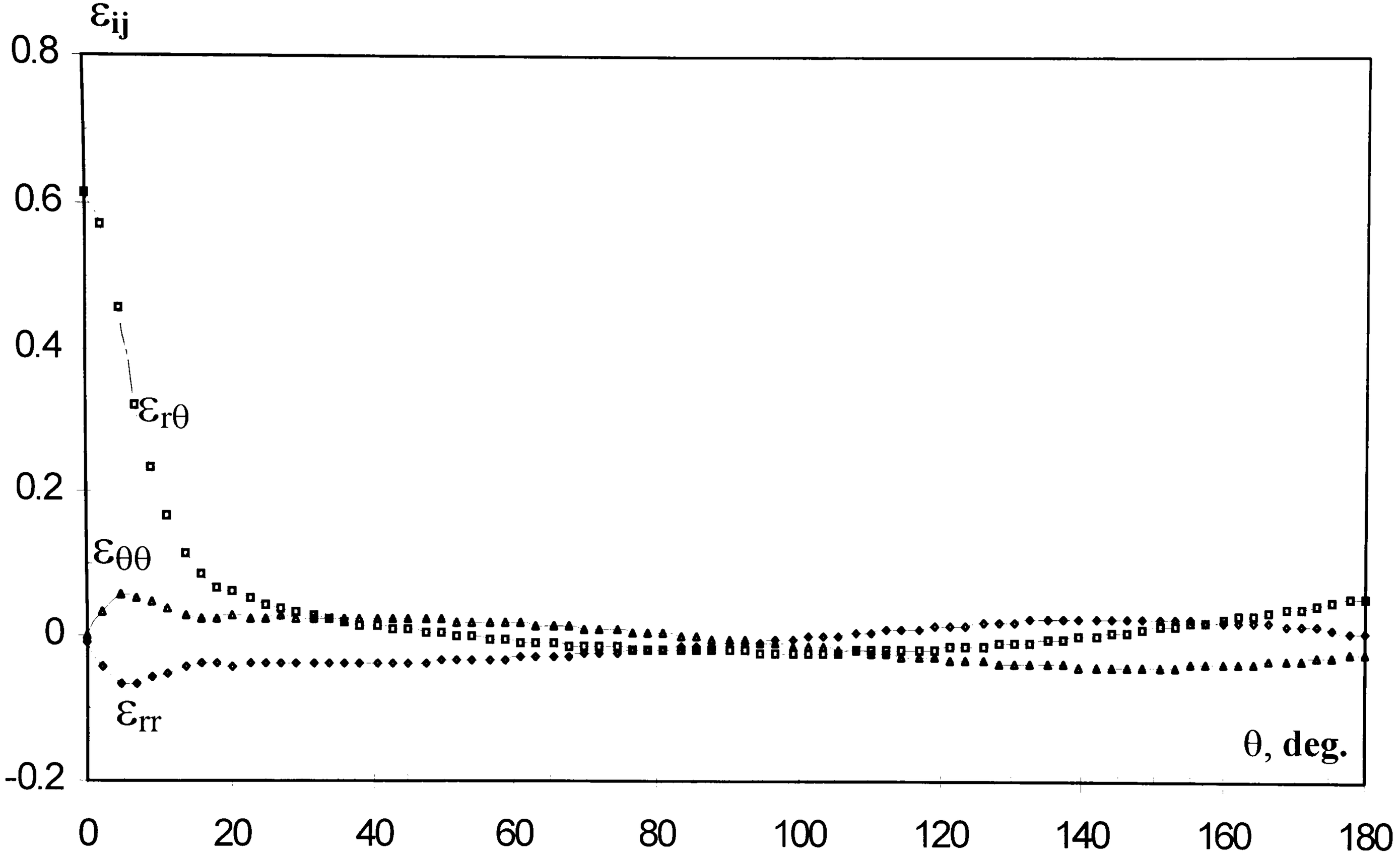

Figure 3.15 Angular variation of strains obtained from elasto-plastic analysis under thermal load for $\Delta T = 50°C$

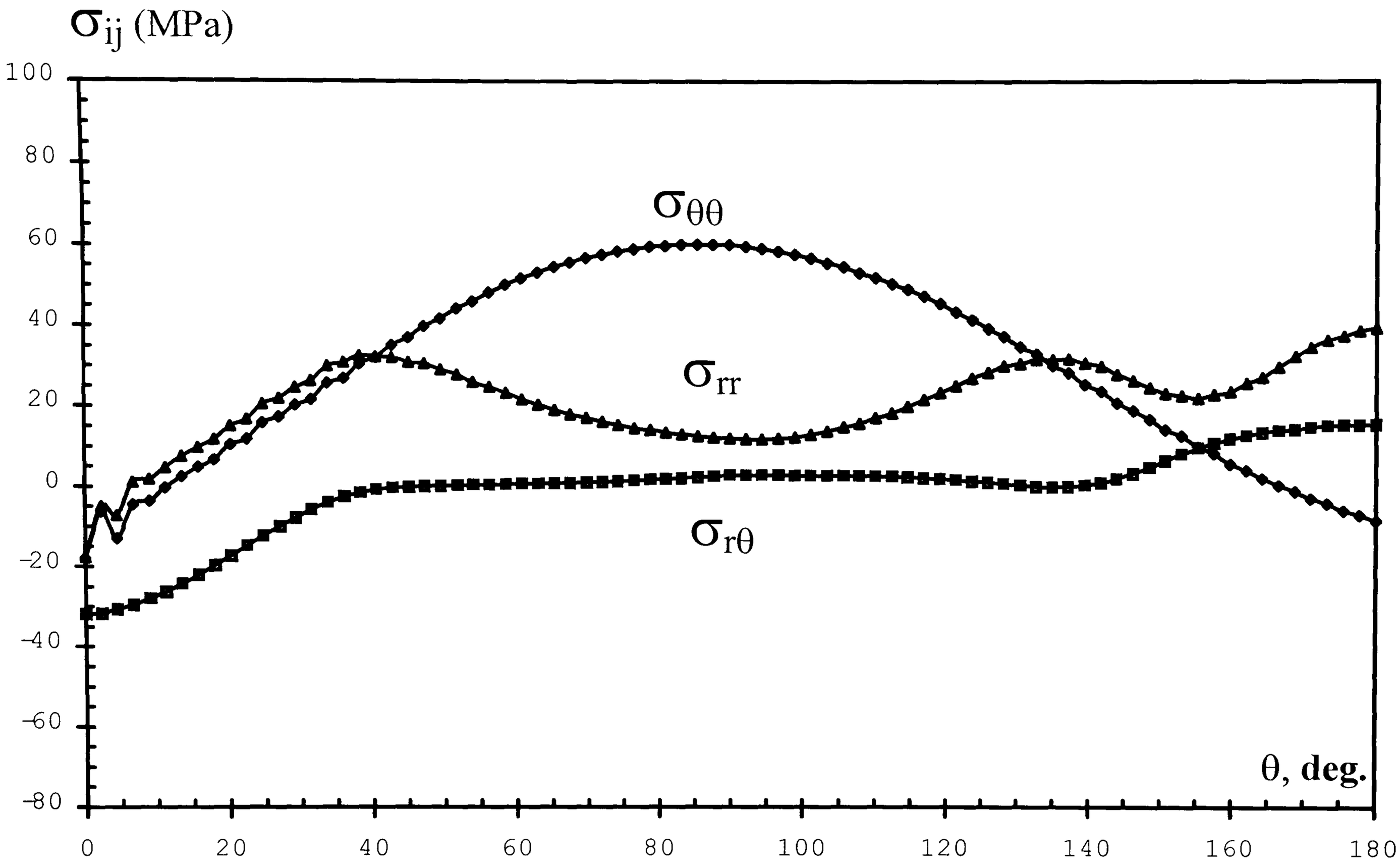

Figure 3.16 Angular variation of stresses under thermal and mechanical load, obtained from elastic-plastic FE analysis, for $\varepsilon_{appl.}$=0.3%

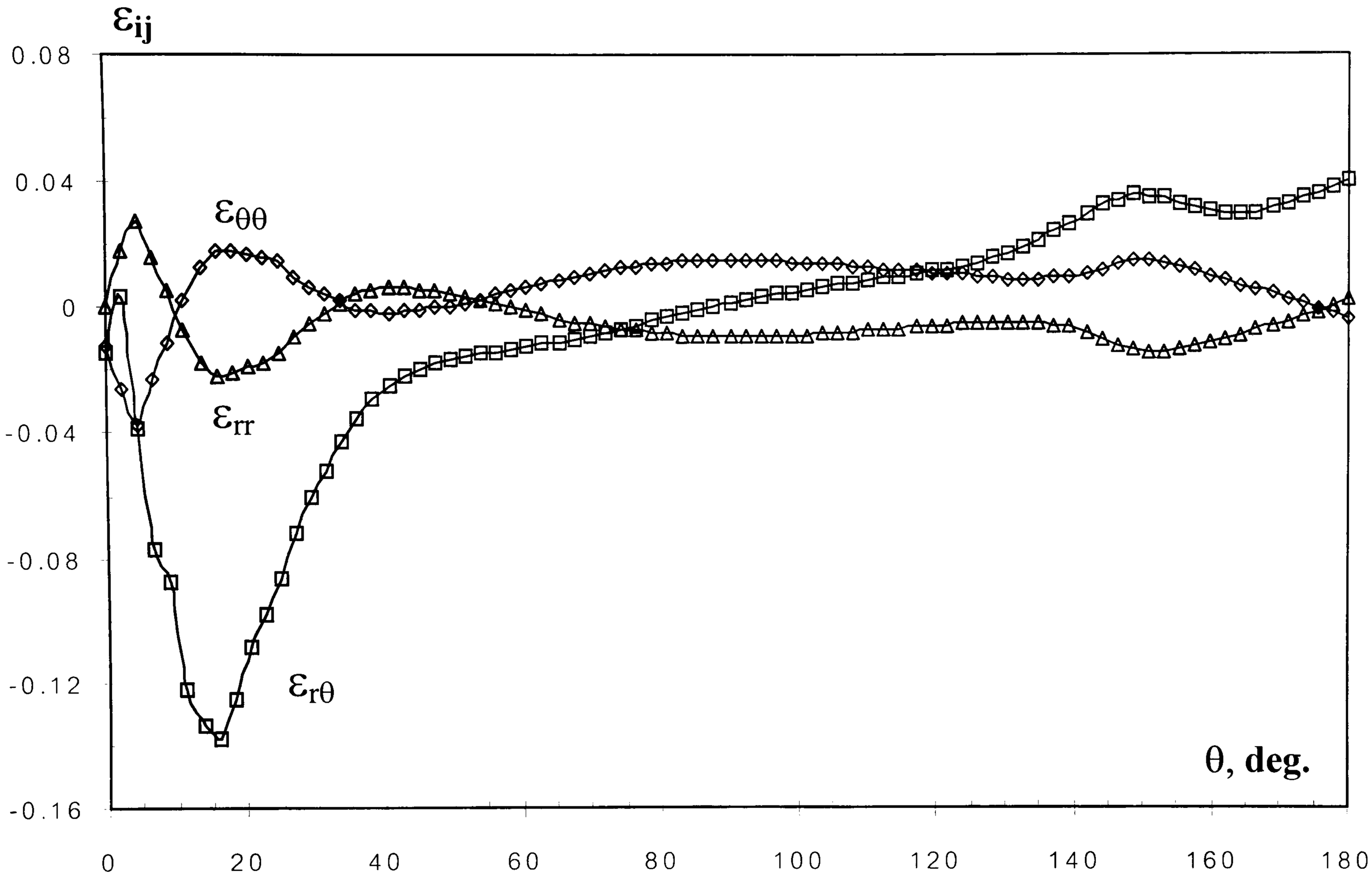

Figure 3.17 Angular variation of strains under thermal and mechanical load, obtained from elastic-plastic FE analysis, for $\varepsilon_{appl.}$=0.3%

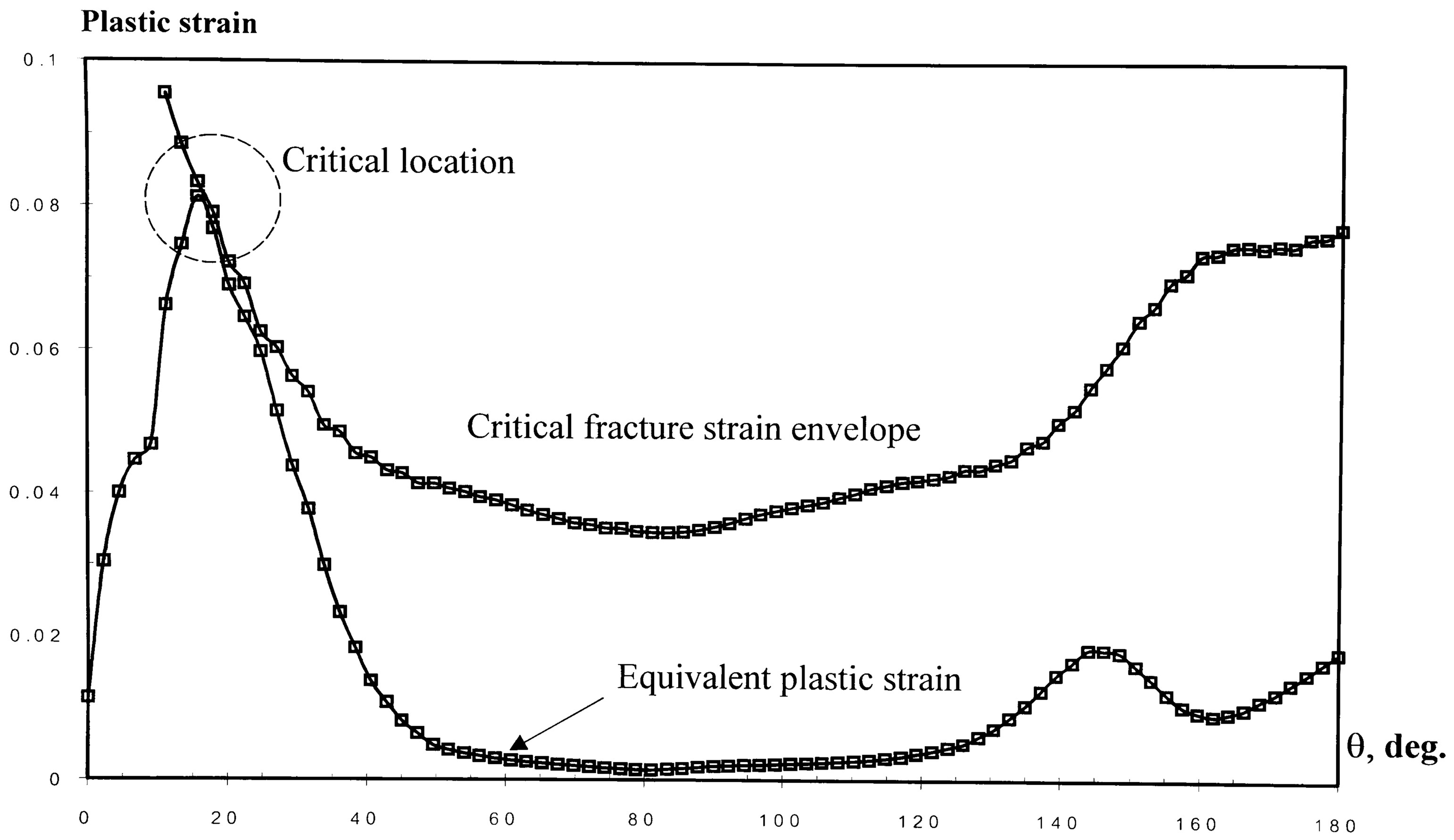

Figure 3.18 Crack initiation condition at r_c =0.2 μm under thermal and mechanical loading with $\varepsilon_{appl.}$=0.3%[9]

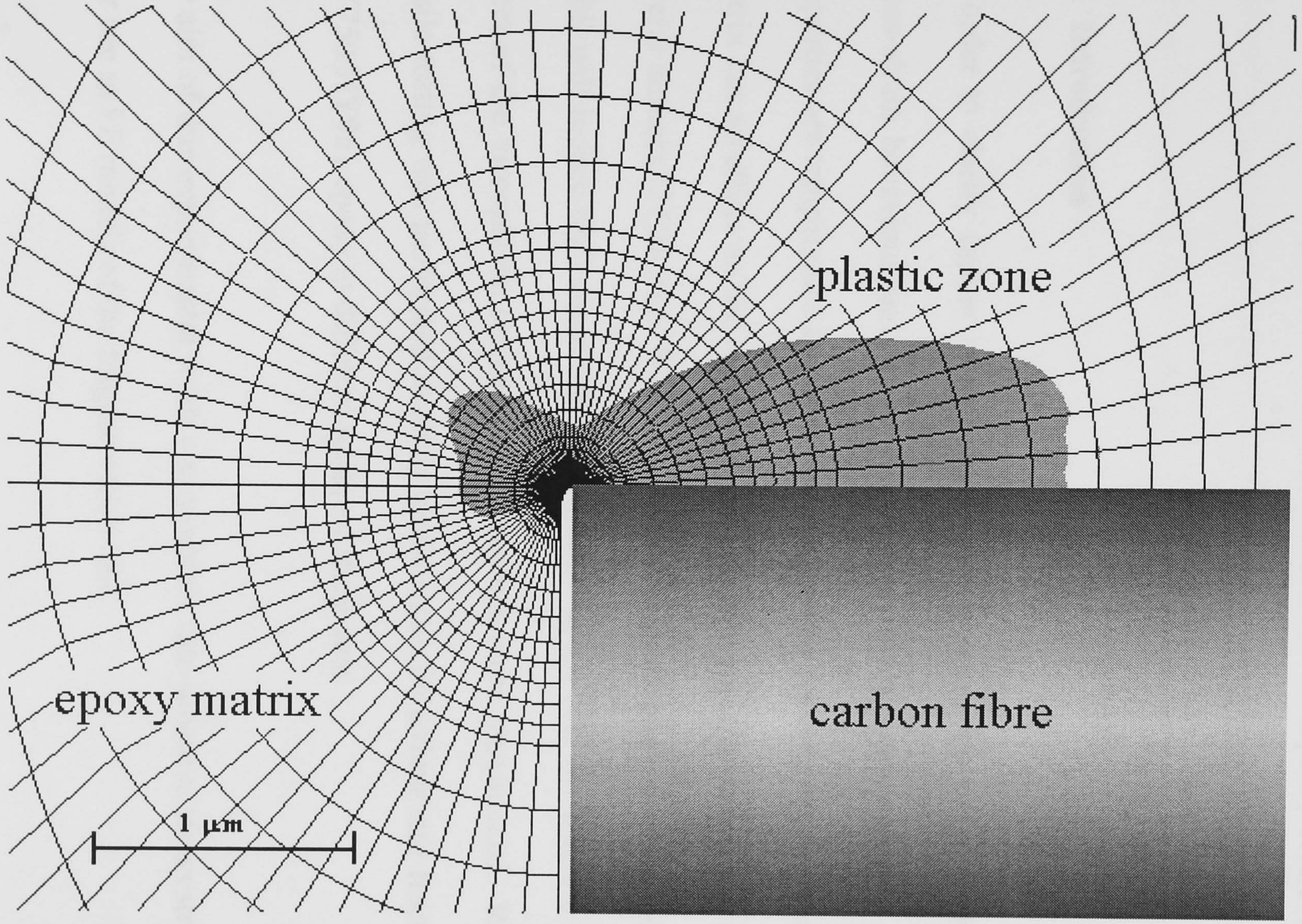

Figure 3.19 Extent of plastic zone for combined thermal and mechanical loading, ε_{appl}=0.3%

CHAPTER 4

Viscoplastic Tensile Behaviour of Epoxy Matrix

4.1 Introduction

In order to clarify failure in a composite, it is necessary to study the viscoplastic stress-strain behaviour and failure mechanisms of the epoxy matrix, for which the properties are temperature and time dependent. The viscoplastic response of an epoxy matrix has an effect on the different types of failure in the composite, as reported by several authors [27,28,34]. When fibre fracture takes place in a composite, the fibre recoil will induce high strain rates in a matrix region near the fracture location. The effect of the viscoplastic response then becomes more pronounced. Rate dependent tensile testing was performed to study stress-strain behaviour and fracture strains of MY750/HY951 epoxy at different levels of strain rate.

The aim of this experimental work was to obtain rate-sensitive stress/strain curves for later use in FE models of the fragmentation test.

4.2 Mechanics of Viscoplasticity

Unlike viscoplasticity in metals, viscoplastic behaviour of polymers is a direct result of their molecular structure. At a low strain-rate, polymer molecules have sufficient

time to move and the internal energy generated by this process must be low, the polymer would easily deform at low stress. At a higher strain-rate, a faster movement of polymer molecules produces high frictional forces between molecular chains. The increase in the internal energy by this event leads to higher stress in the polymer at a similar strain as with lower strain rates. For a rate-sensitive material the true stress σ_{true} can be expressed as [102]:

$$\sigma_{true} = K.\dot{\varepsilon}^{m}.\varepsilon_{p}^{\ n} \qquad \text{provided } \dot{\varepsilon} \neq 0 \tag{4.1}$$

where K is a constant, $\dot{\varepsilon}$ is the strain rate, m is a strain-rate sensitivity exponent, ε_p is the plastic strain and n is a strain hardening exponent. The strain-rate sensitivity exponent m increases with temperature and approaches unity as the equilibrium melting temperature is reached. Generally, $m \leq 0.1$ for most materials. The strain hardening exponent n varies depending on strain hardening at each strain rate.

4.3 Experimental Work

4.3.1 Materials and specimen preparation

Unmodified liquid epoxy resin MY750 and triethylene tetramine hardener HY951 provided by Ciba-Geigy ^{TM} were used in this study. Epoxy tensile specimens were prepared in a two-cavity tensile specimen silicone rubber mould according to ASTM D 638 type I specimen geometry (see Fig. 4.1). Epoxy resin and hardener were degassed for 30 minutes and mixed in a ratio 4:1 by weight at 40°C. This epoxy

mixture was stirred for about half a minute, degassed for 10 minutes then poured into the silicone rubber mould. All these processes were done under full vacuum using the MK-Technology ™ vacuum casting system (see Fig. 4.2). The epoxy tensile specimens were cured while still inside the silicone mould for 2 hours at 60°C in a temperature controlled oven. Complete epoxy specimens are shown in Fig. 4.3.

4.3.2 Rate dependent tensile testing

A universal Instron 4502 ™ testing machine was used for rate dependent tensile testing (see Fig. 4.4 (a)). This machine is a hydraulic position control system, for which the crosshead speed can be controlled precisely. An extensometer with a gauge length of 50 mm, according to ASTM D 638, was mounted on the epoxy specimen (see Fig. 4.4 (b)). The values of load and displacement were obtained through a PC computer at the rate of 25 points/second and converted to stress-strain curves by Series IX ™,provided universal testing software by Instron Corporation. This software also calculated the elastic moduli and yield stresses. The crosshead speeds used in these experiments were 0.5, 1.25, 10, 20, and 60 mm/min. All specimens were tested at 23 °C with the ambient humidity in the range 50-55 %.

4.4 Results Summary

4.4.1 Stress-strain relationship of epoxy

Degassing is a very important process to get rid of air bubbles from the epoxy specimens. When an epoxy resin solidifies air bubbles will be trapped within the epoxy material and remain as voids, which play an important role on reducing the

strength and inducing fracture in the epoxy specimen (see Fig. 4.5). The suitable degassing time, found in this experiment, has to be at least 30 minutes under full vacuum in order to make sure that most of the air bubbles within the epoxy resin have been released. Two specimens were used for tensile testing at each crosshead speed. Stress-strain curves at each strain rate were constructed from the averaged values for the two specimens.

The rate dependent stress-strain relationships of epoxy are shown in Fig. 4.6. The difference between stress-strain curves for the strain rates 0.4 min^{-1} and 1.2 min^{-1} was found minimal. As can be seen from Fig. 4.6, the elastic behaviour is dominant as the strain rate is increased. The averaged elastic modulus E_{avg} of epoxy is 2445 MPa ± 6%, where the details are given in Table 4.1. As the strain rate is increased from 0.01 min^{-1} to 1.2 min^{-1}, the yield stress σ_y, which calculated by offset the yield strength to 0.01 percentage of plastic strain, was found to increase by 51.4 %. Values of yield stress of epoxy at each strain rate are shown in Table 4.1. The true stress-plastic strain relationships of epoxy can be simplified using [103]

$$\sigma = H_i.\varepsilon_p^{\,n_i} \qquad (i=1,2,3,4,5) \qquad (4.2)$$

or in Ramberg-Osgood form [101] as:

$$\varepsilon = \frac{\sigma}{E} + \left(\frac{\sigma}{H_i}\right)^{\frac{1}{n_i}} \qquad (i=1,2,3.4.5) \qquad (4.3)$$

The coefficient of determination $\mathbf{r}^2$ about 95.2 % is obtained from this curve fitting. The strain-hardening exponent n and the strength coefficient H were found to be decreasing as the strain rate is increasing. This may imply that the ability of epoxy to resist necking is reduced as a strain rate is increased. Stress-strain curves obtained by using the Ramberg-Osgood formula are plotted in Fig. 4.7. The relationship between engineering stress and true stress can be obtained by eq. 4.4 [103]

$$\sigma_{true} = \sigma_{eng}(1+ \varepsilon_{nom}) \tag{4.4}$$

for the relationship between engineering strain and true strain can be expressed as

$$\varepsilon_{true} = \ln(1 + \varepsilon_{eng}) \tag{4.5}$$

The true stress-strain curves are plotted in Fig. 4.8. Using eq. (4.1), the true stress-plastic strain relationships of this epoxy system can be characterised as:

$$\sigma_{true} \approx 92.455.\dot{\varepsilon}^{-0.0528}.\varepsilon_p^{\,n_i} \quad \text{provided } \dot{\varepsilon} \neq 0 \tag{4.6}$$

The constant value K = 92.455 MPa and strain-rate sensitivity exponent m = -0.0528 are obtained from the intercept and the gradient of a linear curve fitting of the strength coefficients H and strain rates $\dot{\varepsilon}$ in logarithmic scale, respectively. This curve fitting gives $\mathbf{r}^2$ of about 95.7 %. This formula represents the true stress-plastic

strain relationships for this epoxy as long as the strain-rate is not equal to zero. A negative value for the strain-rate sensitive exponent m indicates decaying of strength coefficients H, as described in Ramberg-Osgood formula, when strain rate is increasing. The strain hardening exponents n_i are varying depending on the strain rates as shown in Table 4.1. The true stress/plastic strain curves from eq. (4.4) are plotted in Fig. 4.9.

4.4.2 Fracture characteristics of epoxy

From a microscopic point of view, yielding and fracture in polymers are different from metals. Polymers consist of long molecular chains and do not contain crystallographic planes, dislocations, and grain boundaries as do metals. Fracture on the atomic level of polymer involves breaking bonds, which is called *chain scission* [104]. There are two types of bond that govern the mechanical response. The first one is the covalent bonds between carbon atoms, which plays a major role in fracture. The second type of bond is the van der Waals forces between molecule segments. This type of bond causes deformation in the polymer, which would lead to fracture when the forces exceed the covalent bond strength.

From a macroscopic point of view, fracture in epoxy is likely to be governed by voids which occur by air bubbles that have been trapped within the epoxy during the fabrication process.

The fracture strain of epoxy matrix obtained from this experiment was found to be approximately 4.5 ± 0.2 %. Epoxy is stiffer and stronger at higher strain rates from its stress-strain behaviour. Unlike modified liquid epoxy resins, unmodified liquid epoxy resins such as MY750 epoxy exhibits a little ductility. Fracture would take place at a percent elongation of only about 2 % after yielding. Details of this experiment are shown in Table 4.2.

At a lower strain rate, between 0.01-0.025 min^{-1}, a very small region of failure by micro-voids was found near the edge of free surfaces. A captured image from the specimen that was tested at the strain rate of 0.01 min^{-1} is shown in Fig. 4.10. This image was produced by inverted grayscale to obtain a clear picture of the fracture surface. Defects, which resulted from an incomplete mixing within a region of lamellae (area A in Fig. 4.10) during a fabrication process, would induce fracture of specimens. Cup and cone fracture appeared conclusively at the strain rate of 0.01 min^{-1}, but it appeared much less pronounced at strain rates between 0.025-0.2 min^{-1} and disappeared as the strain rate increased to 0.4 min^{-1}. Shear bands were observed clearly at the strain rate of 0.2 min^{-1}. A very large zone of failure by micro-voids was observed at a fractured cross-sectional area all around the edges of the free surface in the specimen when testing at a higher strain rate, between 0.4-1.2 min^{-1} in this experiment (see Fig. 4.11-4.12). The images in Fig. 4.11 –4.12 were produced using the same magnification and technique as were used for the image in Fig 4.10. Necking in the specimen is more pronounced at higher strain rate, which is corresponding well with a decrease of the strain hardening exponents n_i.

4.5 Discussion

According to the testing results, viscoplasticity of epoxy matrix has a significant effect when the strain rate is higher than 0.2 min^{-1}, as the yield strength was increased by more than 37 %. In a plastic region at this strain rate level, the stress/strain behaviour has turned to a precipitous slope, which in turn increases the stiffness of the epoxy matrix. As an epoxy matrix is stiffer at a higher strain rate, fracture in epoxy matrix is likely to be governed by a brittle fracture. Micro-void formation in this epoxy material is very difficult to control. An insufficient degassing time resulted in a formation of observable voids, which will be developed to macrocracks in near future.

Crosshead speed (mm/min.)	σ_y (MPa)	E (MPa)	H_i	n_i
0.5	43.3	2597	116.84	0.1206
1.25	46.2	2292	112.25	0.106
10	59.5	2319	100.65	0.065
20	64	2505	101.25	0.0507
60	65.5	2514	94.634	0.0347

Table 4.1 Details of yield stresses, elastic moduli, strength coefficient, and strain hardening exponents for epoxy MY750 at each crosshead speed.

Crosshead speed (mm/min.)	Specimen number	Breaking load (kN)	Breaking displacement (mm)	Breaking time (s)	Cross. area (mm^2)
0.5	I	2.056	1.248	149.76	41.4
	II	1.984	1.939	232.68	38.94
1.25	III	2.301	2.726	130.86	41.4
	IV	2.320	2.156	103.5	39.9
10	V	2.788	2.100	12.6	40.8
	VI	2.87	1.767	10.6	42
20	VII	2.561	2.651	7.95	41.4
	VIII	2.579	2.533	7.6	40.2
60	IX	2.321	3.468	3.47	39.235
	X	2.818	4.502	4.5	41.4

Table 4.2 Details of breaking load, position, time and cross-sectional area of specimens.

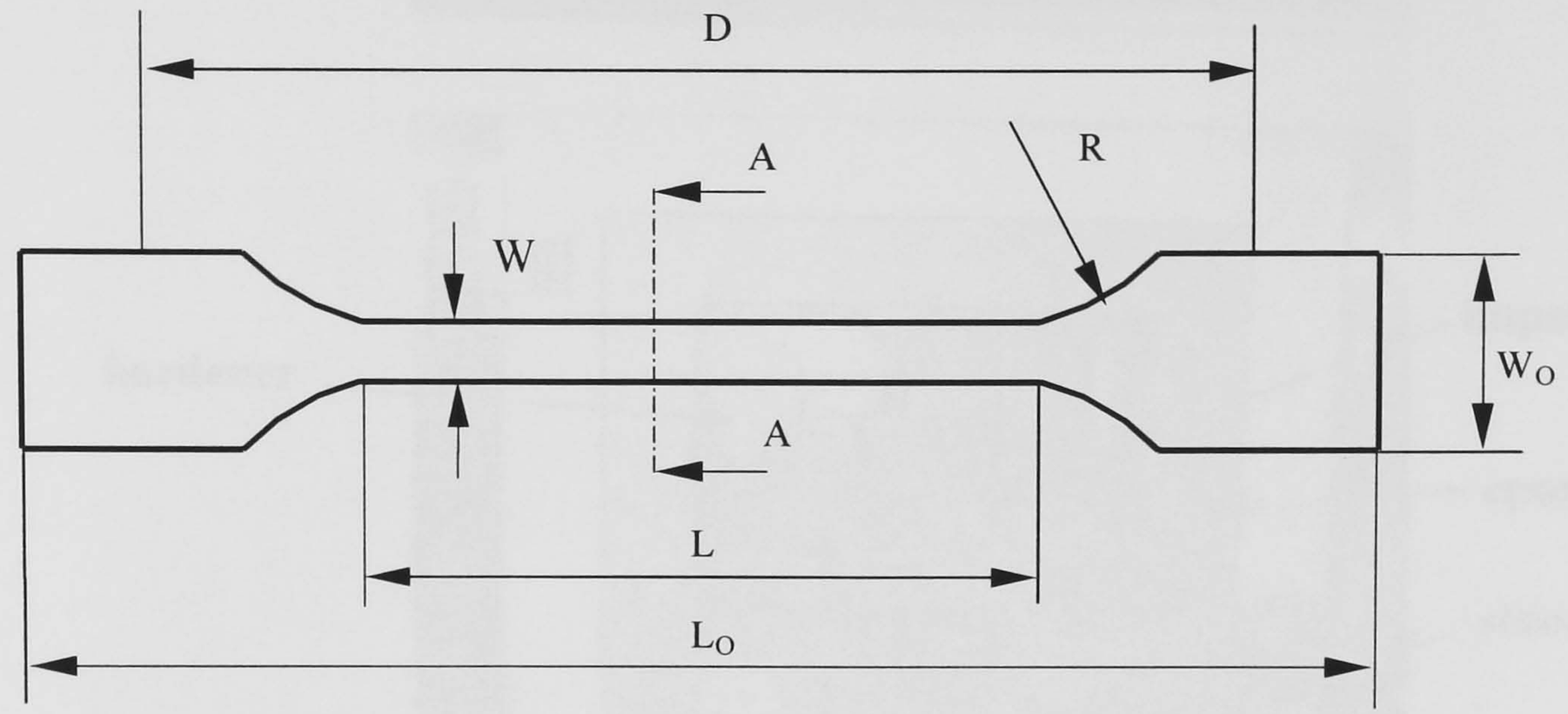

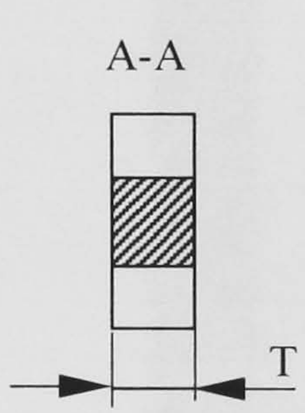

DIMENSIONS	7 OR UNDER
	TYPE I
W	13
L	57
L_O	165
R	76
D	115
W_O	19

Figure 4.1 Details of specimen geometry ASTM D 638 Type I

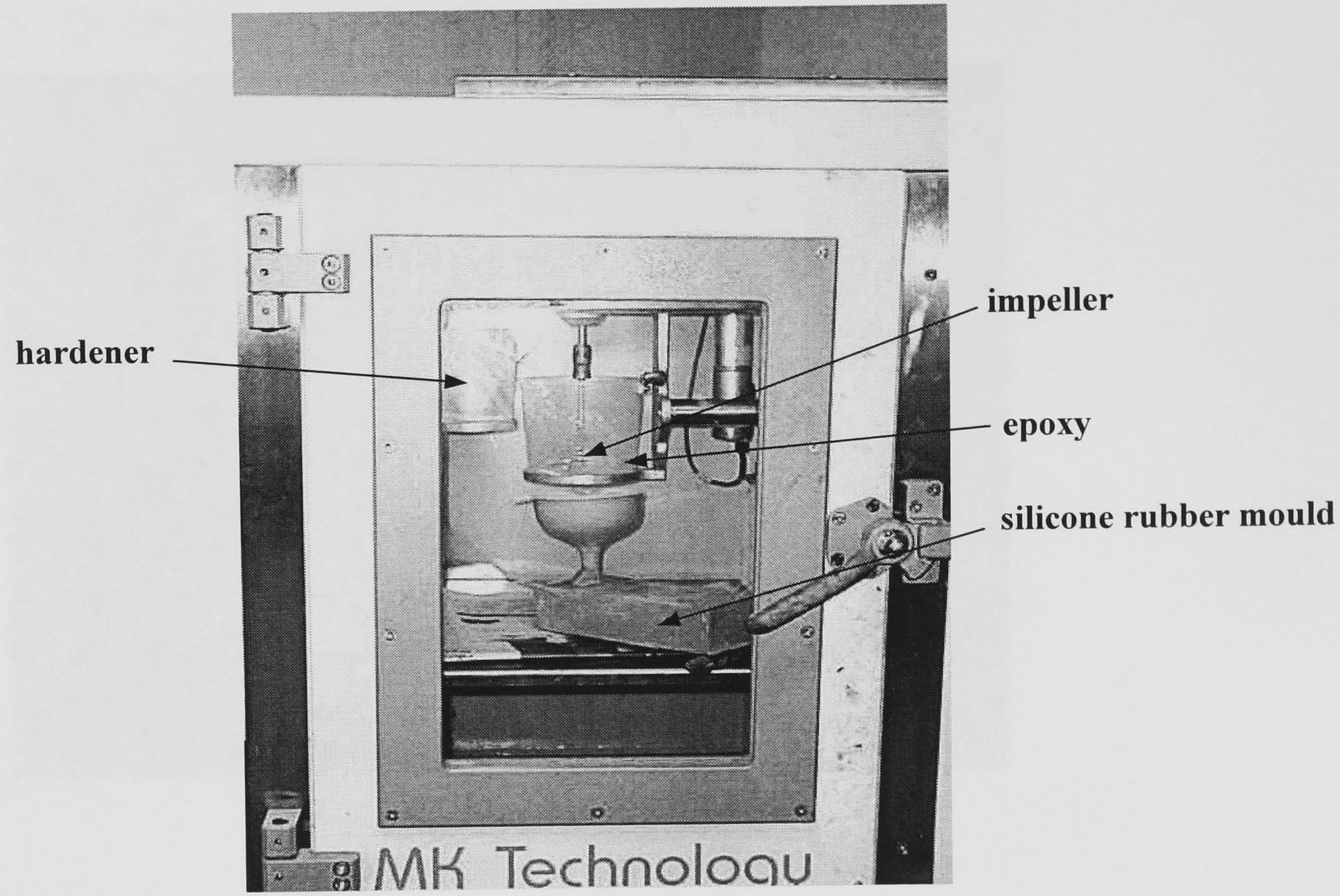

Figure 4.2 Preparation of epoxy specimen inside a vacuum chamber

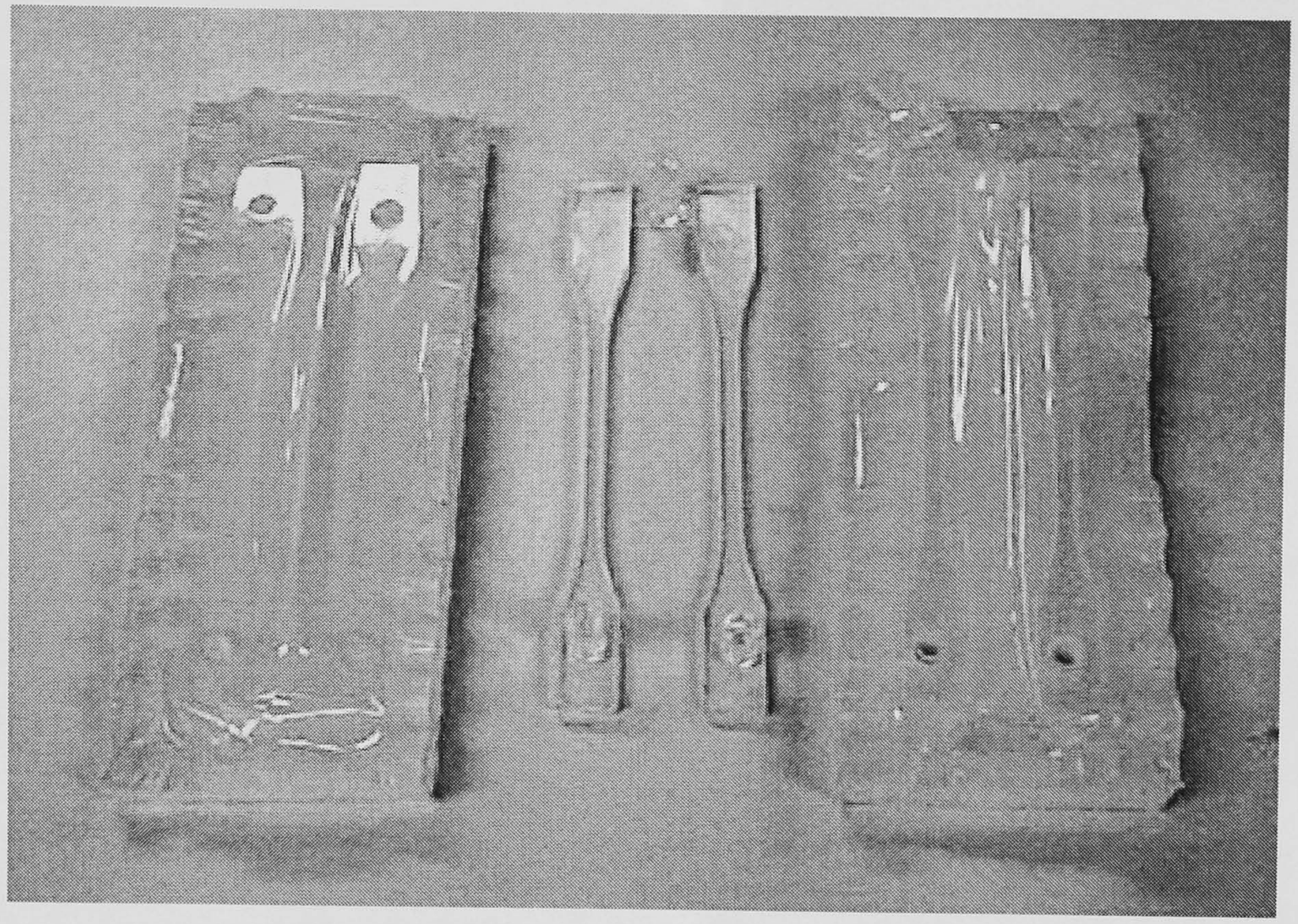

Figure 4.3 Complete epoxy tensile specimens

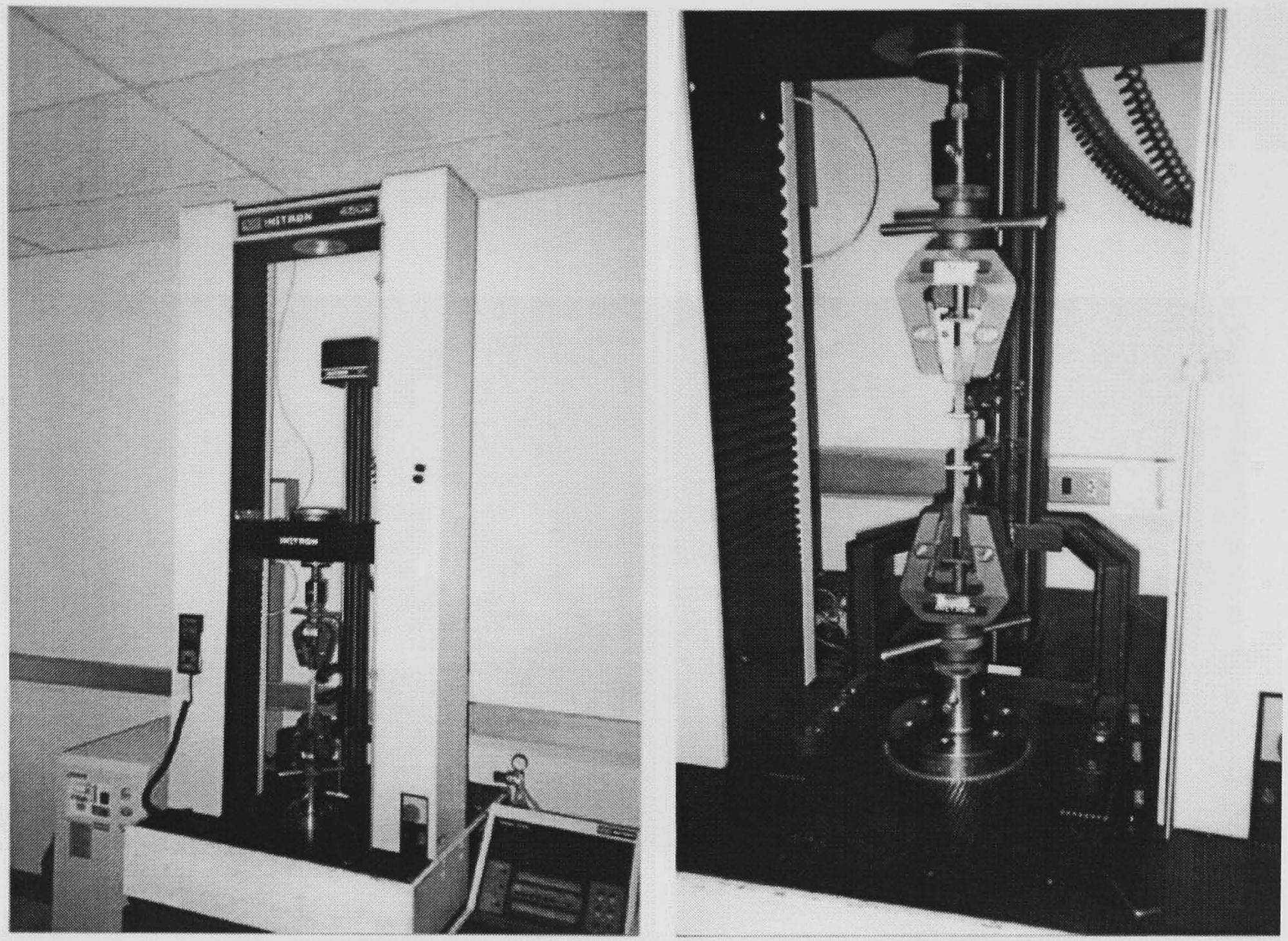

(a) (b)

Figure 4.4 (a) Instron 4502 universal testing machine (b) epoxy specimen on test

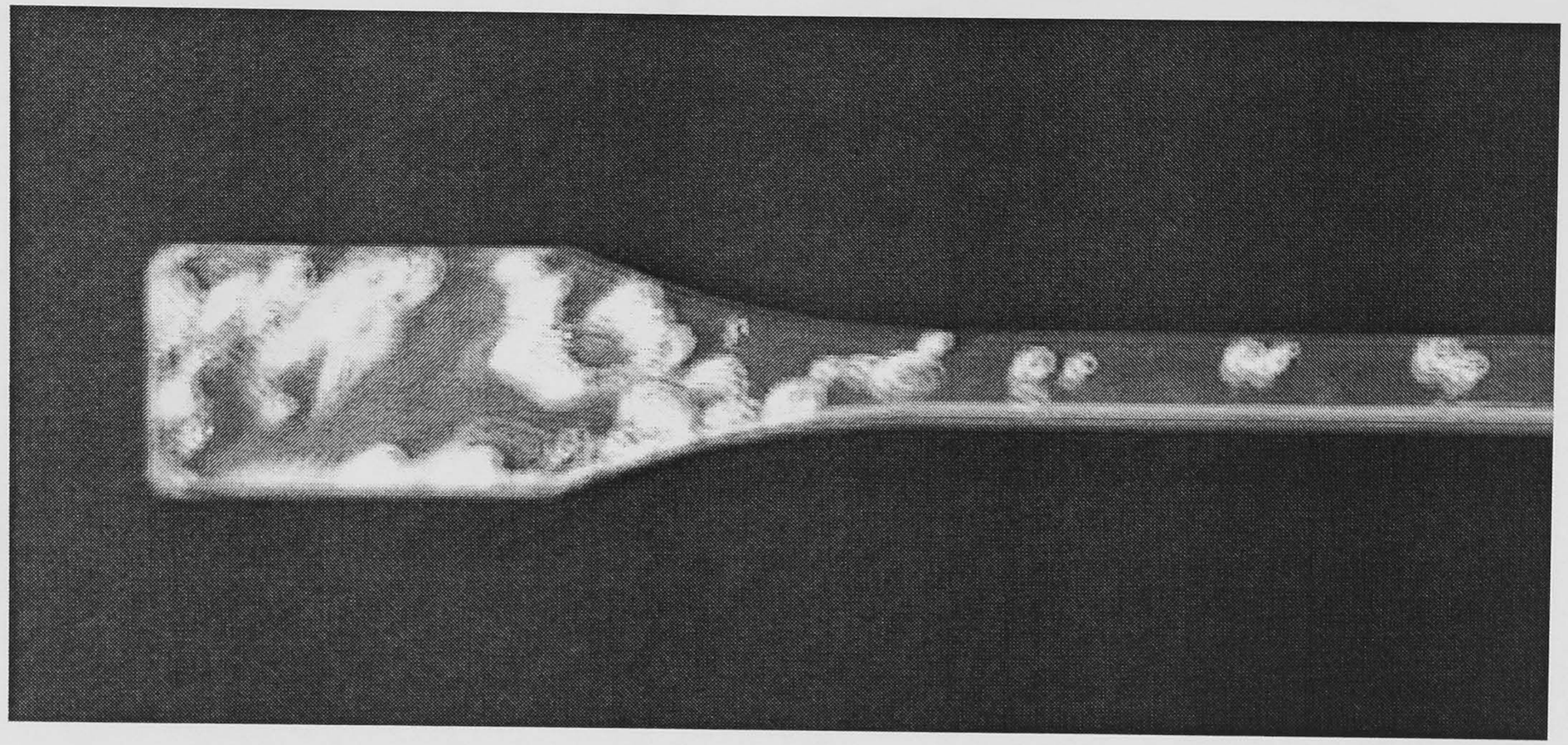

Figure 4.5 Observable voids in a specimen due to the use of improper degassing time

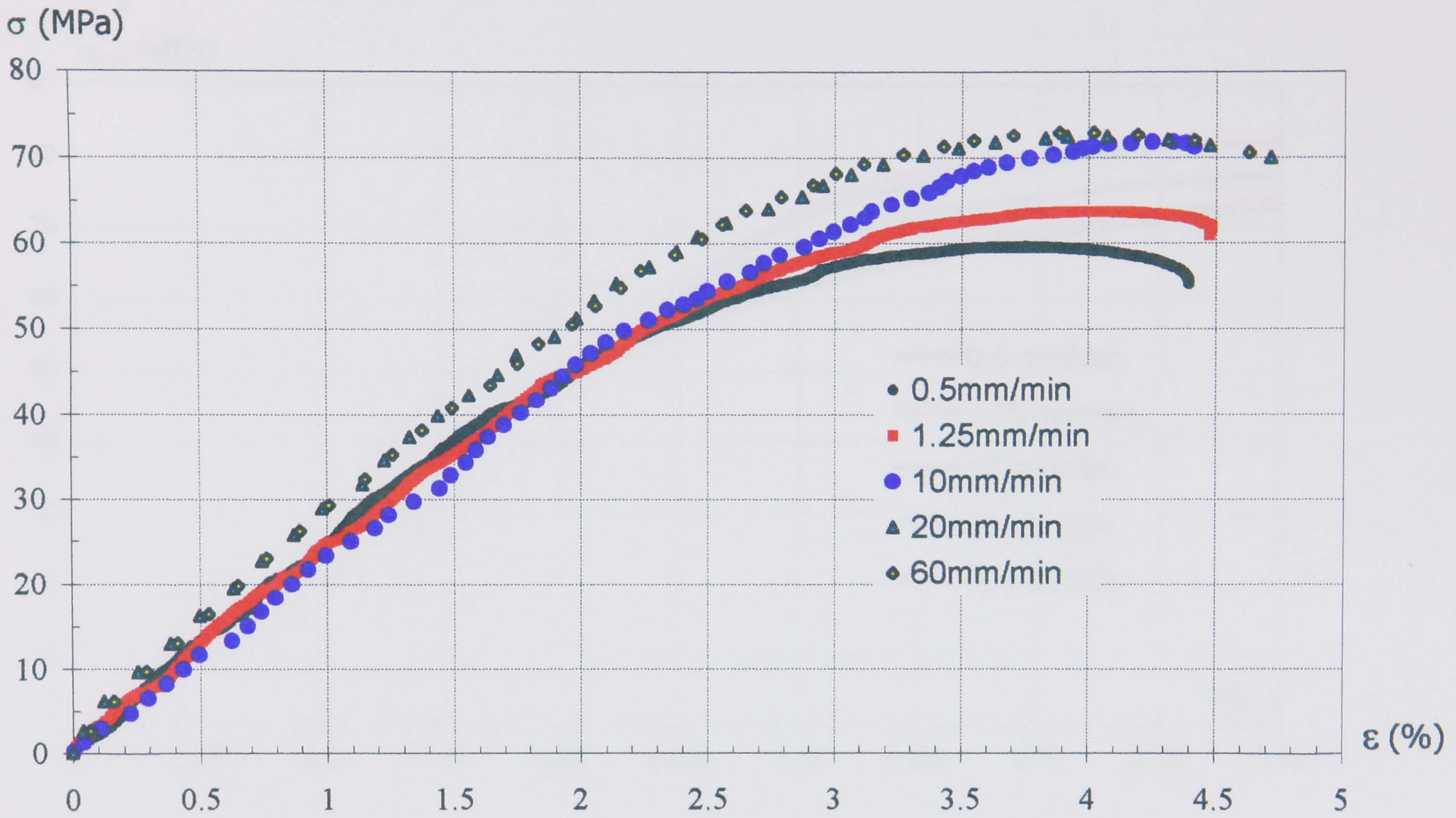

Figure 4.6 Stress-strain relationships, obtained from rate dependent tensile testing

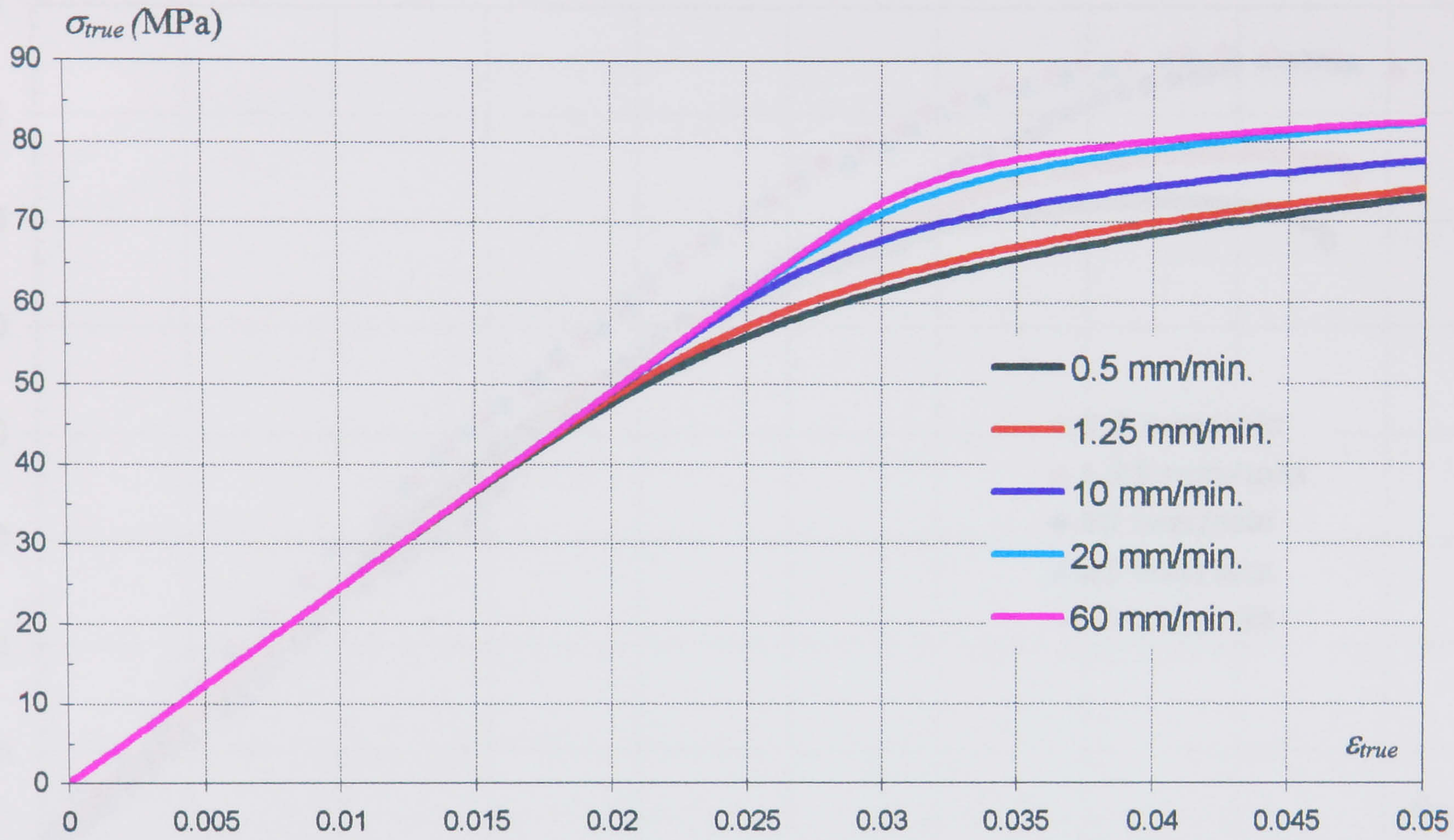

Figure 4.7 True stress-strain relationships of epoxy plotted using Ramberg-Osgood equation

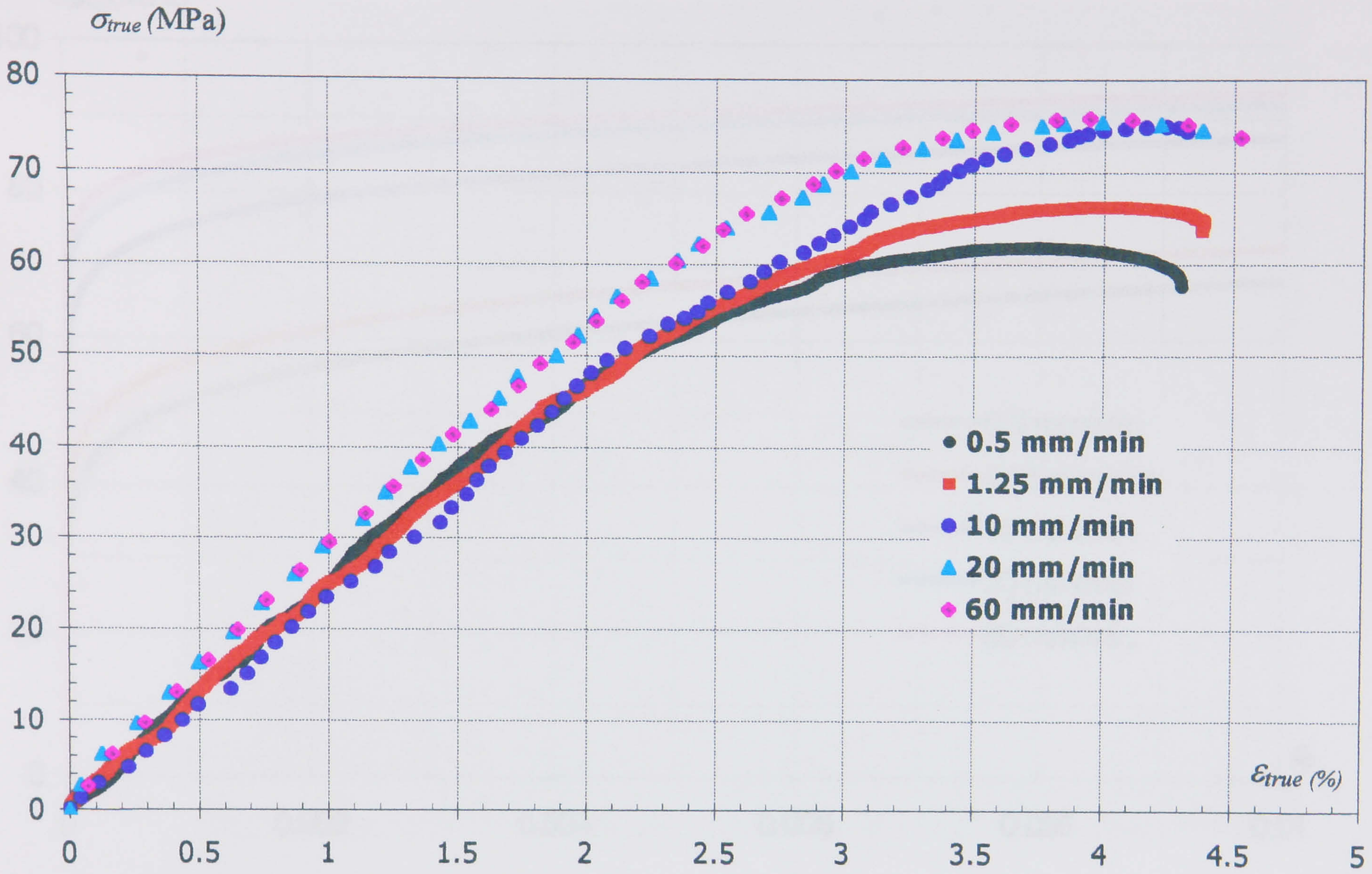

Figure 4.8 True stress-strain relationships, obtained from rate dependent tensile testing

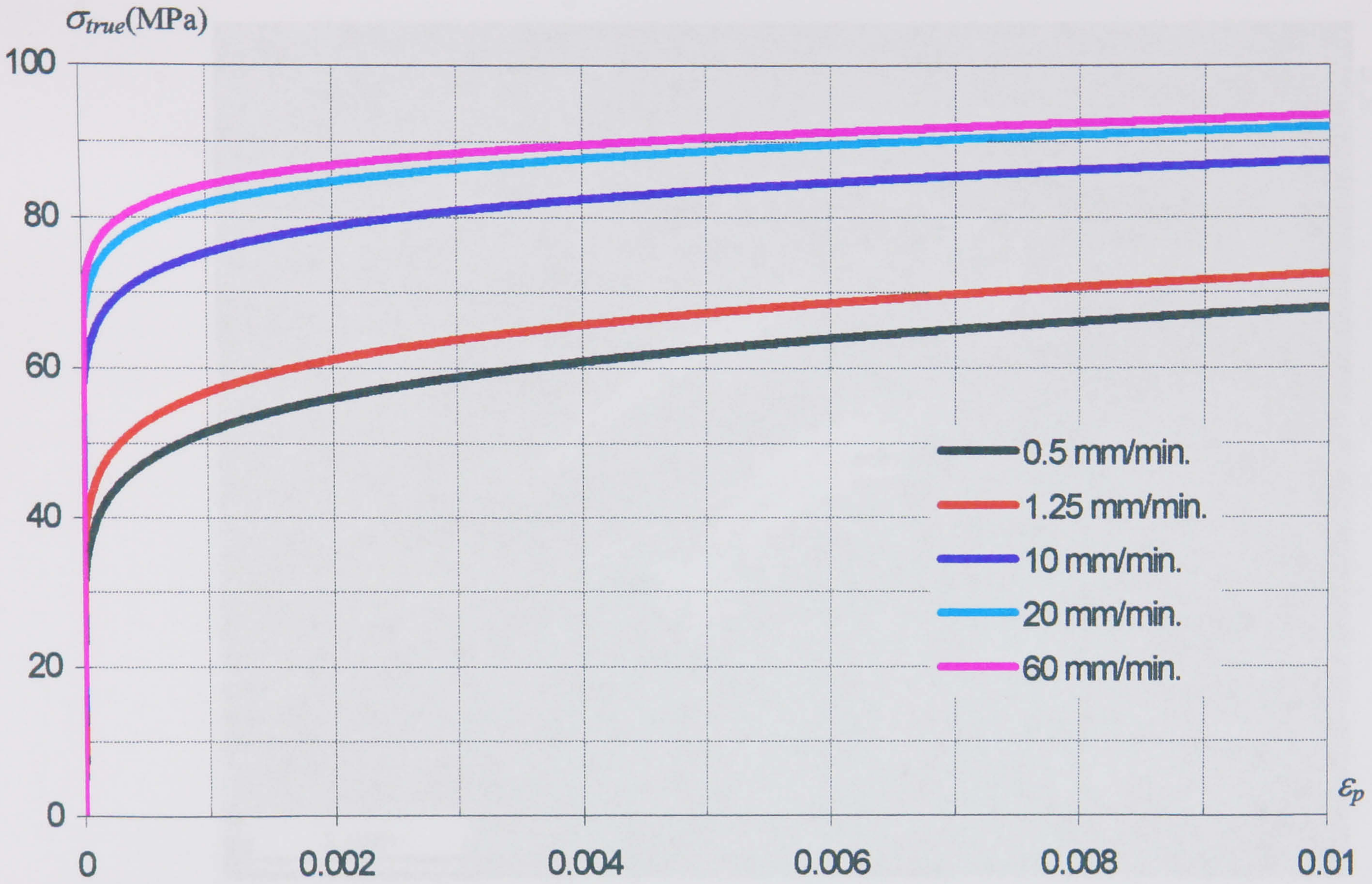

Figure 4.9 True stress/plastic strain curves at different strain rates

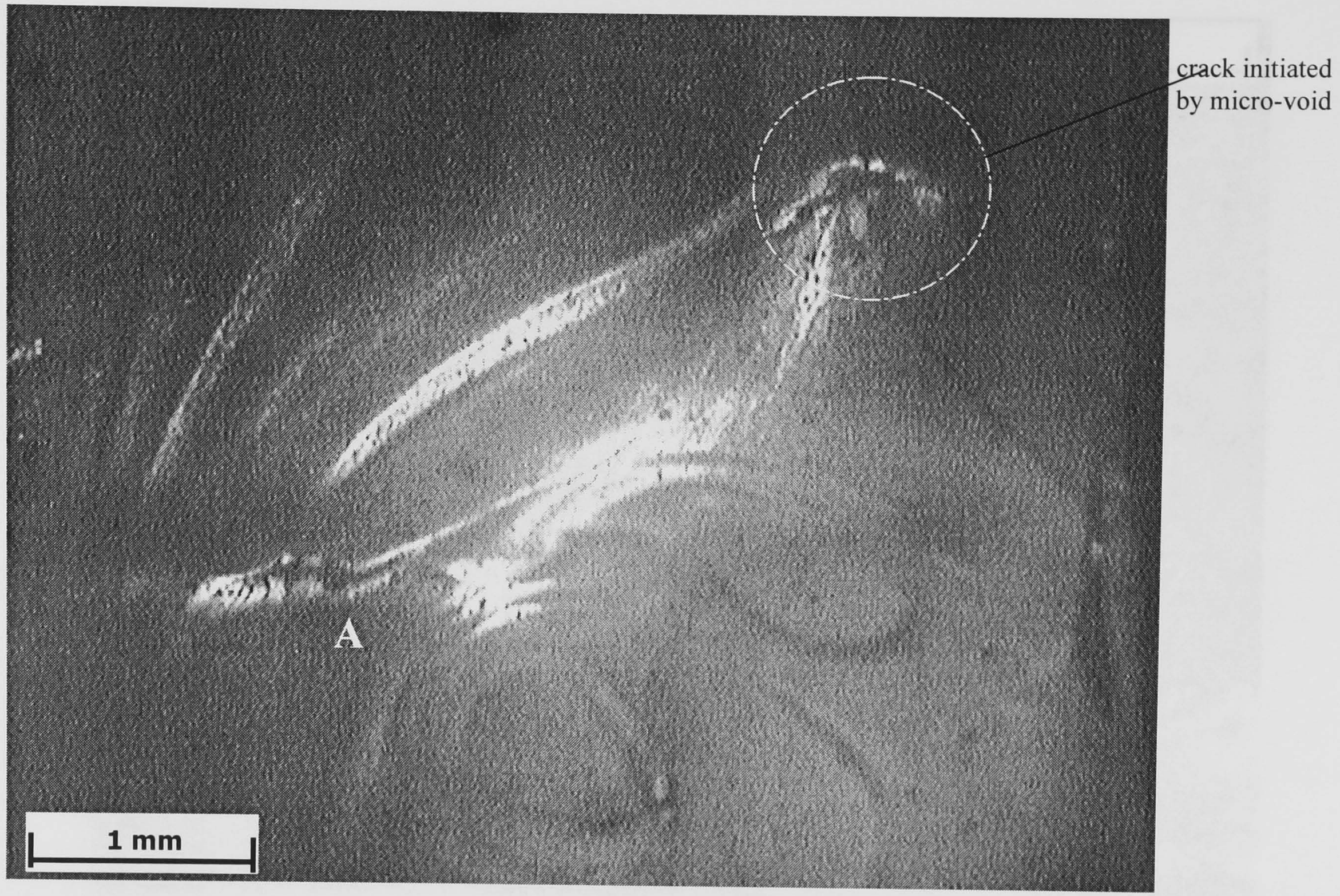

Figure 4.10 Fracture surface of epoxy specimen tested at a strain rate of 0.01 min^{-1}

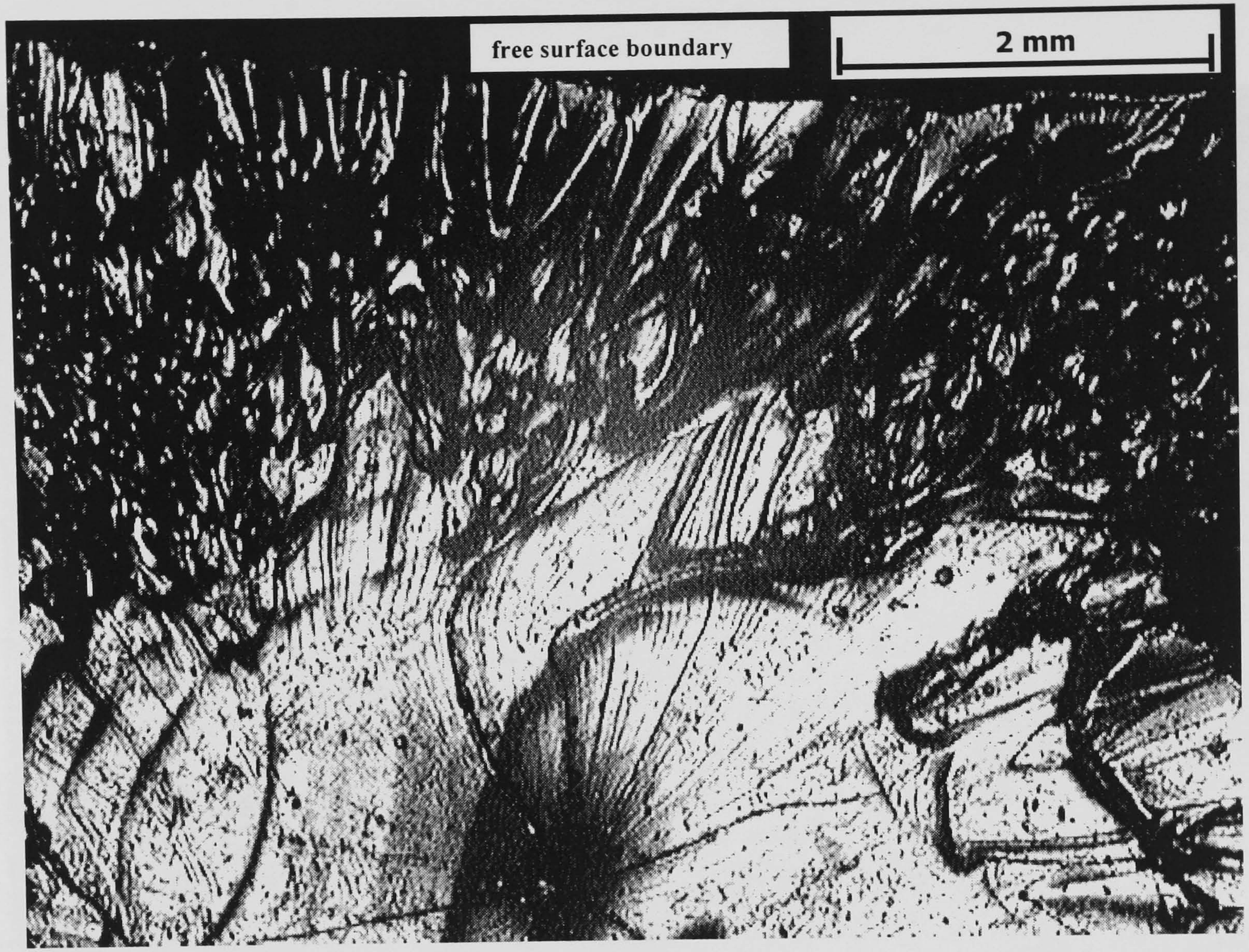

Figure 4.11 Fracture surface on top left side of epoxy specimen tested at a strain rate of 1.2 min^{-1}

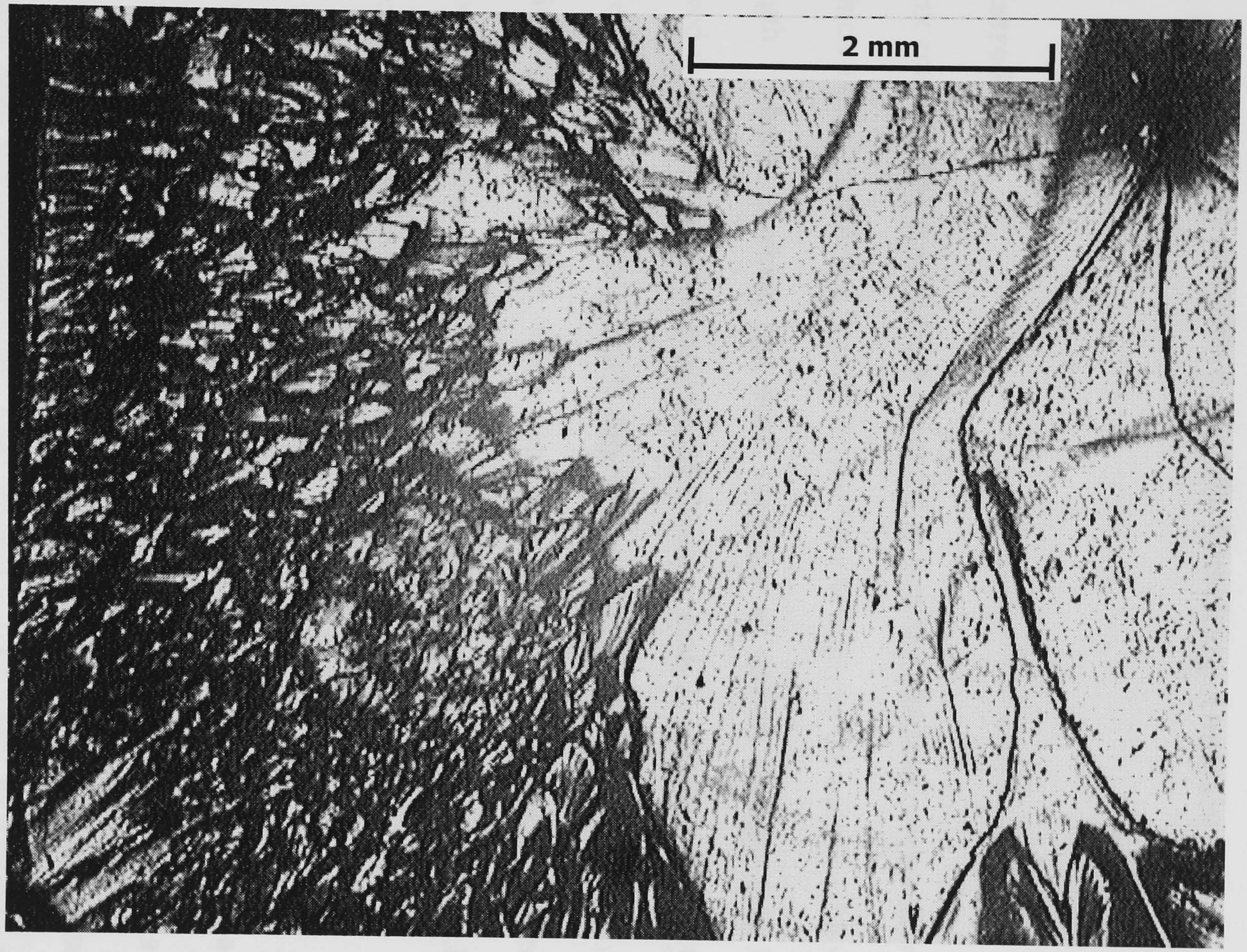

Figure 4.12 Fracture surface on bottom left side of epoxy specimen tested at a strain rate of 1.2 min^{-1}

CHAPTER 5

Rate-sensitive Matrix Cracking Analysis

5.1 Introduction

Matrix cracking has usually been observed in a strong interface composite system in which a coating material is used for the fibre to improve the interfacial bonding strength. Matrix cracking has been classified as serious damage that is not allowed to occur in some composite applications such as pressure vessels [105]. The existence of a matrix crack depends on several factors, such as loading conditions, matrix ductility, viscoelastic or viscoplastic behaviour of the matrix, micro-void concentration etc. Failure mechanisms that induce a matrix crack in a long carbon-fibre composite are discussed in this chapter.

In a typical fragmentation test, a composite is subject to tensile loading at a very slow strain rate (i.e. 0.25×10^{-2} min^{-1}). The stress transfer characteristics of a continuous (long) carbon fibre embedded in an epoxy matrix subjected to such a test have been investigated using laser Raman spectroscopy by Galiotis *et al.* [27,28]. The first fibre fracture in this composite system was found to occur at an applied strain level of about 1.3%, unlike failure in a short carbon fibre system which occurs at a very low applied strain (see Section 3.4.). As a result of fibre fracture, the load previously carried by a broken fibre is then transferred to the weaker matrix material through the fibre/matrix interface. Shear stress, which

transfers across the interface, would induce an interface crack (Mode β) in the composite if the interfacial shear strength of the interface is not strong enough. In the case of a strong interface, the load transferred would induce one or more of several forms of crack in the matrix material [13] (see Fig. 5.1).

The effect of fibre recoil is to induce a higher strain rate in the matrix region near the crack tip. The higher strain rate increases the strength and stiffness of the epoxy (see details in Section 3). The semi cone angle of a matrix crack in a long fibre system is observed from experiment to be a little larger than the angle of a matrix crack in a short fibre composite. Thus, the strain rate in the matrix region near the crack tip would have an effect on the angle of matrix crack and the development of plastic strain in the matrix material. Fracture mechanisms in this case would be a rapid crack-growth process rather than a slow one as found in short fibre system [36]. Only conical-shaped matrix cracks (Mode γ) and interface cracks (Mode β) were observed experimentally for this composite system [27,28]. The matrix crack Mode γ is likely to occur in sized systems only, as described in Section 3.1. The investigation of the fracture mechanisms of a matrix crack (Mode γ) and the prediction of the direction of crack propagation are the aims of the work described in this chapter.

The most suitable analysis tool that makes the investigation of stress/strain characteristics in rate-sensitive material more realistic would be viscoplastic FE analysis. Progressive failure mechanisms in this composite system involve a complex stress field. The energy approach, such as the minimum strain energy

density criterion, would be a good choice since this criterion is easy to apply and the complex stress field will be converted to an energy field. This criterion was used to predict the angle of matrix crack initiation in several unloading conditions [106]. Comparison of the results in this study obtained from linear-elastic, elasto-plastic, and viscoplastic FE analyses are discussed. The predicted angle of crack propagation from this work was also used for modelling pre-existing cracks of variable length in FE models to estimate the crack length in its work discussed in the next chapter.

5.2 Prediction of Matrix Crack Propagation Direction

The fracture mechanisms of short fibre and long fibre composites are different. As mentioned earlier in Section 3.1, a matrix crack in short fibre system is likely to be governed by micro-voids within the matrix material and a slow crack growth process dominates. In the case of the long fibre composite with a strong interface, the fibre fracture event induces the rapid crack growth that would extend the penny-shaped fibre crack into the matrix material to form the disc-shaped or conical-shaped cracks.

Since matrix plasticity, viscoplastic behaviour, and mixed-mode loading are involved in this event, the minimum strain energy density criterion [107] was chosen to predict the crack propagation direction. The strain energy density function *(dW/dV)* is given by:

$$\frac{dW}{dV} = \int_0^{\varepsilon_{ij}} \sigma_{ij} d\varepsilon_{ij} \qquad (5.1)$$

where W is the strain energy, V is a given volume and σ_{ij} and ε_{ij} are the stress and strain tensors, respectively.

It has been observed that at a given scale level, yielding and fracture occur at different locations [107]. This is because yielding involves a permanent shape change in a material due to excessive distortion, while fracture refers to excessive dilatation (see Fig. 5.2). Many locations that have a maximum or minimum value of (dW/dV) would be observed around the area of interest. The variation of the strain energy density would appear as peaks and valleys (see Fig. 5.2). The maximum value of the strain energy density among the other minimum value locations $(dW/dV)_{\min}^{\max}$ implies a critical fracture location. This is consistent with intuition which suggests that a large volume change (macrodilatation) leads to fracture and shape change (macrodistortion) leads to permanent deformation. The area between the maximum and minimum value of the strain energy is subject to macrodistortion and microdilatation, which are responsible for permanent deformation and creation of microcracks.

5.3 FE Model

Since fracture mechanisms are dominated by the viscoplastic behaviour of the epoxy matrix, viscoplastic FE analysis is an appropriate tool to investigate this failure mechanism. ABAQUS has a feature to take account of rate-sensitive material properties. The viscoplastic behaviour of a material in ABAQUS is

defined by entering hardening curves at different equivalent plastic strain rates $\dot{\bar{\varepsilon}}^{pl}$. ABAQUS uses the Lagrangian mechanical modelling capabilities, which will keep all of the loading and deformation history for use in the next step of the analysis. In order to take account of the effect of the rate-sensitive material response during the fibre-breaking event, the unloading time is required in this simulation step. The unloading time refers to a given time for the FE analysis to ramp the residual forces on the fibre end face down to zero with a constant stress rate assumption [100]. ABAQUS calculates the strain-rate by using a rate of change of the spatial position, x, of a fixed material particle with respect to time to define velocity of a material particle, which is expressed as

$$\mathrm{v} = \frac{\partial x}{\partial t} \tag{5.2}$$

and the strain rate can be obtained from

$$\dot{\varepsilon} = \frac{d\mathrm{v}}{dx} \tag{5.3}$$

When inelastic deformation is taking place, this strain rate is defined using the classical *strain rate decomposition* [100], which is expressed as

$$\dot{\varepsilon} \approx \dot{\varepsilon}_{elastic} + \dot{\varepsilon}_{plastic} \tag{5.4}$$

On the basis of experimental observation [27,28], the unloading time was found to be less than one second. Values of unloading time equal to 0.1, 0.5 and 1 second,

which are assumed to cover the range of the actual unloading time, were chosen and used in this FE analysis.

Rate-sensitive stress/strain curves for MY750 epoxy obtained from experiment were used in these FE analyses (see Fig. 4.8). The mechanical properties of carbon fibre are the same as were used in the FE analysis for short fibres system (see Table 2.1). In order to investigate the effect of viscoplasticity on deviation of the angle of crack propagation, linear-elastic, elasto-plastic FE analyses were also performed and the results compared with those from viscoplastic FE analysis.

Axisymmetric FE models used for this work have the outer composite radius R_c = 50 μm, composite length l_c = 260 μm, fibre radius r_f = 3.25 μm and the mesh consists of 2,208 eight-node elements (see Fig. 5.3). The mesh was highly refined in the vicinity of the crack tip and collapsed eight-node axisymmetric triangular crack tip elements [99] were employed around the crack tip.

The 'Progressional Approach' [36] was implemented with all of these FE analyses by separating the analysis into three load steps. The first load step was a simulation of the curing process in which a temperature drop of 60 °C was applied to the entire composite, thereby inducing the thermal residual stresses in the composite. A uniform displacement δ was applied to one side of the boundary of the FE model in the axial direction to produce a mechanical strain of 1.3 % in the second load step. At this strain level, first fibre fracture was found experimentally. Fibre fracture was simulated by removing the constraints in the

y-direction (see Fig. 5.3) from the fibre end face in the last load step. In order to predict the direction of crack propagation, the strain energy density was calculated at every nodal point around a given critical radius r_c. The value of the critical radius of 0.2 μm was chosen (see Section 3.3) to avoid the fluctuation by the effect of collapsed elements (see Fig. 5.3). This value is about 32 times smaller than the fibre diameter.

5.4 Results Summary

5.4.1 Linear elastic FE results

In the case of a brittle matrix, use of linear elastic FE analysis is adequate to investigate the stress/strain behaviour of the composite. In order to understand this fracture mechanism before starting with the complex analysis, brittle fracture was assumed and linear elastic FE analysis was used to investigate the mechanical behaviour of composite. The variation of the strain energy density around a defined critical radius r_c is calculated by linear elastic FE analysis. The maximum value of strain energy density, which was found in the region near the interface, implies the possibility of large deformation that may take place in this region. The strain energy density decreases gradually from the interface and reaches its minimum value at 90° to the fibre axis (see Fig. 5.4). This may imply that a disc-shaped matrix crack is likely to occur in this composite system (see Fig. 5.1). This prediction does not correspond well with experimental observations since a disc-shaped crack has never been observed in this composite system. In reality, MY750 epoxy is not entirely brittle but exhibits localised yielding near the crack

tip [90]. Performing linear elastic FE analysis does not give an accurate prediction for this composite system.

5.4.2 Elasto-Plastic FE results

When the fibre breaks, matrix ductility may absorb the fracture energy by extending its permanent deformation in the vicinity of the crack tip. The direction of crack initiation may deviate by this effect. In order to clarify the exact failure of matrix material, the development of plastic strains near the fibre fracture location must be taken into consideration. A very high equivalent plastic strain of about 400% was developed in the matrix material in the vicinity of the crack tip (see Fig. 5.5). This may imply that catastrophic failure will take place in that region. The maximum value of the strain energy density occurs at the fibre/matrix interface, which is the same result obtained from linear elastic FE analysis. The interfacial shear strength of the fibre/matrix interface plays an important role in preventing an interface crack (Mode β) in the composite. The strain energy density decreases gradually and reaches a minimum value at an angle between 26°-30° to the fibre axis. It then increases up to 90° to the fibre axis (see Fig. 5.6).

Fracture, which would take place after yielding, may occur at the location that the strain energy density turns from the highest peak value to its first minimum value. This criterion implies that a conical-shaped matrix crack would initiate at the angle that lies between 26°-30° to the fibre axis. This analysis predicts a crack initiation angle, which is still slightly lower than the angle observed from experiment.

5.4.3 Viscoplastic FE results

Epoxy matrix is a rate-sensitive thermoset polymer. After the fibre breaks, the fibre recoil may induce a high strain rate in a region near the crack tip leading to a pronounced effect on the mechanical properties of the epoxy matrix. The unloading process after the fibre breaks would be very complicated since the mechanical behaviour of the matrix material depends on the local strain rates. Viscoplastic FE analysis, which takes account of rate-sensitive properties, was used to investigate this process.

At the total unloading time of 1 second, variations of strain rate at a critical radius and at 1 second after the fibre breaks are plotted in Figs. 5.7 – 5.10. The values of these strain rates in the FE calculation do not have the same values as the real strain rates occurring in the fibre-breaking event. Matrix cracking or interface debonding may occur immediately after the fibre fracture, which in turn reduces the value of the strain rates. The variations of these artificial strain rates can be used as a guideline to examine how strain rate develops in the material. Negative values of radial strain rate $\dot{\varepsilon}_{rr}$ were found near the interface and have a maximum value of about -51 min^{-1} at about 34.5 % of the total unloading time. The value of radial strain rate has turned to a positive value around the angle that lies in the range 45°-50° and has its maximum value at about 41 min^{-1} at 90° at the end of the unloading step. The value of axial strain rate $\dot{\varepsilon}_{zz}$ also has a peak value of about 57 min^{-1} at about 34.5 % of the total unloading time. The peak value decreases suddenly to the value about –8 min^{-1} as the unloading time increased only 5.5 % of the total unloading time. The shear strain rate $\dot{\varepsilon}_{r\theta}$ has a highest

value at 137 min^{-1} near the interface, at about 40% of the unloading step. Hoop strain rate $\dot{\varepsilon}_{\theta\theta}$ has negative values about –2.3 to -2.5 min^{-1} near the interface and has a maximum value about –4 min^{-1}.

The development of strain energy density around a critical radius in each unloading time steps is shown in Fig. 5.11. The strain energy at 90° to the fibre axis was built up rapidly in the range 32 – 45 % of the total unloading time and implied the initiation of conical-shaped matrix crack.

At the unloading time of 0.5 second, strain rates were found to have twice compared to the first case. Shapes of strain rates in both cases look similar (see Figs. 5.12-5.15). The maximum negative value of $\dot{\varepsilon}_{rr}$ in this case was found at – 131 min^{-1} at about half unloading step. It then increased gradually and has its maximum value about 79 min^{-1} at the end of unloading time step. The maximum value of strain rate in axial direction $\dot{\varepsilon}_{zz}$ of about 137 min^{-1} occurred near the interface at about half of the unloading step. The values of strain rate in angular direction $\dot{\varepsilon}_{\theta\theta}$ are also about twice compared to the first case. A very high value of strain rate in the shear component $\dot{\varepsilon}_{r\theta}$ of about 478 min^{-1} was found near the interface at about half the unloading step. The critical unloading time that maximum strain rates were induced would be at about half of the unloading time step. The same shapes of strain energy density development around a critical radius in each unloading time steps are shown in Fig. 5.16.

At a very short unloading time about 0.1 second, the values of all components of strain rate are very high (see Figs. 5.17-5.20). The maximum values of $\dot{\varepsilon}_{rr}$, $\dot{\varepsilon}_{\theta\theta}$, $\dot{\varepsilon}_{zz}$ and $\dot{\varepsilon}_{r\theta}$ are –500 min^{-1}, –38 min^{-1}, 650 min^{-1} and 1,930 min^{-1}, respectively. All of those values were found near the interface at about half unloading step. The excessive values of strain rates in this defined unloading time would make the results from this analysis unrealistic since the strain rates in the real event must be lower than these values. The same shapes of strain energy density development around a critical radius in each unloading time steps are shown in Fig. 5.21.

As can be seen from the experimental results (see Fig. 4.6), epoxy matrix exhibits an increase in stiffness as the strain rate is increased. This would lead to a slightly reduction in the equivalent plastic strains in the matrix material. This study has found an equivalent plastic strain decreased from 400 % in an elasto-plastic FE analysis to about 350 % in a viscoplastic FE analysis at a specified fibre-fracture time of about 0.1 second. The first minimum value of strain energy density after the peak value was found to lie between the angle of 32°-36° in all cases (see Fig. 5.22). This corresponds well with the real fibre breaking time observed from the experiment (about less than one second), but the realistic fibre breaking time suggested by these analyses would lie between 0.5 – 1 second. This may imply that the angle of crack initiation would have changed its location according to the strain rate around a region near the crack tip. This analysis gives a better prediction for the angle of crack initiation and corresponds well with experimental observation.

5.5 Discussion

Failure in a long fibre composite in the fragmentation test is quite different from failure in a short fibre composite. Failure in a long fibre composite usually takes place at a high-applied strain level, whereas for a short fibre composite, failure occurs at a low applied strain level and involves a slow crack growth. As can be seen from the FE results (see section 5.4.4), the matrix ductility plays an important role on inducing a conical-shaped matrix crack in this composite system.

The existence of a conical-shaped matrix crack or a disc-shaped matrix crack may rely on the strain rate, which in turn depends upon the fibre-recoil time. The unloading time after the fibre breaks determines the strain rate near the crack tip. If the strain rate in that area is high enough to produce an almost linear stress/strain curve in the matrix material, a disc-shaped matrix crack is likely to be formed. However, only interface debonding and conical-shaped matrix cracks have been observed by experiment for this composite system [27,28]. This means that the strain rate induced by fibre recoil in this composite system was not high enough to bring about the stress/strain relationship to behave linear elastically.

Very high values of the shear strain rates in the matrix near a fracture location, calculated by viscoplastic FE analysis, were found to be varying during the unloading process. This may imply that matrix cracks have already taken place before the unloading process reaches the equilibrium conditions. Although the strain rates calculated by FE analysis are estimates, the development of strain rates during the unloading process can be used to observe trends. By applying the

minimum strain energy density criterion to the FE results, the predicted crack angle lies in the range of 32°-36°. These predicted crack angles are about twice those predicted for a short fibre system (see section 3.4.3).

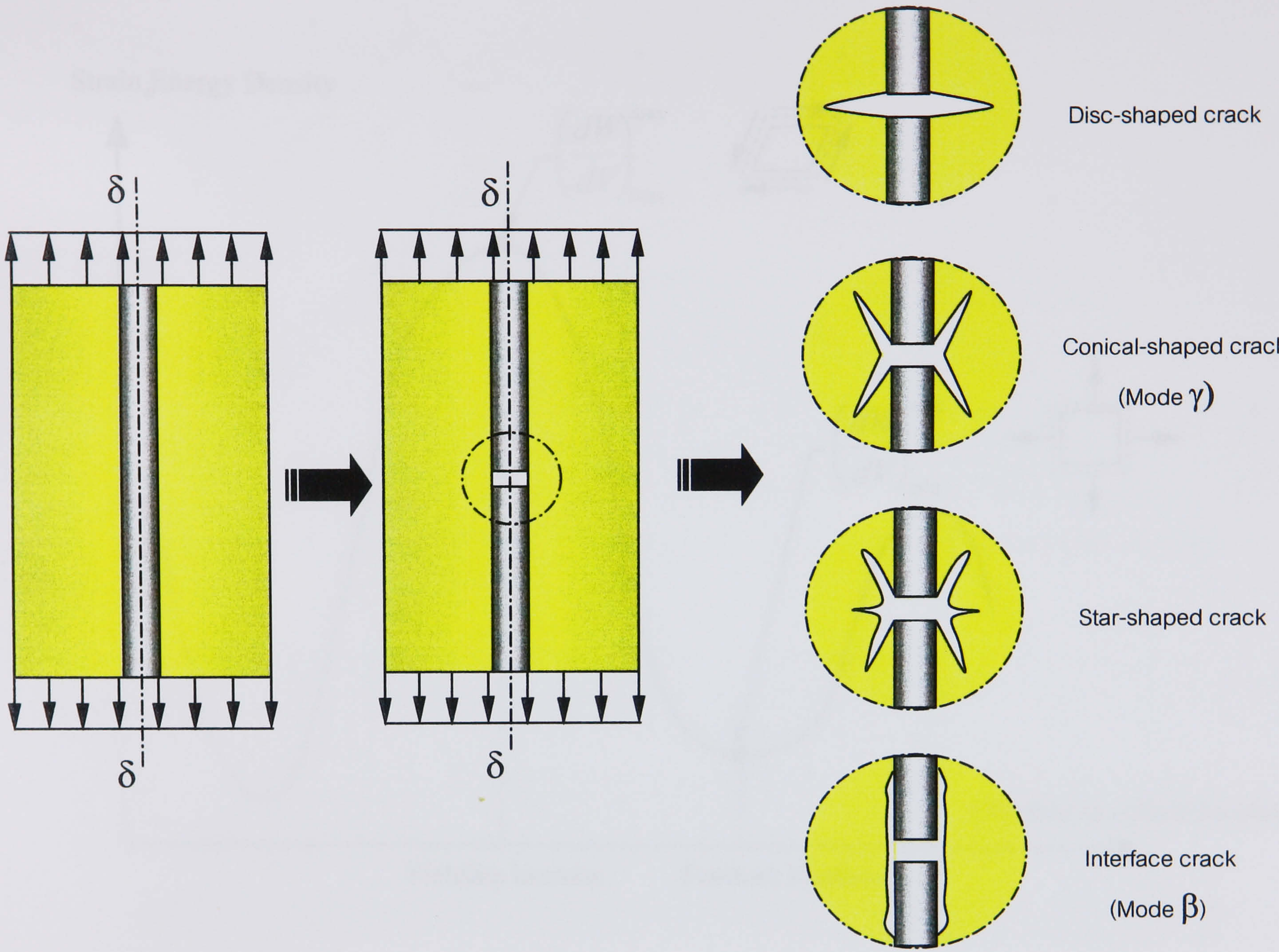

Figure 5.1 Fracture mechanisms of composite in a fragmentation test

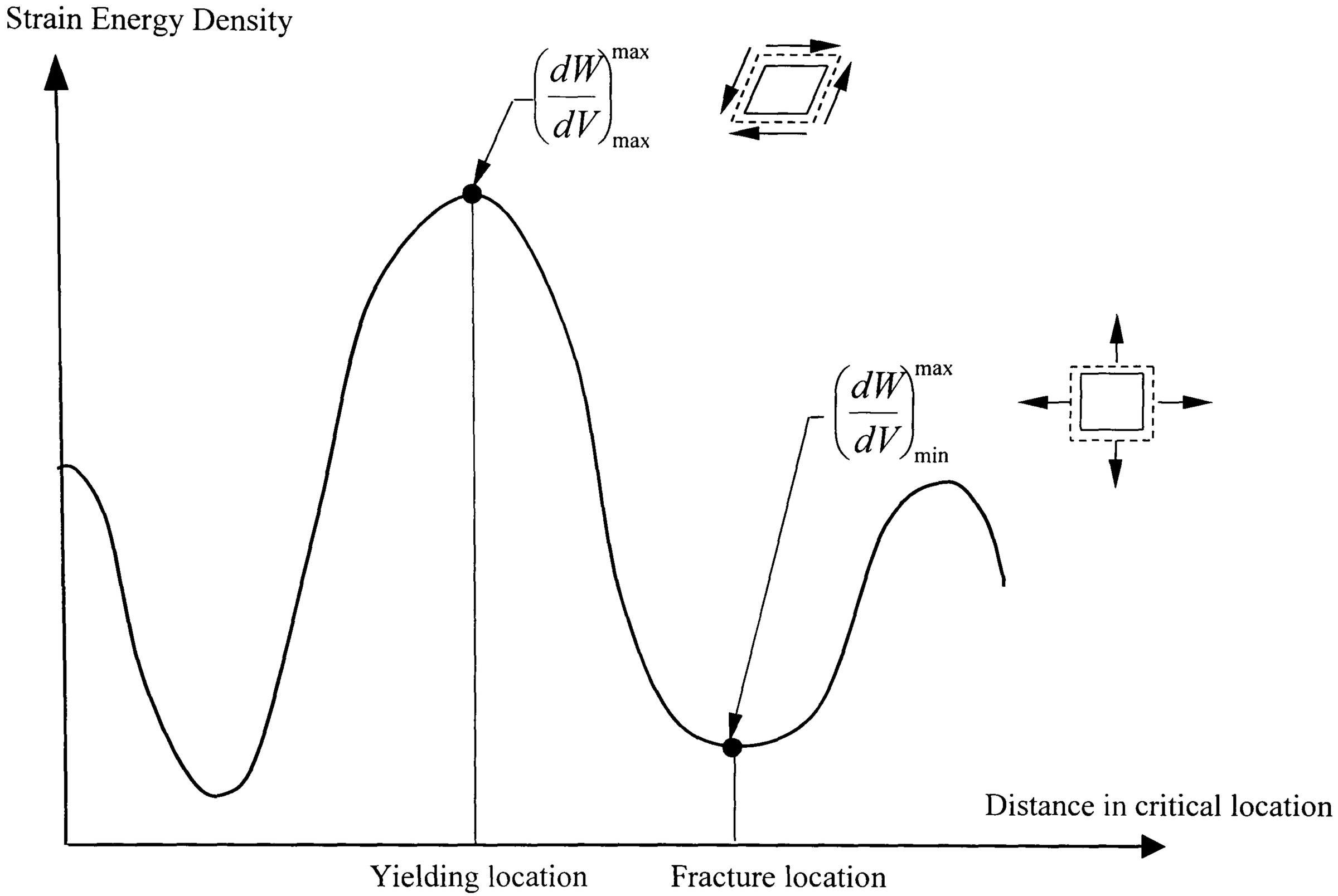

Figure 5.2 Definition of yielding and fracture locations in the fluctuation of strain energy density function

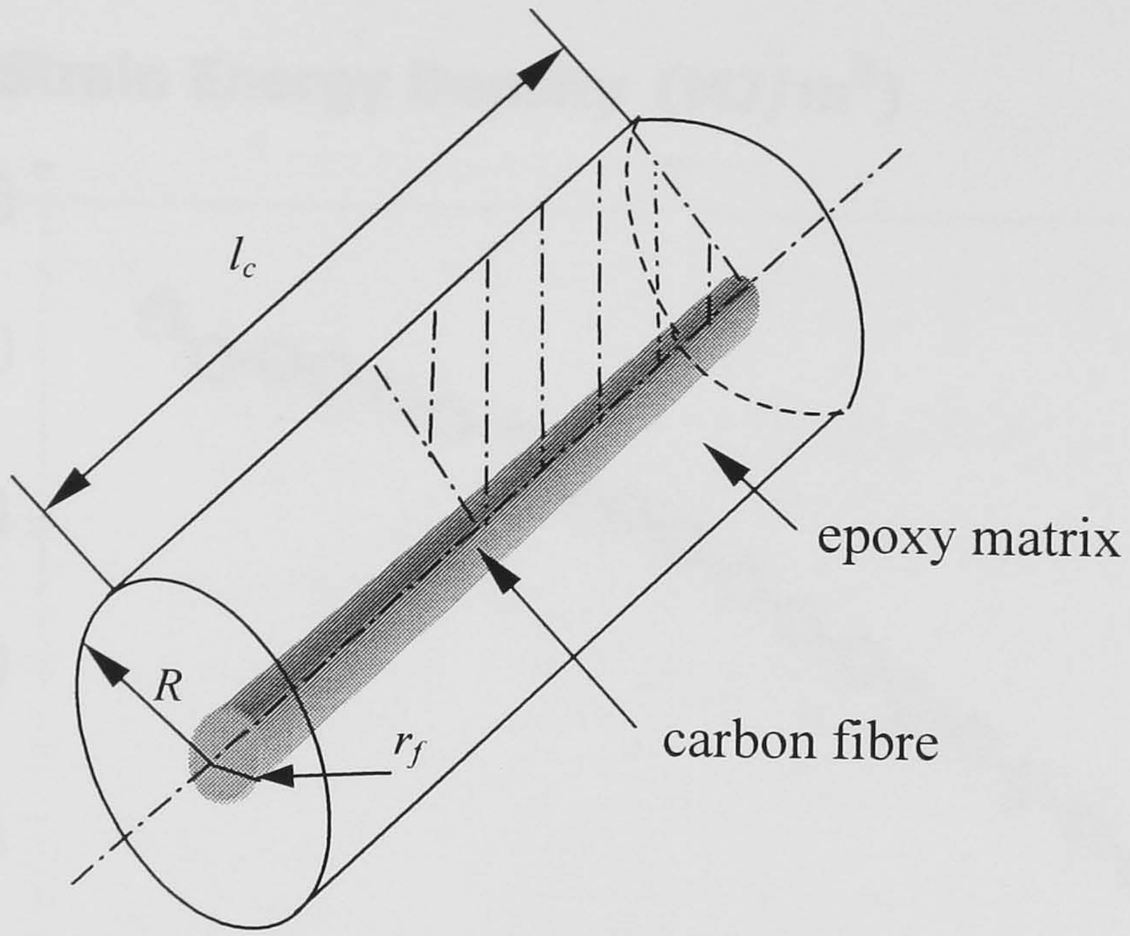

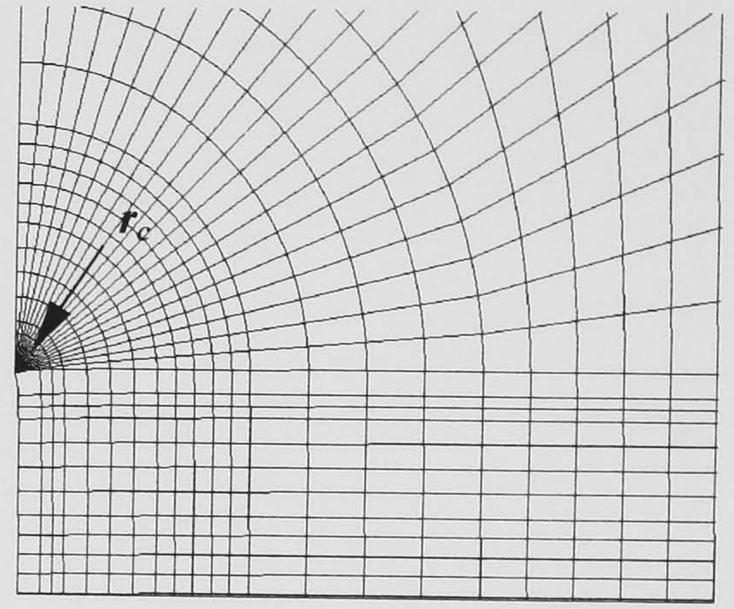

Detail of crack tip mesh

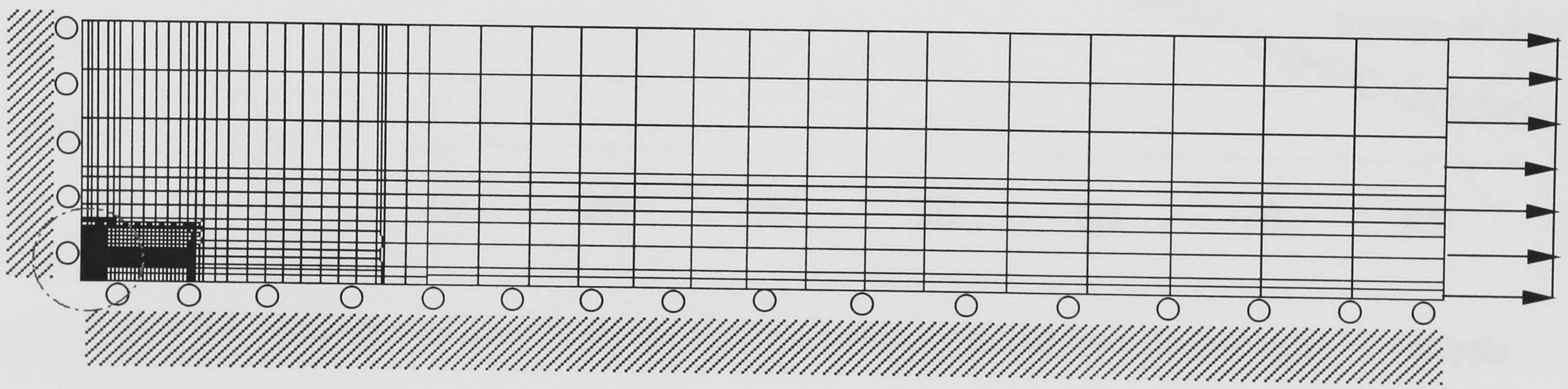

Figure 5.3 Finite element model and mesh detail near a crack tip

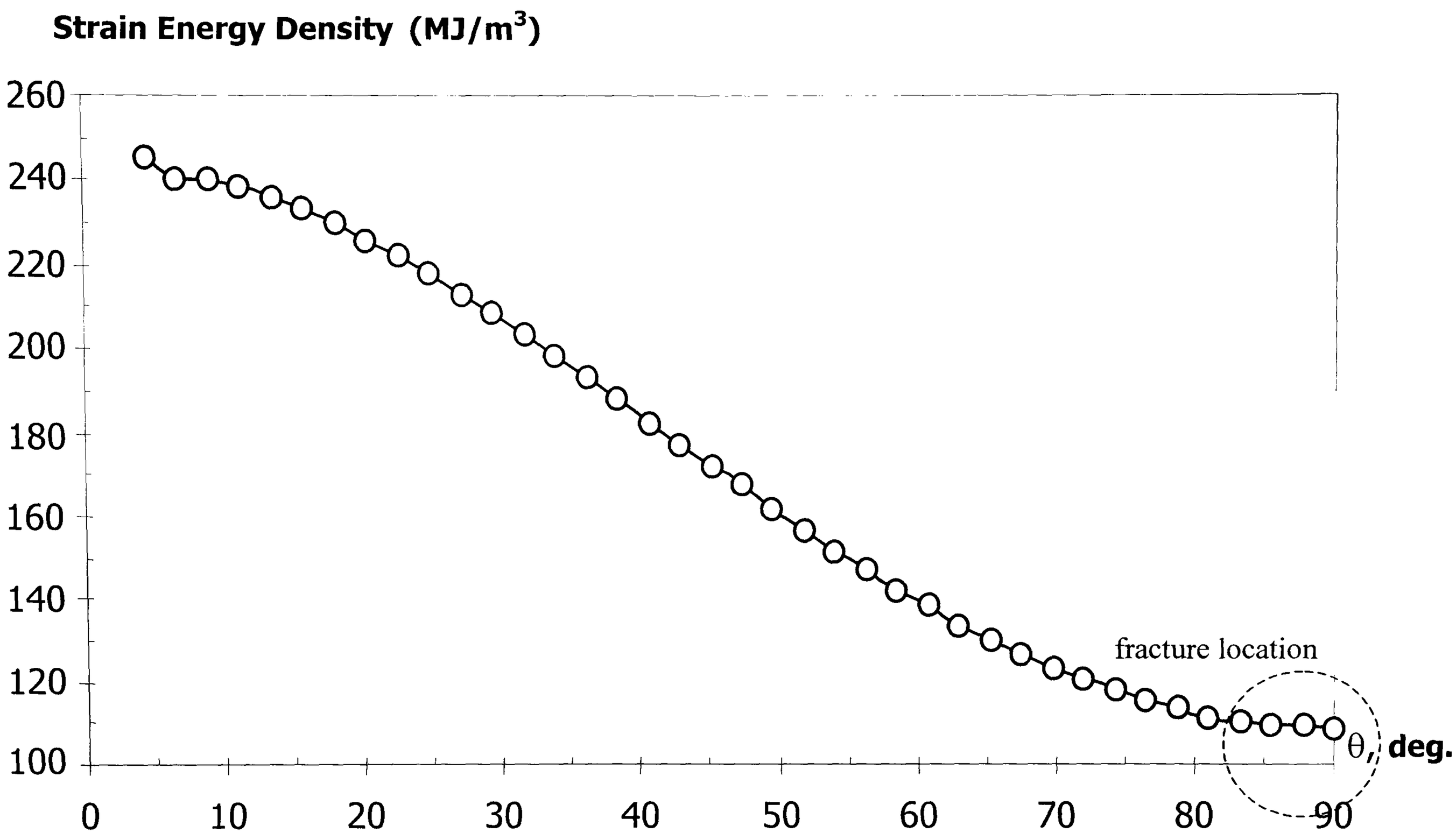

Figure 5.4 Strain energy density around a critical radius, obtained from linear elastic FE analysis

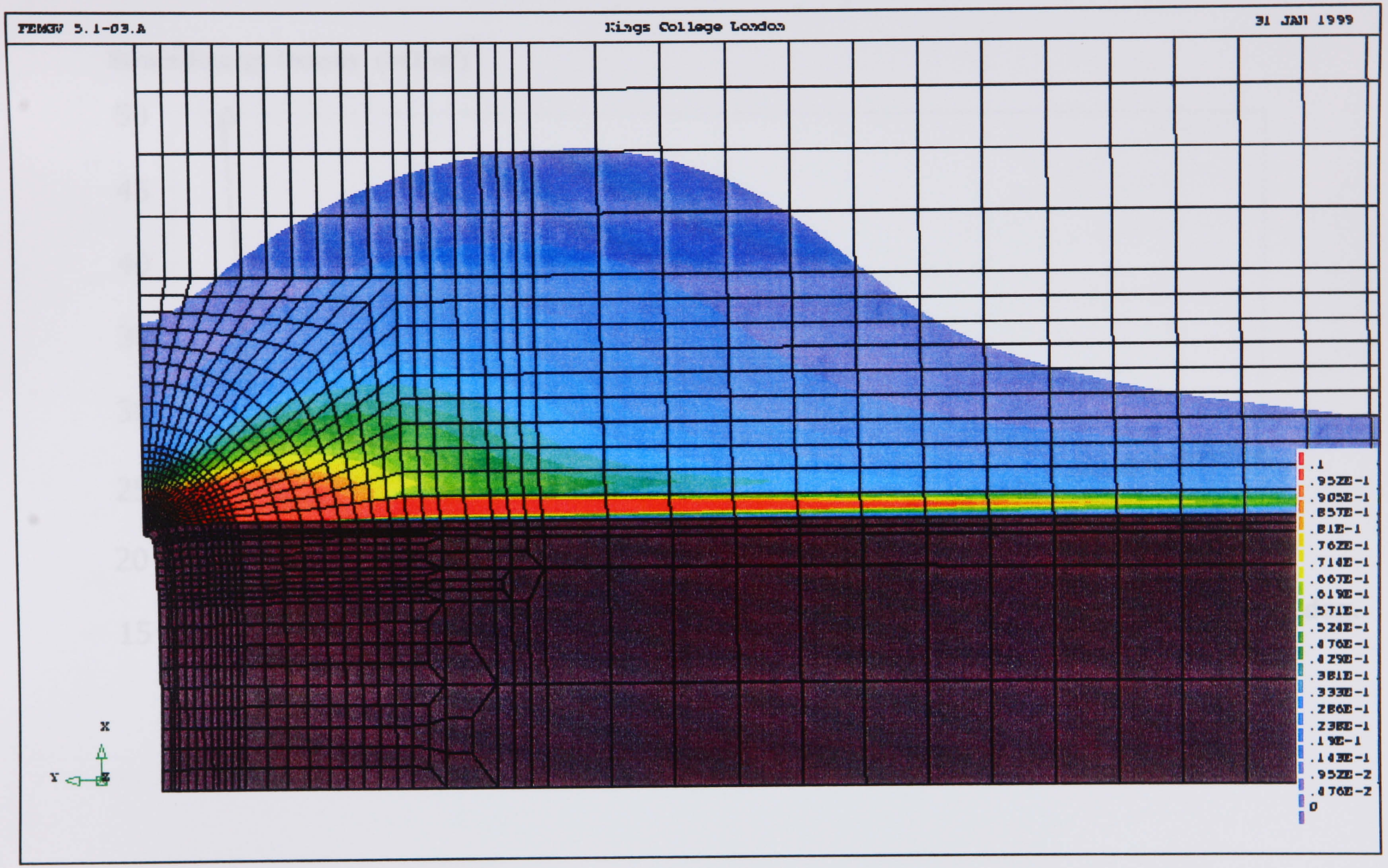

Figure 5.5 Equivalent plastic strain distribution in a region near a crack tip

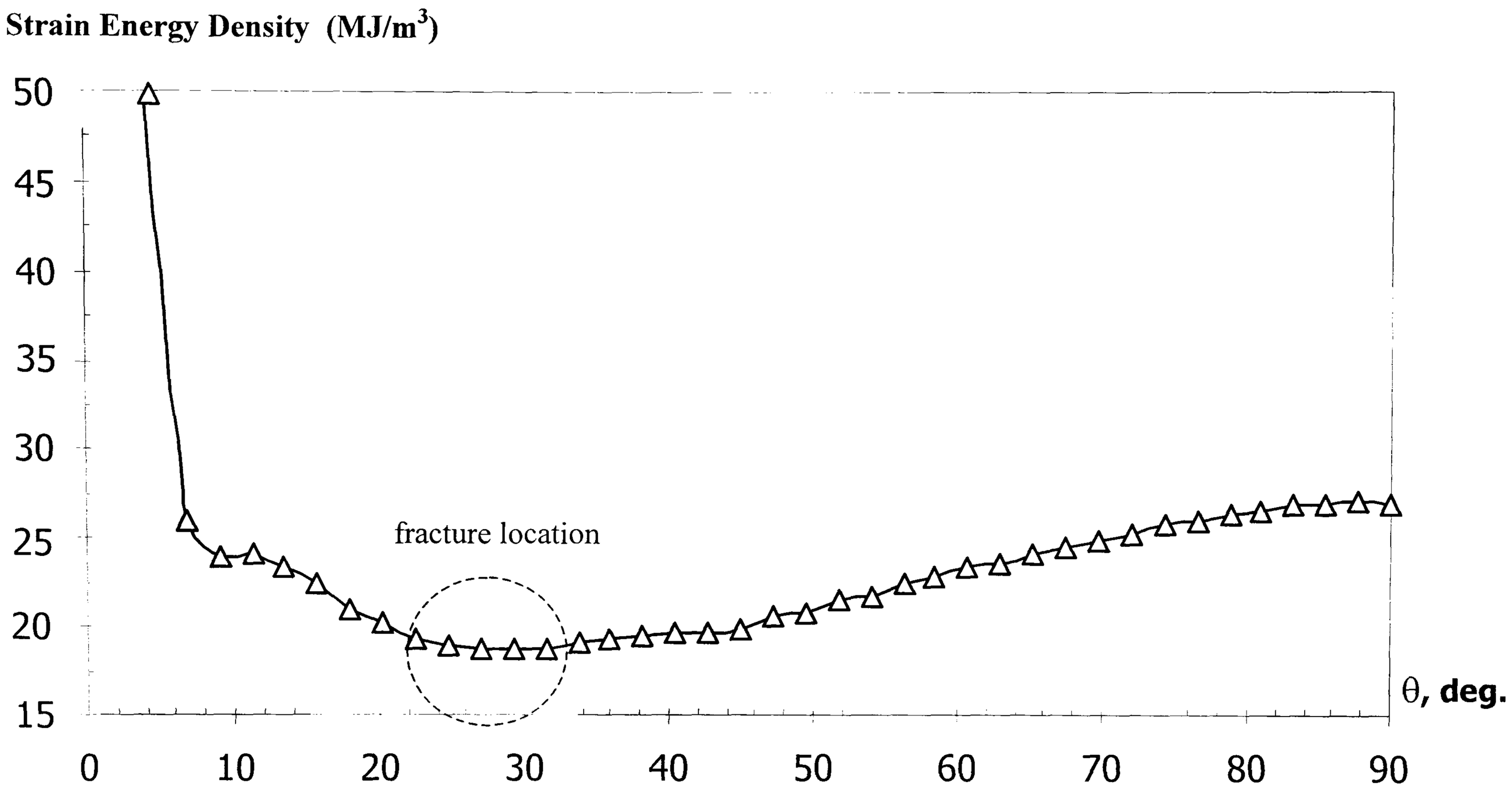

Figure 5.6 Strain energy density around a critical radius, obtained from elasto-plastic FE analysis

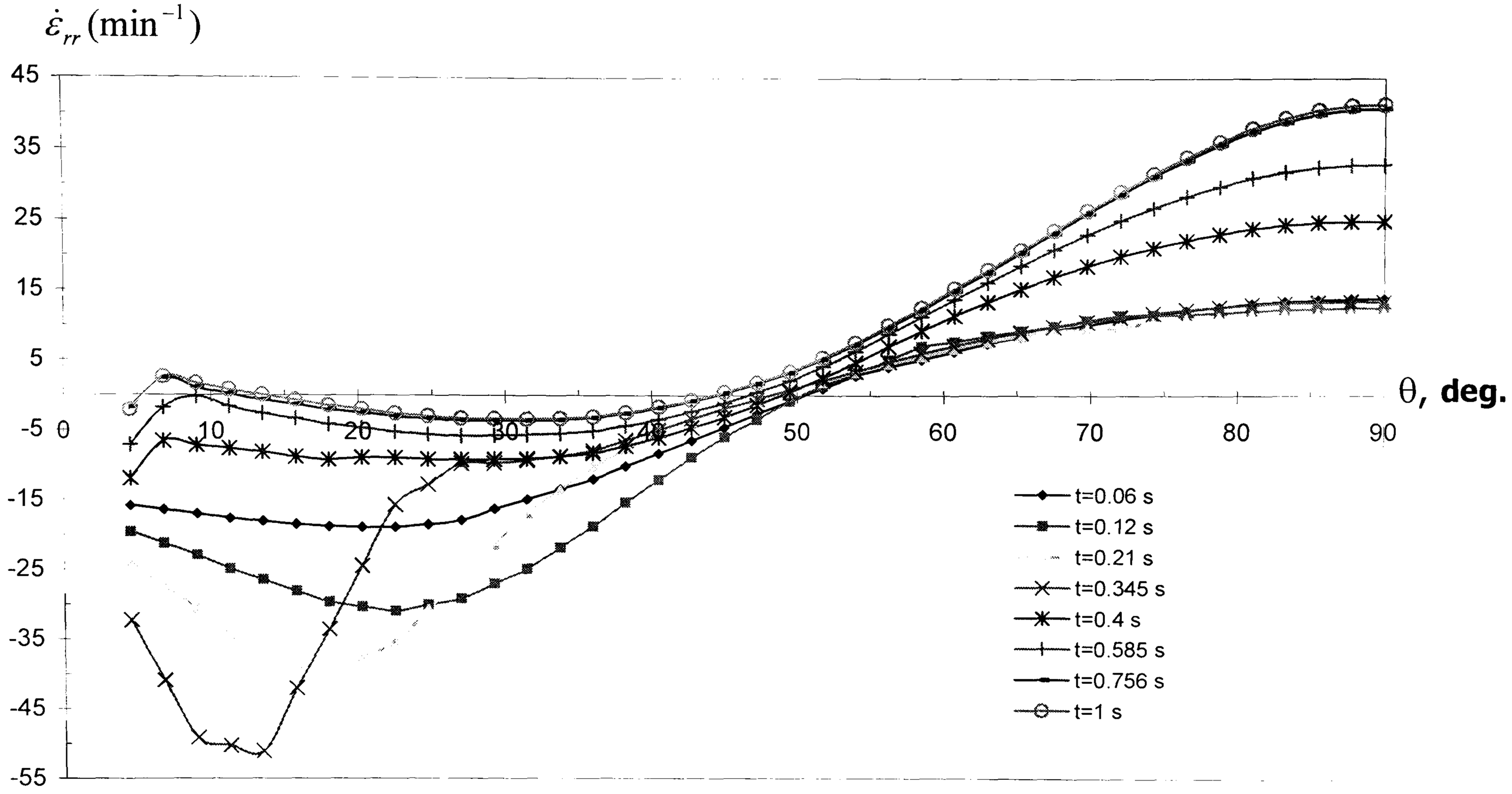

Figure 5.7 Variation of radial strain rate in each unloading step, at the unloading time of 1 sec.

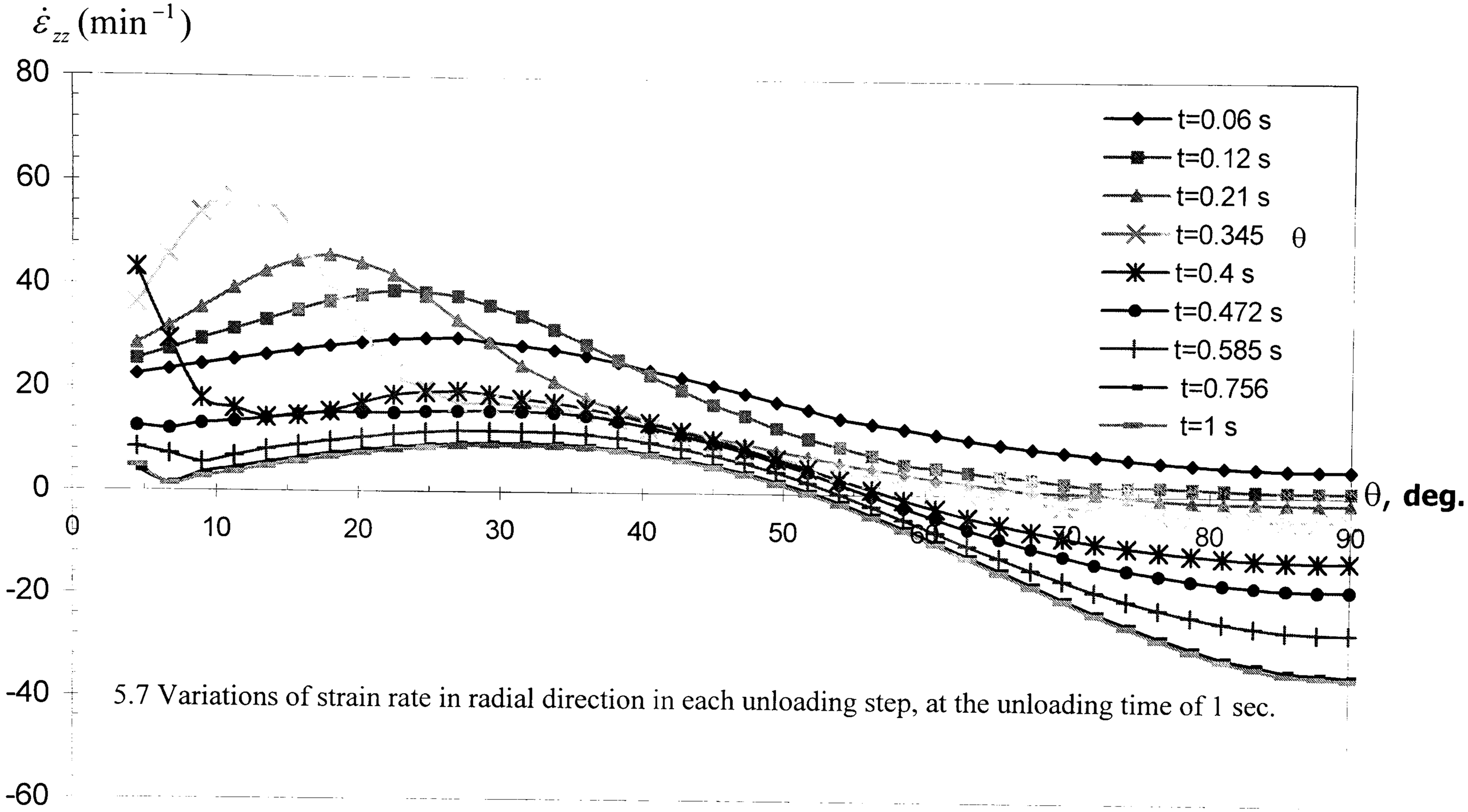

5.7 Variations of strain rate in radial direction in each unloading step, at the unloading time of 1 sec.

Figure 5.8 Variation of axial strain rate in each unloading step, at the unloading time of 1 sec.

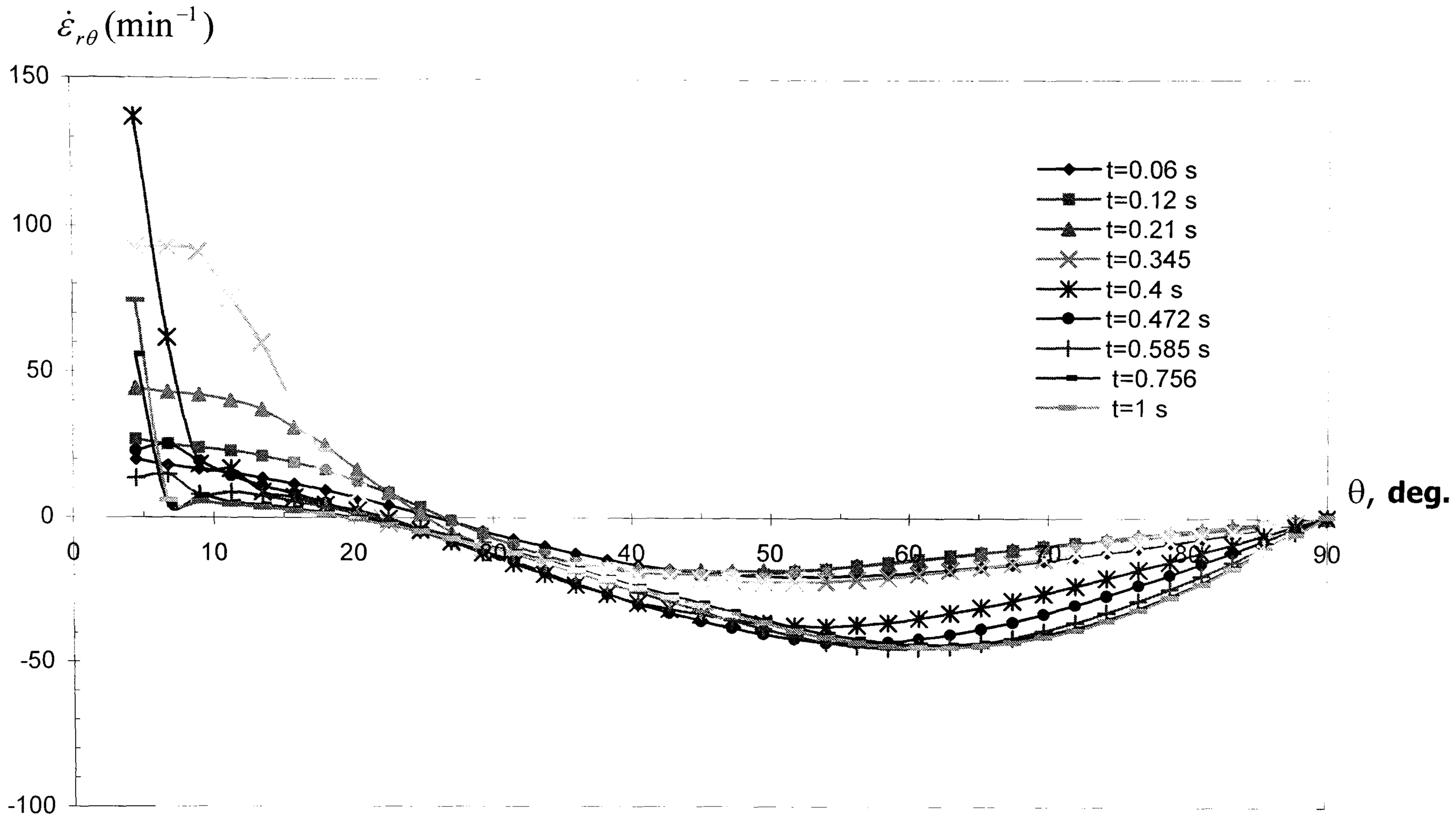

Figure 5.9 Variation of shear strain rate in each unloading step, at the unloading time of 1 sec.

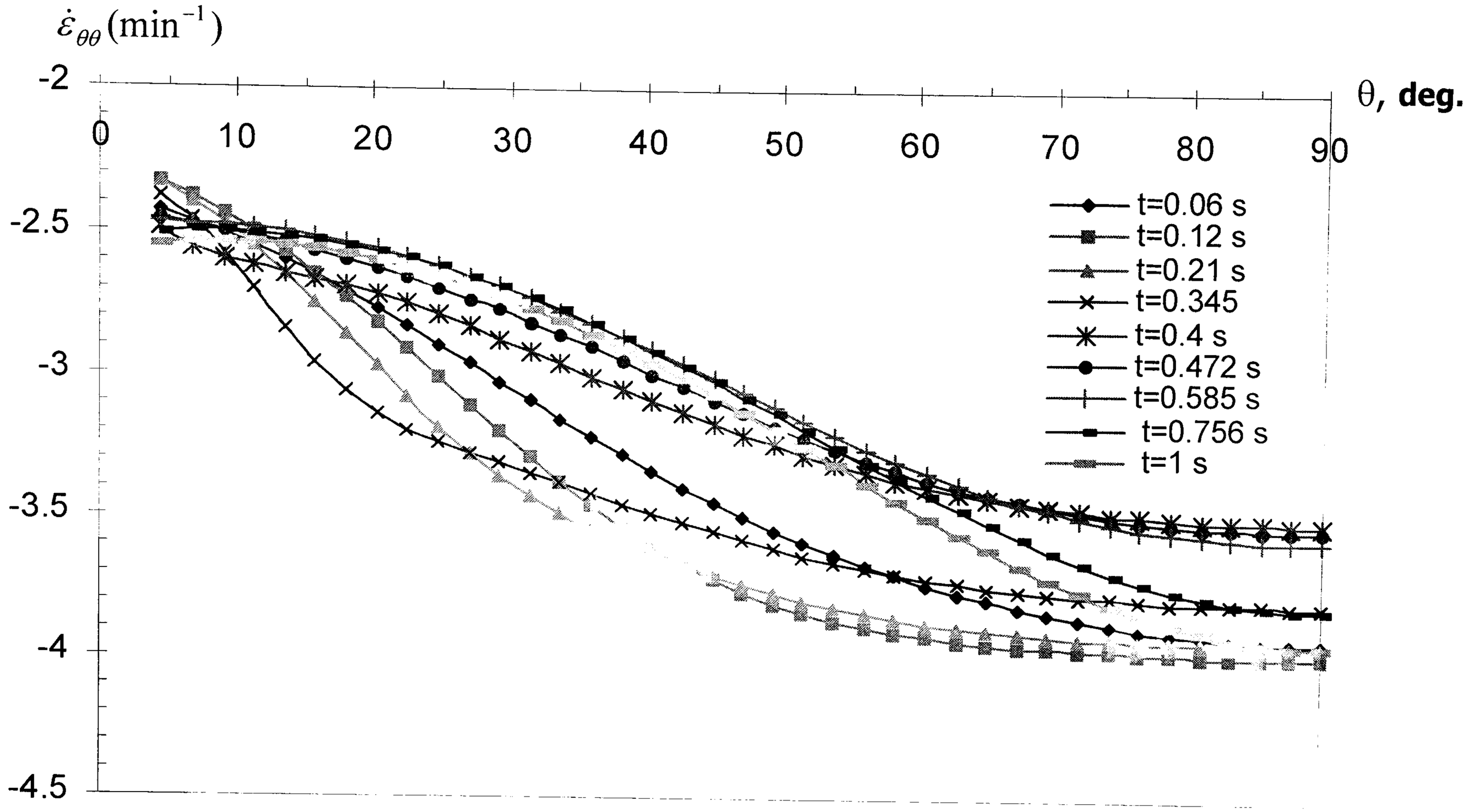

Figure 5.10 Variation of angular strain rate in each unloading step, at the unloading time of 1 sec.

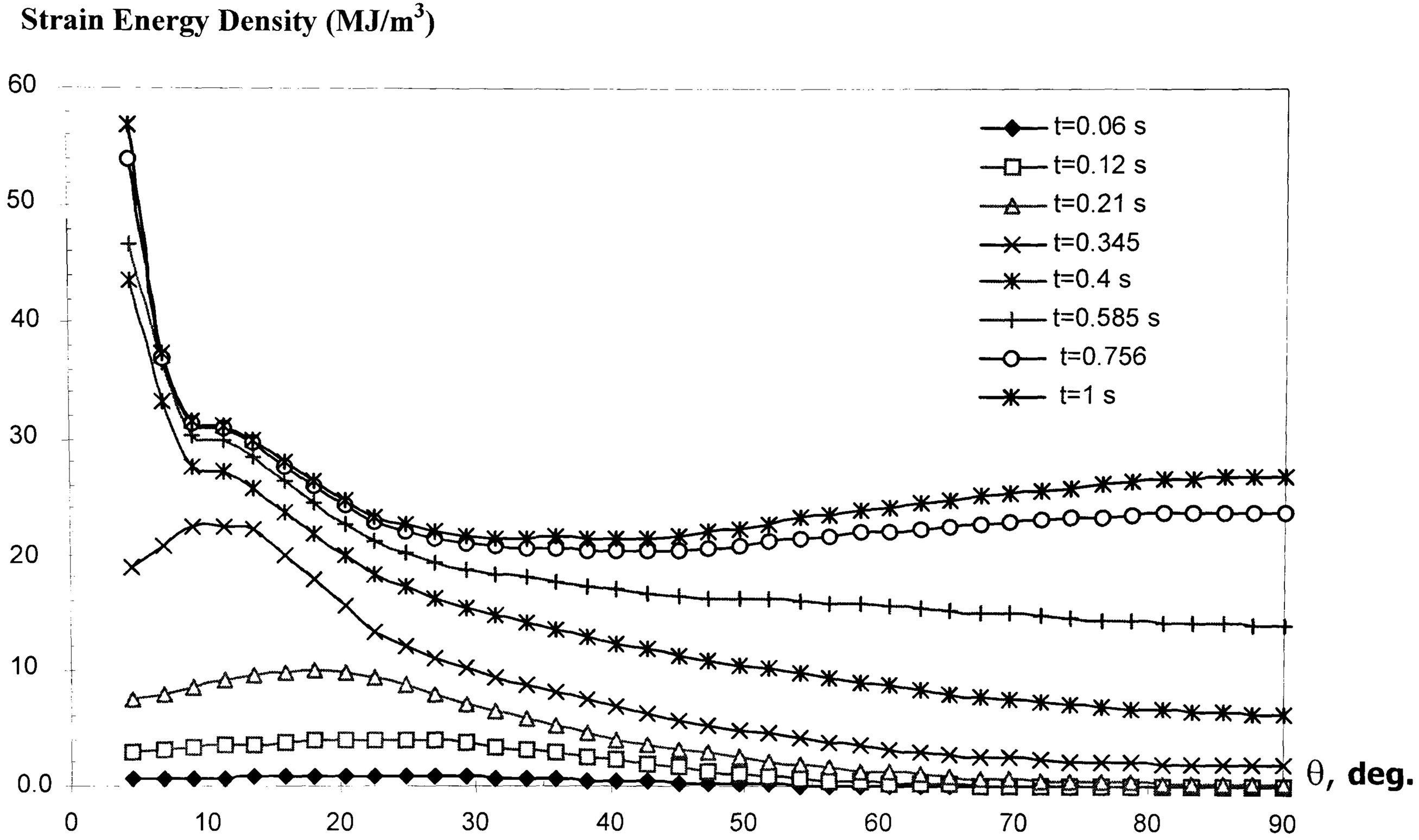

Figure 5.11 Development of strain energy density in each unloading step, at the unloading time of 1 sec.

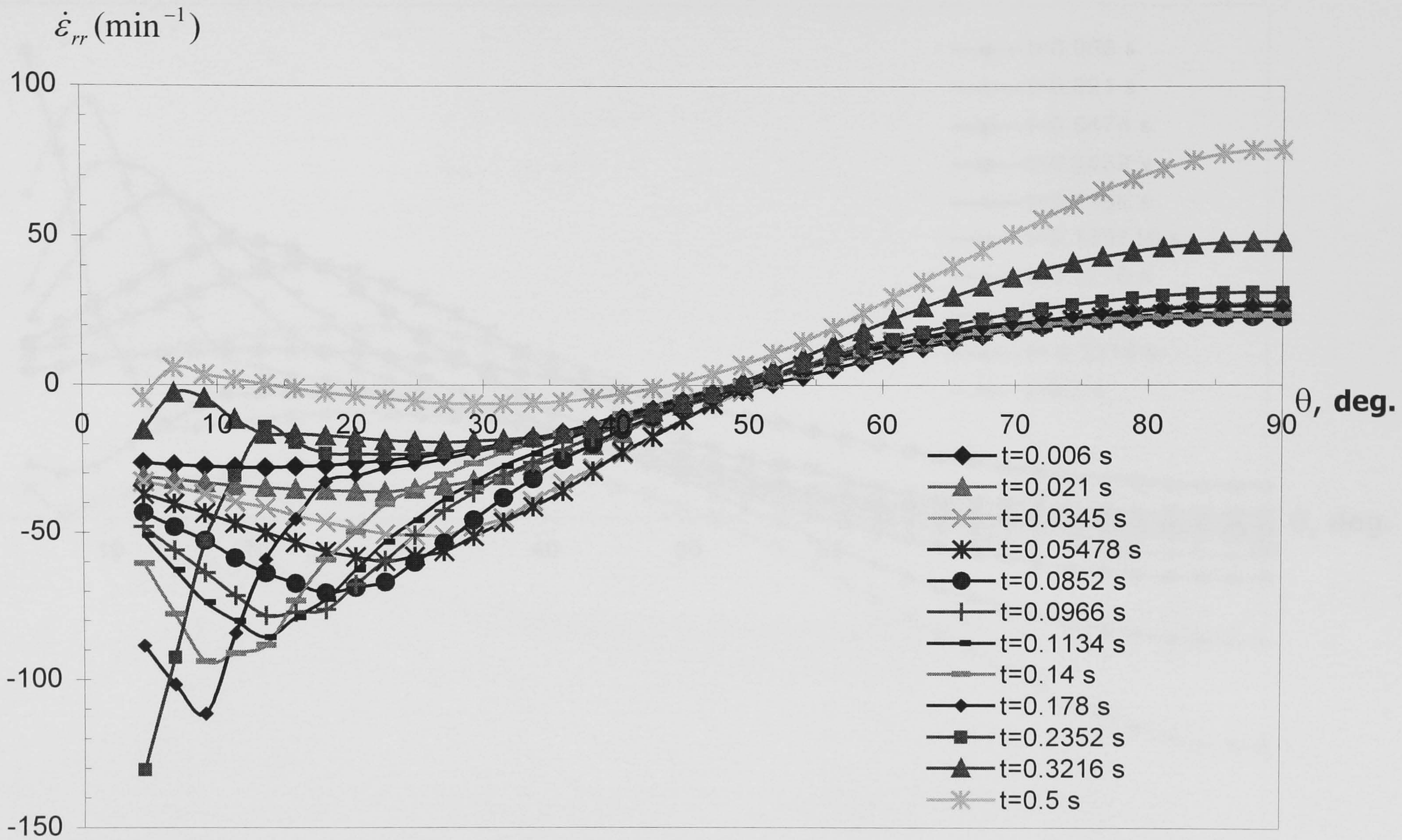

Figure 5.12 Variation of radial strain rate in each unloading step, at the unloading time of 0.5 sec.

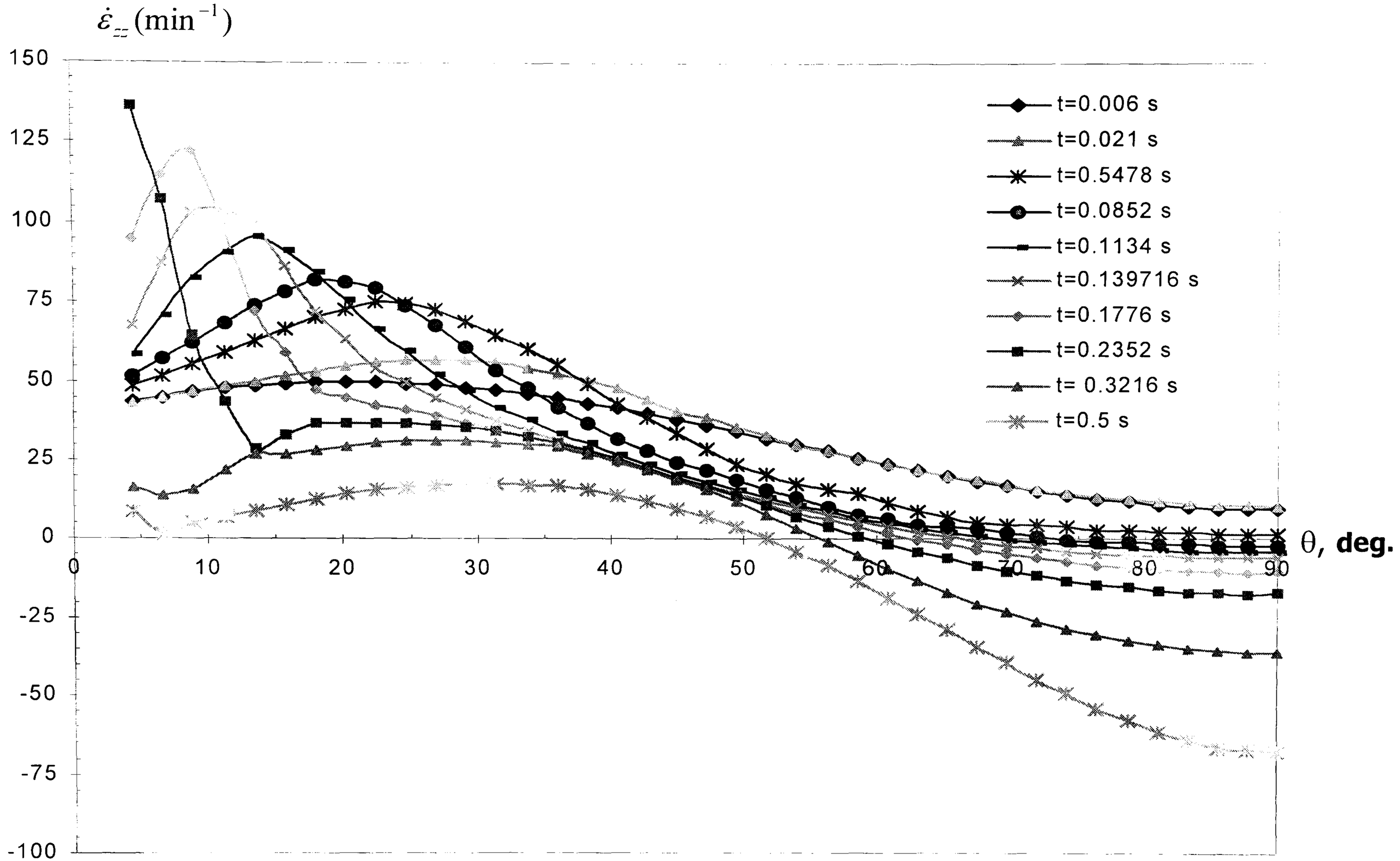

Figure 5.13 Variation of axial strain rate in each unloading step, at the unloading time of 0.5 sec.

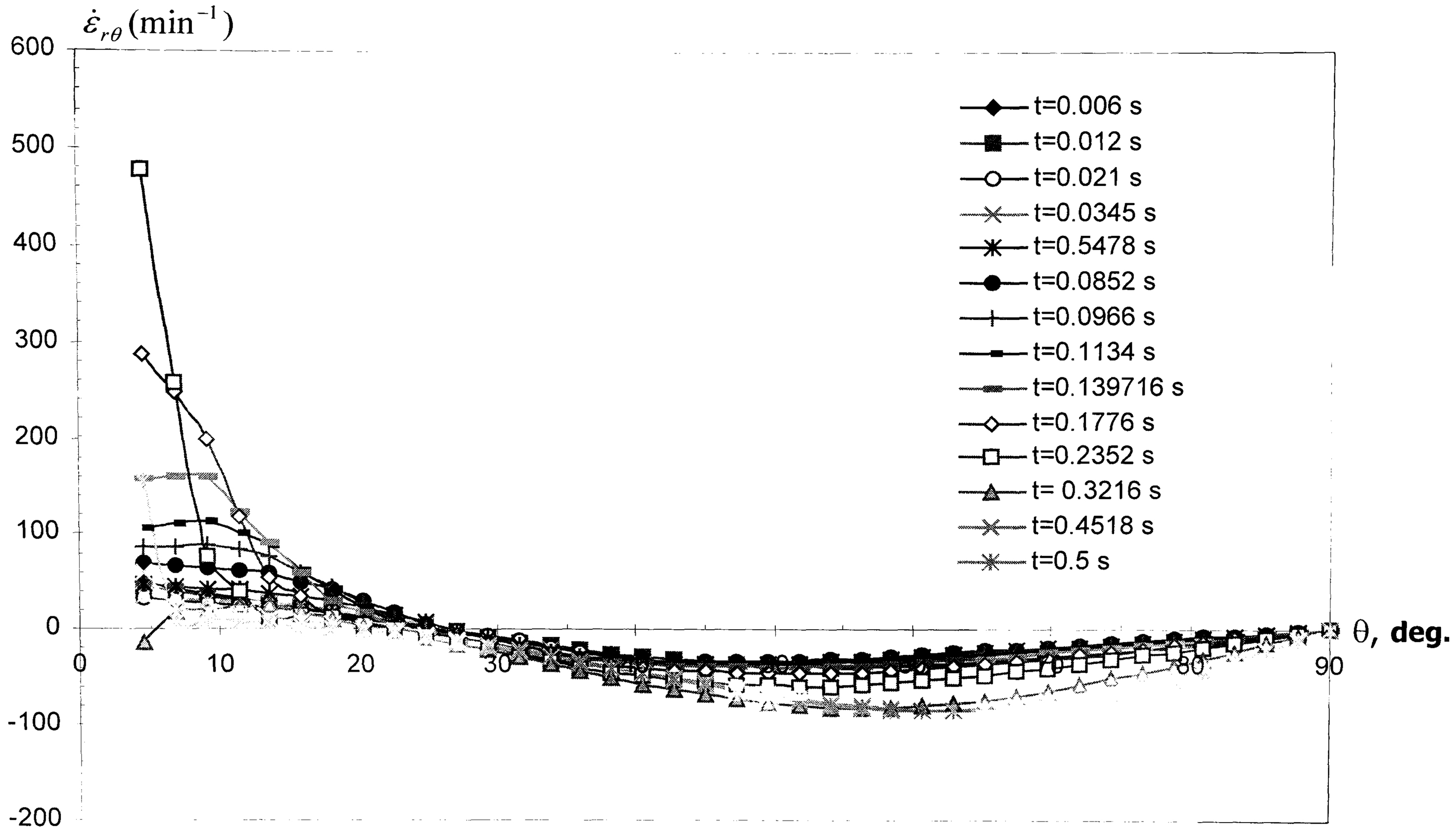

Figure 5.14 Variations of shear strain rate in each unloading step, at the unloading time of 0.5 sec.

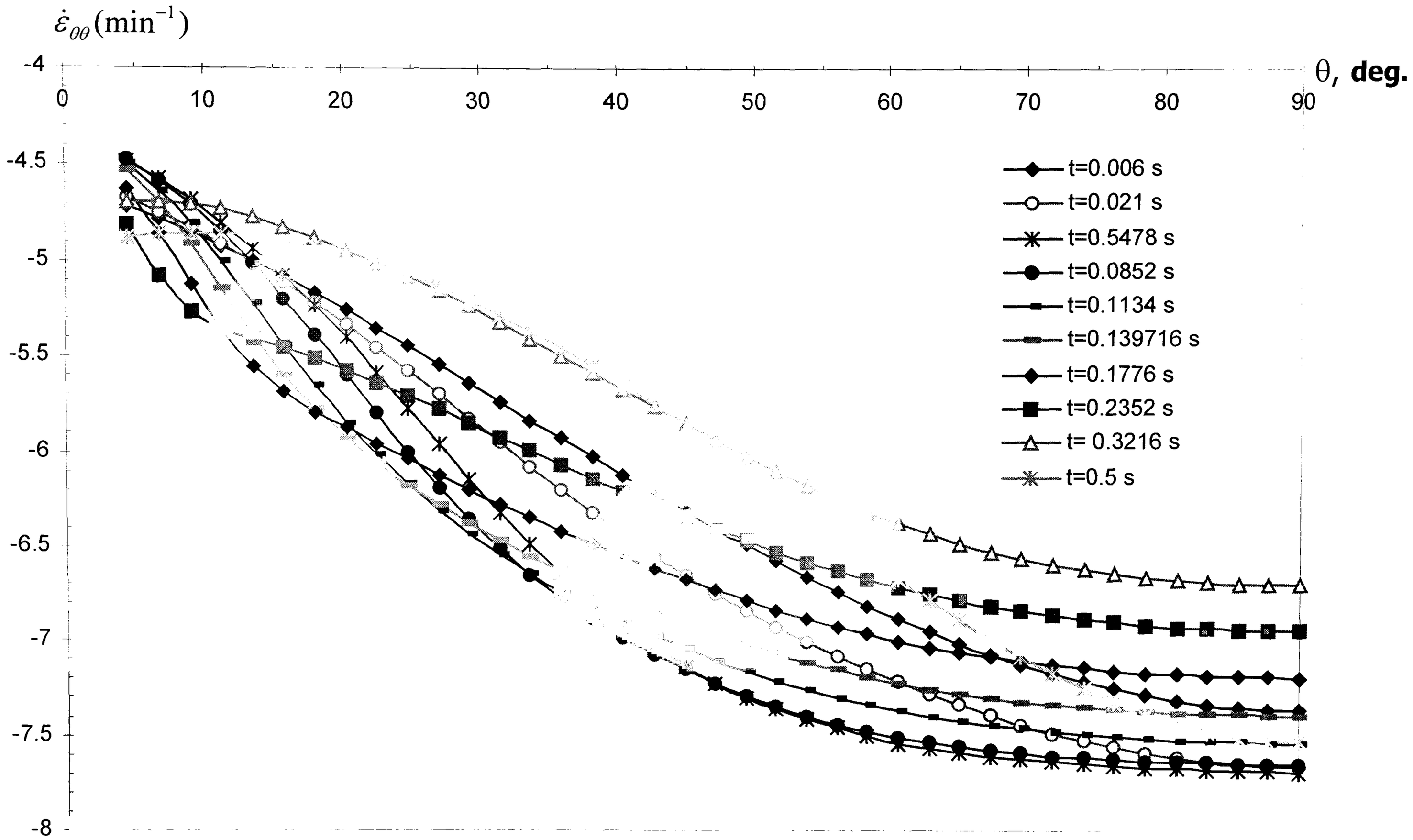

Figure 5.15 Variation of angular strain rate in each unloading step, at the unloading time of 0.5 sec.

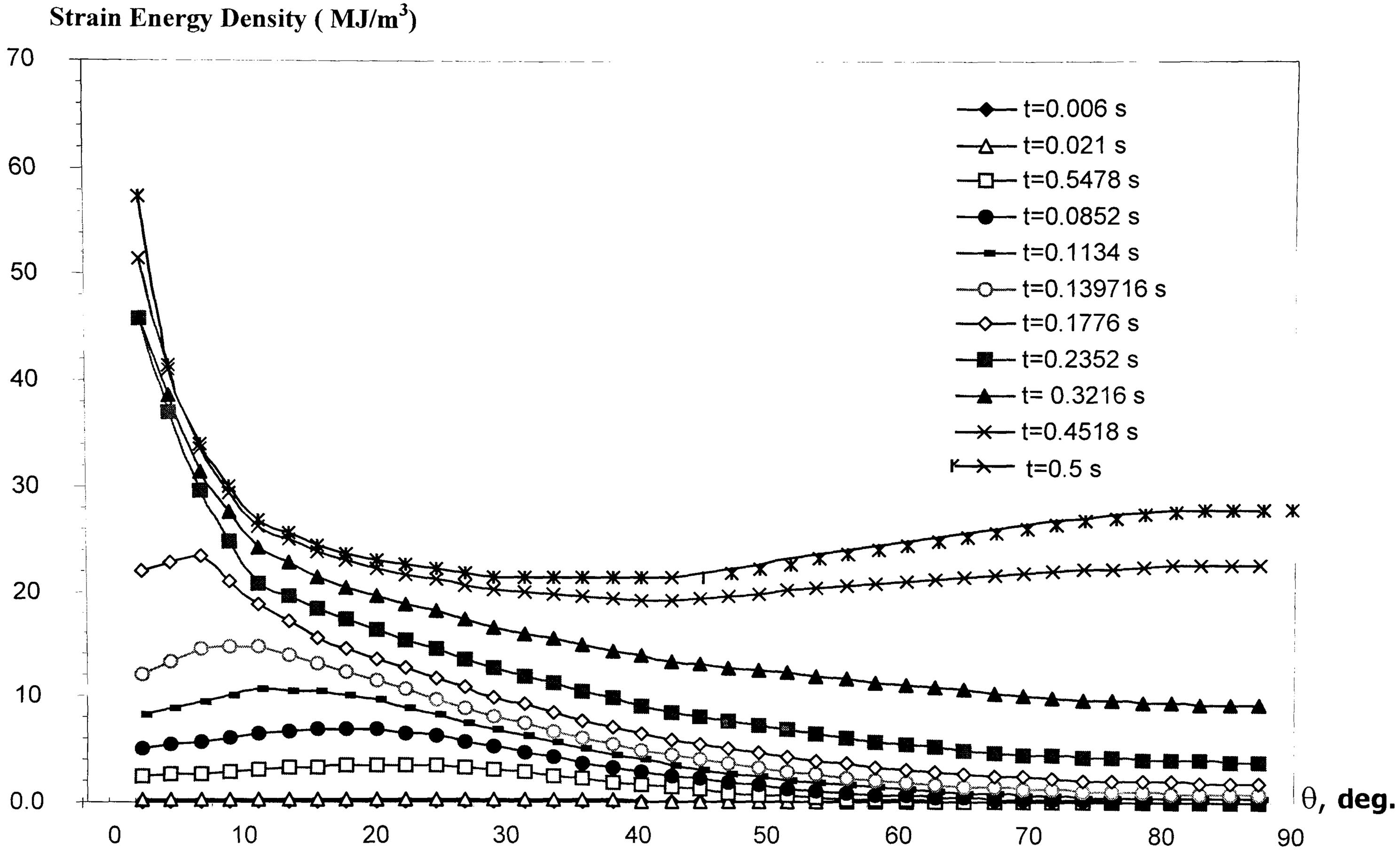

Figure 5.16 Development of strain energy density in each unloading step, at the unloading time of 0.5 sec.

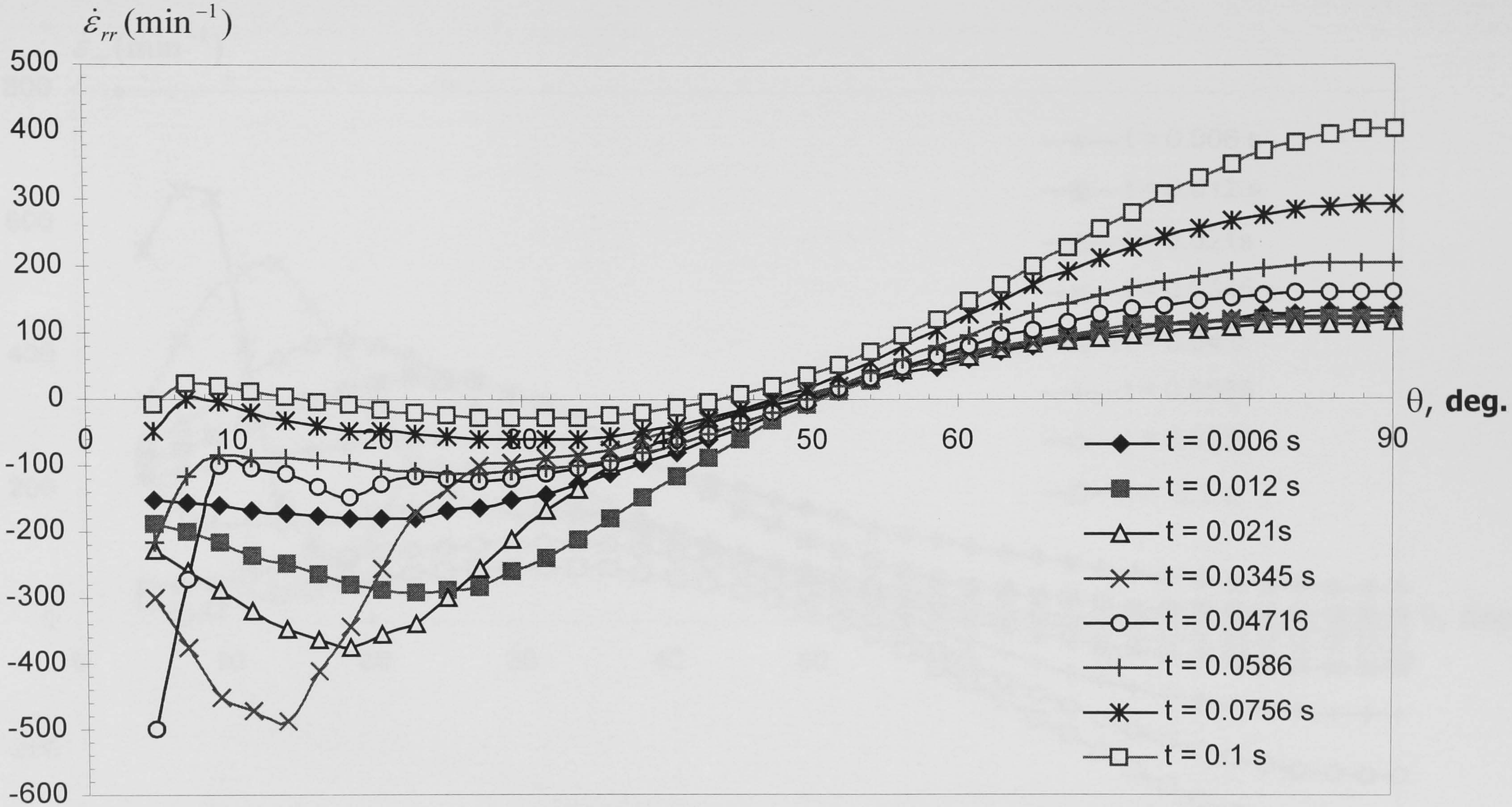

Figure 5.17 Variation of radial strain rates in each unloading step, at the unloading time of 0.1 sec.

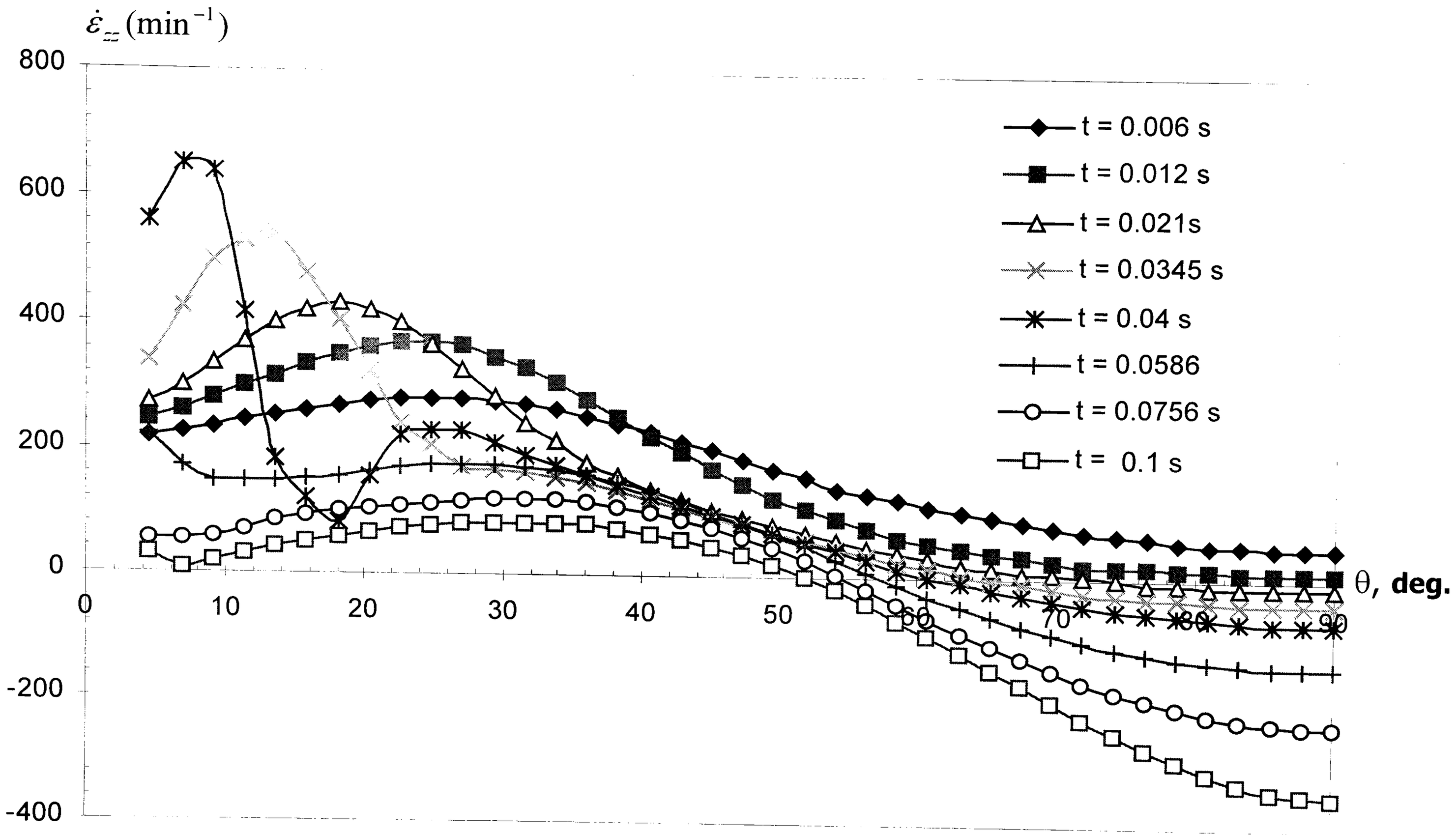

Figure 5.18 Variation of axial strain rates in each unloading step, at the unloading time of 0.1 sec.

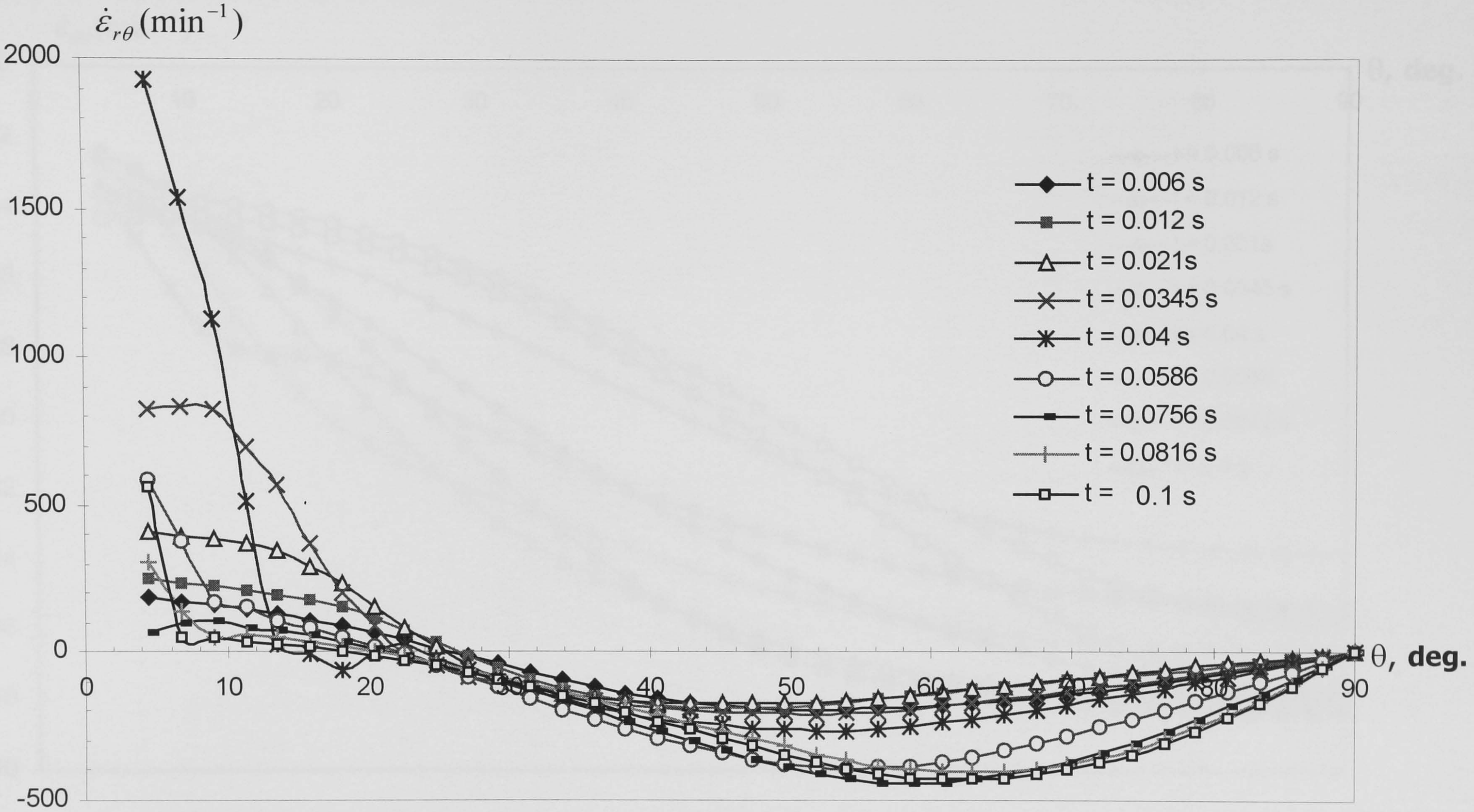

Figure 5.19 Variation of shear strain rate in each unloading step, at the unloading time of 0.1 sec.

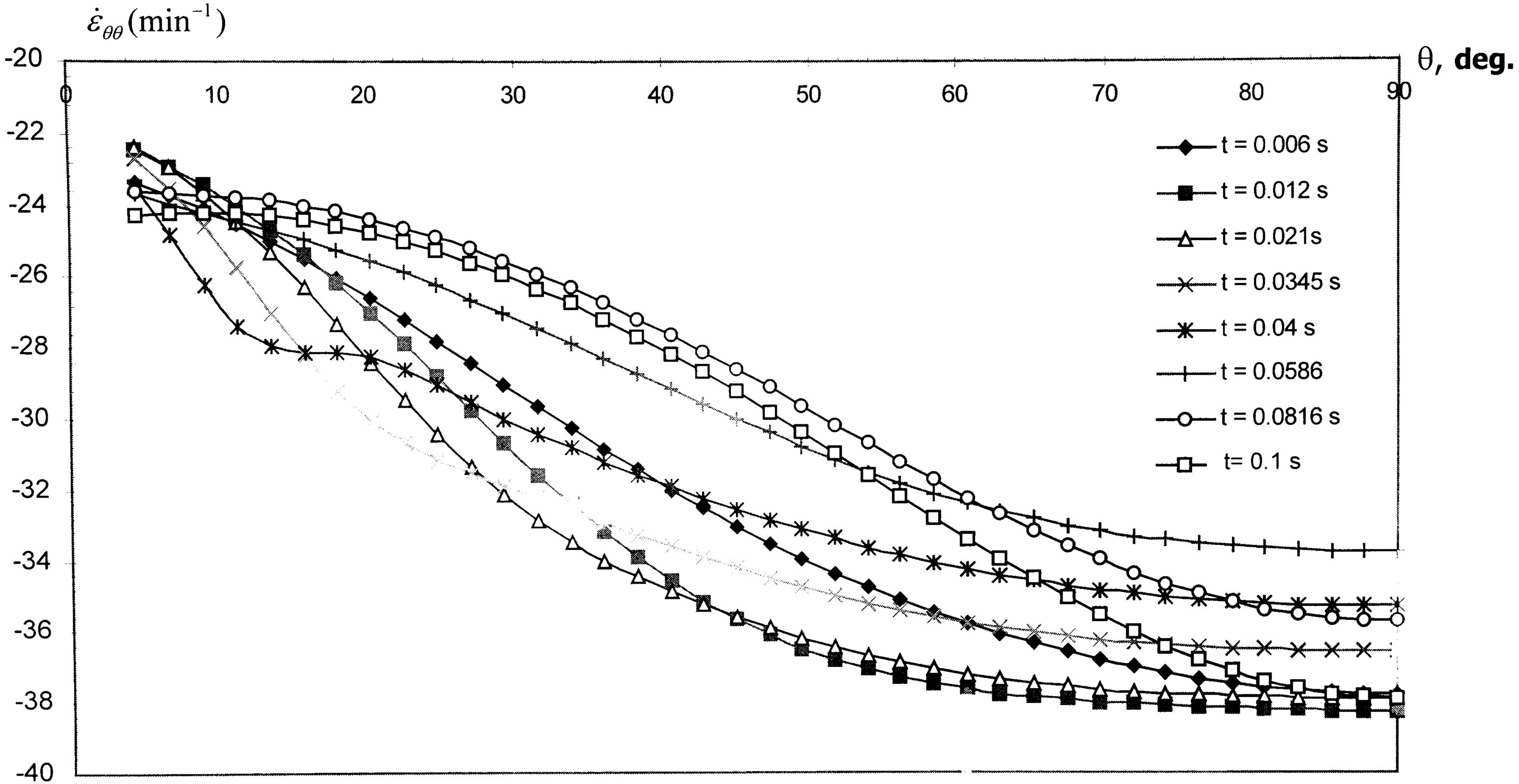

Figure 5.20 Variation of angular strain rate in each unloading step, at the unloading time of 0.1 sec.

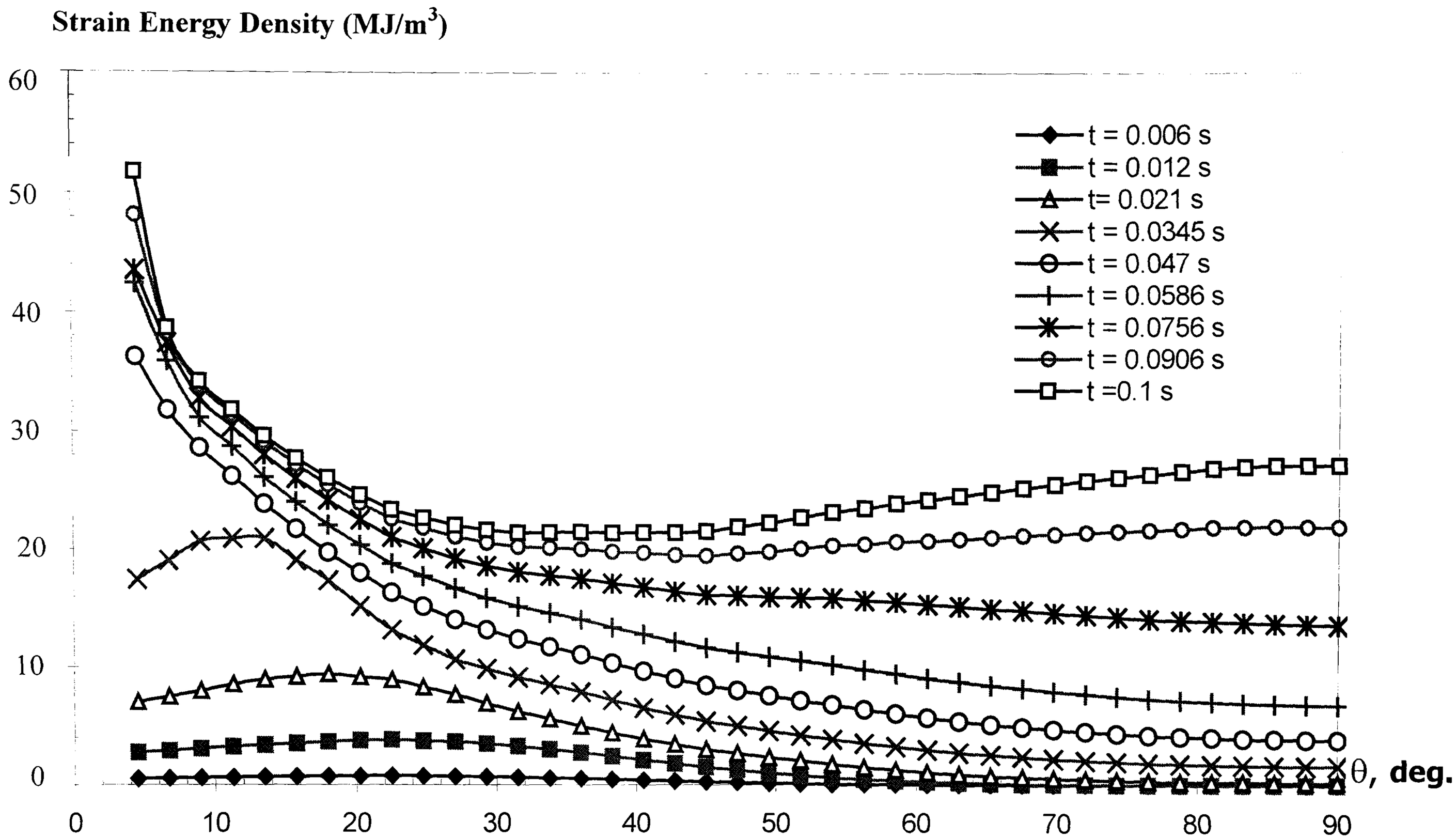

Figure 5.21 Development of strain energy density in each unloading step, at the unloading time of 0.1 sec.

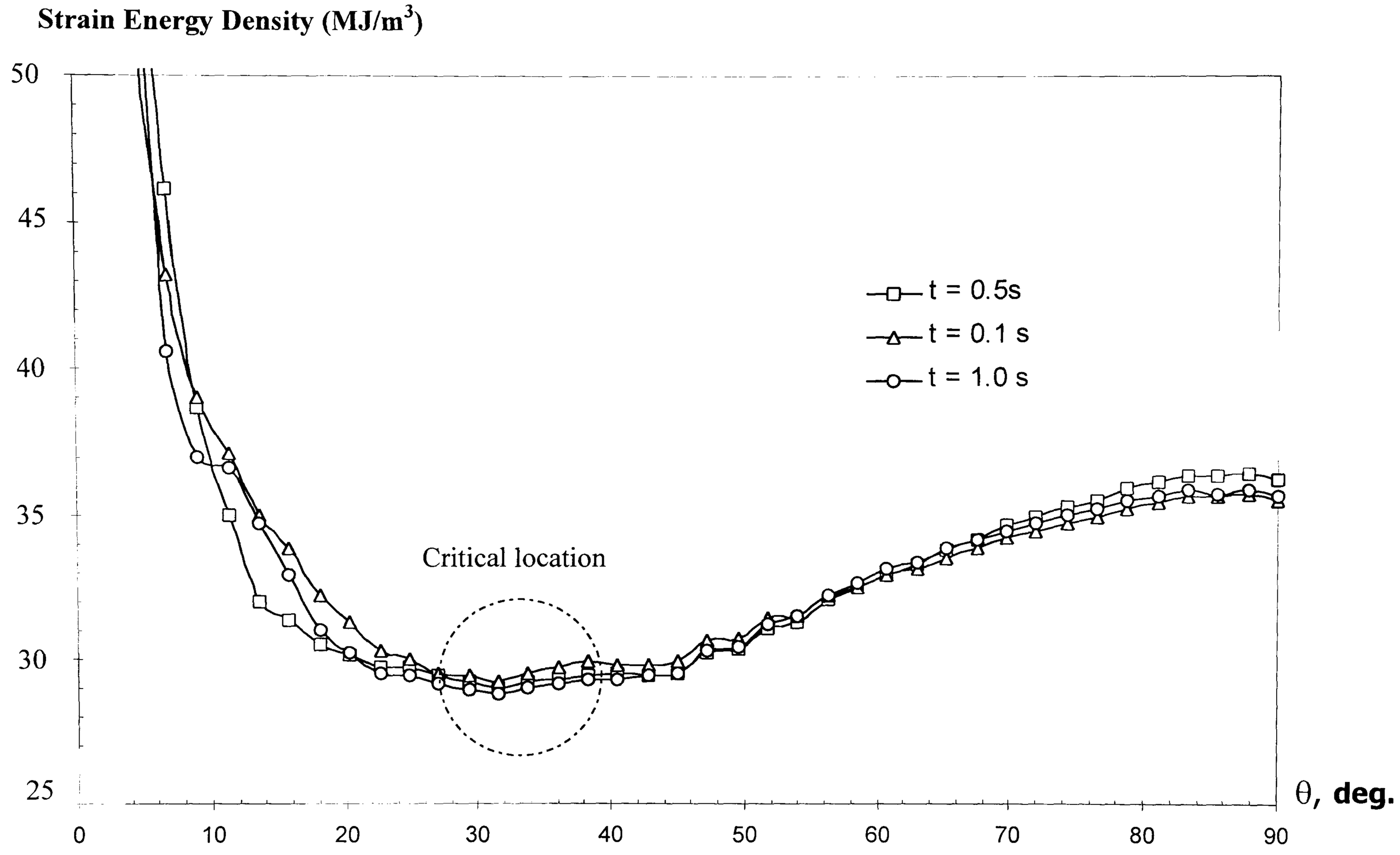

Figure 5.22 Comparison of angular strain energy density around the crack tip for all unloading cases

CHAPTER 6

Crack Propagation Analysis

6.1 Introduction

Failure in a continuous carbon-fibre embedded in epoxy matrix occurs at higher applied strain level in the fragmentation test compared to the short fibre system [27,28]. The large amount of elastic energy stored within the fibre is released after the fibre breaks leading to rapid matrix-crack propagation (Mode γ). The driving force to propagate the matrix crack depends on the net amount of available energy released from the fibre breaks after deducting the energy dissipations in plasticity and the time dependent deformation. Prediction of crack propagation has become a popular subject challenging scientists and engineers for several decades [78,84,85]. However, the prediction of crack propagation in a composite is more difficult than that in a homogeneous material due to the material discontinuities which create a complex stress field ahead of the crack tip. Matrix cracks in polymer composites have been observed experimentally by several authors [27,28,19-22]. Their lengths are extremely short (of the order of a few micrometres) and very difficult to measure. A quantitative study of matrix cracks, reported by Baillie *et al.* [26], has investigated the development of the matrix cracks and the crack growth rate for several matrix crack geometries. This study has also found that the crack growth rate of a conical-shaped matrix crack is faster than that of a disc-shaped matrix crack. Busschen *et al.*

used image-processing techniques to estimate the size of conical-shaped matrix cracks in a sized-glass fibre/polyester composite [20-21]. Their results showed that the matrix crack length is about three times larger than the fibre diameter.

A FE analysis to predict matrix crack propagation in carbon fibre/epoxy composite was performed by Nath *et al.* [34]. The axial fibre stresses obtained from FE models with several crack angles and crack lengths were compared with those obtained from LRS measurement. It was assumed that the axial fibre stress profile is characteristic of the present matrix crack geometry. The crack angle and the crack length that gave good agreement with LRS result were found to be 20° and 100 μm, respectively.

The aim of the work described in this chapter is to use the predicted crack angles obtained from Chapter 4 to estimate the crack length by correlating the axial fibre stress obtained from FE analysis with the results from LRS measurement [27,28]. The energy balance was also employed to estimate the energy available to propagate a penny-shaped fibre crack into the matrix material. Since the energy dissipated by matrix plasticity will lead to an inaccurate estimation of the net amount of the available energy, elasto-plastic and viscoplastic FE analyses were used in this study.

6.2 Matrix Crack Propagation Analysis

6.2.1 Energy balance in matrix crack

As mentioned in section 6.1, the matrix crack propagation is made possible by the energy released from the fibre-breaking event. The energy released when a fibre

fractures can be calculated by using the energy balance model. However, the domination of matrix plasticity and the thermal residual stresses have created a difficulty in mathematical modelling of the energy balance for this fracture phenomenon. Fortunately, the complex energy change in this progressive fracture can be calculated accurately by FE analysis. The energy balance model, which was proposed by Detassis *et al.* [108], has been modified to take account of the entire failure process. Therefore, the energy available to produce matrix cracks can be approximated as:

$$U_{avai} = \left([U_f^{thermal} + U_m^{thermal}] + [U_f^{prior} + U_m^{prior}]\right) - \left([U_f^{break} + U_m^{break}]\right) - \left(U_m^{plas.dis.}\right) \qquad (6.1)$$

$U^{thermal}$ refers to strain energy stored in the curing process, U^{prior} refers to the strain energy before the fibre breaks, and U^{break} refers to the recoverable strain energy after the fibre breaks. $U^{plas.dis.}$ is the energy dissipated by matrix plasticity. The subscripts *f* and *m* refer to fibre and matrix, respectively. The dynamic effects related to rapid fibre fracture, such as energy dissipated by shock waves, are neglected in this energy balance model due to the carbon fibre used in this specimen is very light and small; the carbon fibre density is only about 1.78 g/cc. The presence of an interphase, which is a thin layer between the fibre and matrix in a sized system, was also neglected because its mechanical properties are not fully understood. To take account of the viscoplastic loading and unloading in the matrix material, the rate-dependent

plasticity model was also included in this calculation. According to all of these assumptions, the internal energy U_i can be obtained by ABAQUS [100] as:

$$U_i = U_s + U_p + U_c \tag{6.2}$$

or it can be written in the full form as:

$$U_i = \underbrace{\int_0^t \left(\int_V \sigma^c : \dot{\varepsilon}^{el} dV \right) dt}_{U_s} + \underbrace{\int_0^t \left(\int_V \sigma^c : \dot{\varepsilon}^{pl} dV \right) dt}_{U_p} + \underbrace{\int_0^t \left(\int_V \sigma^c : \dot{\varepsilon}^{cr} dV \right) dt}_{U_c} \tag{6.3}$$

where U_s is the recoverable elastic strain energy, U_p is the energy dissipated by plasticity and U_c is the energy dissipated by time dependent deformation.

6.2.2 Crack propagation in FE analysis

A mismatch between the coefficients of thermal expansion of the fibre and the matrix induced thermal residual stresses in the composite during the fabrication process. When the composite is subject to tensile loading, the stresses and strains in the matrix material are superimposed onto the residual stresses/strains from the initial stage. After the fibre breaks, the viscoplastic unloading creates complex stress/strain fields near the fracture location. In order to clarify this fracture mechanism and to take account all of the effects, the entire process needs to be simulated continuously. Since this analysis contains two materials and the crack propagation was also

simulated, the use of special crack-tip elements for J-integral calculation [81] would be inappropriate for this problem.

6.3 FE models

The representative volume element (RVE) model [8], which is often used for the micromechanical analysis of a composite, was assumed to create FE models for this problem (see Fig. 6.1 (a)). Axisymmetric FE models with a pre-defined crack path of about 100 μm along the predicted angle of 32° and 34° to the fibre axis were created. Both FE models contain 3,551 4-node quadrilateral elements and 60 surface-to-surface contact elements. The material properties as were used in Chapter 5 were applied to these FE models. The outer matrix radius R_m, the composite half-length l_c and the fibre radius r_f are 100 μm, 400 μm, 3.25 μm, respectively (see Fig. 6.1 (b)). The composite half-length, assumed in FE models, is a minimum length giving a uniform far field stress as in the LRS specimens. The FE models with disc-shaped matrix cracks were created to confirm that the axial fibre stress profile is different from that in the conical-shaped crack model. The FE model consists of 2,250 4-node quadrilateral elements (see Fig. 6.2).

A progressional approach was implemented in FE analysis with the consecutive simulations of the curing process in the first load step, applied mechanical strain of 1.3 % in the second load step, and the fibre fracture with the addition of matrix-crack propagation in the last load step (see Figs. 6.3 (a-d)). A constant crack growth rate with a constant stress rate unloading were assumed in these FE analyses. The time

step in the curing process simulation was set to 200 minutes. The time step in the second load step, applied strain of 1.3%, was also set to 200 minutes in order to keep the strain rates minimum. The crack propagation option in ABAQUS enables a pre-defined crack path to debond to the desired length within a defined debonding time of 0.5 second, which was chosen by the approximated result discussed in section 5.4.4. In the case of a disc-shaped crack simulation, all boundary conditions along the pre-defined crack path will be removed to form the disc-shaped crack from a penny-shaped fibre crack (see Fig. 6.4).

6.4 Results Summary

6.4.1 Prediction of matrix crack length

Comparison of the axial fibre stresses from experiment and FE analysis was used to estimate the matrix crack length. Viscoplastic FE results of the model contains the crack angle of 32° with variations of the matrix crack lengths of 30, 50, 70, 100 μm were compared with the LRS result. The axial fibre stresses calculated by FE analysis for the crack length of 30, 50, 70 μm were found to have steeper slope than the axial fibre stress measured by LRS (see Fig. 6.5). The slopes of axial fibre stress reduced as the crack length was increased implying that the fibre stresses are likely to be relieved by a longer crack length. Good agreement for this crack angle was obtained at the crack length of about 90-100 μm (see Fig. 6.5). The value of the axial fibre stress obtained from elasto-plastic FE analysis with the same crack length (100 μ m) is a little lower than the value obtained from viscoplastic FE analysis, good agreement in this analysis was obtained at the crack length of 90 μm (see Fig. 6.6).

The results have shown that using elasto-plastic FE analysis may lead to the prediction of a shorter crack length due to the fact that the use of rate-sensitive material properties in viscoplastic analysis resulted in smaller amount of the energy dissipated in plasticity.

Good agreement in the model with the crack angle of 34° was also obtained at the same crack length of about 86 μm in both elasto-plastic and viscoplastic FE analyses (see Fig. 6.7). FE results for both crack angles have shown that the axial fibre stress is likely to be more sensitive to the crack length than the angle of crack propagation. The axial fibre stress obtained from the model with the crack angle of 34° matches slightly better with the experiment than the model with the crack angle of 32° (see Fig. 6.8). This result implies that the matrix crack may prefer to initiate at the angle of 34°.

To prove that the axial fibre stress profile is characteristic of the existing matrix crack size and type, comparison of fibre stresses in disc-shaped and conical-shaped matrix crack models were compared. Viscoplastic FE result for disc-shaped crack models gives good agreement with experiment at the crack length of 78 μm (see Fig. 6.9). The magnitude of the fibre axial stress is lower than the values obtained from conical-shaped crack models (see Fig. 6.8). According to the FE results, in some circumstances the assumption that the axial fibre stress profile is a characteristic of the crack type is adequately acceptable.

6.4.2 Variations of strain energy matrix crack model

The results presented here are the total strain energy for the full RVE model; double the amount of the energy values calculated by FE analysis was presented. The fabrication process has induced strain energy in the epoxy matrix of about 0.258 x 10^{-6} J. A very small value of strain energy of about 2.002 x 10^{-11} J was found in the fibre, as a result of the matrix material has contracted more than the fibre. When the composite is subject to an applied strain of about 1.3 %, both elasto-plastic and viscoplastic FE analysis give the strain energy at about 6.78 x 10^{-6} J for the matrix and 0.75 x 10^{-6} J for the fibre. By applying the values of strain energy from the model with the crack angle of 32° and with the crack length of 100 μm to eq. 6.1, the available strain energy to propagate the crack in viscoplastic analysis was found to be

$$U_{avai}^{visco.32^\circ} = \left(\overbrace{0.75}^{U_f^{ther+prior}} + \overbrace{6.78}^{U_m^{ther+prior}} \right) - \left(\overbrace{0.26}^{U_f^{break}} + \overbrace{6.30158}^{U_m^{break}} \right) - \left(\overbrace{0.07842}^{U_m^{plas.dis.}} \right) \times 10^{-6} J$$

$$= 0.89 \text{ x } 10^{-6} \text{ J}$$

In the case of elasto-plastic FE analysis for the model that contains the same crack angle with the crack length of 100 μm, the available energy to propagate the crack was found to be

$$U_{avai}^{elasto.plas.32^\circ} = \left(\overbrace{0.75}^{U_f^{ther+prior}} + \overbrace{6.78}^{U_m^{ther+prior}} \right) - \left(\overbrace{0.222}^{U_f^{break}} + \overbrace{6.098}^{U_m^{break}} \right) - \left(\overbrace{0.592}^{U_m^{plas.dis.}} \right) \times 10^{-6} J$$

$$= 0.618 \text{ x } 10^{-6} \text{ J}$$

The results have shown that viscoplastic model has more energy to produce a crack than that in elasto-plastic model.

Variation of the available energy as a function of the crack length, calculated using eq. 6.1, have shown that the available strain energy increases non-linearly with larger crack length (see Fig. 6.10).

In the case of a crack angle equal to 34°, where good agreement was obtained at the crack length of 86 μm, the available strain energy in viscoplastic FE analysis was found to be

$$U_{avai}^{visco.34^\circ} = \left(\overbrace{0.75}^{U_f^{ther+prior}} + \overbrace{6.78}^{U_m^{ther+prior}} \right) - \left(\overbrace{0.290}^{U_f^{break}} + \overbrace{6.40714}^{U_m^{break}} \right) - \left(\overbrace{0.07286}^{U_m^{plas.dis.}} \right) \times 10^{-6} J$$

$$= 0.76 \times 10^{-6} \text{ J}$$

$$U_{avai}^{elasto.plas.34^\circ} = \left(\overbrace{0.75}^{U_f^{ther+prior}} + \overbrace{6.78}^{U_m^{ther+prior}} \right) - \left(\overbrace{0.254}^{U_f^{break}} + \overbrace{5.928}^{U_m^{break}} \right) - \left(\overbrace{0.512}^{U_m^{plas.dis.}} \right) \times 10^{-6} J$$

$$= 0.836 \times 10^{-6} \text{ J}$$

The available strain energy to propagate the crack to the same length as in the former case (100 μm) was found to be 0.98×10^{-6} J in the case of viscoplastic analysis, and

1.29×10^{-6} J in the case of elasto-plastic analysis. The variations of the available strain energy as a function of the crack length for this case are plotted in Fig. 6.11.

In the case of a disc-shaped crack, where good agreement was obtained at the crack length of 78 μm, the available strain energy in viscoplastic FE analysis was found to be

$$U_{avai}^{visco.disc.crack} = \left(\overbrace{0.75}^{U_f^{ther+prior}} + \overbrace{6.78}^{U_m^{ther+prior}} \right) - \left(\overbrace{0.236}^{U_f^{break}} + \overbrace{5.528}^{U_m^{break}} \right) - \left(\overbrace{0.206}^{U_m^{plas.dis.}} \right) \times 10^{-6} J$$

$$= 1.56 \times 10^{-6} \text{ J}$$

It has been seen that a higher amount of the available energy is needed to propagate a disc-shaped crack to the same length as in the former cases. On the limited data available, a higher crack angle is likely to require more energy, per unit crack extension. The variations of the available strain energy as a function of the crack length for a disc-shaped crack case are plotted in Fig. 6.12.

6.5 Discussion

Good agreement between the LRS measurement and the viscoplastic FE analysis was found when the matrix crack length lies in the range 90-100 μm (see section 6.4.1). For the models containing disc-shaped cracks, the fibre axial stress profiles for any crack length did not agree well with the experiment see also section 6.4.1. The

assumption that the fibre axial stress profile is characteristic of the presence of a defined crack geometry is reasonably acceptable.

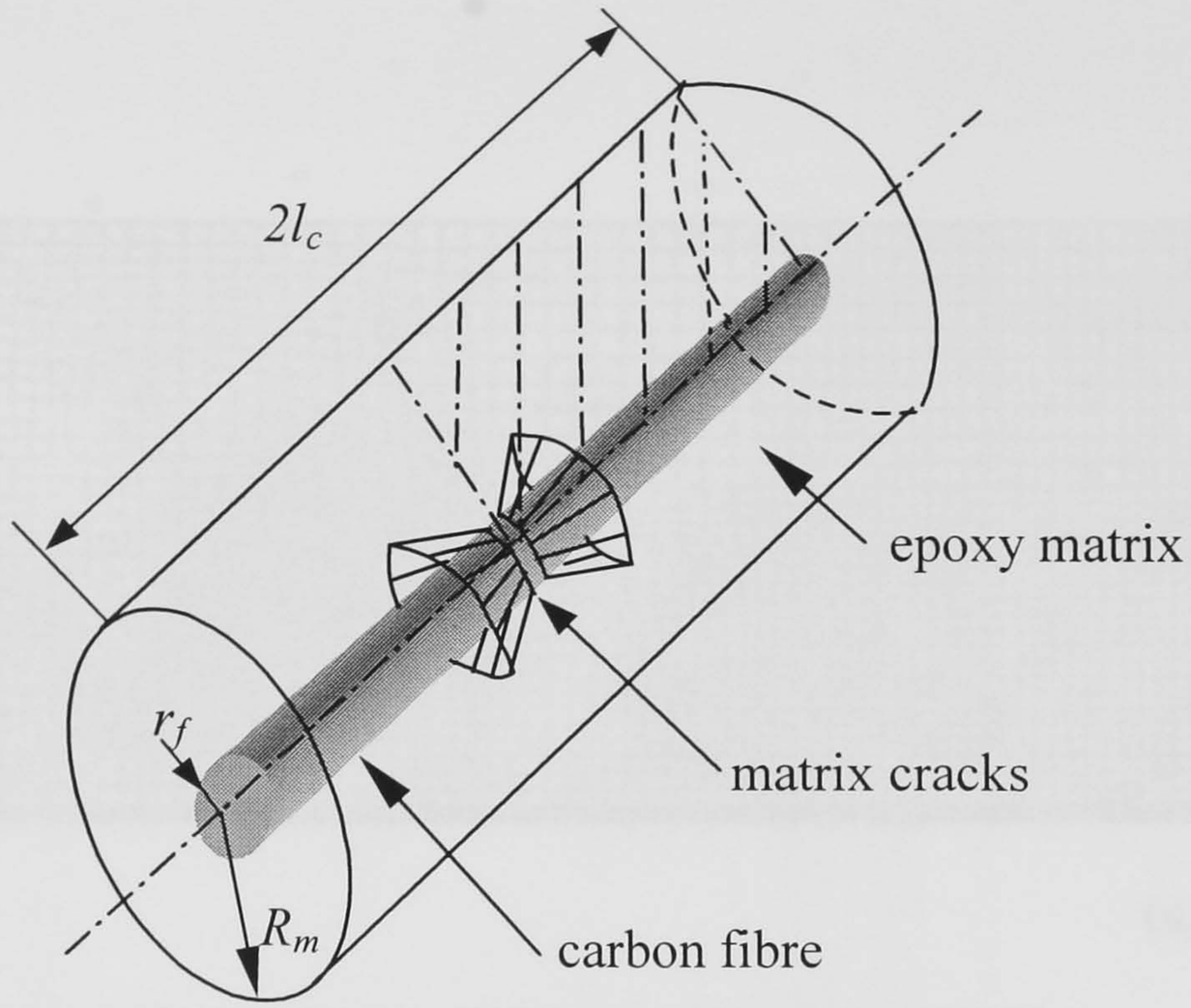

(a)

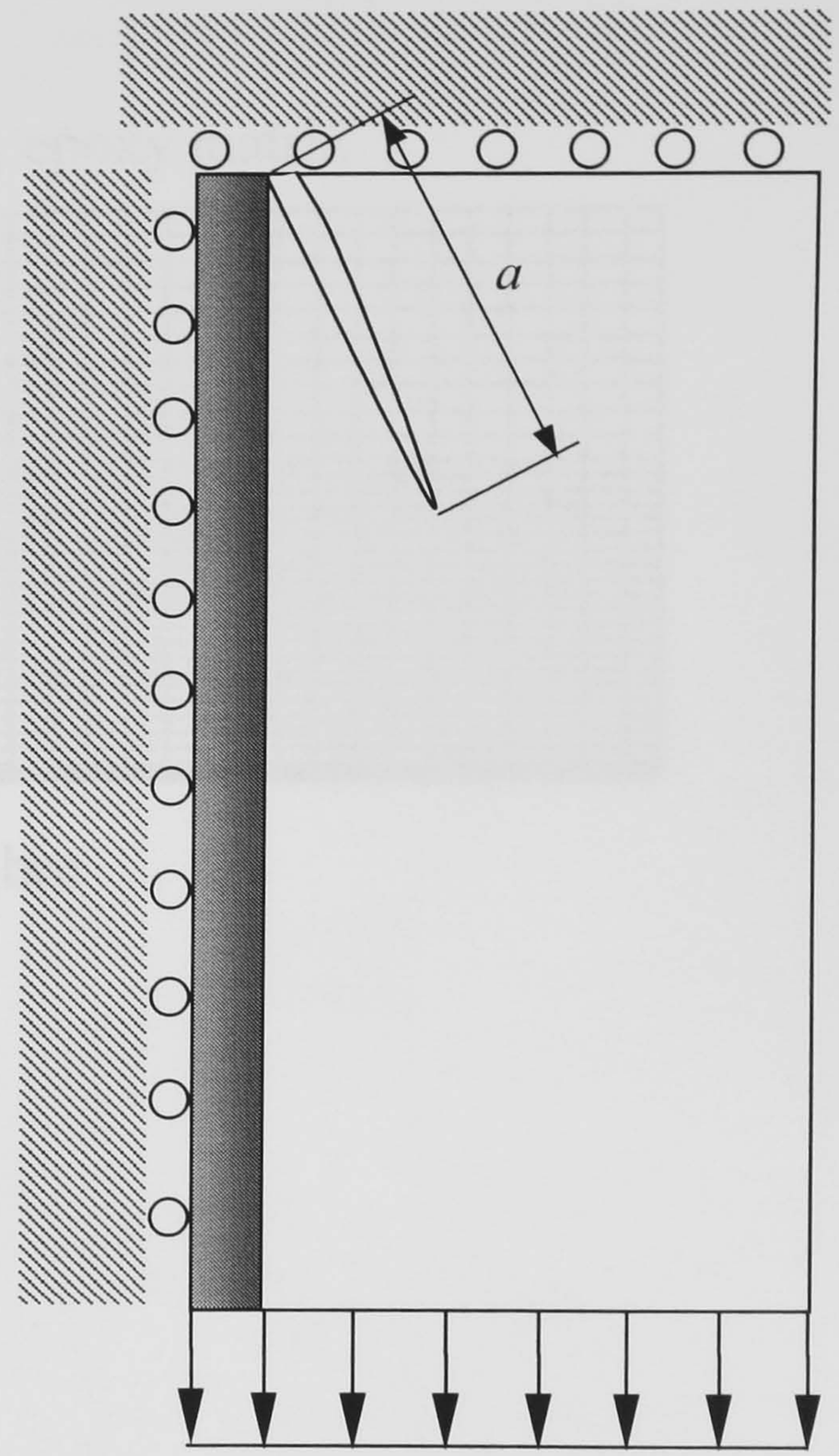

(b)

Figure 6.1 (a) RVE model (b) FE model

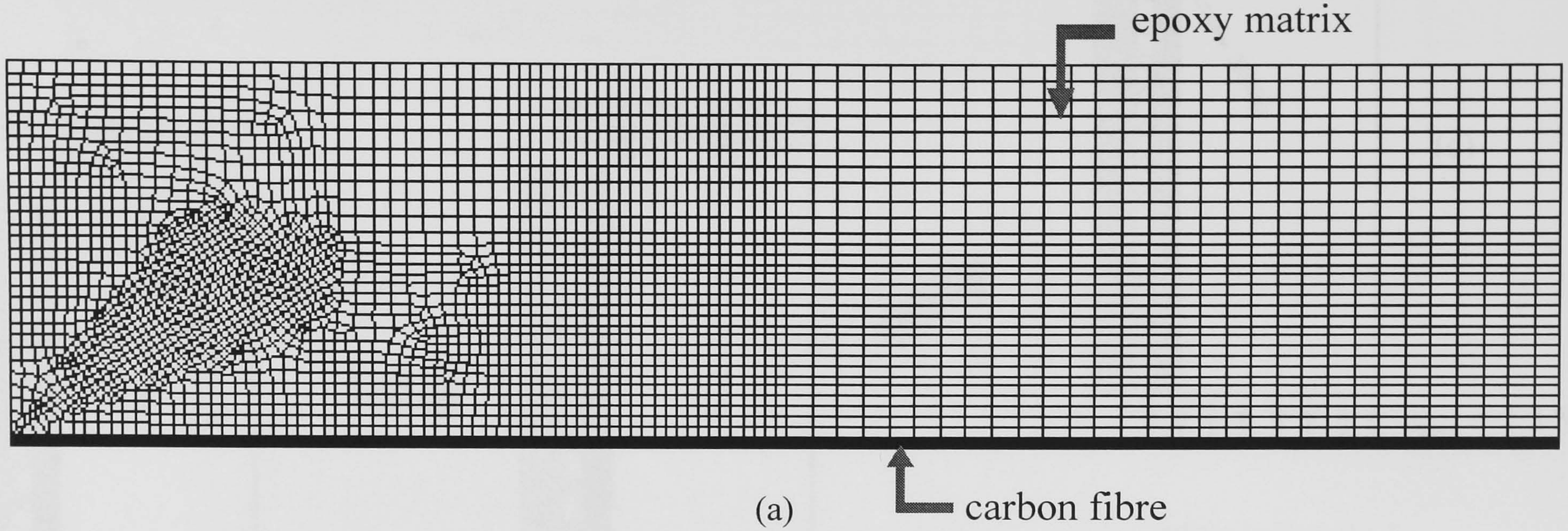

(a)

(b)

Figure 6.2 (a) FE mesh for conical-shaped crack models (b) mesh detail; red arrow indicates the crack propagation direction

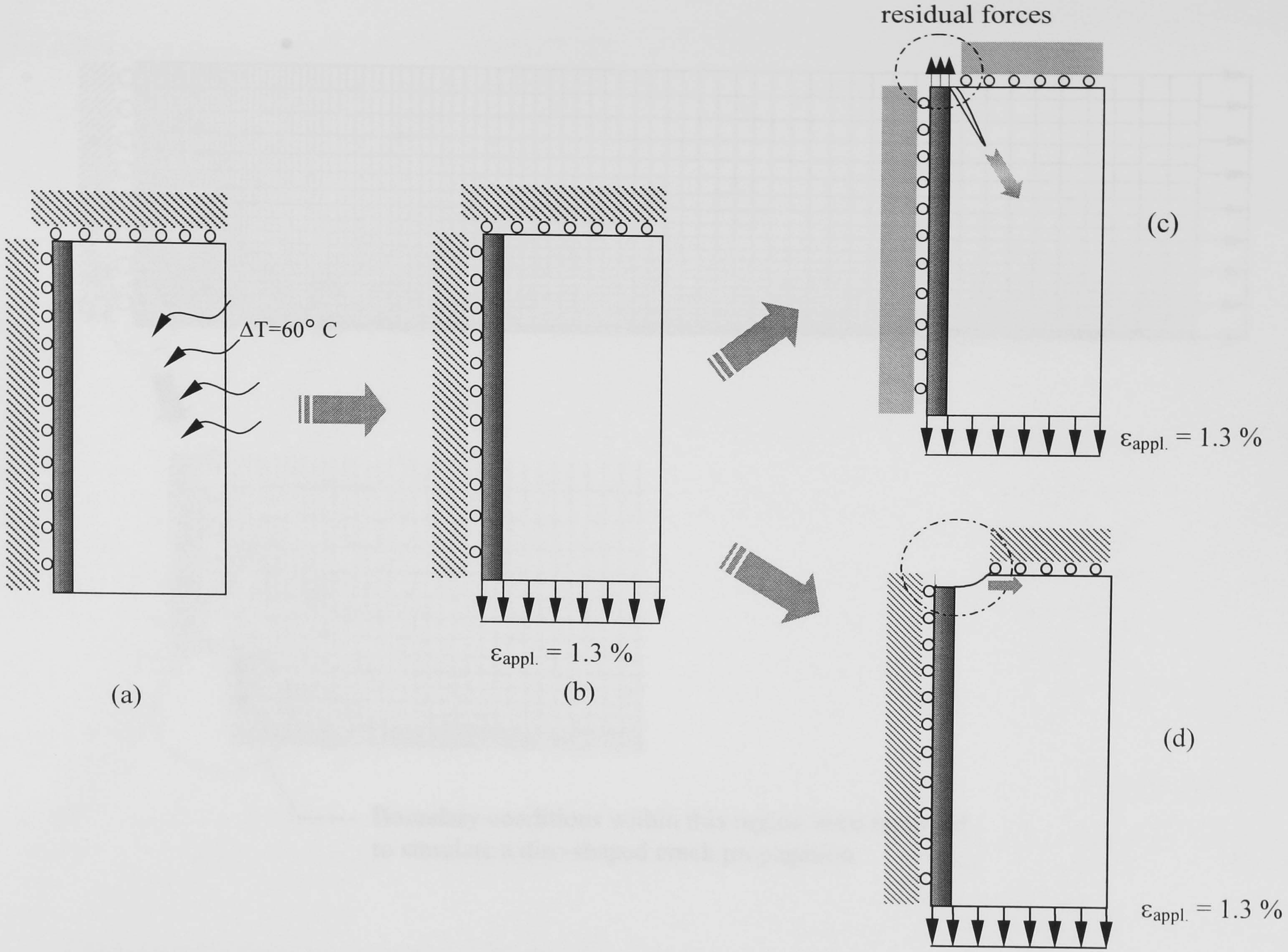

Figure 6.3 Progressional approach in FE analysis (a) curing process (b) applied strain 1.3 %
(c) fibre fracture followed by matrix crack propagation along the arrow direction
(d) fibre fracture followed by disc-shaped crack propagation along the arrow direction

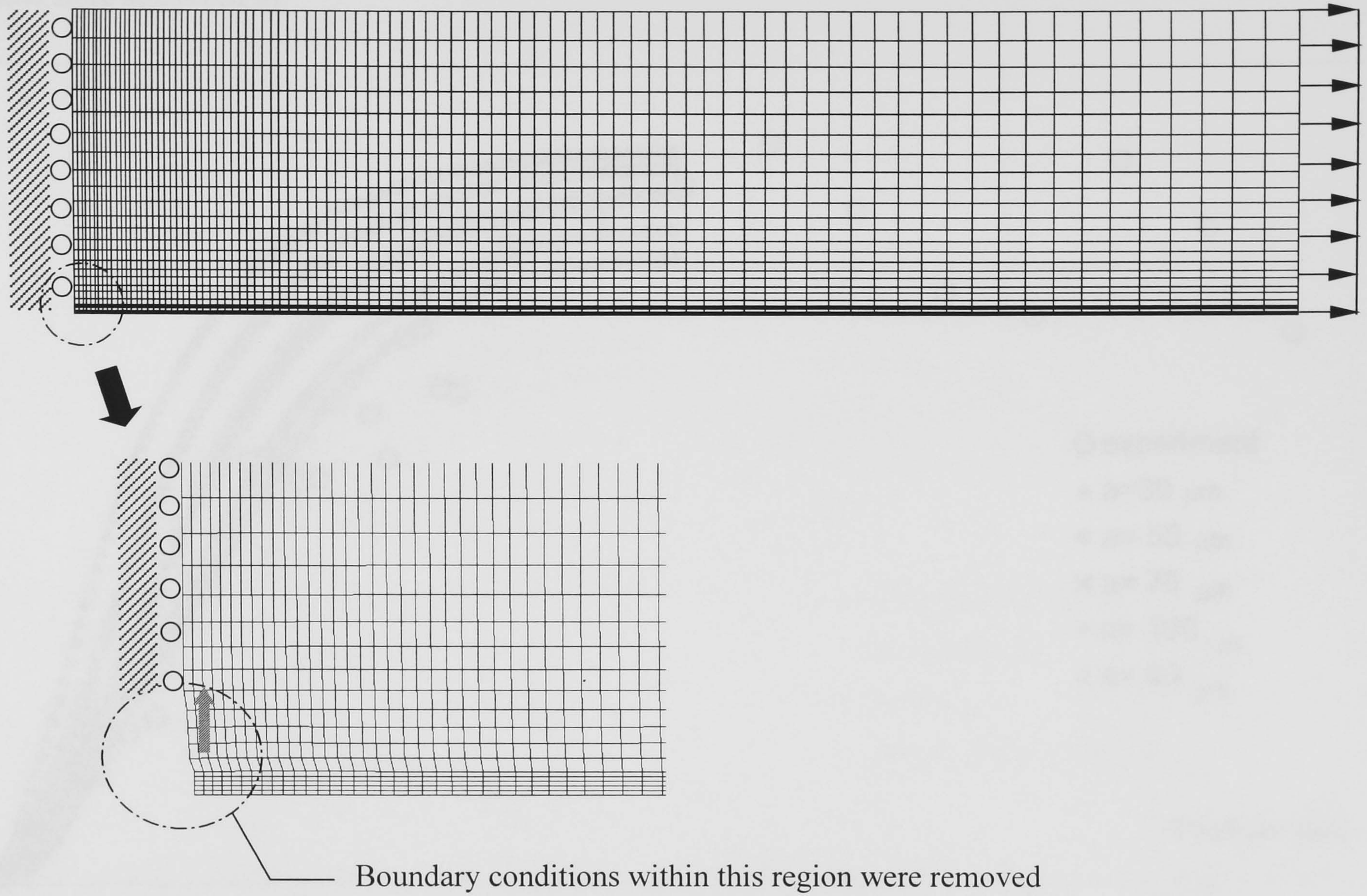

Figure 6.4 FE mesh for disc-shaped crack models

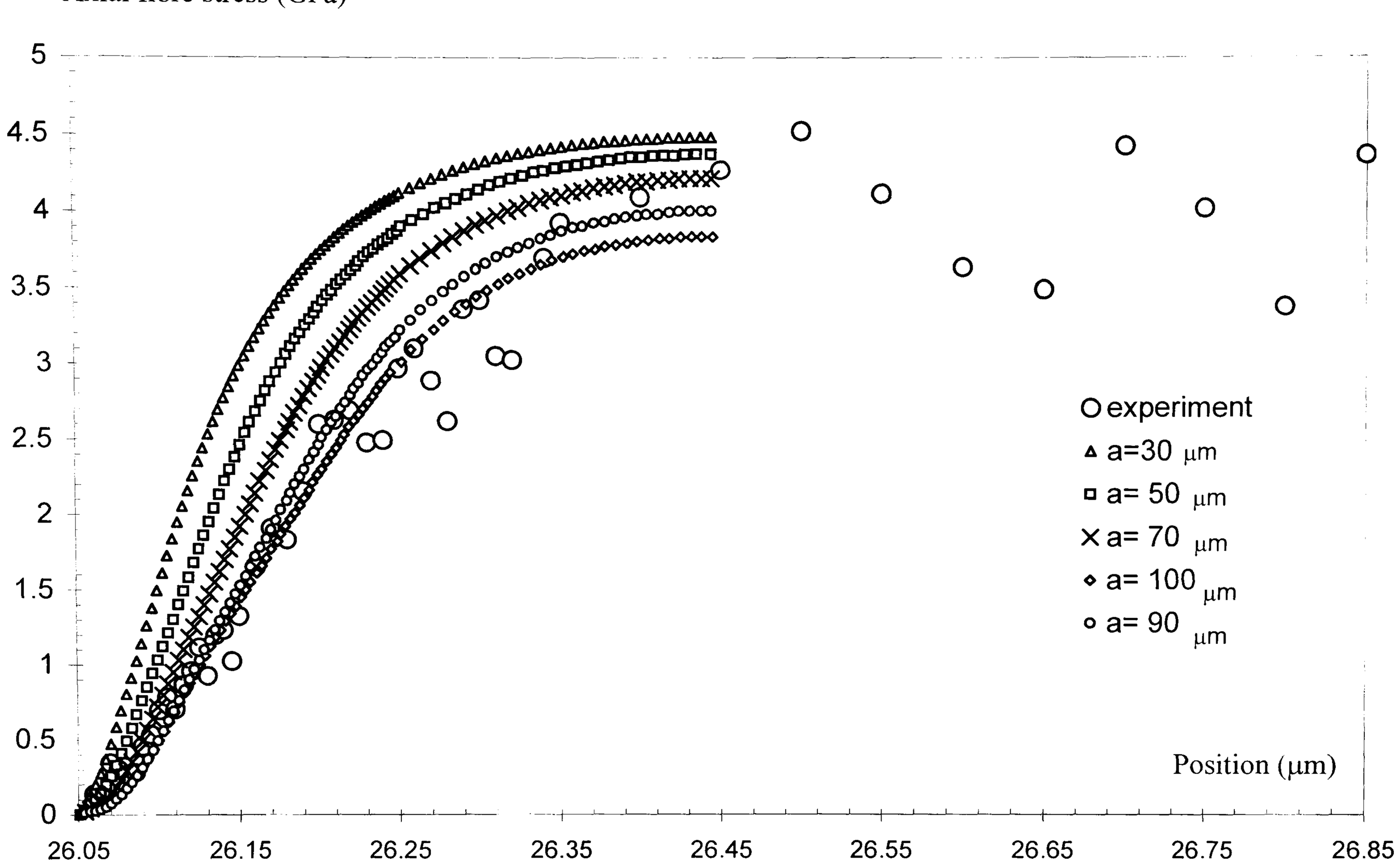

Figure 6.5 Comparison of axial fibre stresses at different crack lengths, in conical crack models with a semi cone angle of 32 ° with experiment

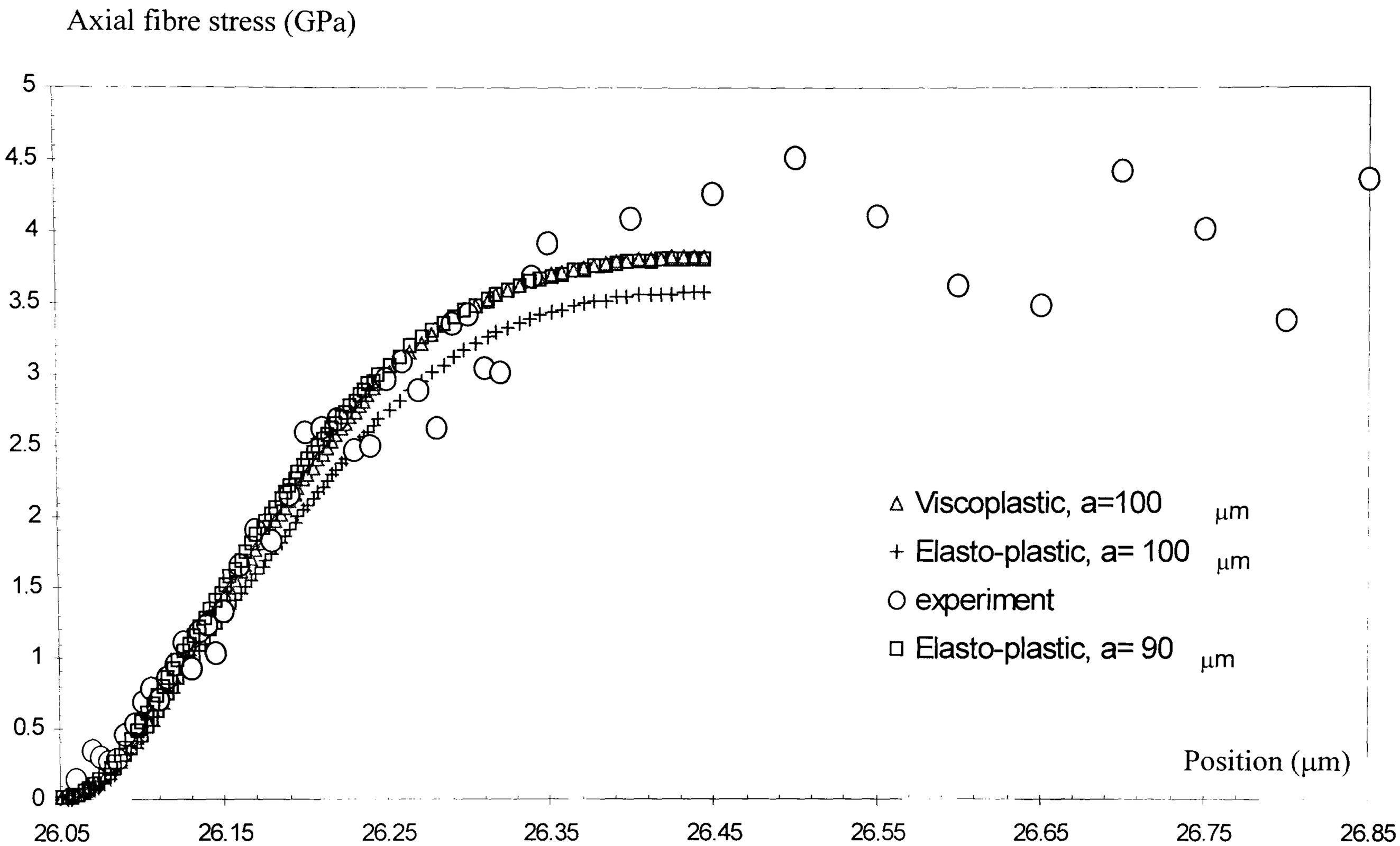

Figure 6.6 Comparison of axial fibre stresses in viscoplastic and elasto-plastic FE analyses for the conical crack models with a semi cone angle of 32 °

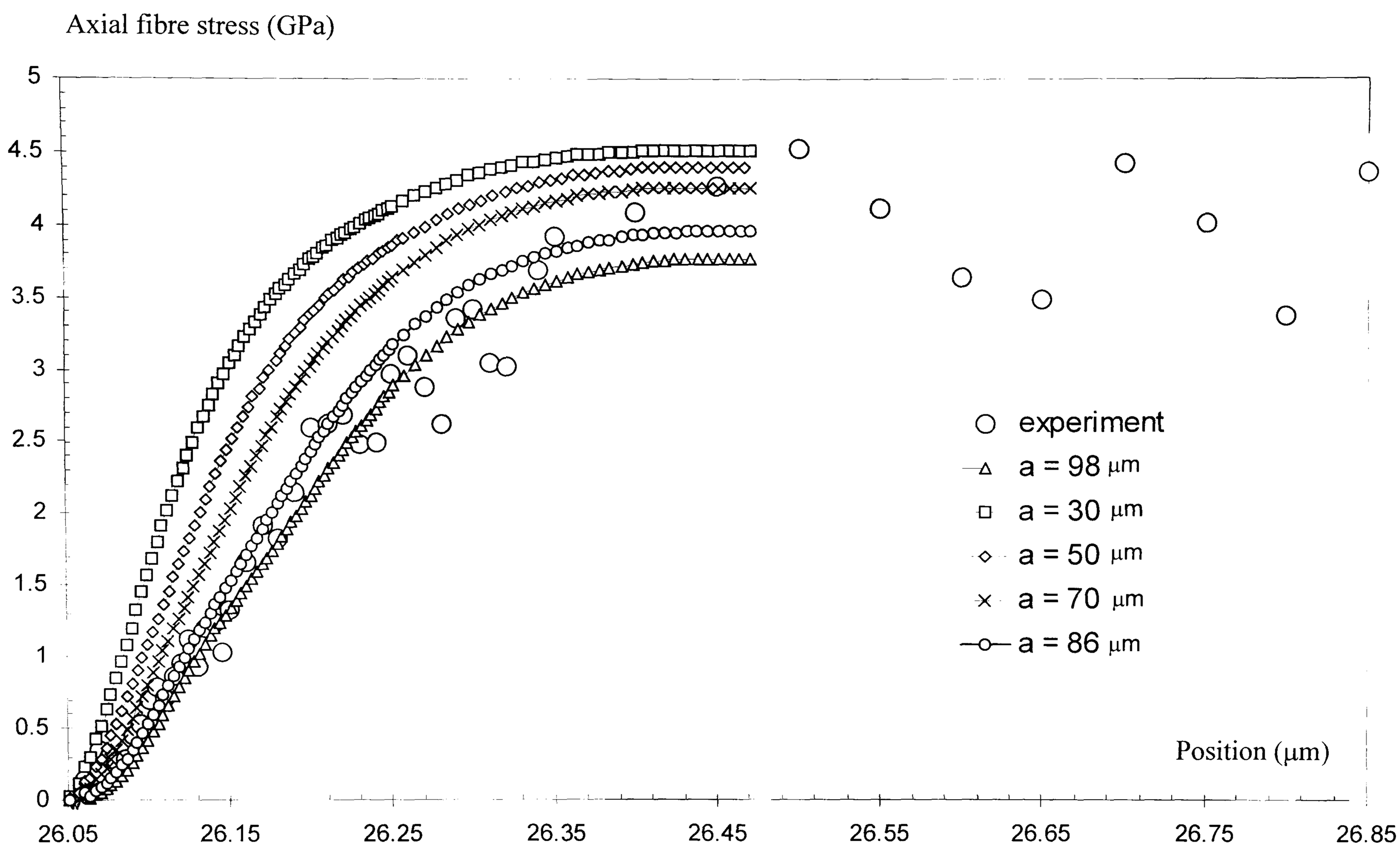

Figure 6.7 Comparison of axial fibre stresses at different crack length in conical crack models with a semi cone angle of 34 ° with experiment

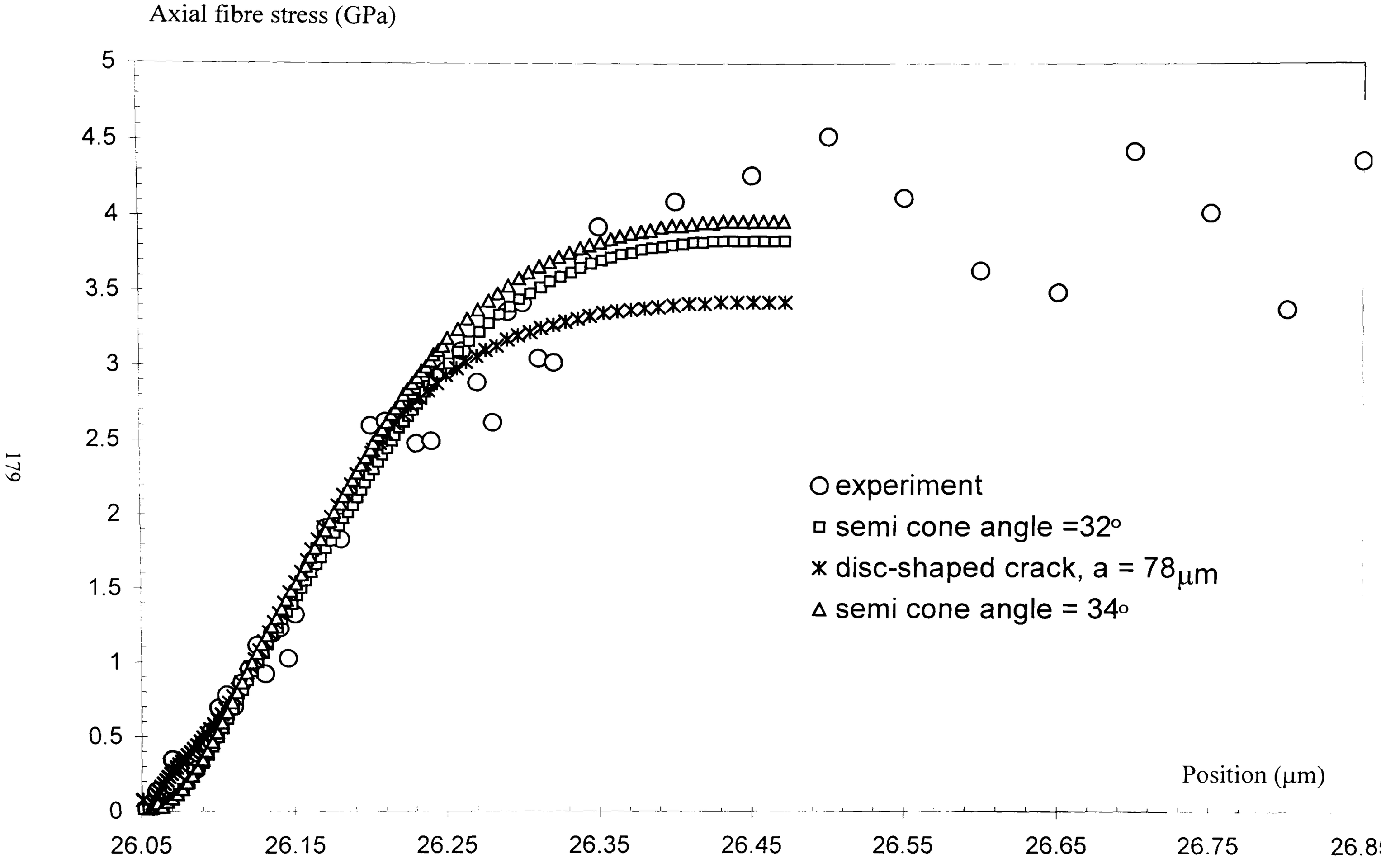

Figure 6.8 Comparison of axial fibre stresses obtained from viscoplastic FE analysis in the conical crack models and disc-shaped crack model

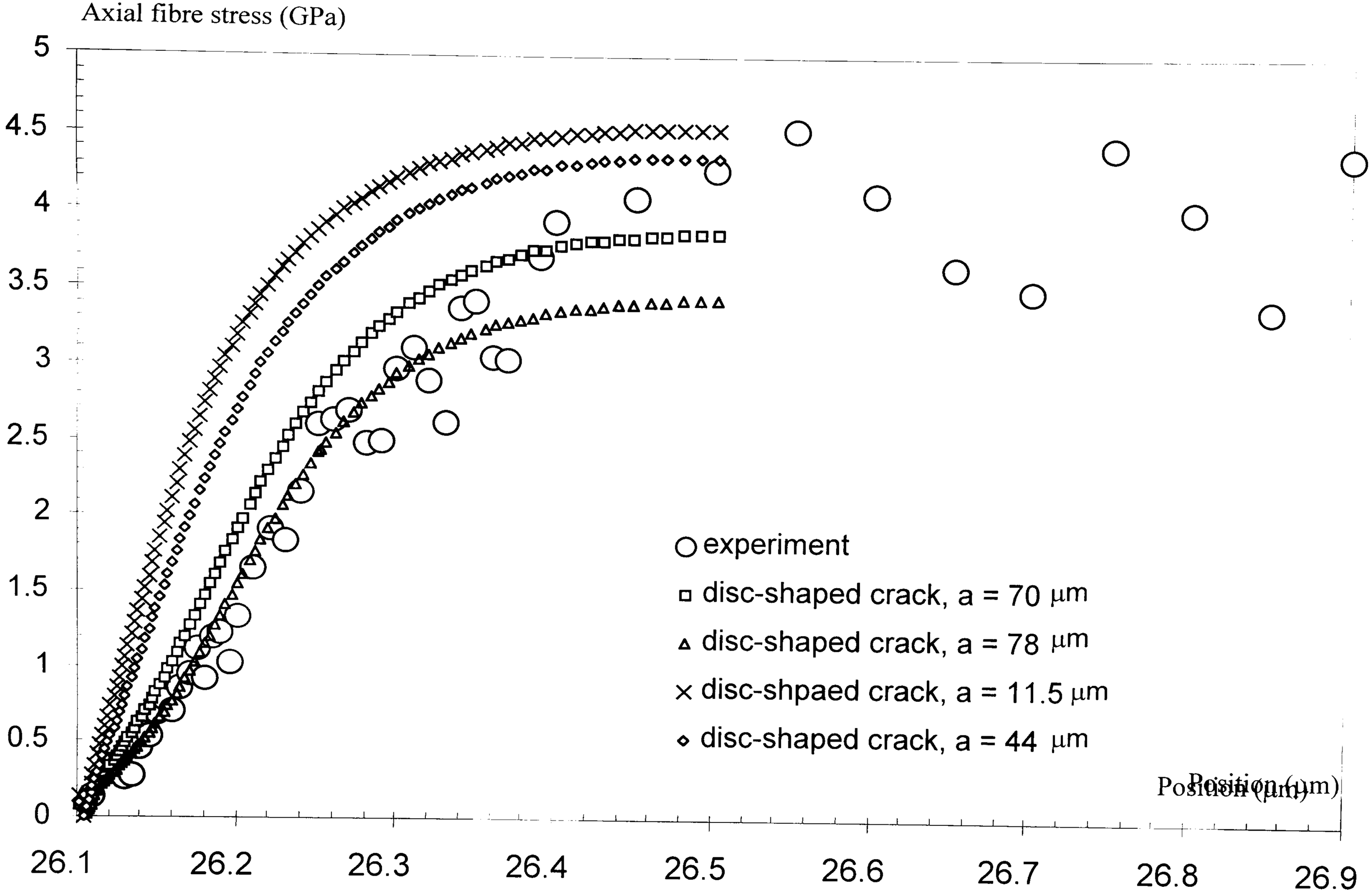

Figure 6.9 Comparison of axial fibre stresses at different crack length in disc-shaped crack models with experiment

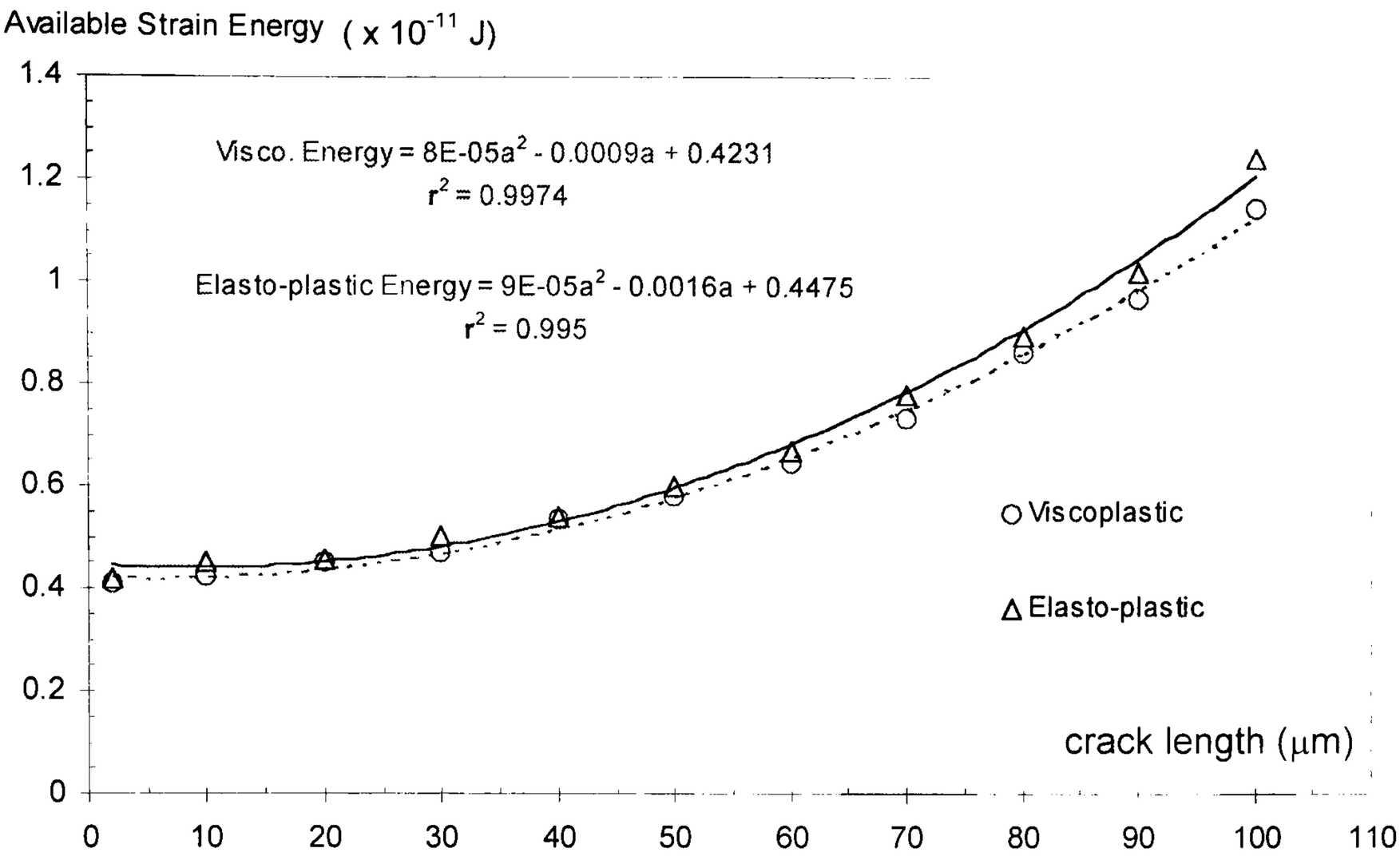

6.10 Variations of the available strain energy in viscoplastic and elastoplastic FE analyses for a conical model with a semi cone angle of 32 °

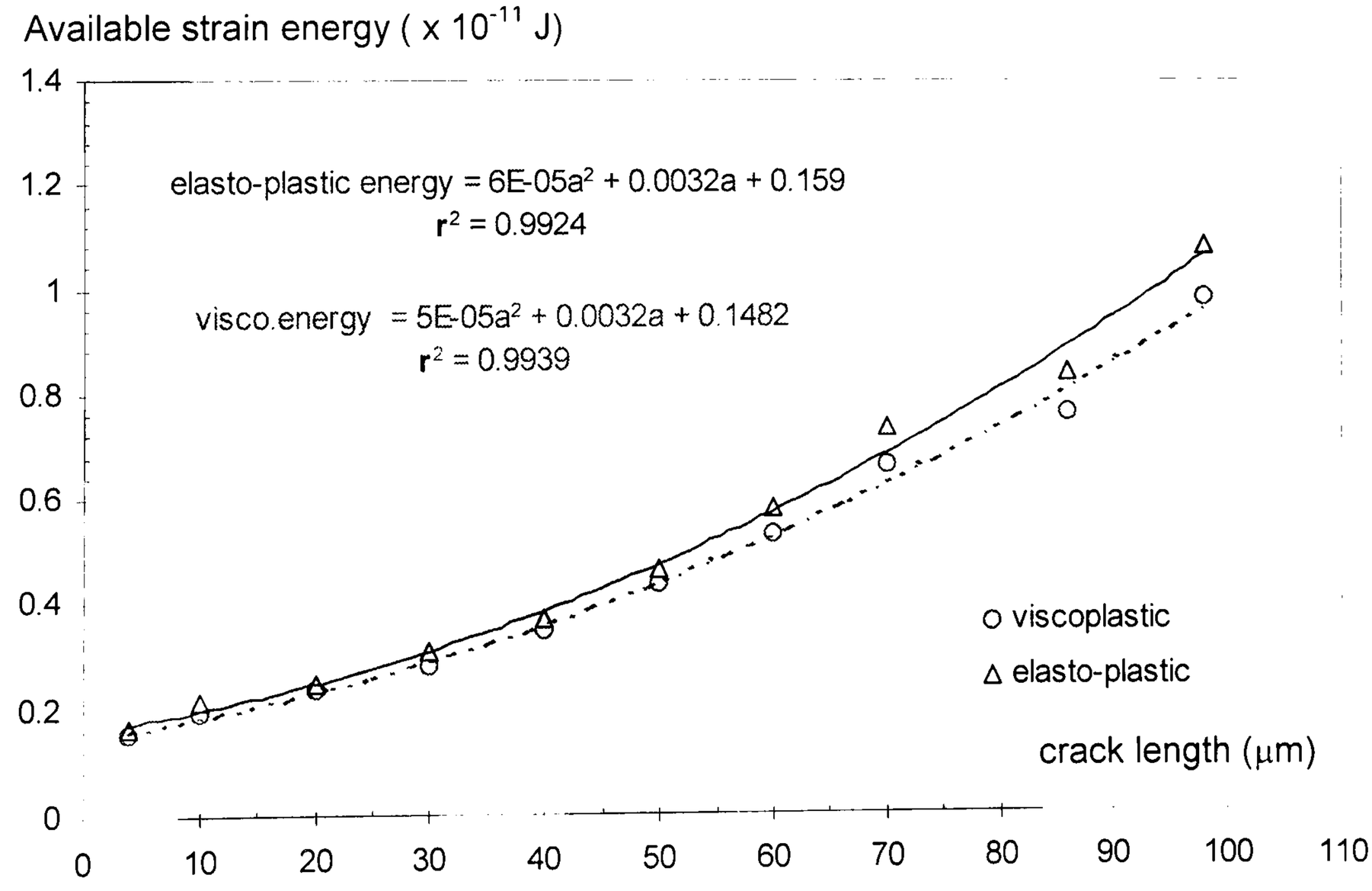

6.11 Variations of the available strain energy in viscoplastic and elastoplastic FE analyses for a conical model with a semi cone angle of 34 °

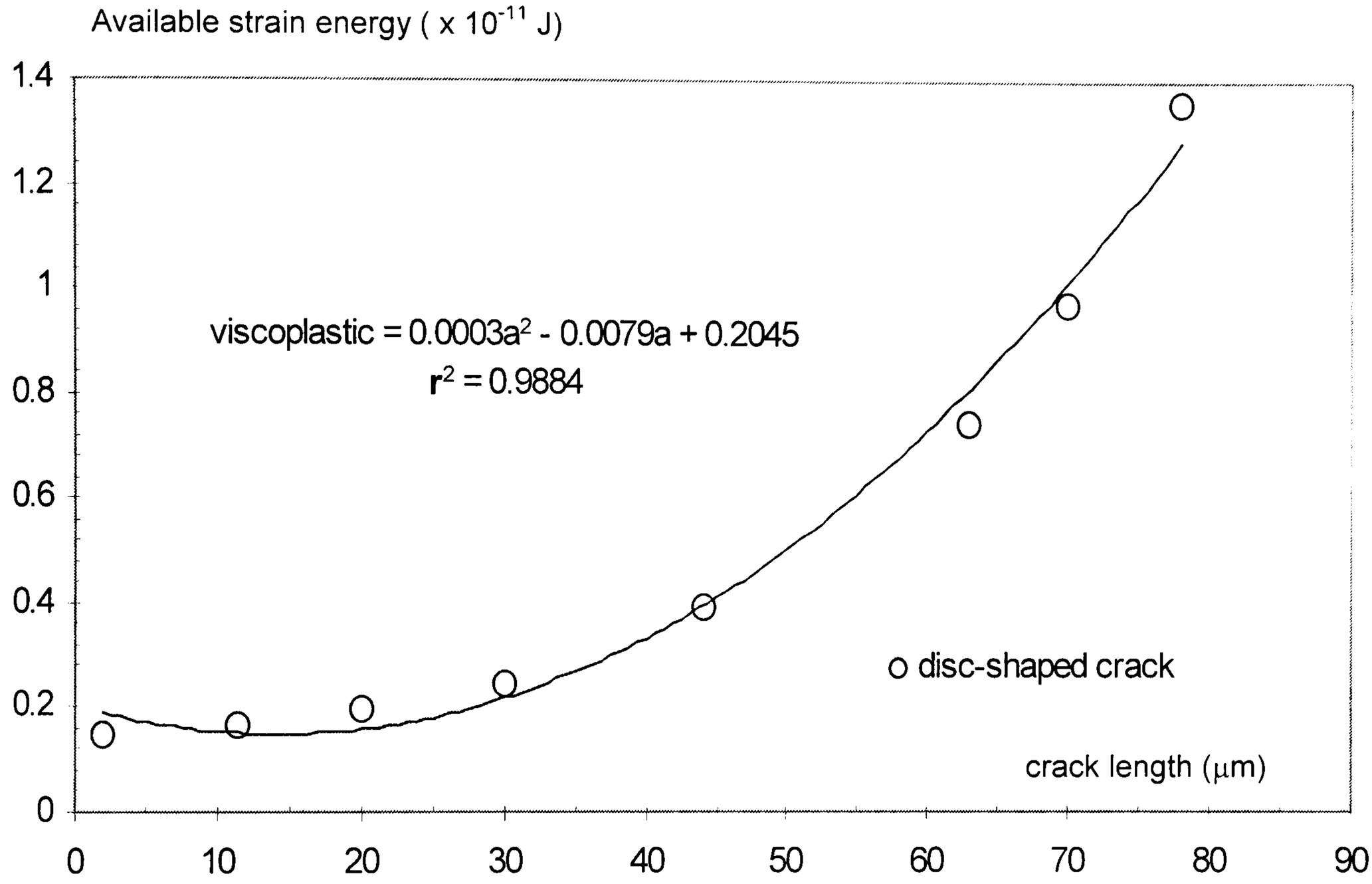

6.12 Variations of the available strain energy in viscoplastic FE analysis for a disc-shaped crack model

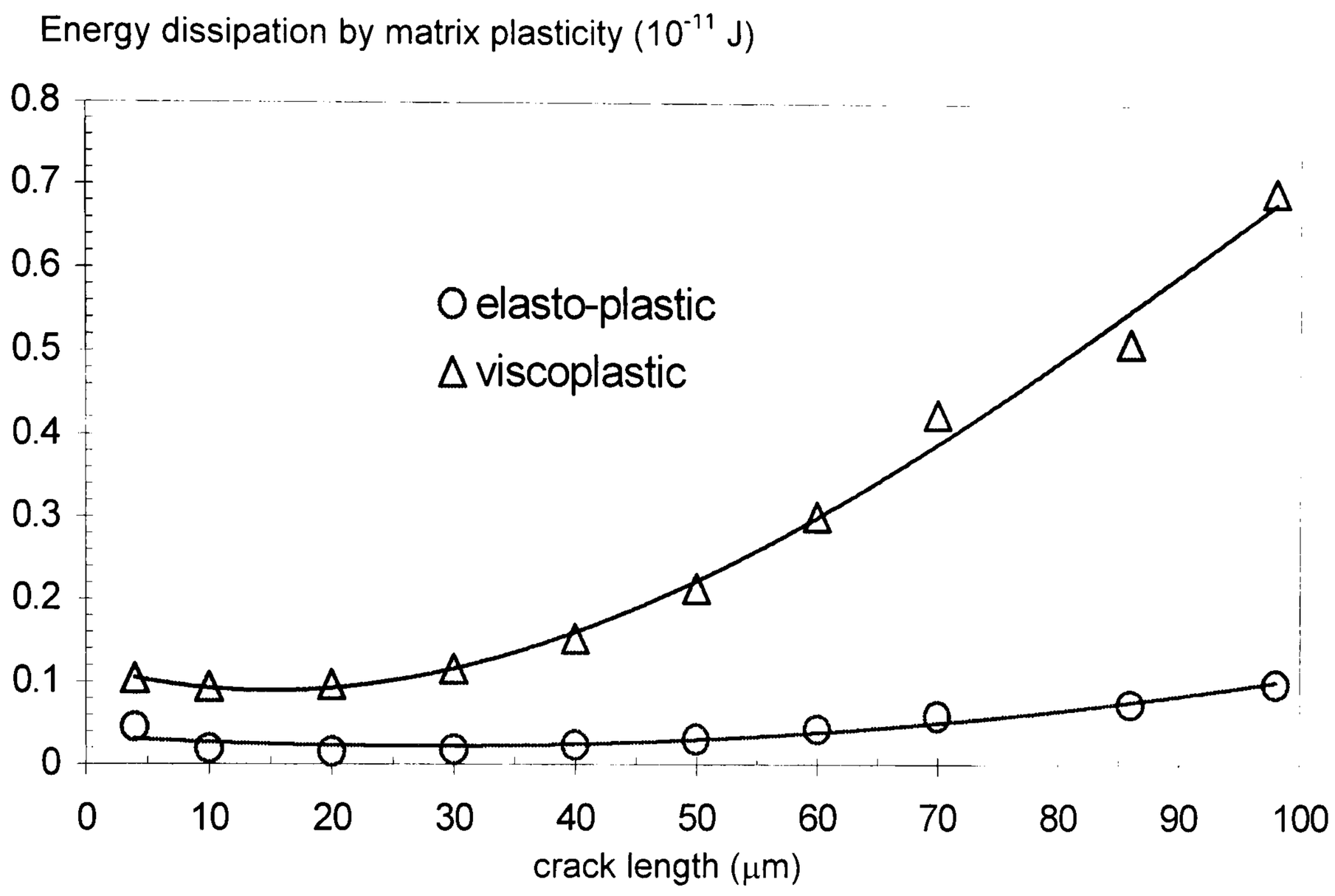

Figure 6.13 Variations of strain energy dissipated to matrix plasticity in viscoplastic and elasto-plastic FE analysis for models with a semi cone angle crack of 32 °

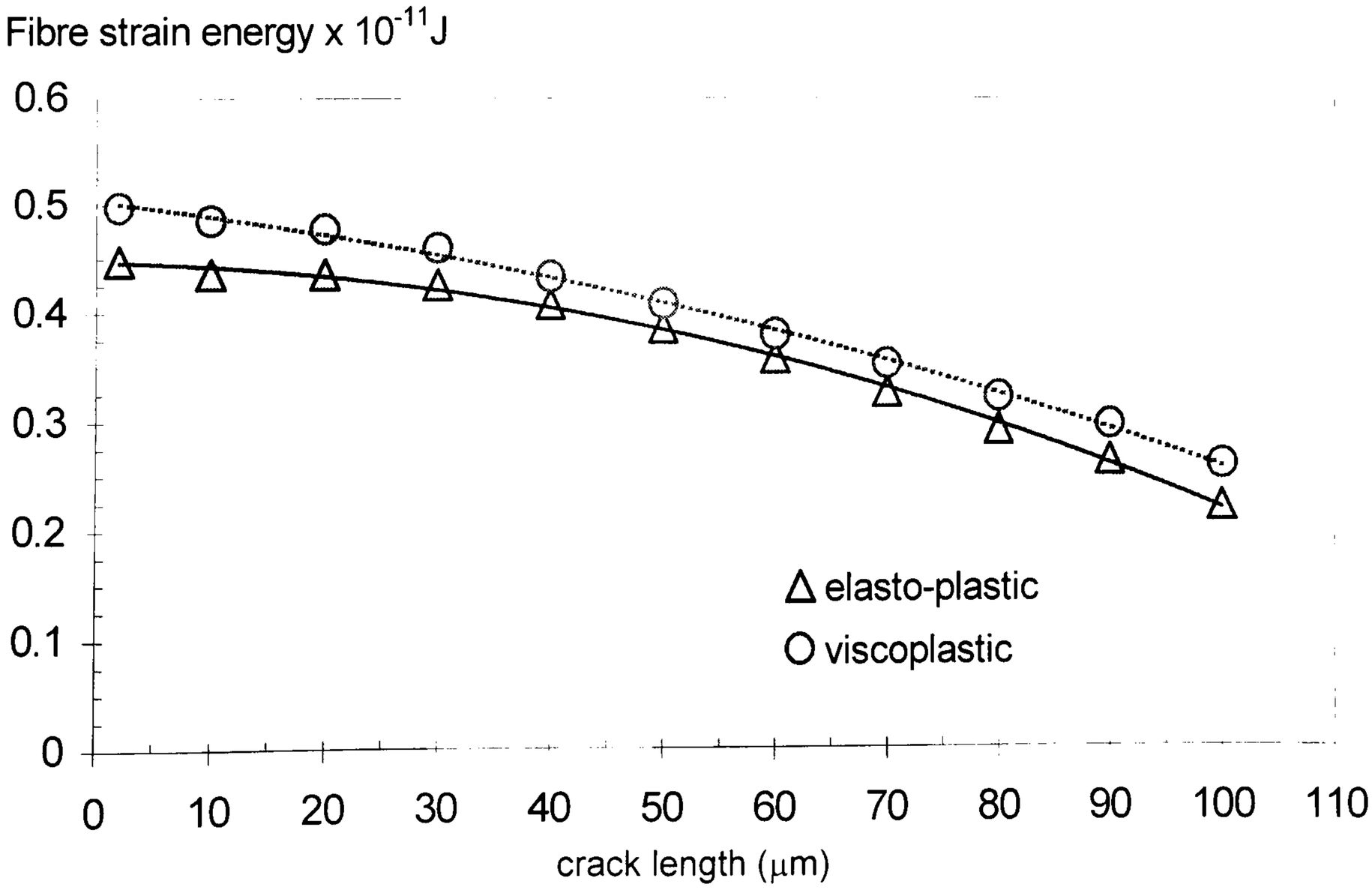

Figure 6.14 Variations of fibre strain energy in viscoplastic and elasto-plastic FE analysis for models with a semi cone angle crack of 32 °

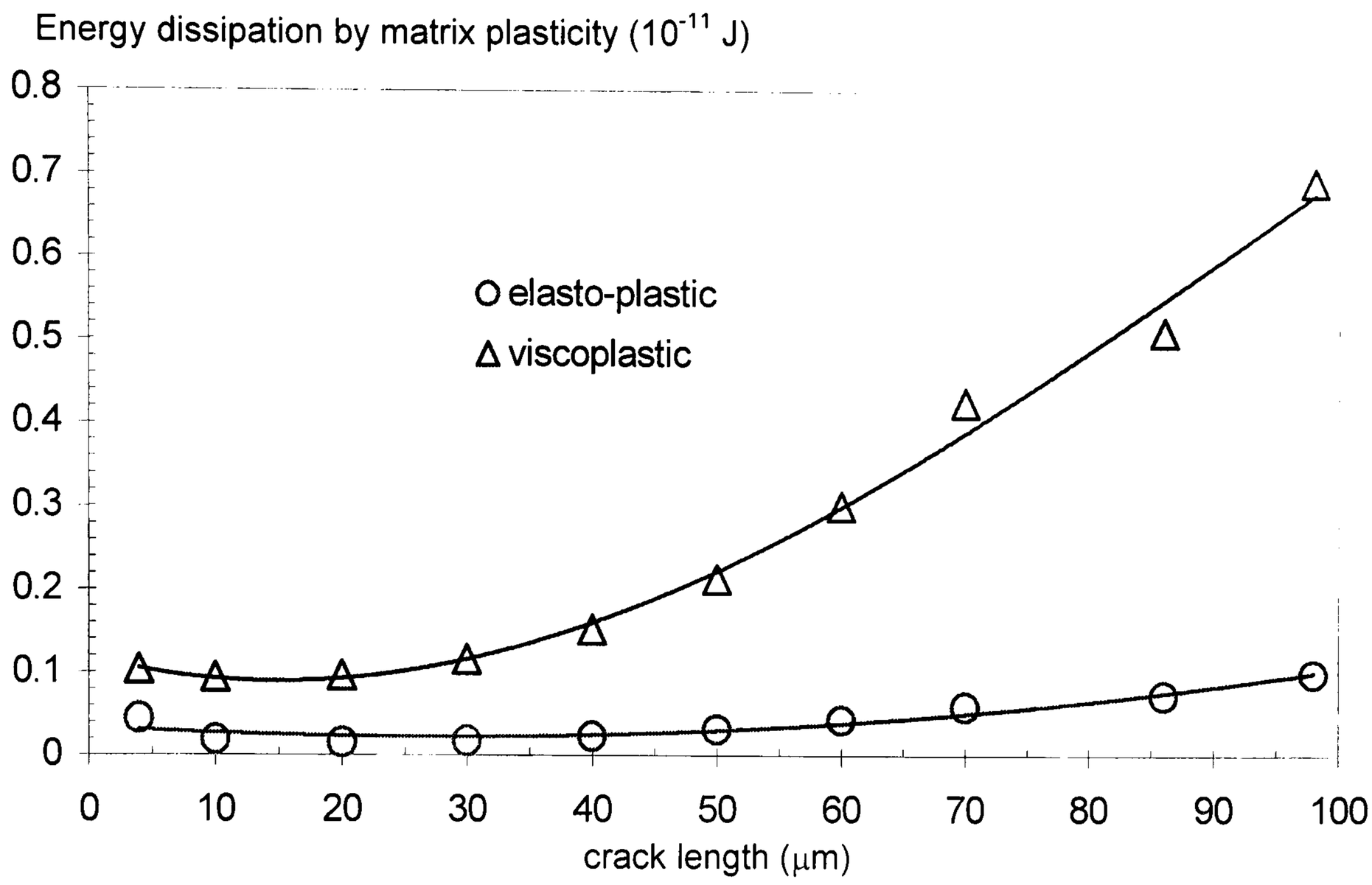

Figure 6.15 Variations of strain energy dissipated to matrix plasticity in viscoplastic and elasto-plastic FE analysis for models with a semi cone angle crack of 34 °

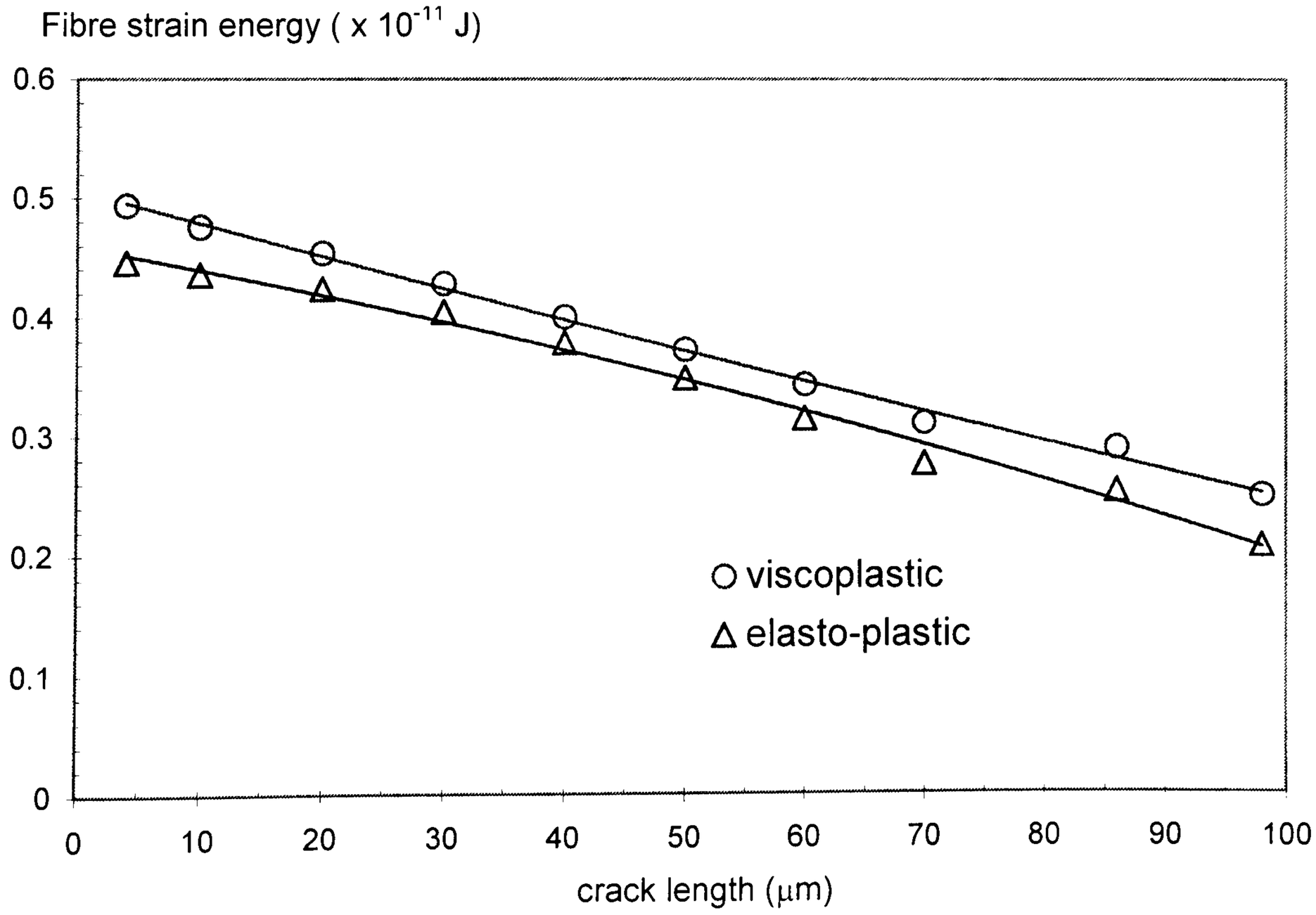

Figure 6.16 Variations of fibre strain energy in viscoplastic and elasto-plastic FE analysis for models with a semi cone angle crack of 34 °

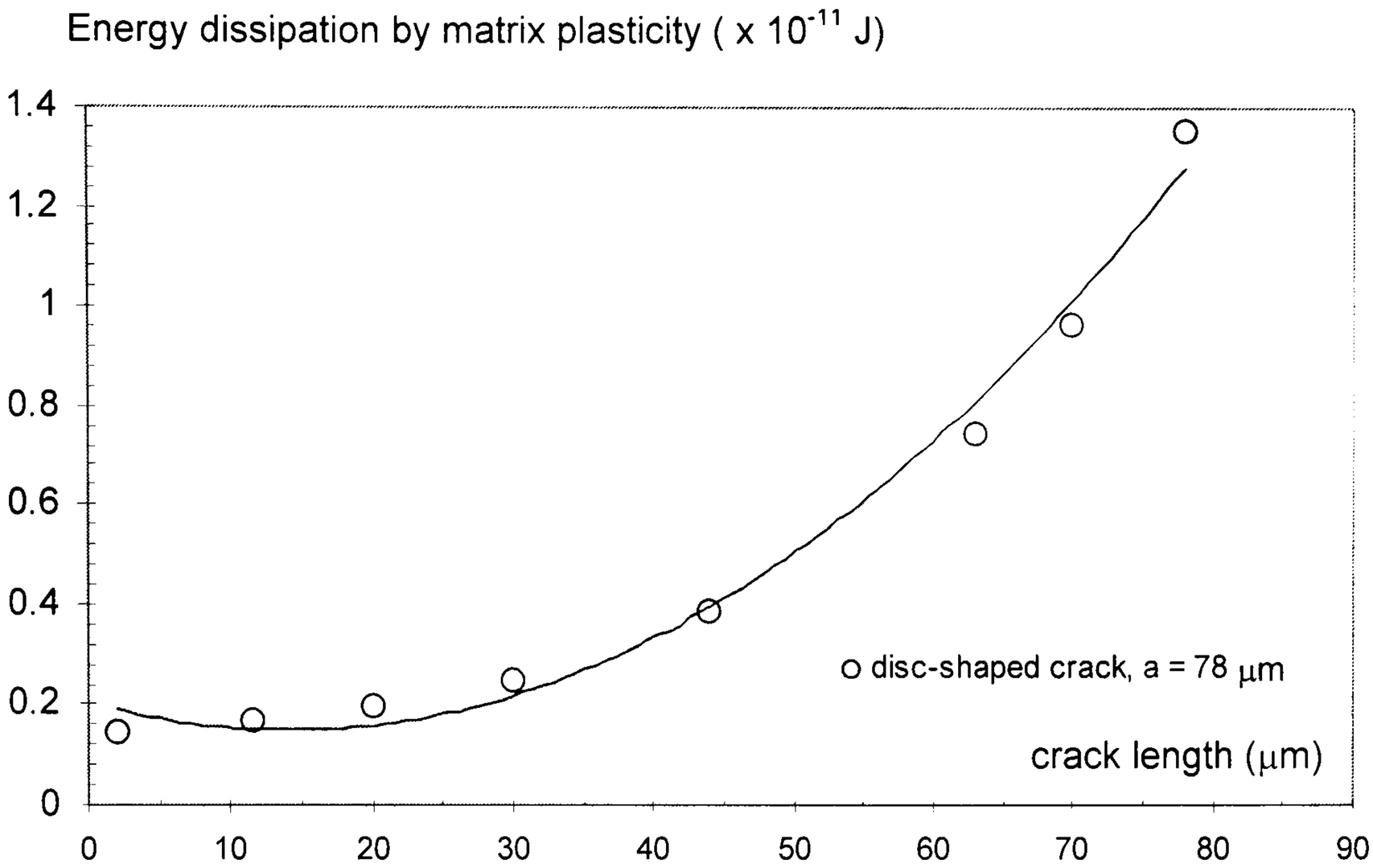

Figure 6.17 Variations of strain energy dissipated to matrix plasticity in viscoplastic FE analysis for disc-shaped crack model

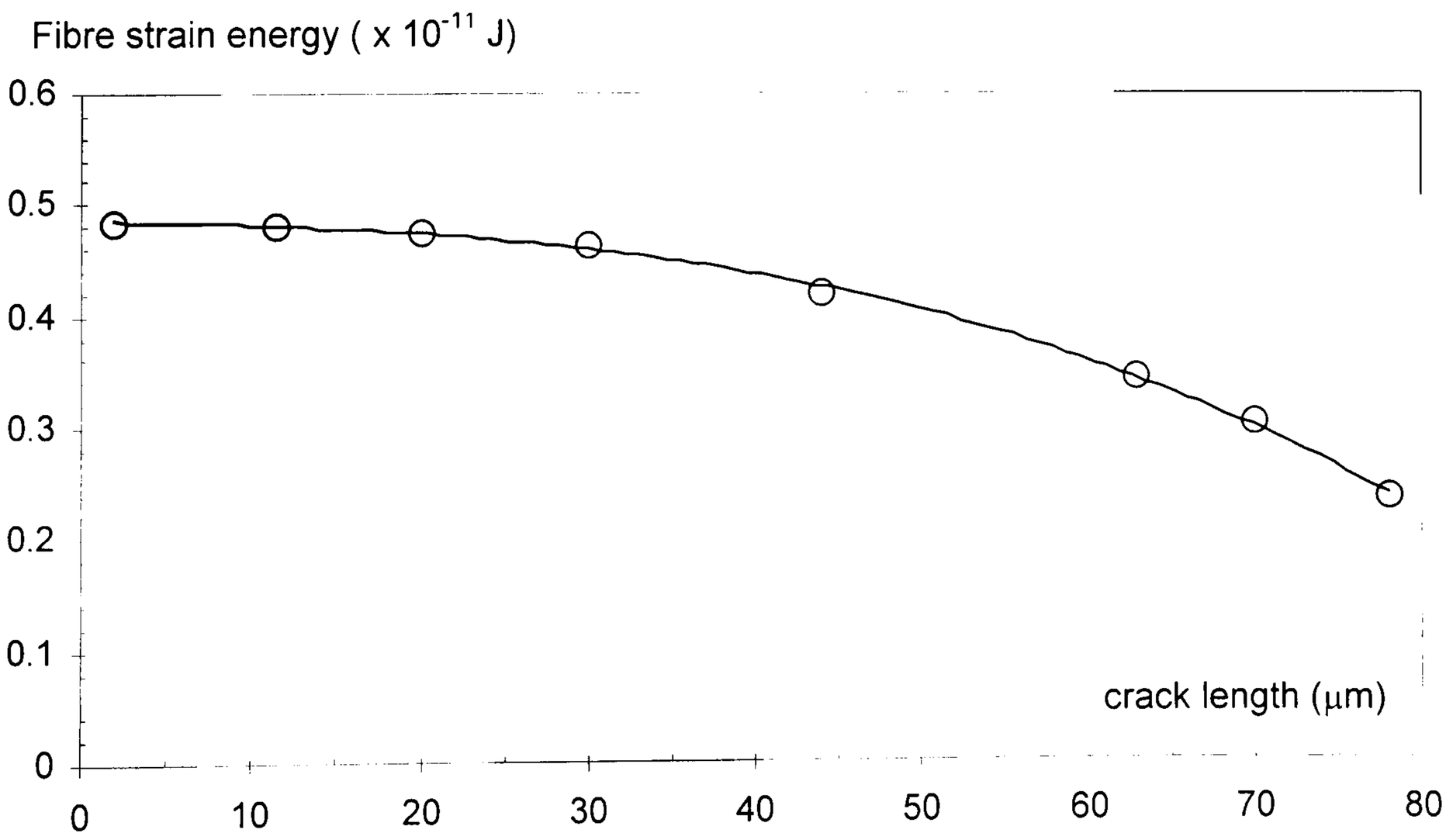

Figure 6.18 Variations of fibre strain energy in viscoplastic FE analysis for disc-shaped crack model

CHAPTER 7

Effects of Inter-fibre Spacing and Matrix Cracks in Planar Array Composites

7.1 Introduction

When an individual fibre in a composite breaks the load is transferred through the matrix to the neighbouring intact fibres and this may induce failure in these fibres. The load carrying capacity of a composite depends on the fibre volume fraction, which in turn determines the inter-fibre spacing. In order to investigate the effect of fibre volume fraction in the composite, the inter-fibre spacing was defined and used by several authors [56,57] in a micromechanical analysis. The inter-fibre spacing, R, is the distance between the centre of a broken fibre and the centre of the adjacent fibres (see Fig. 7.1). To quantify the effect of stress redistribution near the fracture location, the stress amplification factor (SAF) is defined as:

$$SAF = \frac{\sigma_{peak}}{\sigma_{far}} \tag{7.1}$$

Here σ_{peak} refers to the peak value of the axial fibre stress in the adjacent fibres, σ_{far} refers to the far field axial fibre stress (see Fig. 7.1). Some authors refer to this ratio as the stress concentration factor while others refer to it as the stress intensity factor [56,57]. Both names are more commonly employed in different contexts. In order to

avoid possible confusion, the term stress amplification factor (SAF) is used from now on in this work. This name seems appropriate because the axial stresses in the remaining intact fibres are amplified near the fracture plane [36].

The value of the SAF depends on several factors, including the inter-fibre spacing, mechanical properties of the materials and the types of failure. The magnitude of the stress redistribution in the intact fibres is governed by the mechanical properties of the matrix material [109]. Failure in a composite, generally, relies on the strength of the fibre/matrix interface [13]. Debonding usually occurs along the interface for an unsized system whereas matrix cracking occurs in a sized system. The region of the stress amplification in an intact fibre is expressed in terms of a positively affected length (PAL) (see Fig. 7.1). The alternative approach to specifying the region of stress amplification is to use the stress transfer length (L_f) (see Fig. 7.1) which is equal to half the PAL [56].

A 3-D finite element (FE) analysis has been used to study stress concentrations in multiple fibre model composites by Fiedler *et al.* [110]. They used a fibre with a pre-existing crack extending out into the matrix in their FE model. This approach is, strictly speaking, only valid for a linear elastic analysis. For an elasto-plastic analysis, the correct order of events should be modelled starting with an intact fibre-end followed by the simulation of fibre fracture. If a pre-existing crack is used the plastic strain in the matrix material near the fracture location is underestimated.

The effect of inter-fibre spacing on stress transfer in multi-fibre model composites was studied by van den Heuvel *et al*. [57]. They performed a 3-D linear elastic and elasto-plastic FE analysis, which incorporated three load steps. A thermal load was applied in the first load step to simulate the thermal residual stresses, resulting from the curing process. Several small increments of mechanical strain were then applied in a second load step. When the mechanical applied strain reached 0.40 % the fibre fracture was simulated by releasing the nodal constraints in the axial direction from the fibre-end face in the third load step. Their linear elastic and elasto-plastic FE results gave a reasonable approximation of the trend for the SAF, but the magnitudes predicted for SAF were much lower than their experimental results obtained using a LRS. This discrepancy probably resulted from an unrealistic failure mechanism assumed in the model. Lane *et al*. [58] performed 3-dimensional FE analysis with the inclusion of the interphase to investigate the effect of matrix plasticity on the strain transfer characteristics. Nevertheless, the associated failure after fibre fracture was not included. This would lead to an overestimate of the matrix strains due to the fact that matrix cracking and interface debonding have the effect of relieving the stresses in the matrix material.

It is necessary to include a realistic failure mechanism in the FE model of the composite in order to obtain a good approximation for the SAF. The presence of conical-shaped matrix cracks may have the effect of reducing the load-carrying capacity of the matrix and increasing the load carried by adjacent intact fibres. The effect of a conical-shaped matrix crack on the fibre stresses and the SAF is

investigated in this study. Using ABAQUS [100], 3-D elasto-plastic FE analysis for a composite with a planar array of fibres has been performed to investigate the influence of the fibre volume fraction on this effect. A *Progressional Approach* [76] in the FE analysis was used to simulate the thermal residual stresses from the fabrication process and the fibre fracture. The FE results were compared with the measurements obtained using LRS by Chohan *et al.* [56]. This is because LRS cannot be used to investigate the stress in a broken fibre located at the centre of the hexagonal array.

7.2 Finite Element Models

A composite with a planar array of fibres has been modelled using 3-D elasto-plastic FE analysis (see Fig. 7.2). The FE model had the same geometry as the LRS specimen [56] so that predictions of the model could be compared with the experimental results. The effect of the inter-fibre spacing on the stress redistribution near the fibre fracture location was examined by varying the ratio of the fibre centre distance R to the fibre diameter d. Values of the ratio R/d equal to 1.1, 1.25, 1.5, 2, 3, 4, 5 and 8 were used to create the FE models which comprised 11,000 linear brick elements (see Fig. 7.3).

The effect of matrix cracking on the stress redistribution was investigated by introducing conical shaped matrix cracks, initiated from the crack in the fibre, into the FE model using an additional load step. Contact elements were used to bond a pre-defined matrix crack path during the preliminary simulation steps. Crack propagation

was then simulated by deactivating the contact elements along the crack path during the final load step. The FE mesh for the models with a conical-shaped matrix crack consisted of 14,144 linear brick elements and 32 surface-to-surface contact elements with a sticking contact condition (see Fig. 7.4).

The quasi-static FE analysis was divided into 3 or 4 sequential ABAQUS load steps (see Fig. 7.5), depending on the types of analysis, to implement the *Progressional Approach* as follows:

i) Thermal Pre-load: A temperature drop $\Delta T = -60°$ C was applied in this load step in order to simulate the curing process in the specimen. Matrix contraction leads to residual compressive stresses in the fibres. The displacement constraints in the axial direction of the composite were applied to every node on the pre-defined fibre fracture surface.

ii) Applied Mechanical Load: A uniform displacement δ, corresponding to an applied strain of 0.4 %, was applied to every node on the end face of the composite (see Fig. 7.2). At this strain level, the matrix material was everywhere yielded.

iii) Fibre Fracture: Fibre fracture was simulated by removing all displacement constraints on the fibre-end face to form a penny-shaped crack. This was achieved by ramping the forces on the fibre-end face linearly down to zero within the time step defined in ABAQUS. The applied strain of 0.4 % was held constant during this step.

iv) Matrix Cracking: For models with a matrix crack, a conical-shaped matrix crack with a semi cone angle of 40° and a crack length ranging from 2-8 μm was introduced in this load step. This simulation was performed by removing all constraints on the fibre end face and deactivating the contact elements along the pre-defined crack path according to the desired crack length. By using this technique, the residual contact forces will be ramping down to zero within a time defined in this load step [100]. The crack length increment used was 2 μm and the applied strain was held constant during this step.

The carbon fibre is a transversely isotropic material with linearly elastic behaviour. The material properties of high-modulus M40-3k-40^{TM} carbon fibre (Toray Industries) were used in the FE model (see Table 7.1). The elasto-plastic behaviour of the matrix material was modelled using the relaxed properties of LY5052/HY5052^{TM} (Ciba-Geigy) epoxy matrix (see Fig. 7.6) [86]. These properties were used because the strain-rate used in the LRS experiment was approximately $0.25x10^{-2}$ min^{-1}.

7.3 Results Summary

7.3.1 Comparison of FE Predictions with Experimental Results

Experiments have shown that the first fibre fracture occurs when the applied strain is 0.4 % [56]. In order to compare with the LRS results, a FE model with a fibre spacing of 10.8 μm, as used in the experimental specimens. The FE analysis of the

effects of thermal pre-load predicted a residual longitudinal strain ε_{zz} and the residual lateral strains ε_{xx} and ε_{yy} in the matrix material of about -0.00191, –0.00593 and -0.00053, respectively. The shear strain components in the matrix material were found to be very small at this stage. The thermal residual axial stress σ_{zz} in the fibre of about 14.4 MPa was predicted by FE analysis. The von Mises stress and von Mises strain induced by the curing process are shown in Fig. 7.7 and Fig. 7.8, respectively. The FE analysis predicted the fibre stress in an intact fibre adjacent to the crack of the same order as that measured by LRS, but the predicted stress variation is significantly different (see Fig. 7.9). The axial stress in the broken fibre obtained from FE analysis does not compare well with the result from LRS, at the region close to fibre fracture (see Fig. 7.10). Both FE and LRS results give the same maximum fibre axial stress of approximately 1.75 GPa. The maximum interfacial shear stress (ISS) predicted by FE was found to be about 27 MPa, while Chohan *et al*. [56] obtained the maximum value of about 30 MPa (see Fig. 7.11). Chohan *et al*. obtained the ISS profile by fitting the fibre axial stress profile with a cubic spline function and then converted it to ISS using the result:

$$\tau_{(rx)} = -\frac{r_f}{2}\left[\frac{d\sigma_f}{dx}\right] \tag{7.2}$$

where r_f is a fibre radius and x is a distance along the fibre length. The value of the PAL from FE analysis is a little lower than experimental results when the conical-shaped matrix crack was neglected in the FE model. A critical zone with a very high

value for the equivalent plastic strain, ranging from 1 % to 13 %, in the matrix material ahead of a crack tip implied a catastrophic failure in the matrix material (see Fig. 7.12). This would lead to an initiation of matrix crack propagation. The FE results obtained from this model have also predicted a value for the SAF lower than the experimental results. In reality, an individual fibre fracture would be followed either by debonding along the fibre/matrix interface for the unsized system or by conical-shaped matrix crack propagation for the sized systems [13]. A conical-shaped matrix crack has also been observed during LRS measurements for this composite [27,28].

In the fragmentation test for a single fibre system, the semi cone angle of a conical-shaped matrix crack was found to lie in the range 30°-60° [19-21,27]. In order to investigate the effect of a matrix crack on the SAF, a semi cone angle of 40° was assumed. The effect of crack length is more important than the effect of crack angle (see section 6.4). Good agreement was obtained using a crack length of 4 μm in 3-dimensional FE analysis (see Fig. 7.9). The PAL and L_f are increased by the presence of a conical-shaped matrix crack. The FE results have shown that neglecting a conical-shaped matrix crack in the FE model leads to an underestimate the values of the SAF and PAL. The axial stresses in a broken fibre with and without a matrix crack are compared with the experimental results in Fig. 7.10. It is seen that the axial fibre stress obtained using a FE model with a matrix crack gave better agreement with experimental results than using a model without a matrix crack. The ISS was found to have approximately half the value for the model without a matrix crack (see Fig.

7.11). The critical location, which contains high value of the equivalent plastic strain, was confined adjacent to the crack (see Fig. 7.13).

7.3.2 Effect of Inter-Fibre Spacing on SAF

In order to study the effect of fibre volume fraction upon SAF, the ratio R/d was used in a dimensionless study of the effect of inter-fibre spacing (see Fig. 7.2). Values of the ratio R/d equal to 1.1, 1.25, 1.5, 2, 3, 4, 5 and 8 were used to create FE models. The variation of the SAF with the ratio R/d is shown in Fig. 7.14. The SAF calculated by FE analysis for the ratios 1.5, 2, 3, 4, 5 and 8 are lower than the values obtained by experiment [56]. The values of SAF decrease gradually and reach a constant value when the ratio R/d is greater than 8 (see Fig. 7.14). This is because the presence of a conical-shaped matrix crack was neglected in the FE models. Matrix cracking in composites reduces the stress redistribution efficiency, which would have the effect on increasing the axial stress in the intact fibres and increasing the PAL. Matrix cracks do not have an effect on SAF when the ratio R/d is close to unity. This is because the maximum crack length that could occur for R/d near unity will be very small. The fibre axial stress in the neighbouring fibres has the same value as the far field stress when the ratio R/d reaches the value of 8.

7.3.3 Effect of Matrix Crack on SAF

The presence of matrix cracks in composites has been neglected in all previous FE studies [57,58,87]. After a fibre fractures in a sized system, the fibre recoil may initiate a conical-shaped matrix crack from the fibre crack [36]. This will lead to a

reduction in the stress redistribution area, which in turn will increase the axial stress in the intact fibres. A conical-shaped matrix crack with a semi cone angle of 40° was included in all FE models. It has been found that for values of the ratio R/d in the range 1.1 to 3, a crack length of 4 μm gave good agreement with experimental results. When the ratio R/d is greater than 4, a crack length of 8 μm gave better agreement. The FE results have confirmed that a longer matrix crack length is required at larger inter-fibre spacing to obtain good agreement with experimental results (see Fig. 7.14).

7.4 Discussion

It has been shown that the inter-fibre spacing plays an important role in determining the stress redistribution in the intact fibres adjacent to cracked fibre in a planar fibre array composite. Disregard of a realistic failure mechanism in the composite will lead to an erroneous estimation of SAF and fibre stresses. A large inter-fibre spacing has less effect on the stresses in the neighbouring fibres, but would lead to catastrophic failure in the matrix material. A matrix crack has a significant effect on the SAF when the ratio R/d is greater than 2. A low inter-fibre spacing leads to a high value of SAF, which would induce another fracture in the adjacent intact fibres. An appropriate inter-fibre spacing is required to improve a composite toughness in order to prevent the domino effect of the fibre fracture to occur.

Material Properties	Carbon fibre	Matrix LY5052/HY5052 (relaxed properties)
Axial Tensile Modulus, GPa	392	1.78
Transverse Modulus, GPa	20	1.78
Axial Tensile Strength, GPa	3.2 *(fracture)*	31×10^{-3} *(yield)*
Axial Fracture Strain, %	0.8	4.2
Transverse Poisson's ratio, $\nu_{R\Theta}$	0.27	0.36
Poisson's ratio in R-Z direction, ν_{RZ}	0.03	0.36
Axial Coefficient of Thermal Expansion, K^{-1}	-0.25×10^{-6}	58×10^{-6}
Transverse Coefficient of Thermal Expansion, K^{-1}	25×10^{-6}	58×10^{-6}

Table 7.1 Material properties of carbon fibre and epoxy matrix

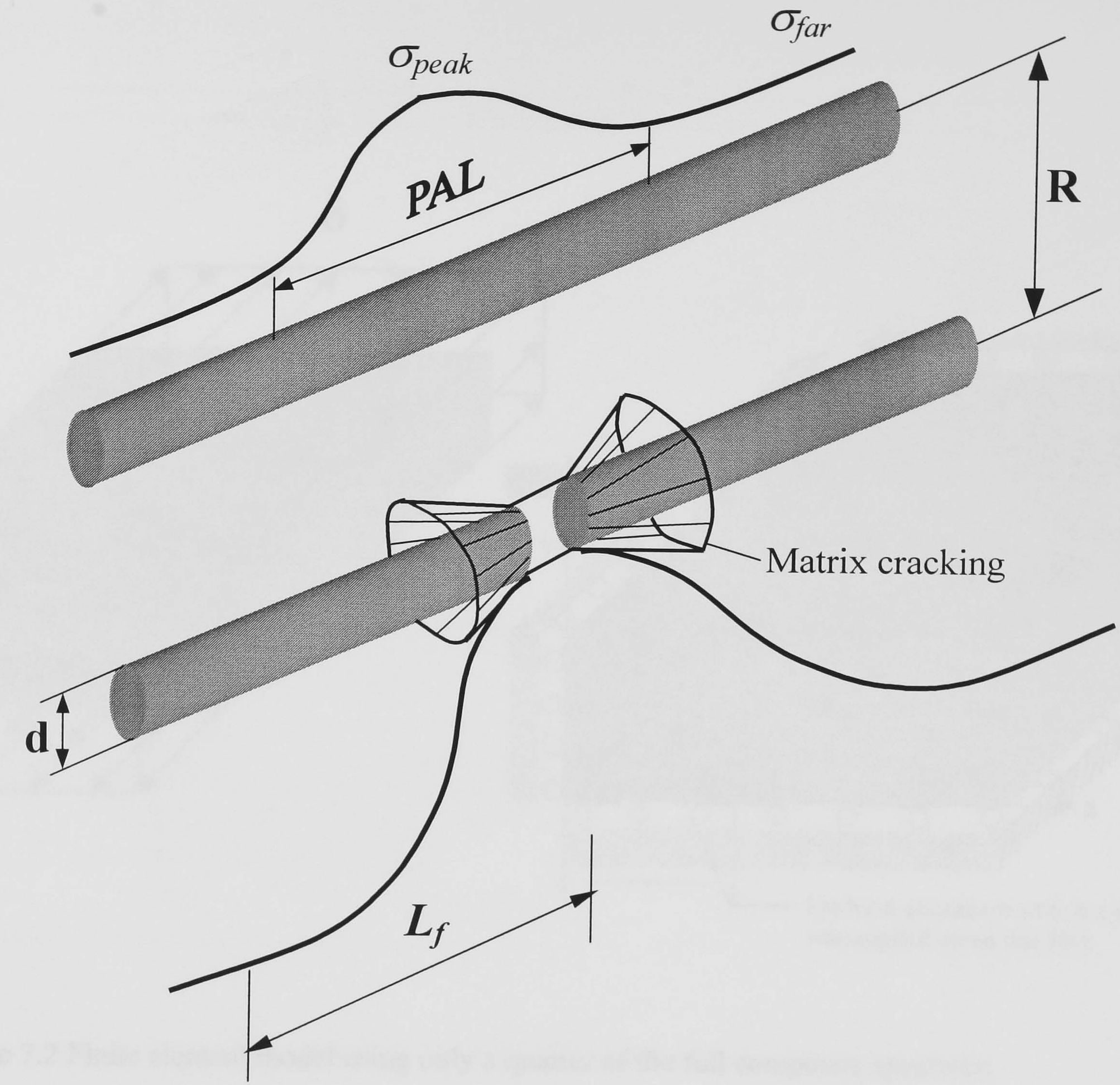

Figure 7.1 Variation of axial stress in a fractured fibre and an adjacent intact fibre.

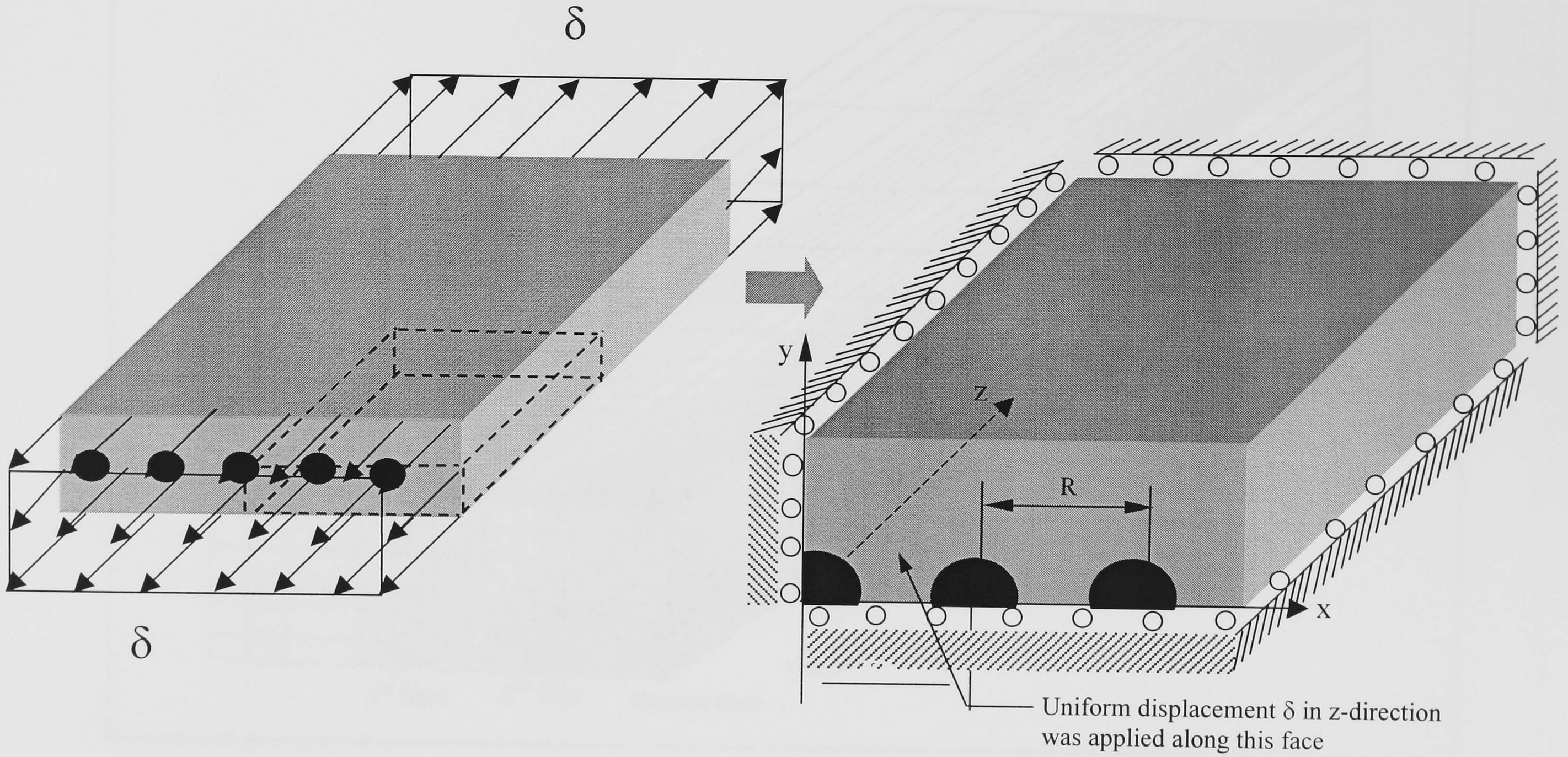

Figure 7.2 Finite element model using only a quarter of the full composite specimen

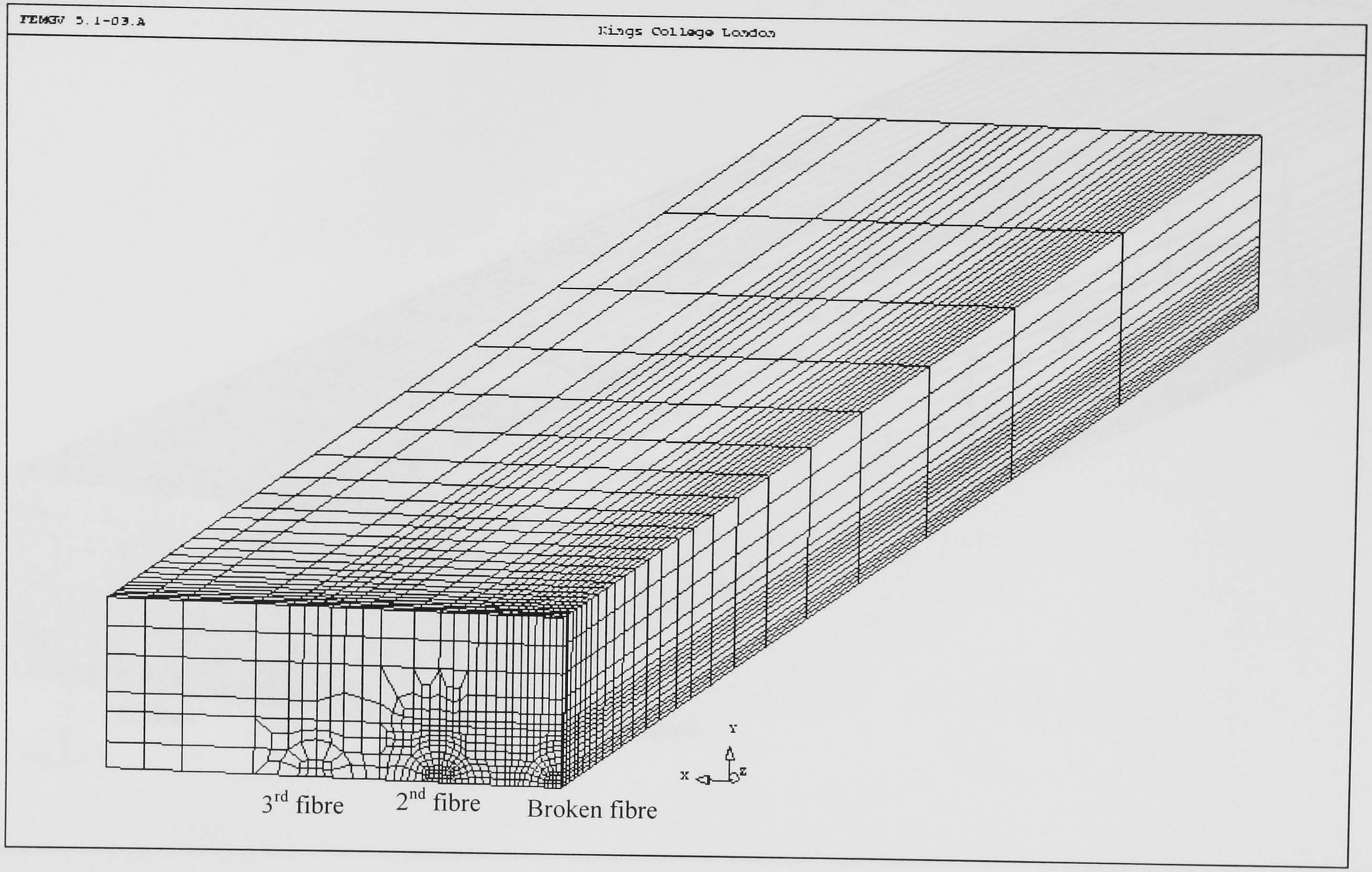

Figure 7.3 FE mesh without matrix crack

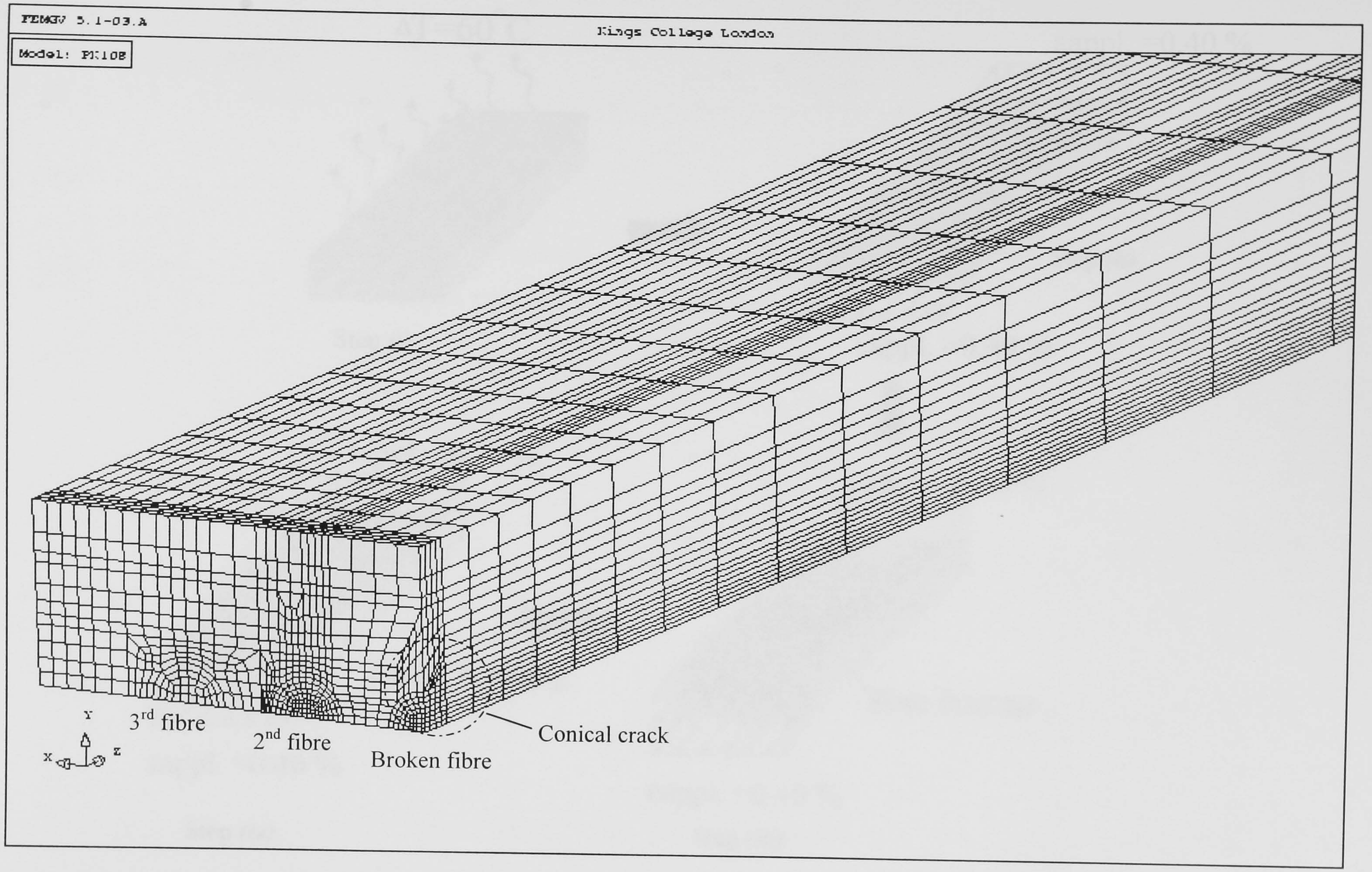

Figure 7.4 FE mesh with matrix crack

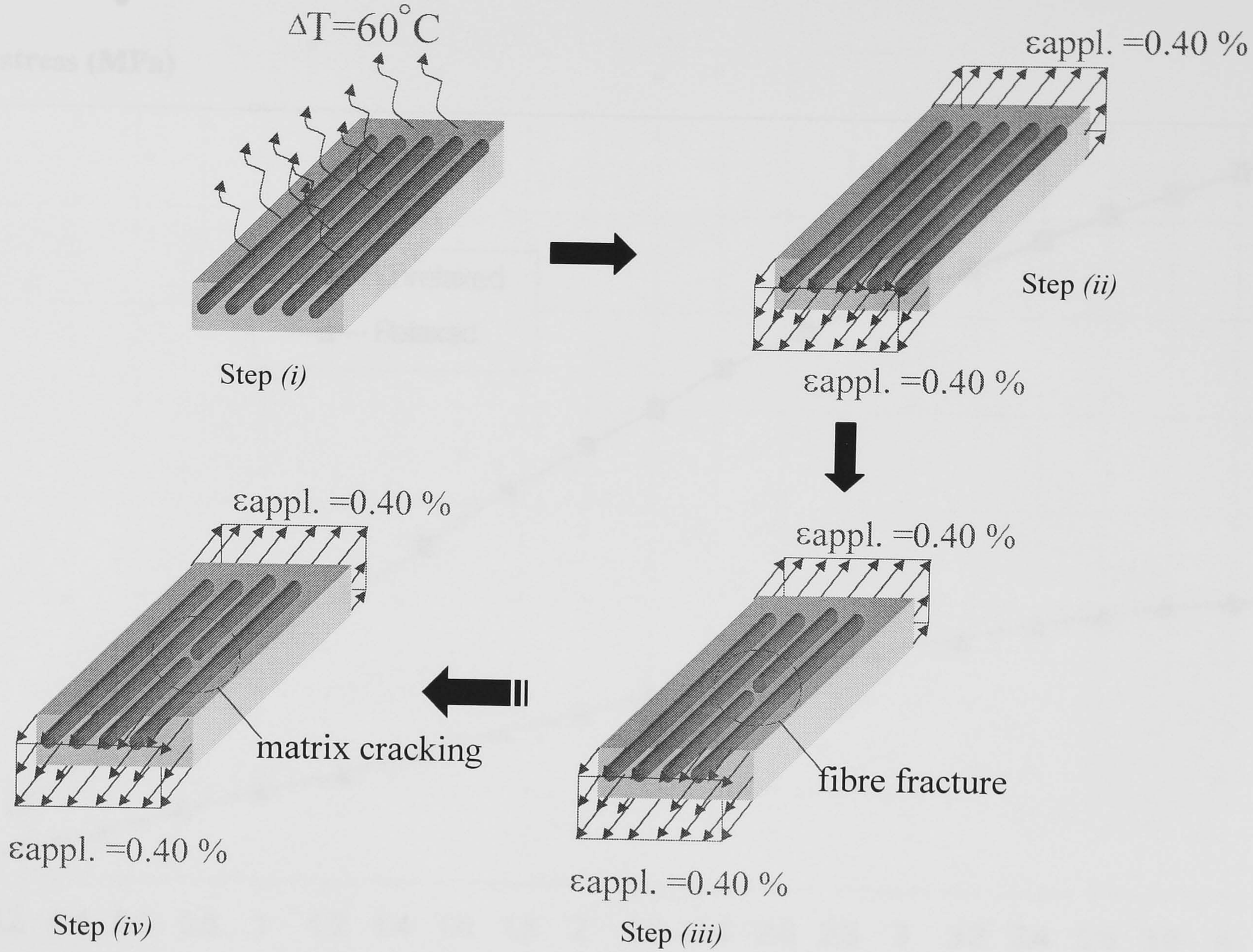

Figure 7.5 Progressional Approach in FE analysis

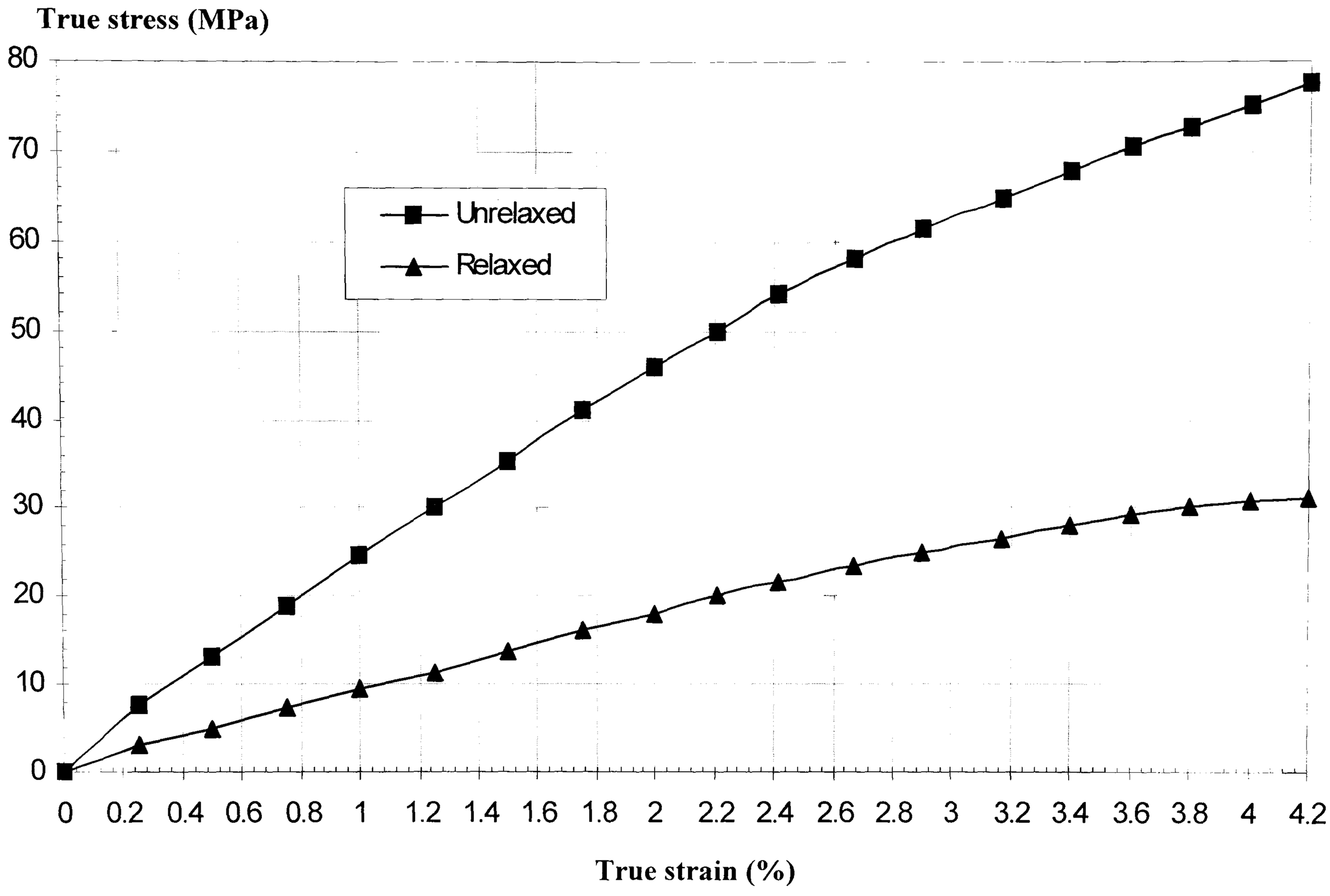

Figure 7.6 Stress-strain relationship for epoxy matrix at low-applied strain rate used in Nath *et al.* [75] (Reproduced with permission)

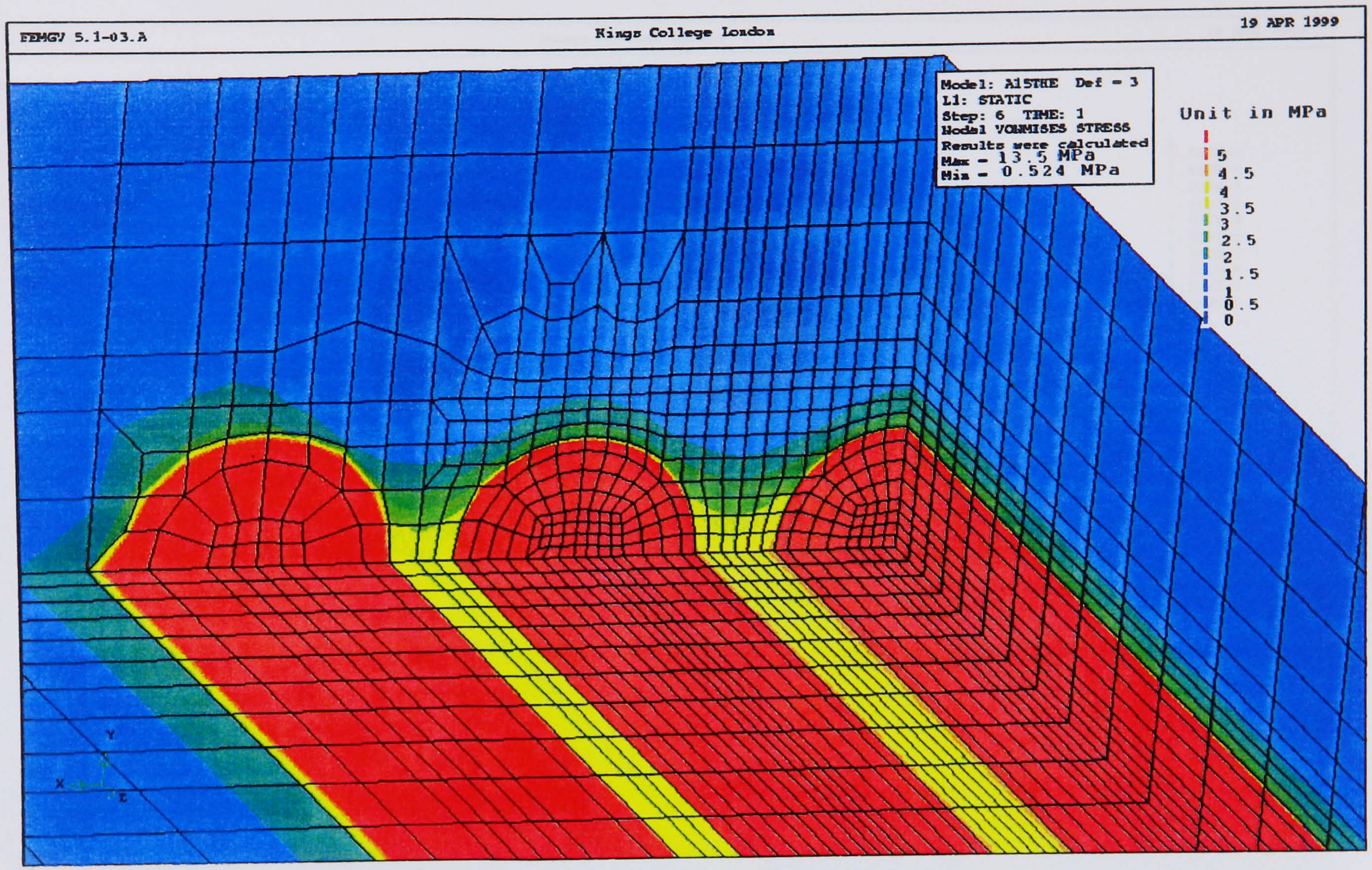

Figure 7.7 Residual thermal von Mises stress induced by curing process

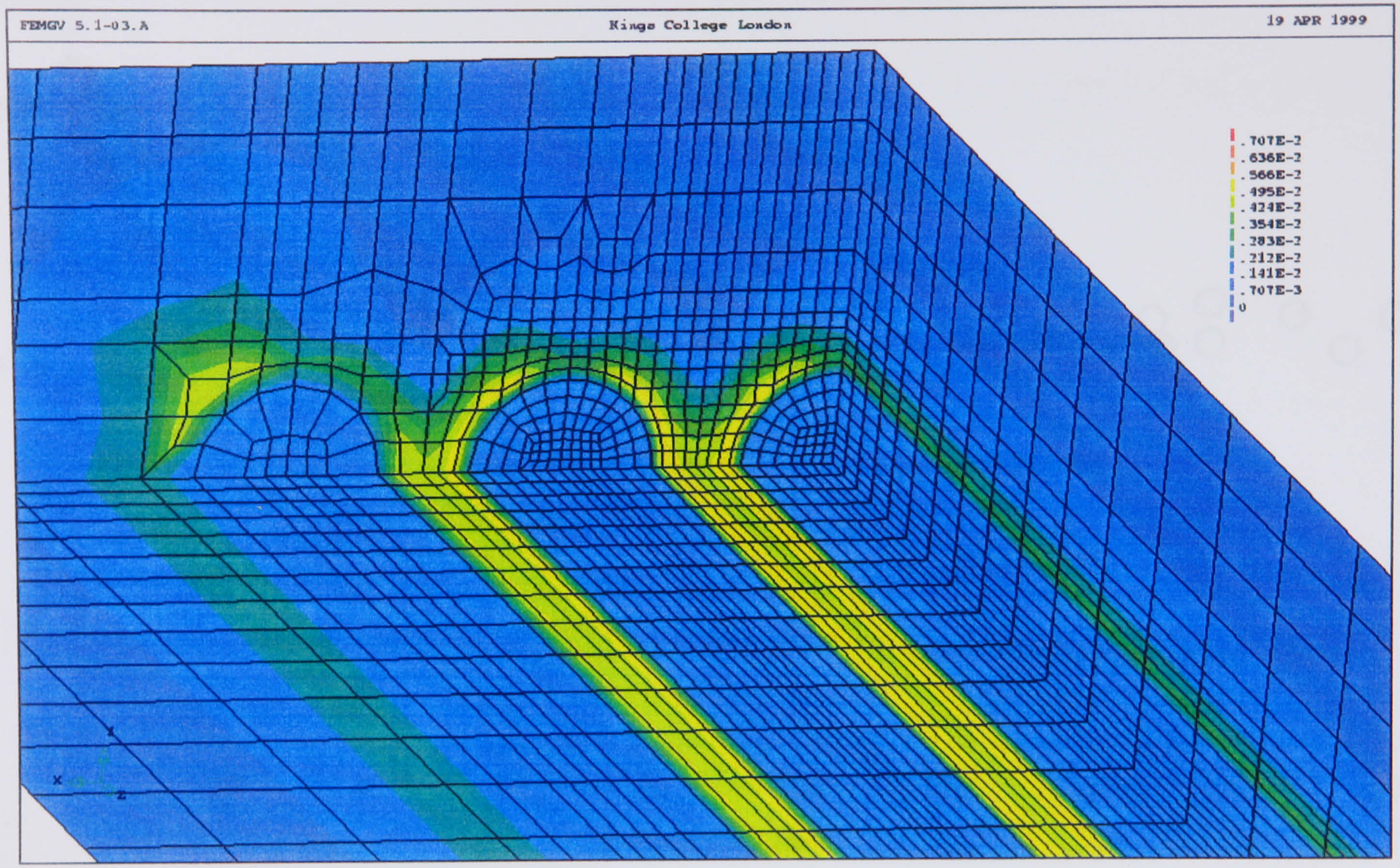

Figure 7.8 Residual thermal von Mises strain induced by curing process

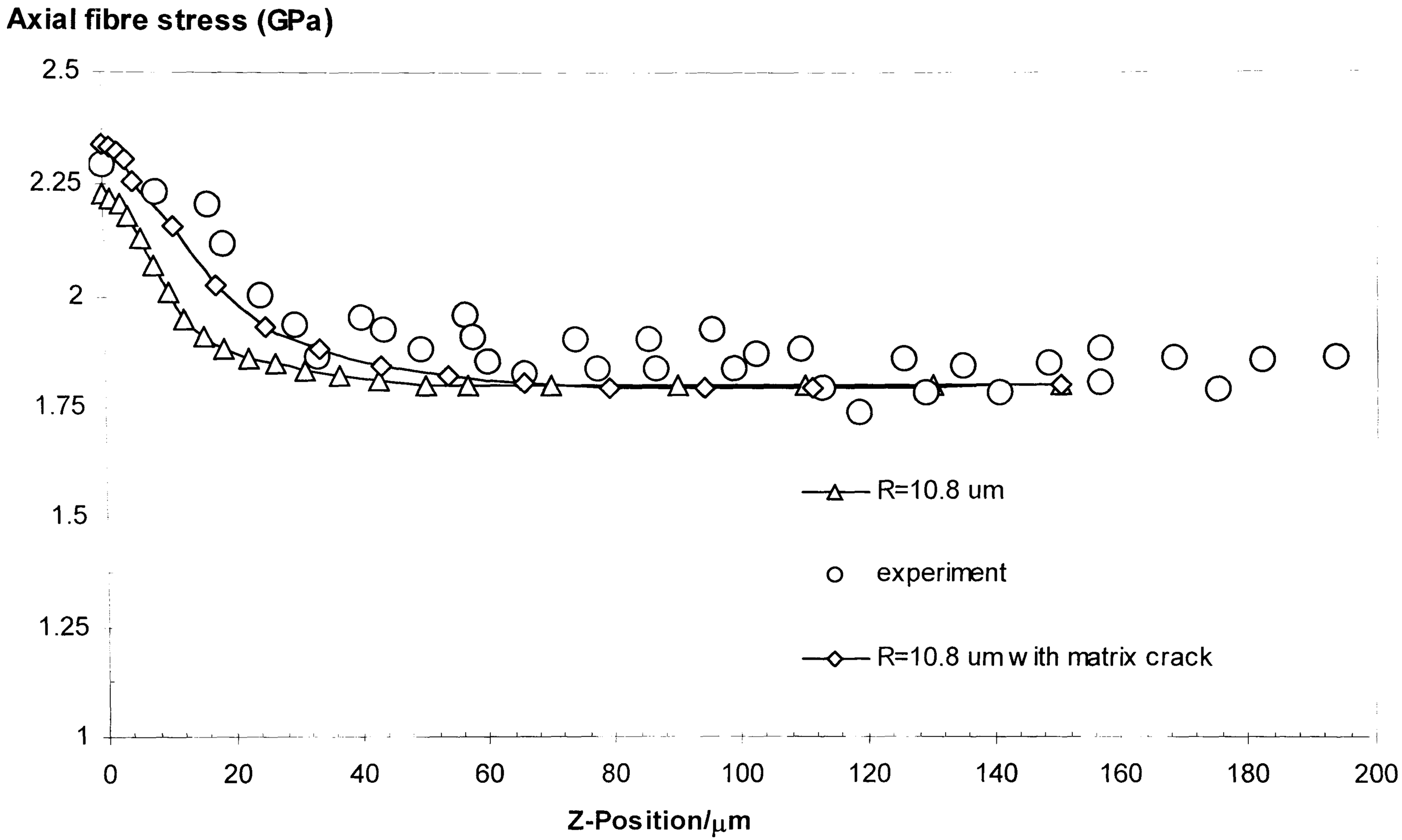

Figure 7.9 Variation of the axial stresses in an adjacent intact fibre, at the inter- fibre spacing of 10.8 μm

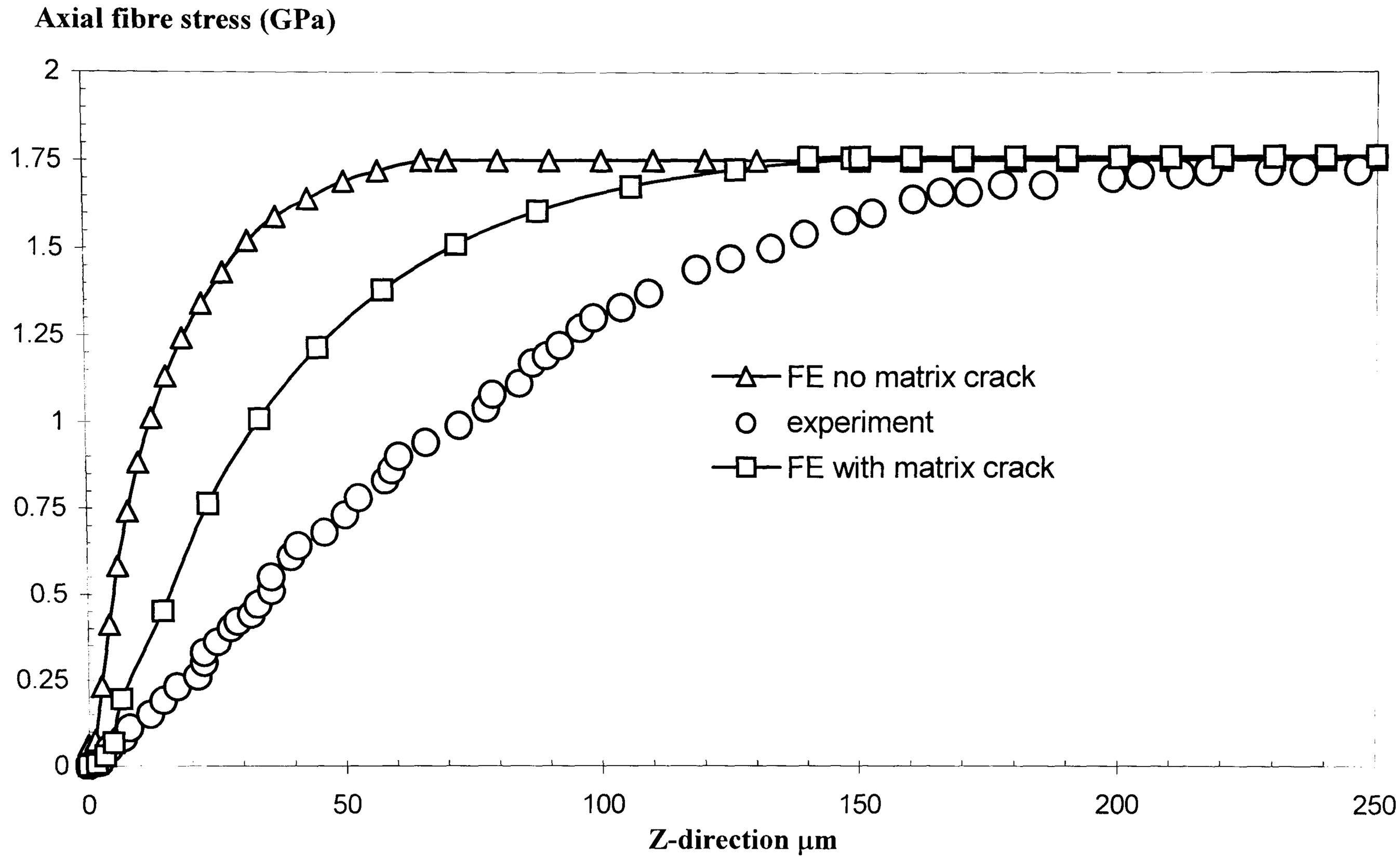

Figure 7.10 Variation of axial stresses in a broken fibre with and without a matrix crack, at the inter- fibre spacing of 10.8 μm

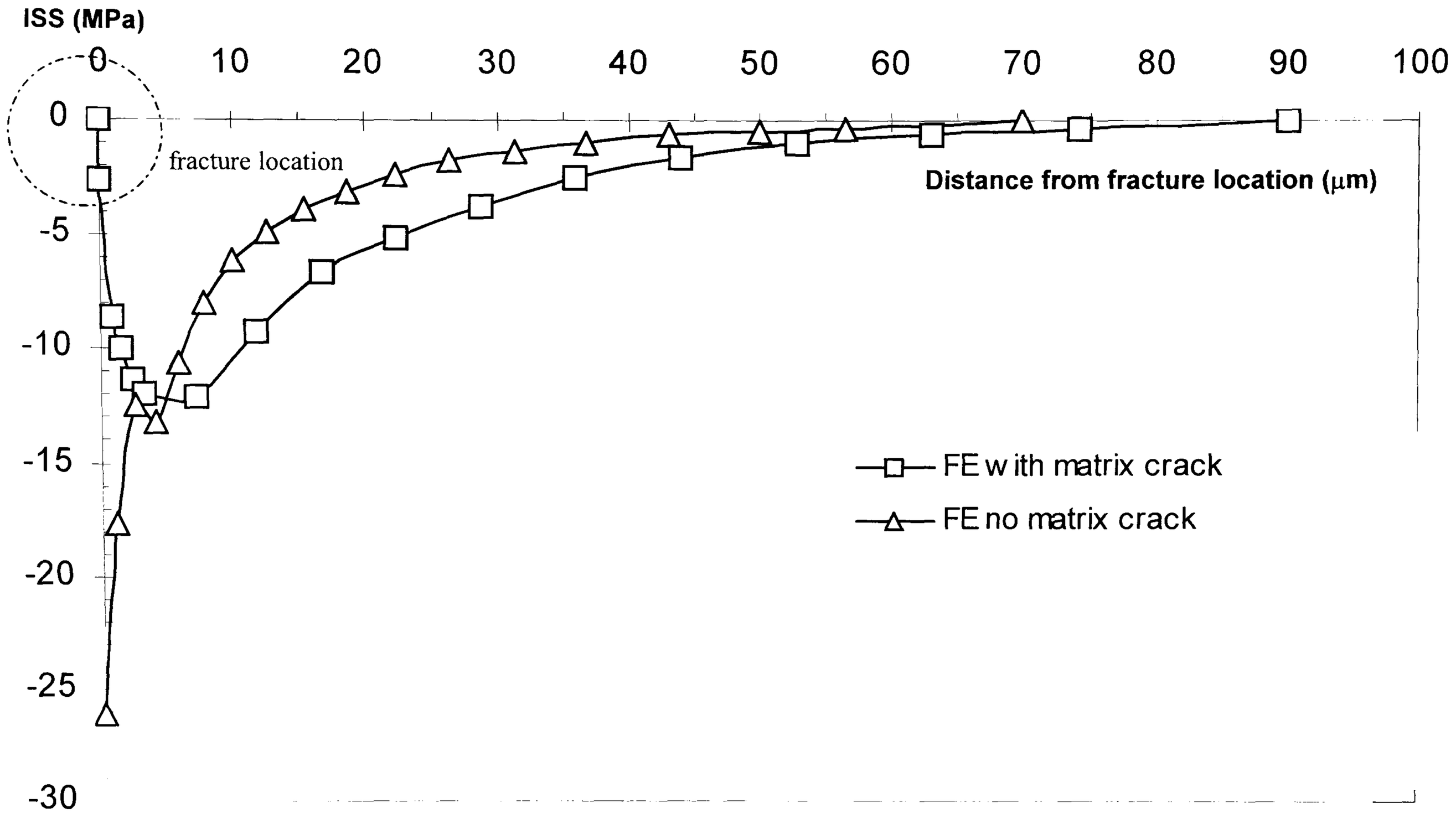

Figure 7.11 Variation of shear stresses in a broken fibre with and without a matrix crack, at the inter-fibre spacing of 10.8 μm

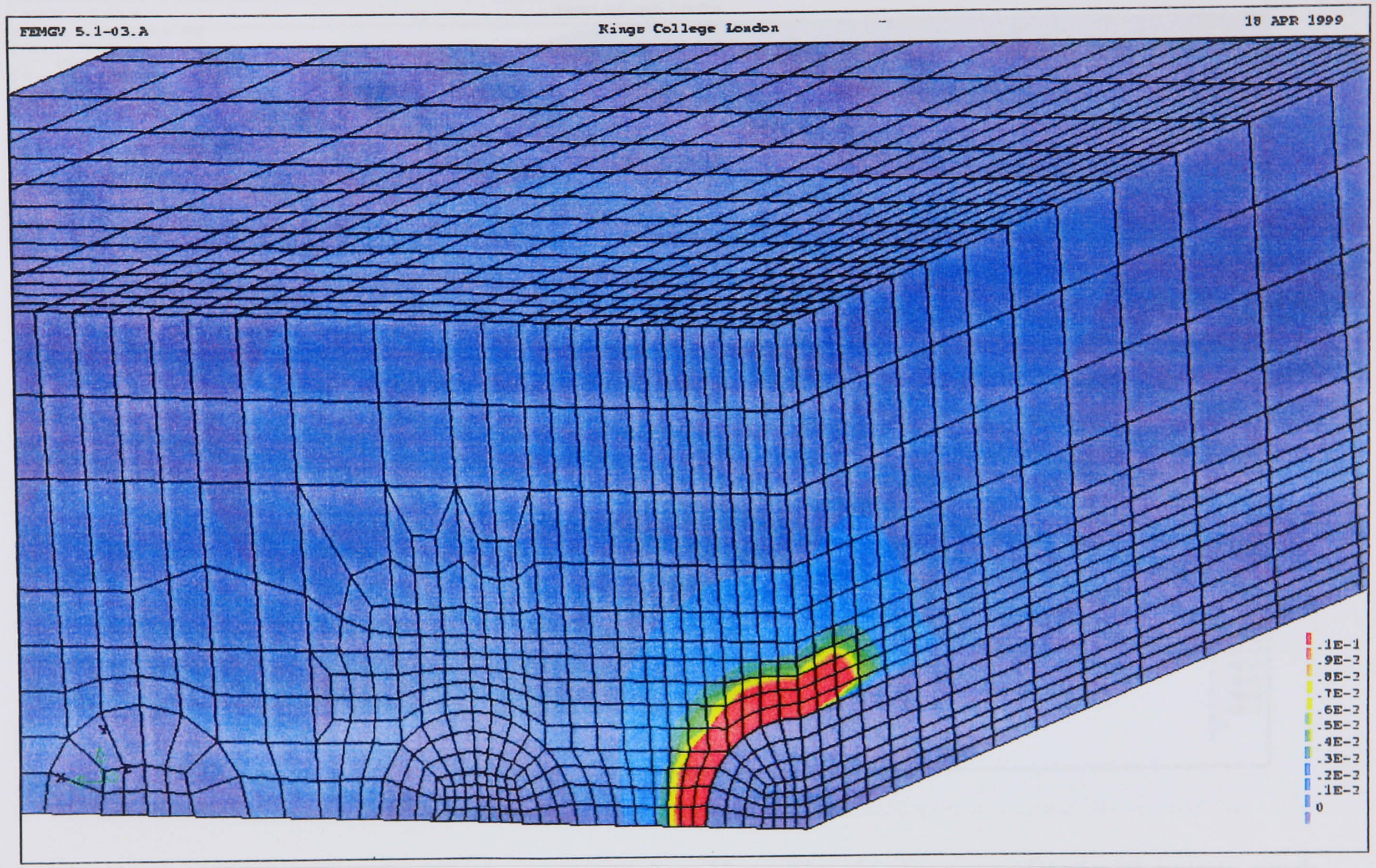

Figure 7.12 Critical area of high value of equivalent strain induced by a fibre fracture

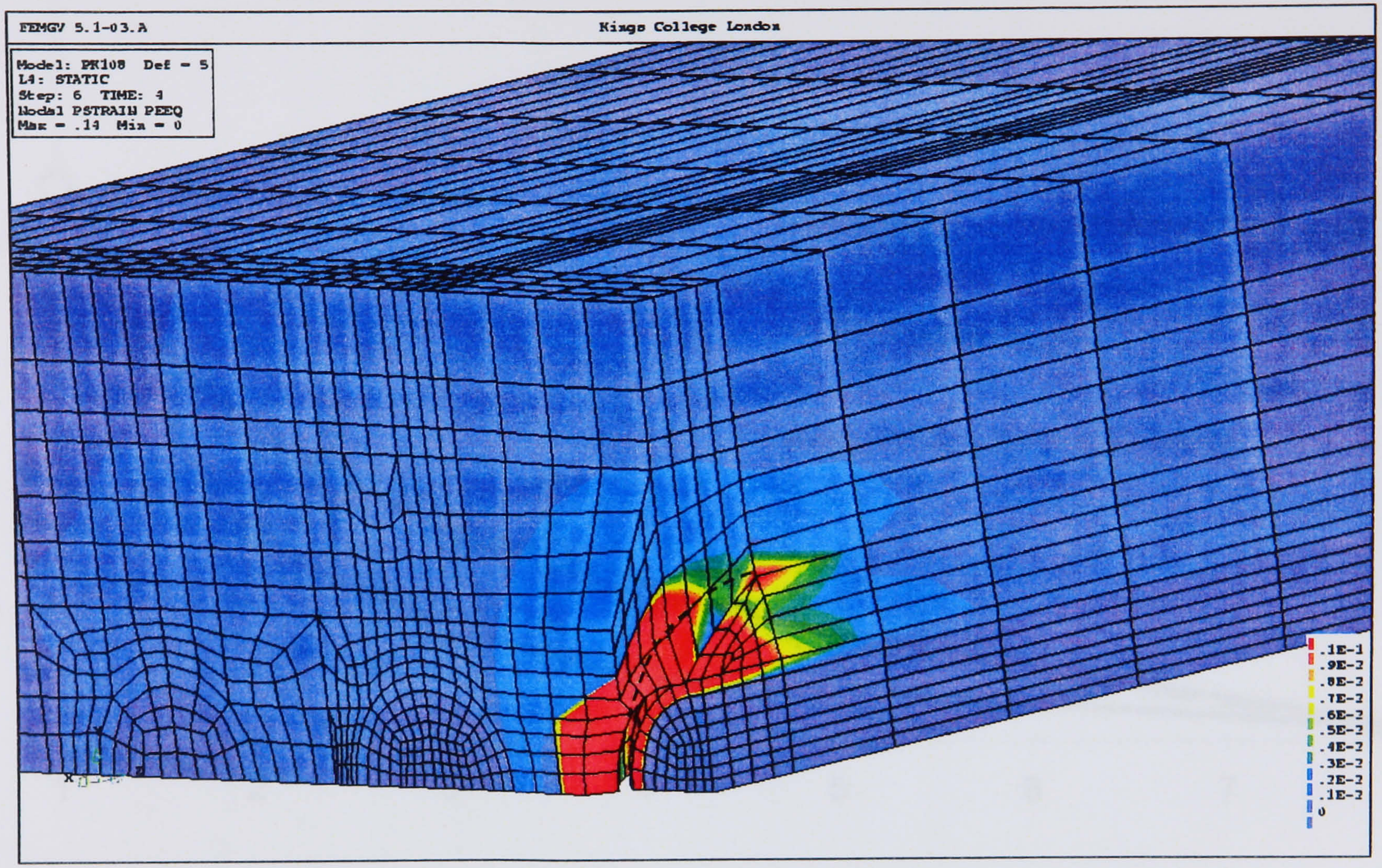

Figure 7.13 Critical area of high value of equivalent strain induced by a fibre fracture associated with matrix crack

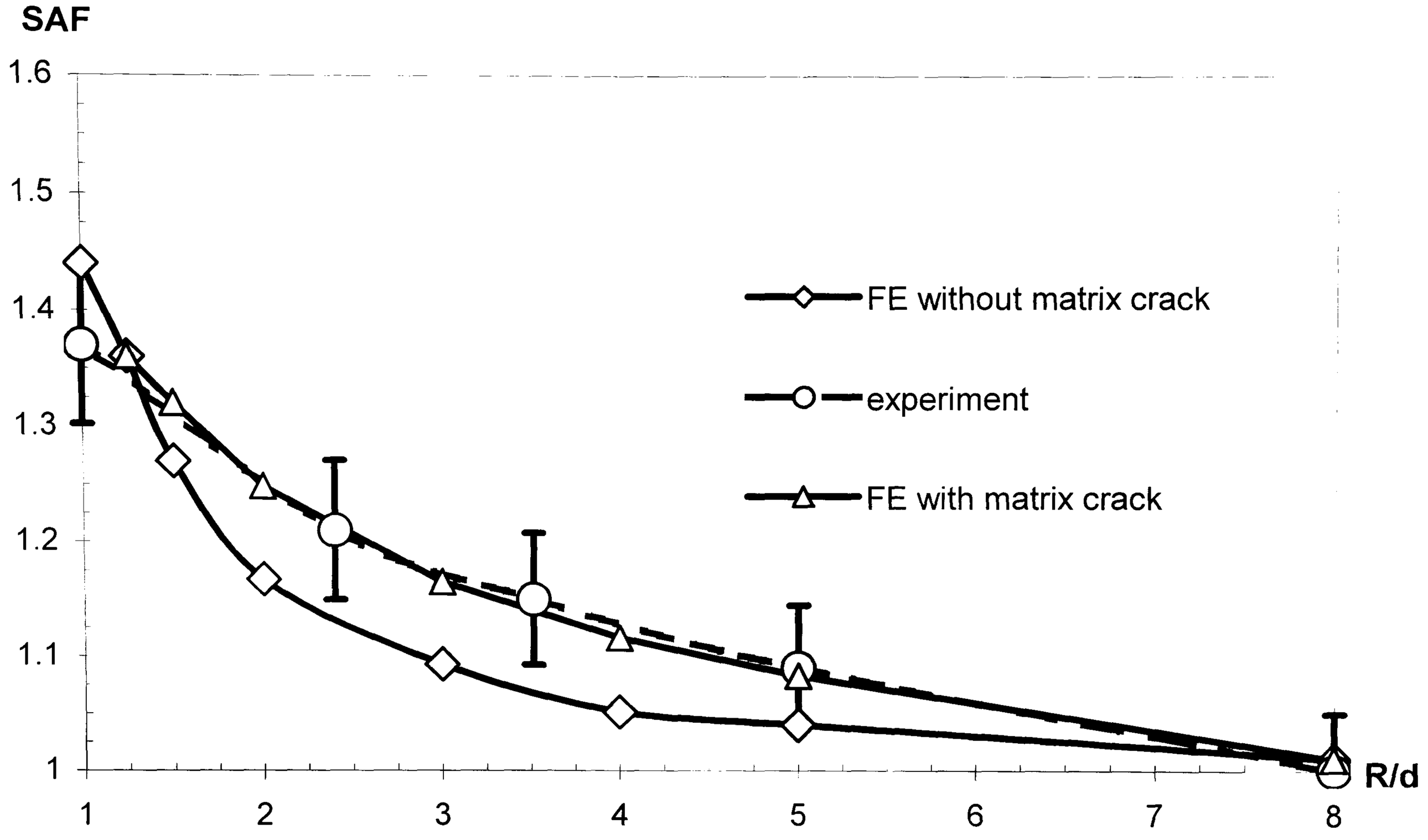

Figure 7.14 Variation of SAF in a neighbouring intact fibre at different inter-fibre spacings

CHAPTER 8

Effect of Inter-Fibre Spacing and Matrix Cracks in Hexagonal Array Composites

8.1. Introduction

The fibre volume fraction in a composite depends on the fibre packing arrangement. The most effective fibre packing arrangement is the hexagonal array (see Fig. 8.1 (a)). This arrangement gives a theoretical maximum fibre-volume fraction up to 0.907 when the fibres touch to each other (see Fig. 8.1 (b)). A micromechanical analysis for this model can be accomplished in the same manner as for the planar array composite. Unfortunately, LRS is unable to measure the stress in the internal broken fibre located at the centre of the model (see Fig. 8.2) due to a reflection of the Raman waves by the surrounding fibres. An attempt to predict the value of the SAF for the hexagonal array of carbon fibres/epoxy composite was performed by Chohan *et al.* [56]. They used LRS surface measurement to measure the fibre stresses in a 2-D planar array and a semi hexagonal array composite to predict the SAF (see Fig. 8.3). Another attempt was made by Sastry *et al.* [111]. They performed a single-fibre pullout from the microbundle to investigate the interfacial failure in a hexagonal array of fibres polymer-matrix composite. They used three mechanical models to verify their experimental results and described the stress transfer characteristics. However, an

experimental technique to examine fibre stresses for this model has not yet successfully been developed. The possible way to investigate the stress distribution in this model is to use numerical analysis. A 2-dimensional boundary element analysis, performed by Eischen *et al.* [112], was used to determine the effective elastic moduli of the hexagonal array models with different fibre volume fractions. Choi *et al.* [113] used the boundary element method to investigate the stress transferred through the interphase under the transverse loading. They found that the interphase has little effect on the stress transfer characteristic in this model. The presence of the interphase is believed to improve the bonding strength of the fibre/matrix interface [27,28,36]. Galiotis [35] has observed the thickness of the interphase in a sized-carbon fibre/epoxy composite to lie in the range 0.15-0.6 μm. The presence of an interphase produces stronger bonding, and matrix cracking is likely to occur.

The aim of the work in this chapter is to investigate the effect of fibre volume fraction on SAF and the stress transfer characteristics in the hexagonal array of fibres composites. The effects of an interphase and matrix viscoplasticity are neglected in this work since only the fibre stresses are of interest (see Chapter 5). The effect of the inter-fibre spacing on the domino effect of fibre fracture was also investigated. Finite element analysis was employed to examine the stresses in the fibres and the stress redistribution in the hexagonal array models. The validation of this FE model is based on good correlation between the FE results in a previous study of a planar array model and LRS measurement (see Chapter 7).

8.2 Finite Element Models

Since the boundary and loading conditions are symmetric, this problem can be modelled using only a quarter of the actual specimen (see Fig. 8.4). The hexagonal array FE models have been created with the ratio R/d equal to 1.5, 2, 3, 4, and 5 using FEMGV [114]. The FE models without a matrix crack consist of 12,096 linear brick elements (see Fig. 8.5). The stage-by-stage '*Progressional Approach*' technique proposed by Nath *et al.* [76], was employed to perform this FE analysis. The FE analysis for these models is divided into 3 sequential ABAQUS load steps for a fibre fracture analysis, and 4 sequential ABAQUS load steps for the analysis of fibre fracture followed by matrix cracking (see section 7.2). The material properties are the same as those used by Nath *et al.* [76] (see Table 7.1).

8.3 Results and Discussion

8.3.1 Effect of Fibre Volume Fraction on SAF

The FE results show that the axial fibre stress in the intact fibres decreases as the ratio R/d increases, and the fibre volume fraction in the composite decreases. A reduction of fibre volume fraction may lead to catastrophic damage in the matrix material when an individual fibre breaks. Details of the maximum fibre axial stress in each intact fibre are shown in Table 8.2.

The fibre axial stress profiles in the hexagonal array for the ratio R/d ranging from 1.5 to 5 are shown in Fig. 8.6. The fibre axial stress in the nearest neighbouring fibres was decreased gradually from the fibre-fractured location. The maximum fibre axial stress

in the nearest neighbouring fibres at the ratio R/d of 1.5 is about 13 % higher than those values in the other intact fibres. As the ratio R/d increased to 5, the difference between the fibre stress in the nearest neighbouring fibres and the other intact fibres was reduced to 2 %. A very high value of shear stress was found in the models having a low value of the ratio R/d. The shear stress was reduced by approximately half when the R/d ratio is equal to 5 (see Fig. 8.7). The fibre stresses in the nearest neighbouring intact fibres is shown in Fig. 8.8.

The FE results for the ratio R/d of 1.5 show a maximum value of the von Mises strain of about 25 % in the matrix material (see Fig. 8.9). This is greater than the failure strain in the matrix material. When the ratio R/d increased to 5, the von Mises strain in the matrix material was reduced to about 4.5 % (see Fig. 8.10). Although the magnitude of strain was reduced, the region, where the plastic strain is greater than the fracture value (critical plastic strain), was enlarged. A large inter-fibre spacing has more space for stress redistribution, which in turn leads to a larger region of plastic strain. A comparison of critical plastic strain at the ratio R/d of 1.5 and 5 is shown in Fig. 8.11 (a) and Fig. 8.11 (b).

The criterion used here to determine whether intact fibres fail is based on the SAF. The values of SAF in the hexagonal array models are much lower than those values in the planar array models, for the same R/d ratio (Fig. 8.12).

8.3.2 Effect of Matrix Cracking

As described in section 6.5, ignoring the matrix cracks may lead to an underestimate of SAF, and therefore in this analysis a matrix crack was included in the FE models. The loading conditions in this analysis are the same as for the FE analysis of the planar array with a matrix crack (see section 7.5), except a matrix crack of maximum length 8 μm was used. As a matrix crack was introduced in this analysis, in order to save the computing time, this problem was modelled using only one-sixth of the actual specimen (see Fig. 8.13). The FE mesh, which consists of 22,120 linear brick elements, is shown in Fig. 8.13.

The maximum value of the fibre axial stress in a broken fibre for the models with a matrix crack is about 6.6 % higher than in the models without a matrix crack (see Fig. 8.14). The shear stresses in the models with the ratio R/d equal to 1.5 and 2 were about 3 times higher than those values in the models without a matrix crack (see Fig. 8.15). This may be caused by the insufficient space at this ratio for the stress redistribution. As the ratio R/d was increased beyond 3, the maximum shear stresses were reduced to about half but they are still twice as high as those values in the models without a matrix crack (see Fig. 8.15). This could be due to the fact that conical-shaped matrix cracks restrict the redistribution of shear stress. The maximum fibre stress in the nearest neighbouring intact fibres for the FE model with a matrix crack at the ratio R/d of 1.5 is about 5.6 % higher than in the model without a matrix crack (see Fig. 8.16). When the ratio R/d is greater than 2, only a slight difference between the fibre axial stress in the models with and without matrix crack was found (see Table

8.1). The increase of PAL of about 75 % compared to the model without a matrix crack was found (see Fig. 8.16).

As can be seen in Fig. 8.17, the value of the SAF in the FE models with and without a conical-shaped matrix crack was only slightly different. The biggest difference was found at the ratio R/d of 1.5. This discrepancy may result from an insufficient space for stress redistribution. A very high value of axial stress in the nearest neighbouring fibres at this ratio may induce fracture in the intact fibres when an additional mechanical strain is applied, which could lead to a domino effect of the fibre fracture. A suitable inter-fibre spacing must be chosen to increase the toughness of composites. The FE results have shown that conical-shaped matrix cracks in the hexagonal array models have less effect on the intact fibres when compared with the planar array models.

8.4 Discussion

The inter-fibre spacing and fibre-packing geometries, which control the fibre volume fraction in a composite, have a strong effect on the stress transfer through the intact fibres. A small inter-fibre spacing induces more fibre axial stress in the neighbouring intact fibres when a single broken fibre was found in the composite. A small inter-fibre spacing may confine the matrix damage area within the pocket of nearest neighbouring intact fibres. In contrast to the larger inter-fibre spacing, that has the effect of enlarging the damaged sone in the matrix due to a reduction of composite strength, as a result of lower fibre volume fraction. The fibre axial stress in the

neighbouring fibres was a little different to the far field stress at higher ratios compared to the fibre axial stress in the planar array. Matrix cracks in the hexagonal array models have less effect on SAF in the neighbouring intact fibres than in the planar array of fibres composites.

The ratio R/d (no matrix crack)	Fibre stress in FB2 (GPa)	Fibre stress in FB3 (GPa)	Fibre stress in FB4 (GPa)	Fibre stress in FB5 (GPa)	Fibre stress in FB6 (GPa)	Fibre stress in FB7 (GPa)
1.5	2.16	1.88	2.16	1.90	1.90	1.88
2	2.06	1.88	2.06	1.89	1.89	1.87
3	1.96	1.85	1.96	1.86	1.86	1.85
5	1.88	1.84	1.88	1.84	1.84	1.84

The ratio R/d (matrix crack)	Fibre stress in FB2 (GPa)	Fibre stress in FB3 (GPa)	Fibre stress in FB4 (GPa)	Fibre stress in FB5 (GPa)	Fibre stress in FB6 (GPa)	Fibre stress in FB7 (GPa)
1.5	2.29	1.84	2.33	1.95	N/A	2.05
2	2.04	1.88	2.04	1.89	N/A	1.88
3	1.97	1.86	1.97	1.87	N/A	1.86
5	1.83	1.83	1.83	1.83	N/A	1.83

Table 8.1 Maximum fibre axial stresses in the intact fibres for the hexagonal array with and without matrix crack

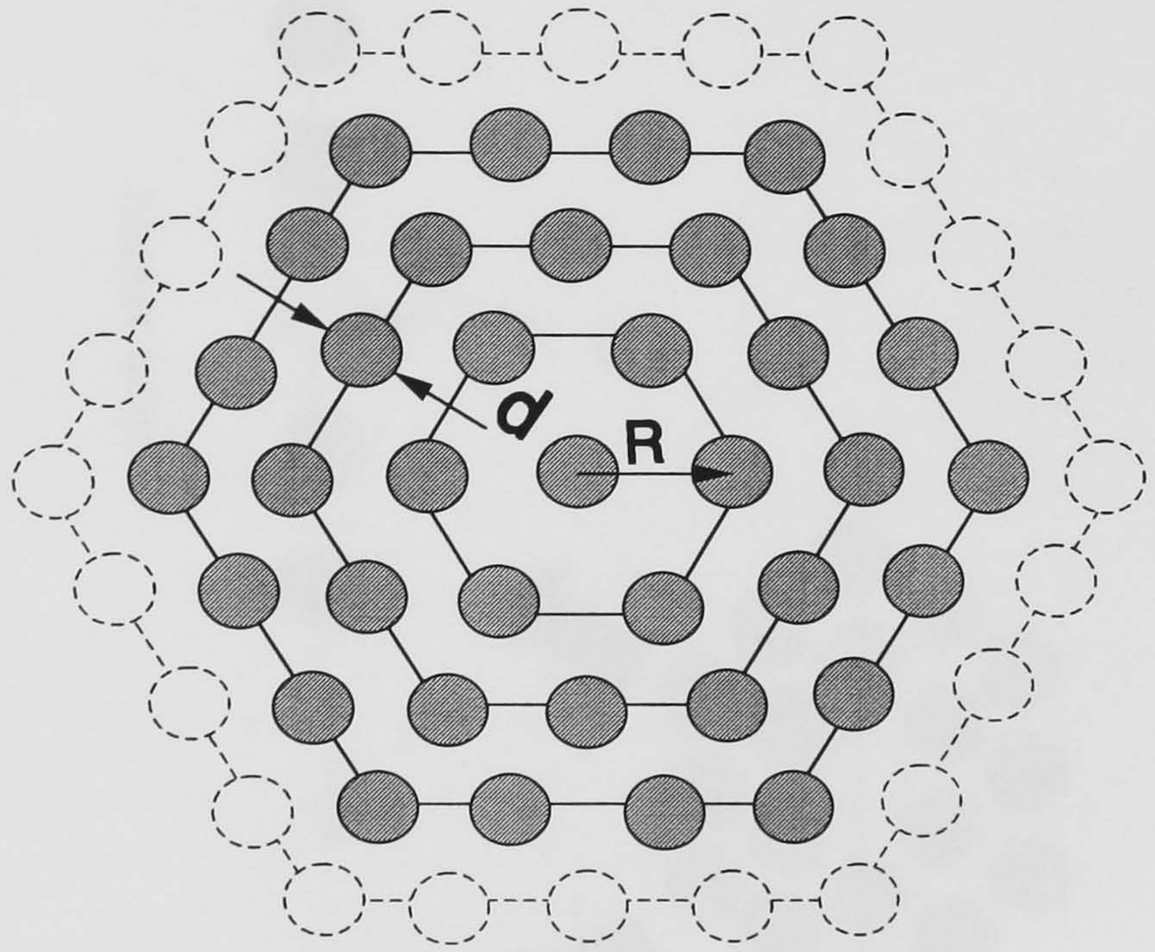

(a)

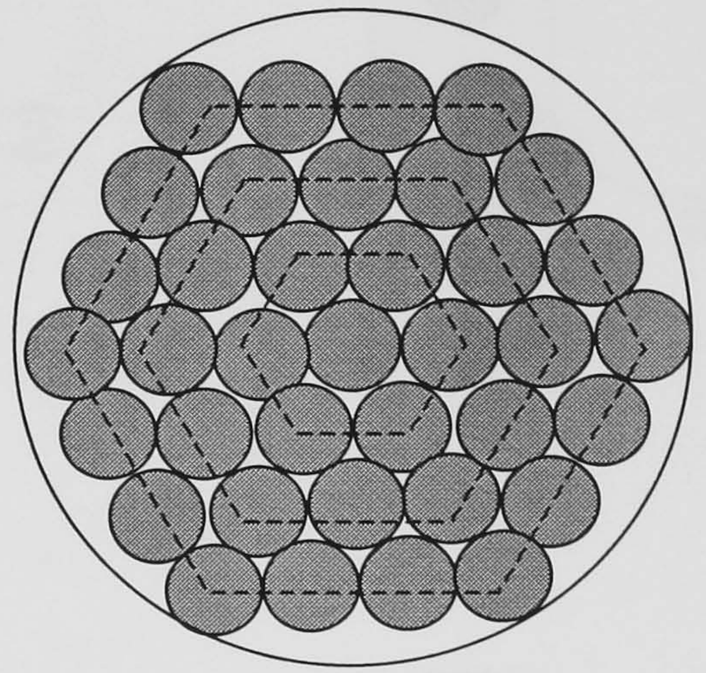

(b)

Figure 8.1 Geometry of fibre packing arrangement used in this work (a) dimension of hexagonal packing of fibres (b) geometry of hexagonal array which gives the highest effective fibre volume fraction

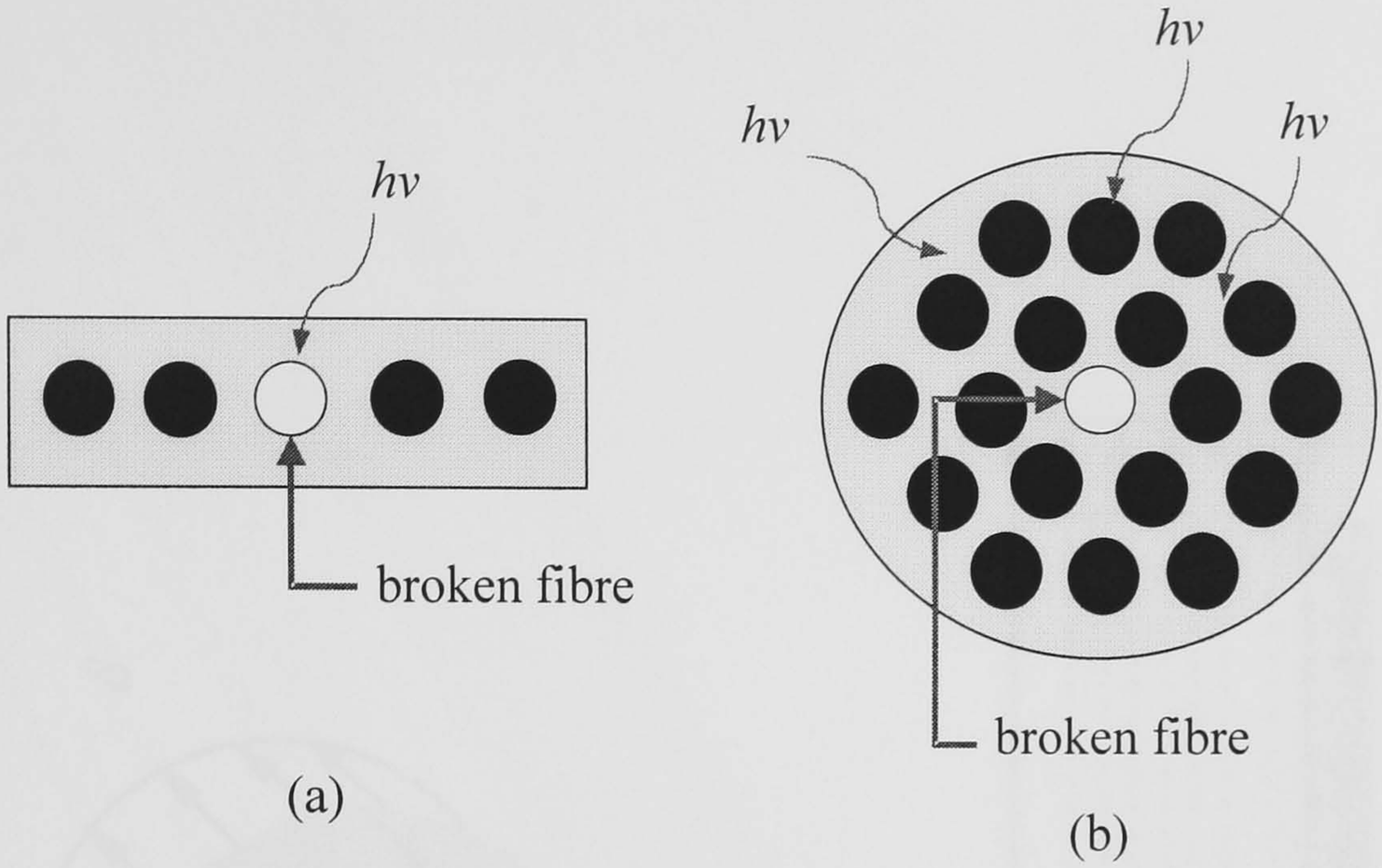

Figure 8.2 (a) surface measurement of planar array (b) difficulty in LRS measurement

* *hv* refers to photon energy

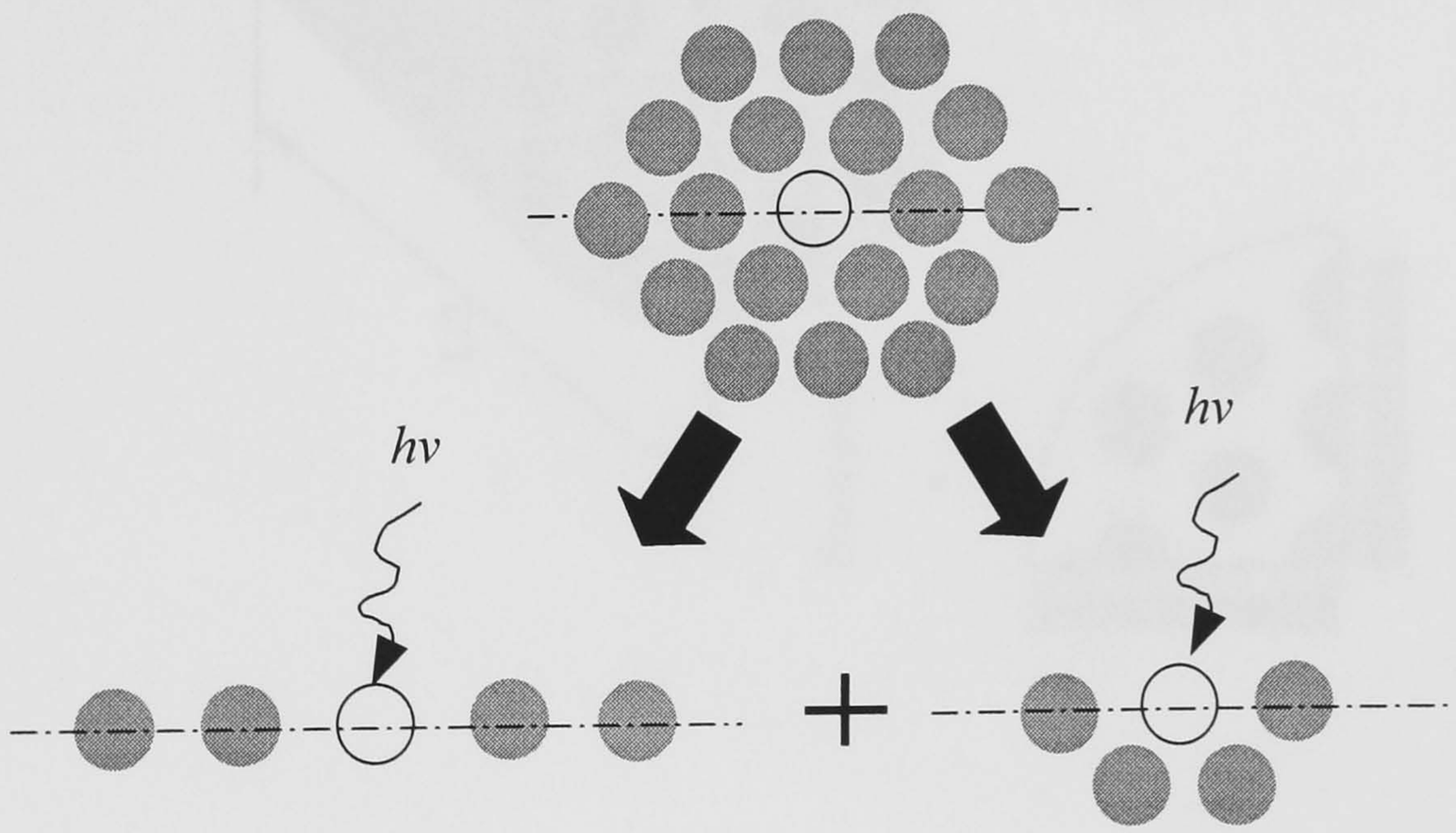

Figure 8.3 LRS surface measurement technique used by Chohan *et al*. [56] for hexagonal arrays

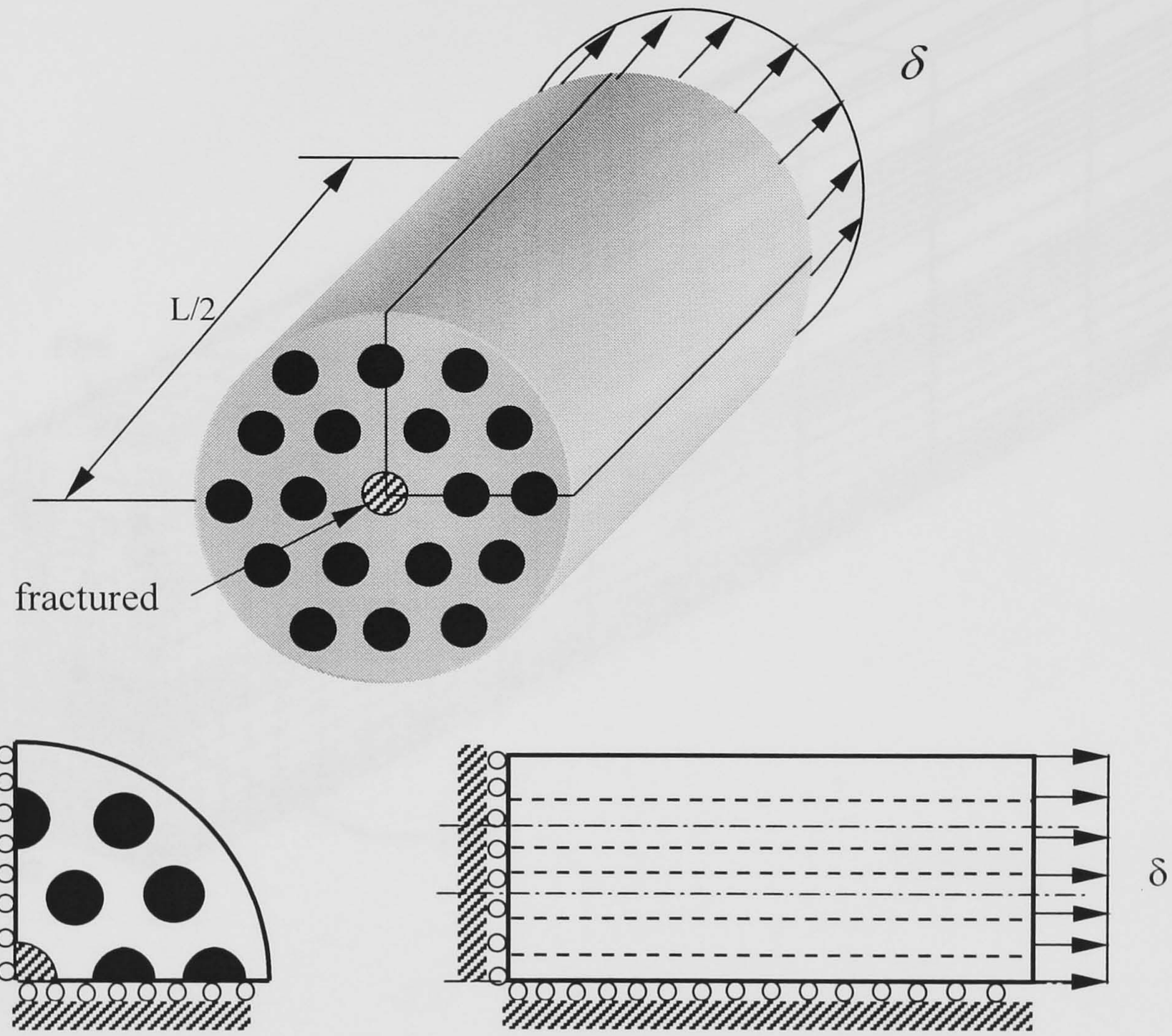

Figure 8.4 Hexagonal array FE model without matrix crack

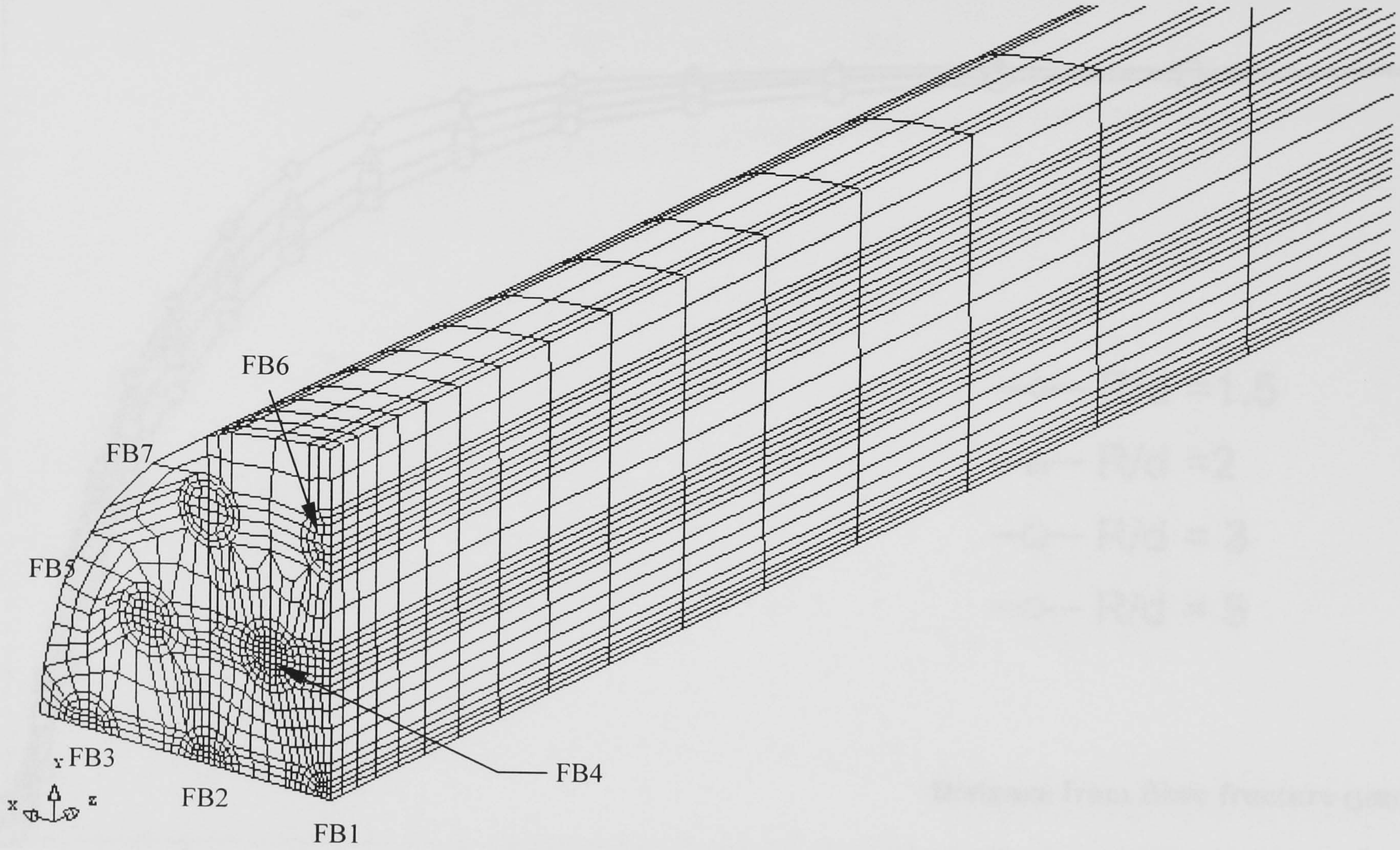

Figure 8.5 FE mesh for hexagonal array models without matrix crack

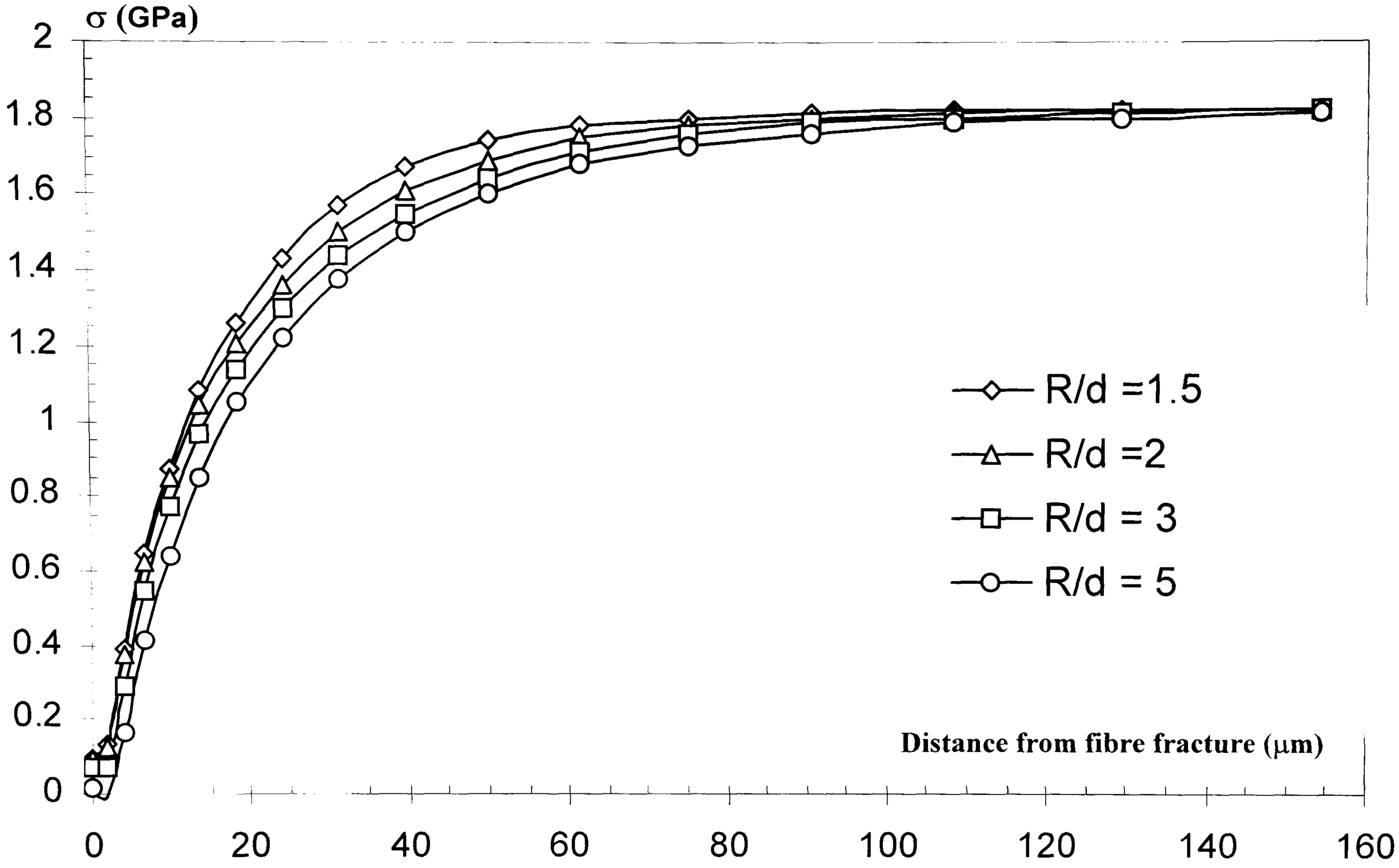

Figure 8.6 Variation of fibre stresses in the models without matrix crack

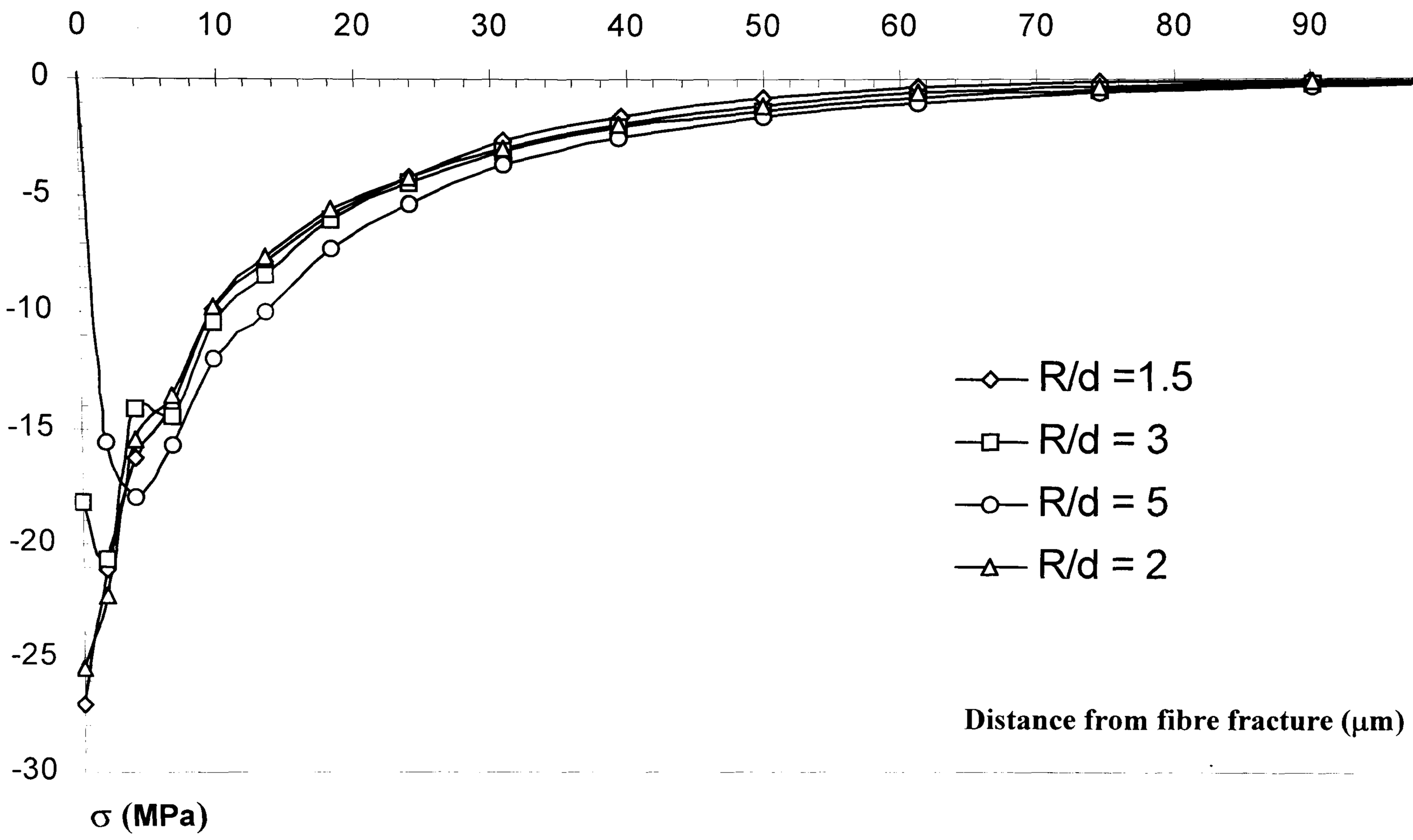

Figure 8.7 Variation of interfacial shear stresses in the models without matrix crack

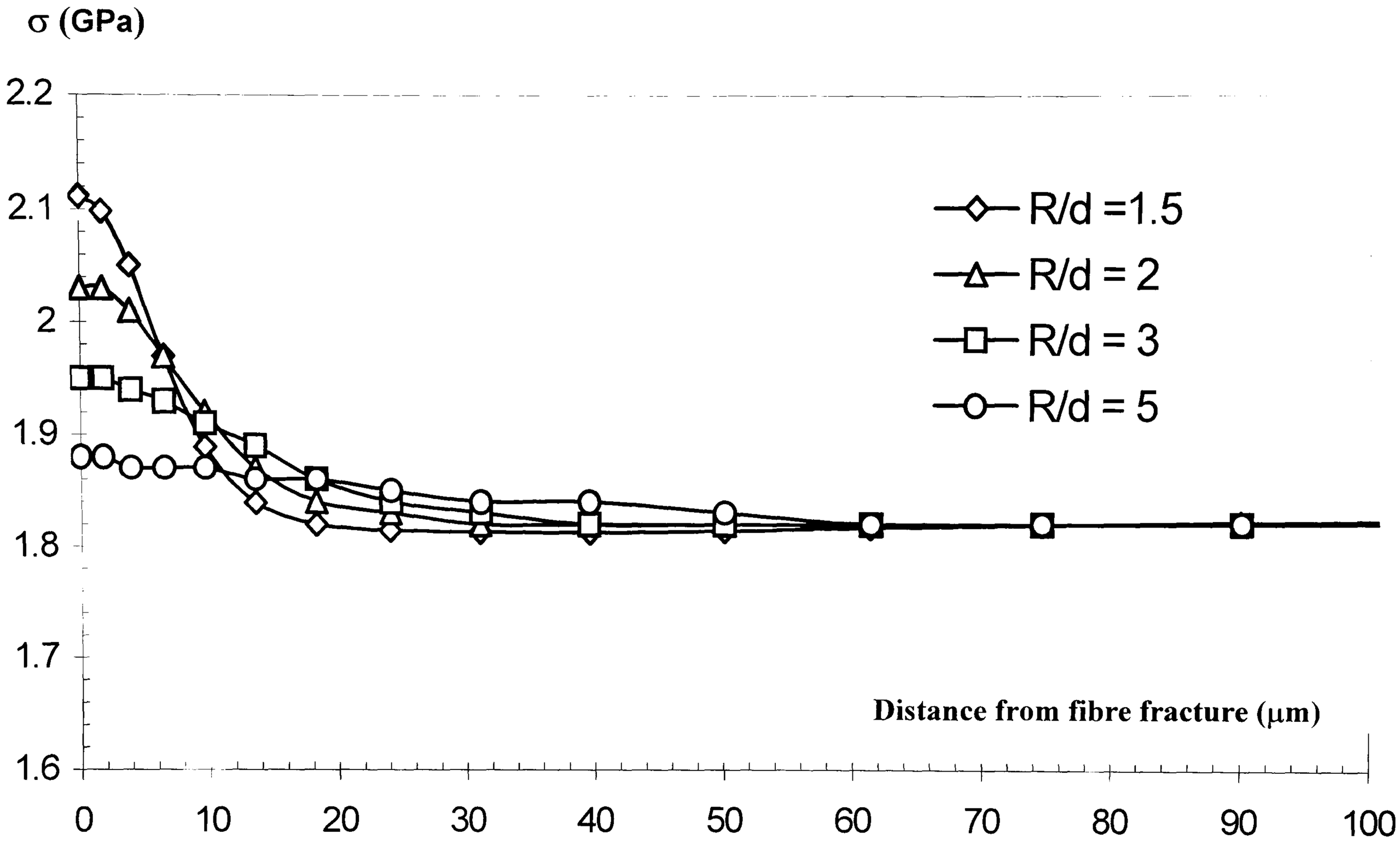

Figure 8.8 Variation of fibre stresses in the nearest neighbouring fibres for the models without matrix crack

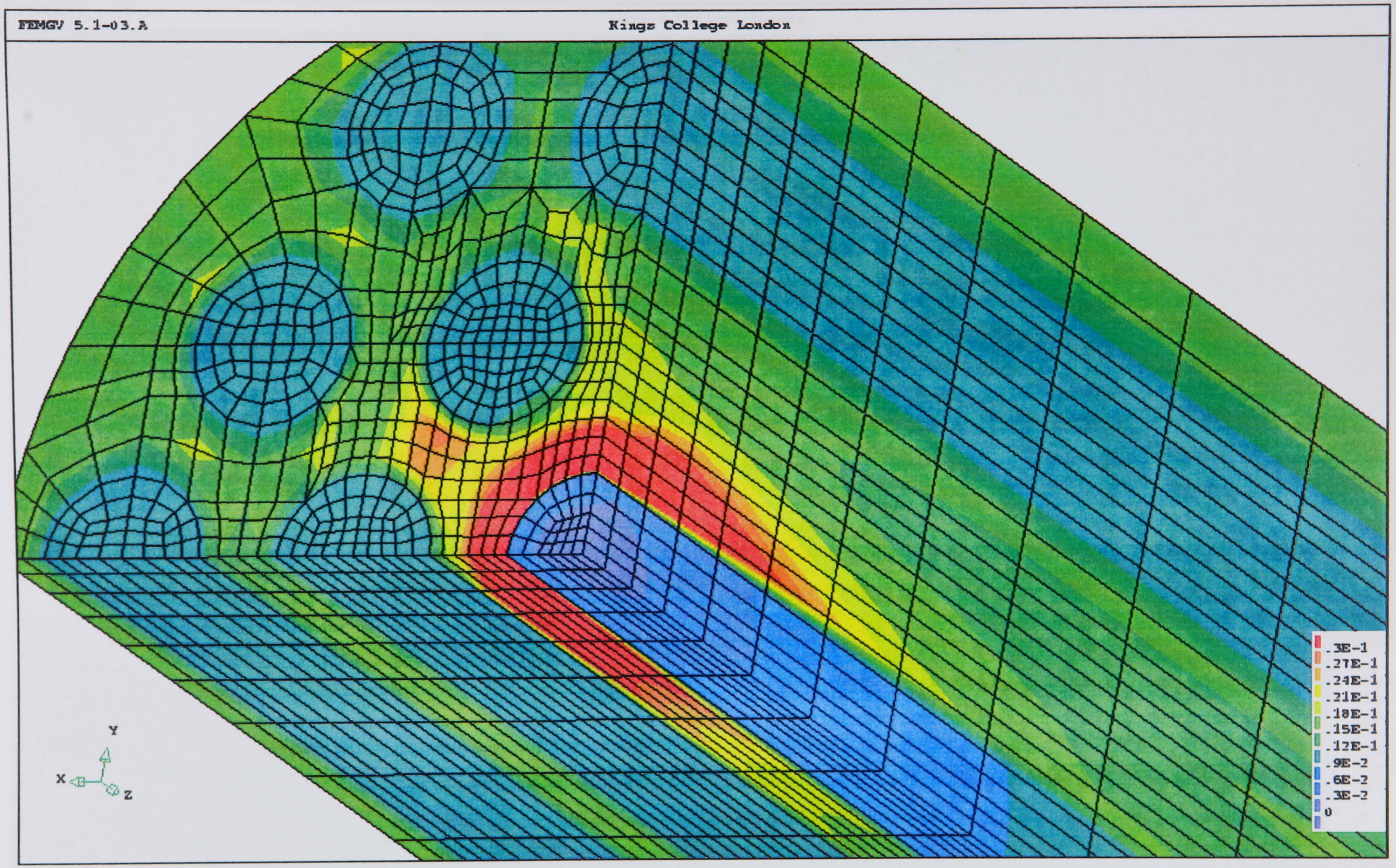

Figure 8.9 von Mises strain in the FE model without matrix crack, at the ratio R/d = 1.5

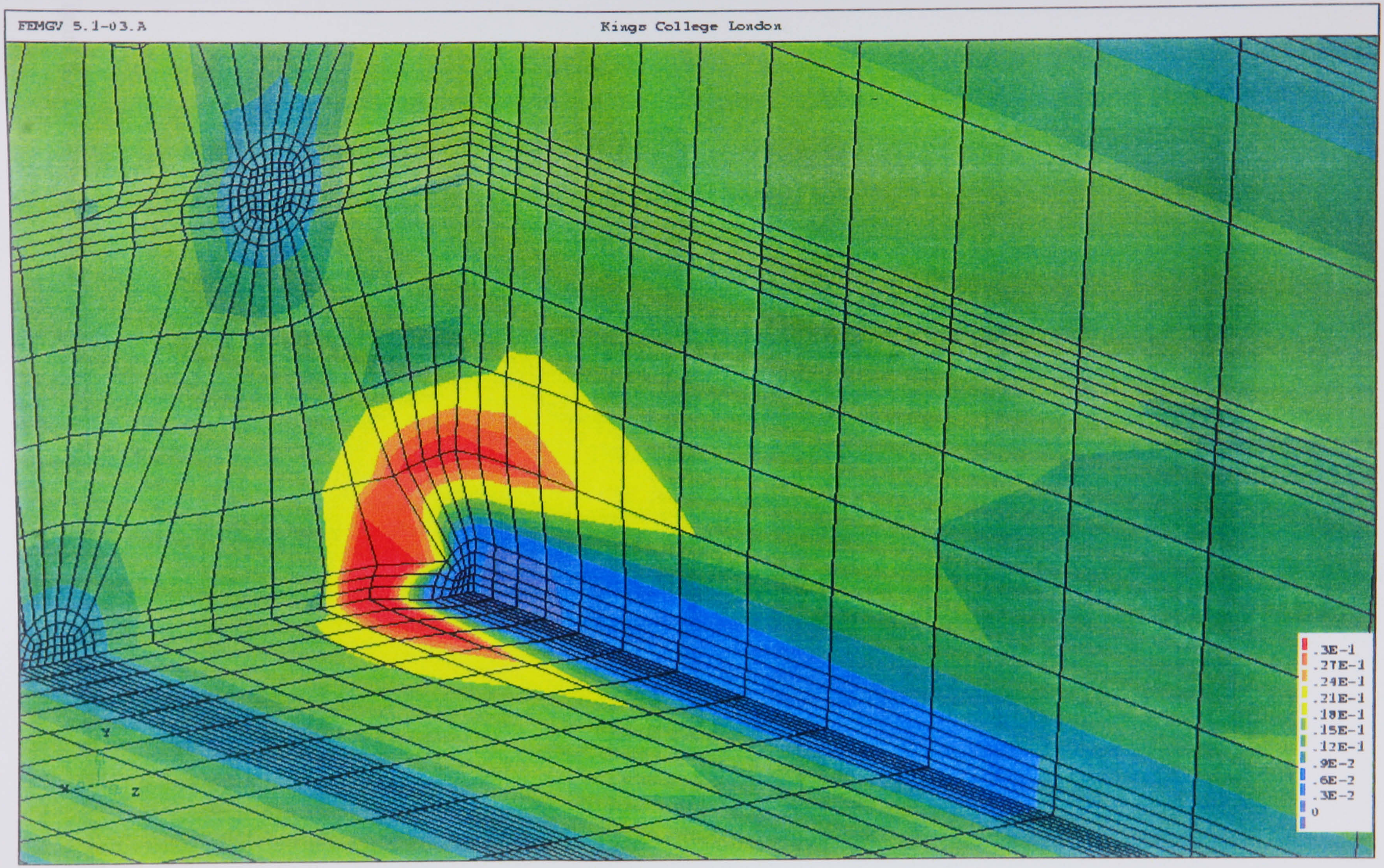

Figure 8.10 von Mises strain in the FE model without matrix crack, at the ratio R/d = 5

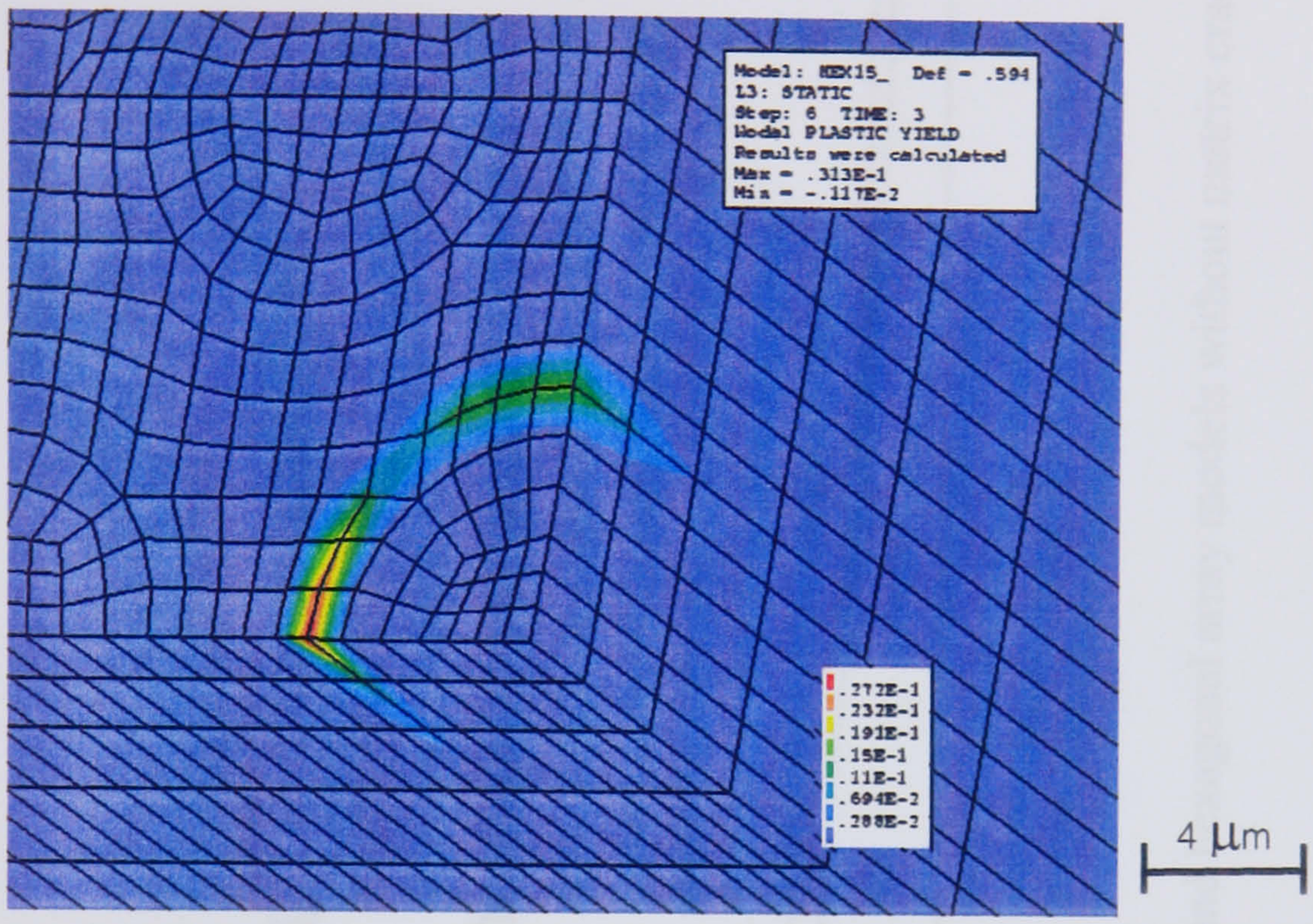

(a)

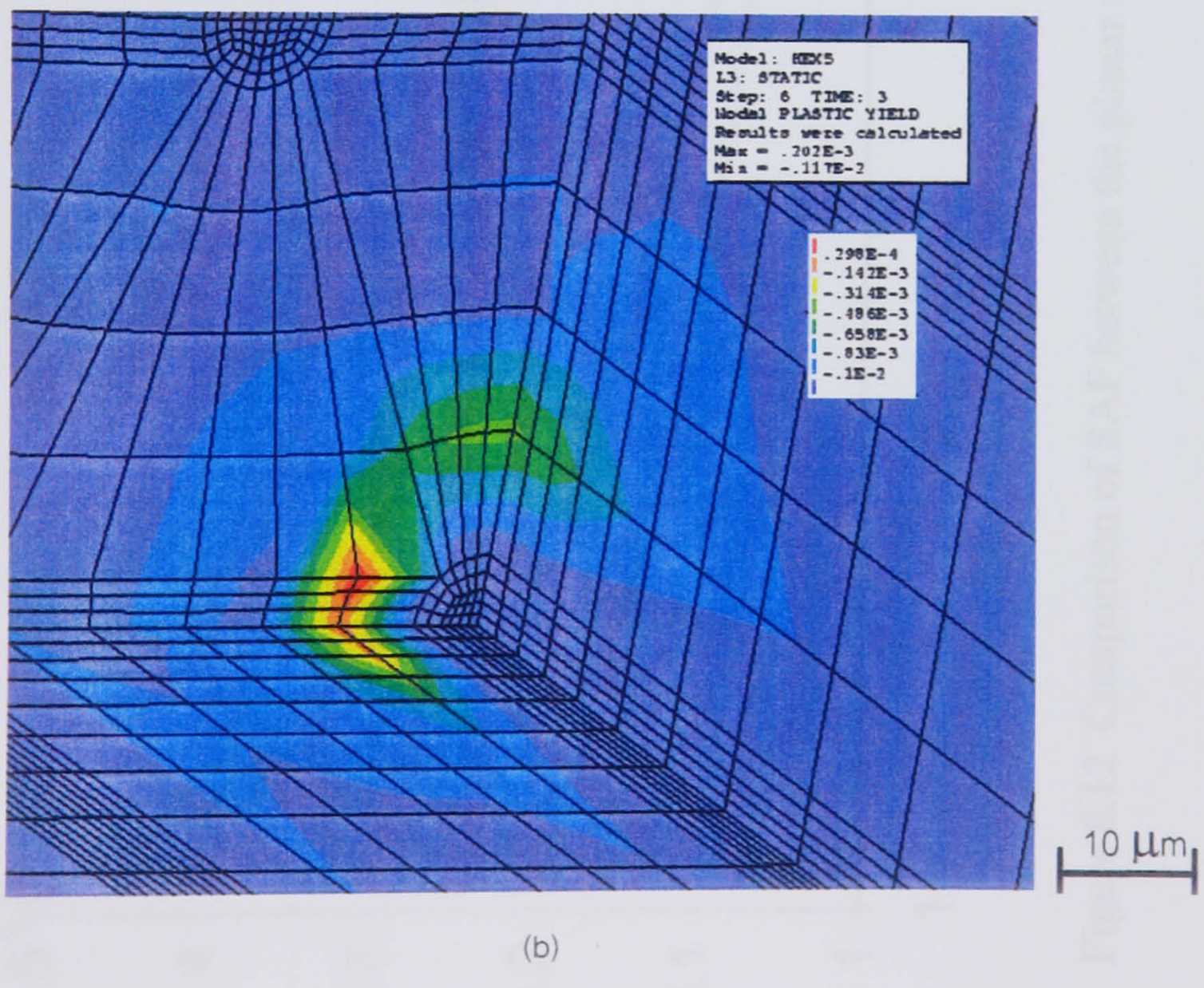

(b)

Figure 8.11 Areas of critical plastic strain in (a) FE model without matrix crack at R/d = 1.5 and (b) FE model without matrix crack at R/d = 5

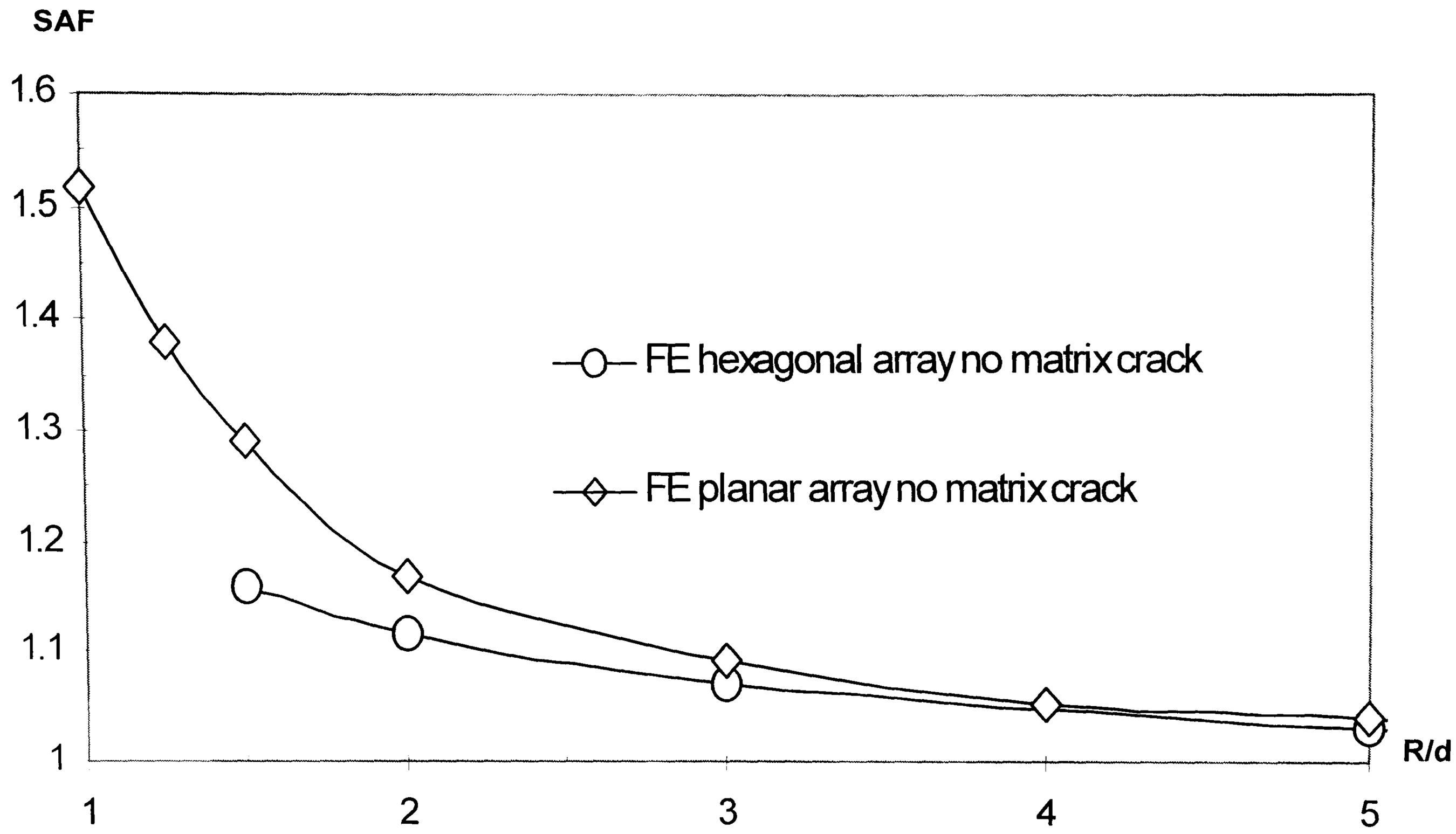

Figure 8.12 Comparison of SAF between the planar array and hexagonal array models without matrix crack

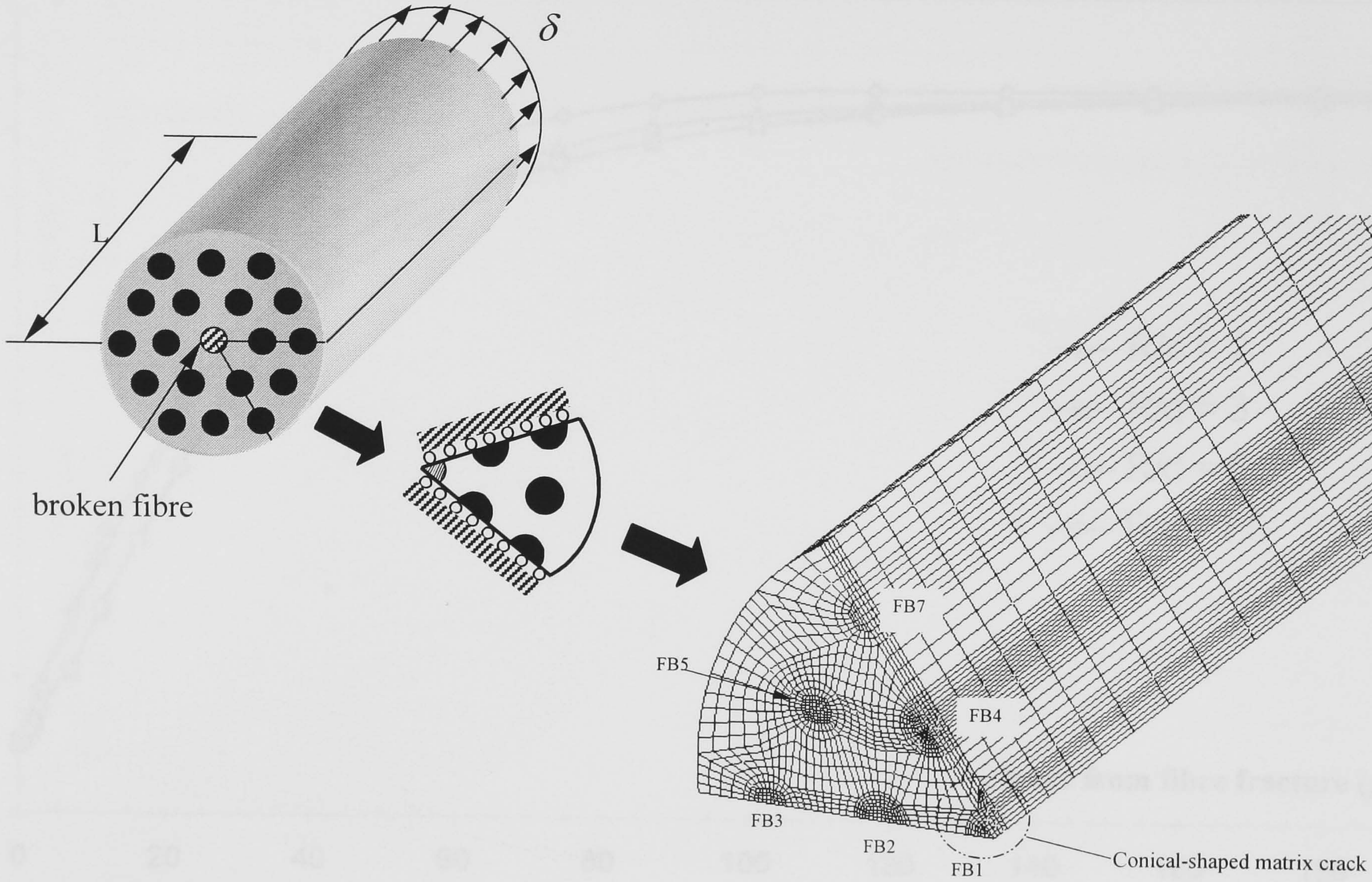

Figure 8.13 Hexagonal array FE model with matrix crack

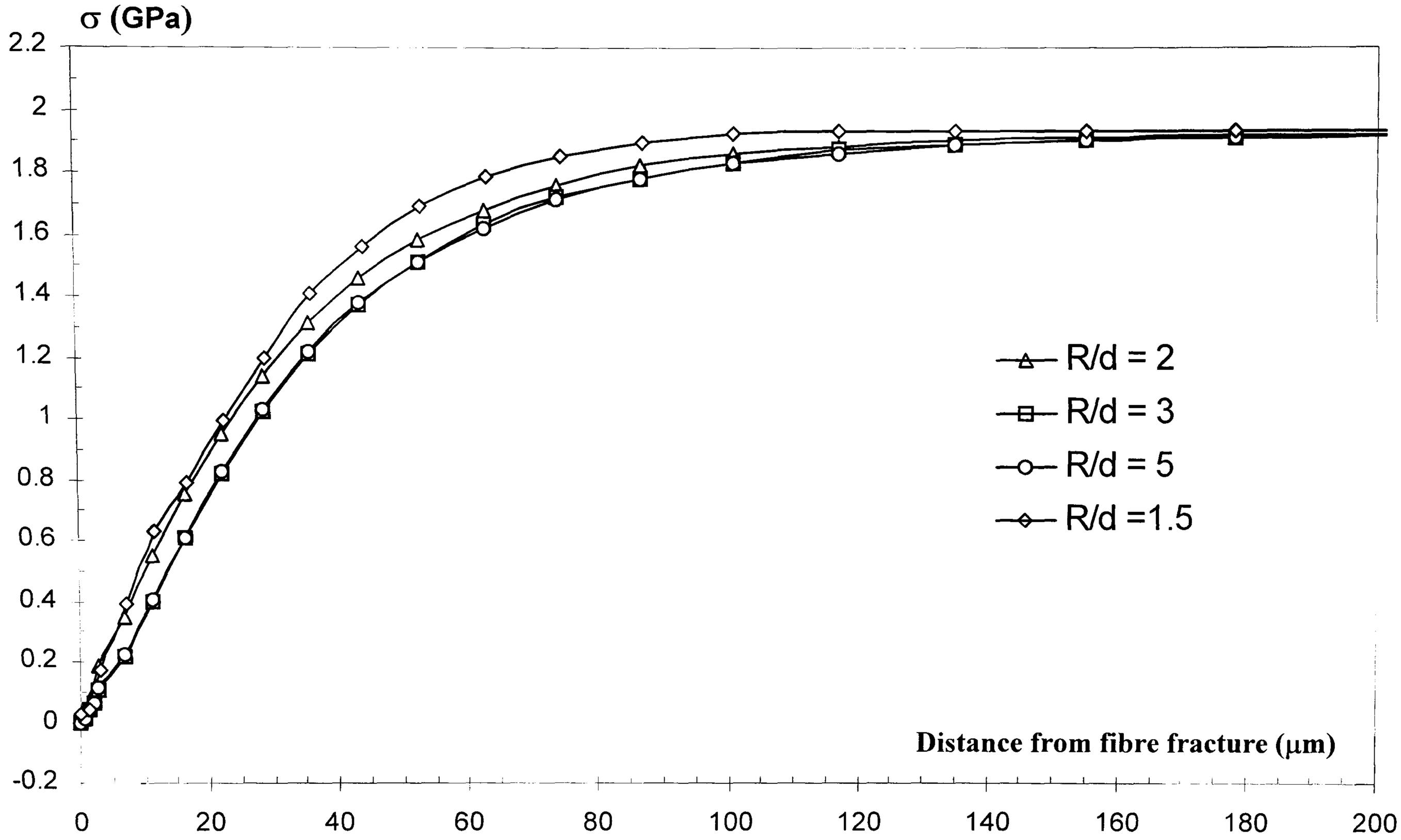

Figure 8.14 Variation of fibre stresses in the models with matrix crack

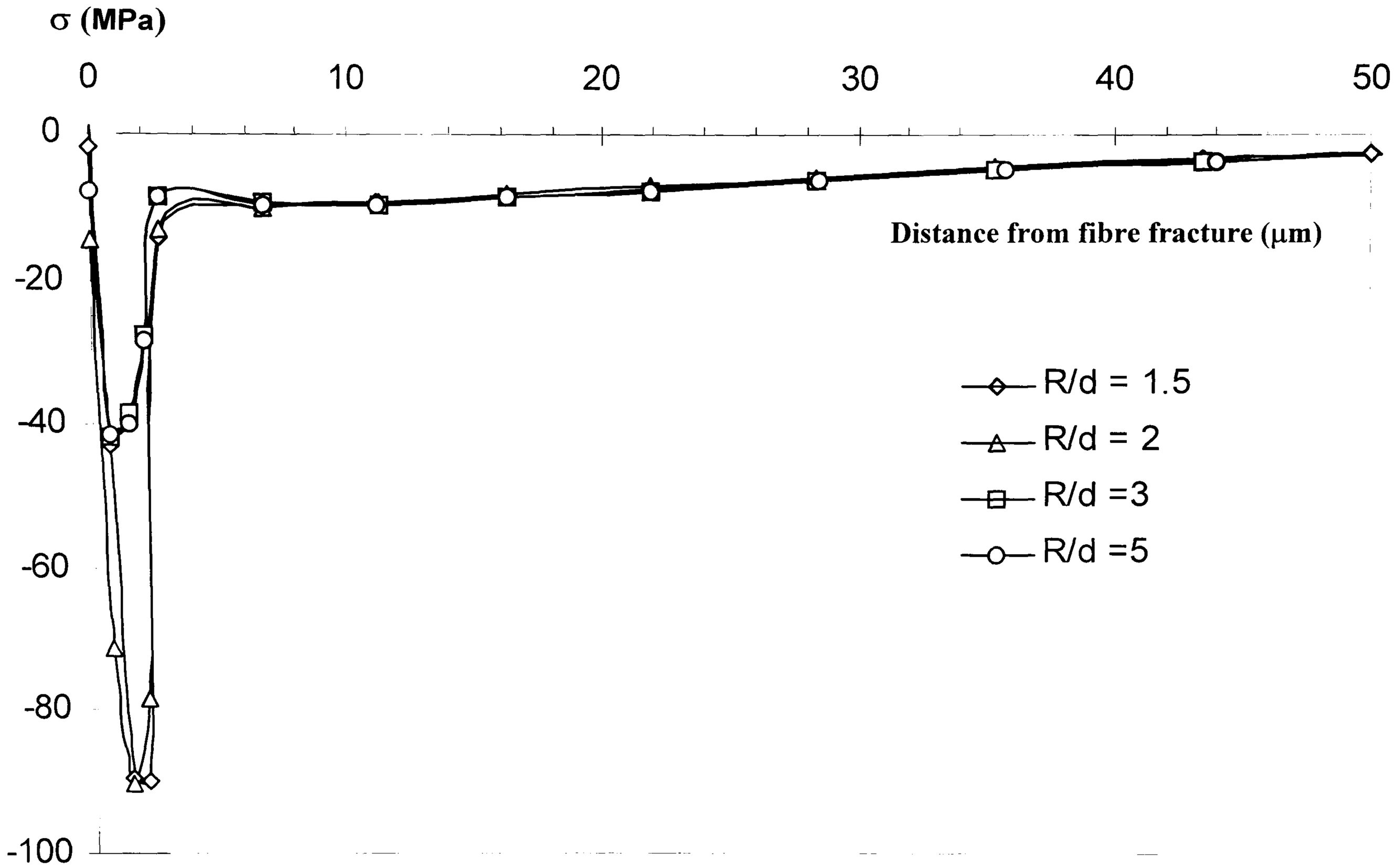

Figure 8.15 Variation of interfacial shear stresses in the nearest neighbouring fibres for the models with matrix

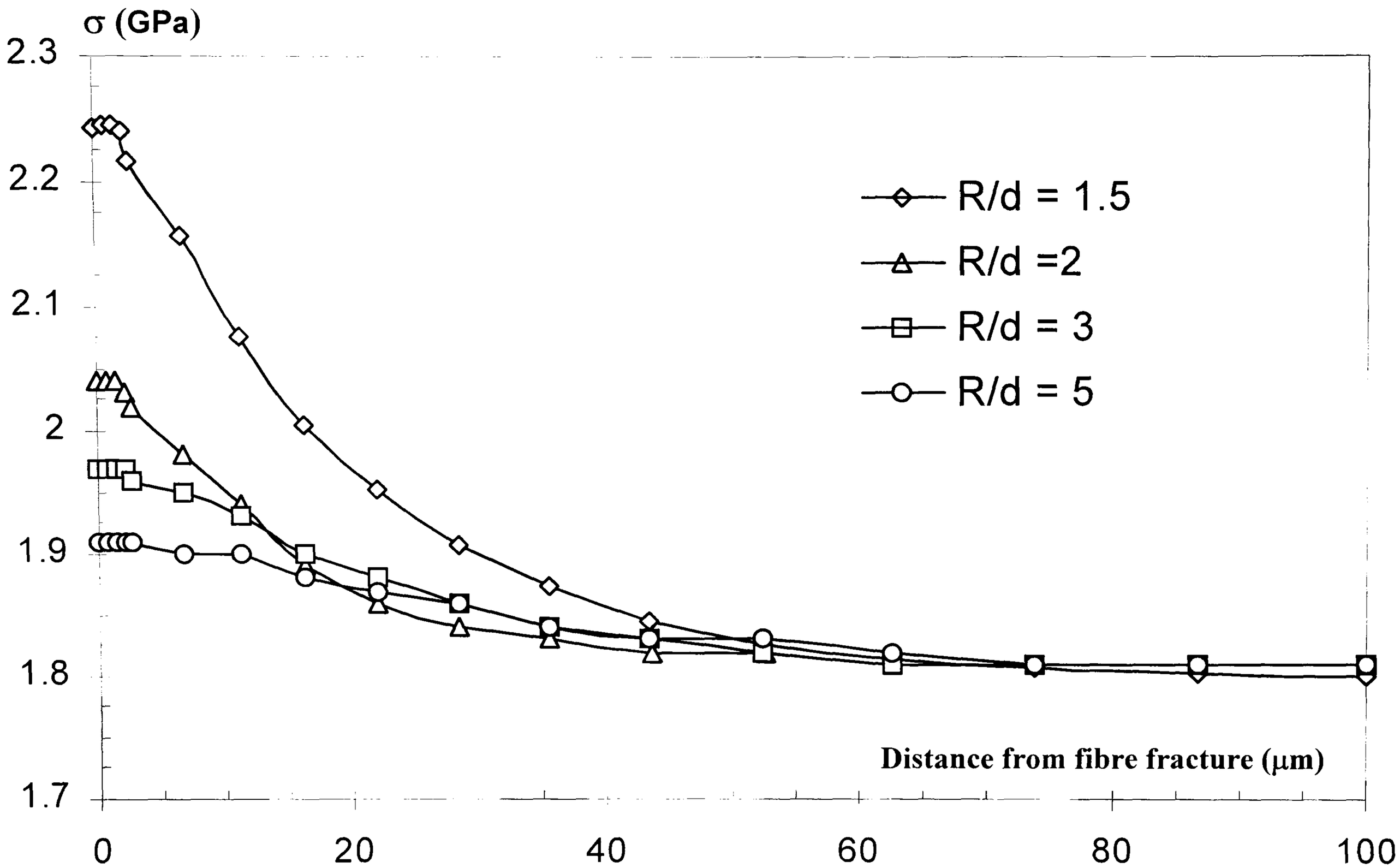

Figure 8.16 Variation of fibre stresses in the nearest neighbouring fibres for the models without matrix crack

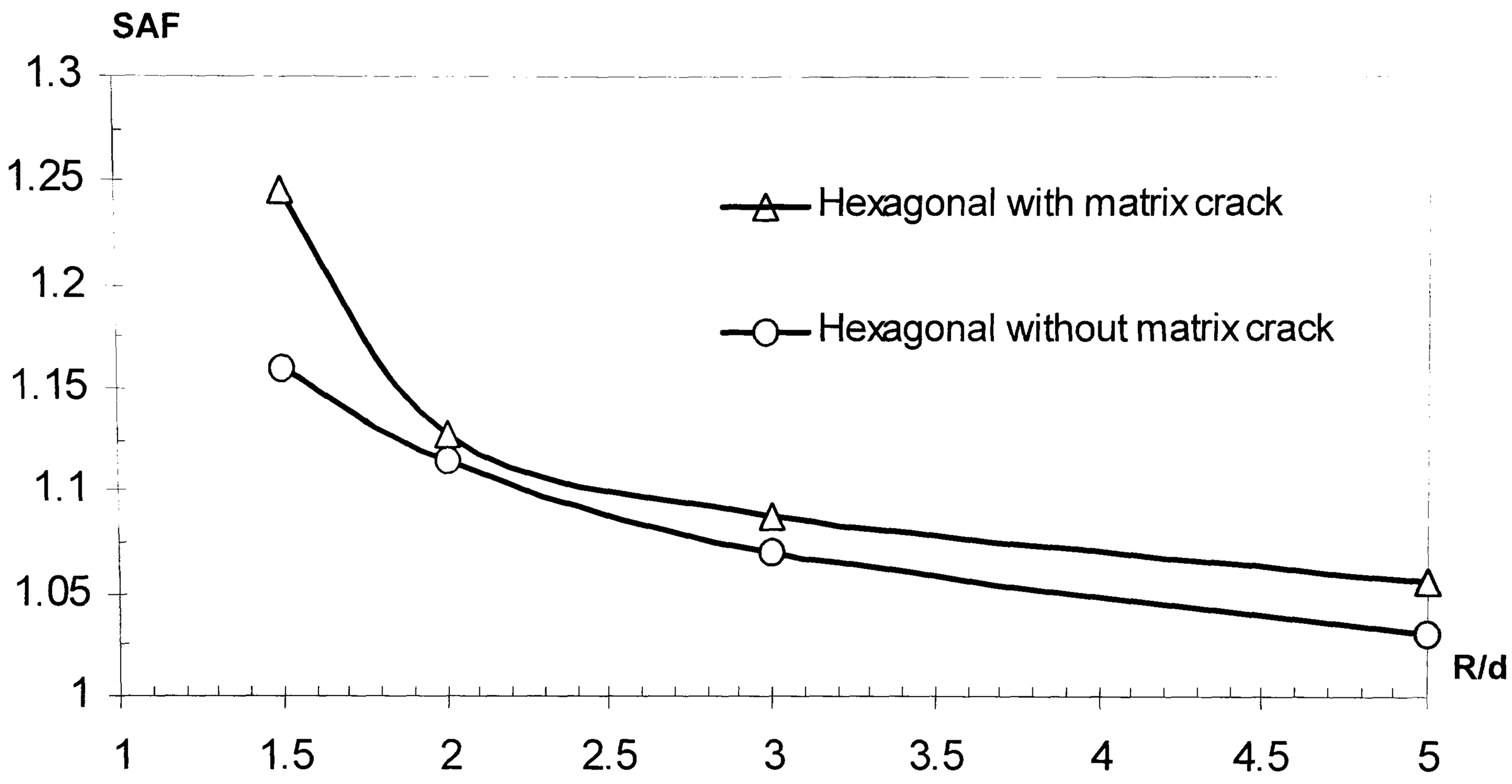

Figure 8.17 Comparison of SAF between the hexagonal array with and without matrix crack

CHAPTER 9

Conclusions and Future Research

9.1 Conclusions

The micromechanics of progressive failure in fibre-reinforced composites have been successfully investigated using FE analysis, and the LRS results were used to validate FE models. The micromechanical analysis of progressive failure began with the investigation of the effect of an interphase. The interphase model was based on a linear elastic material with a radial variation of moduli throughout the thickness. The elasto-plastic FE results have shown that the interphase has little effect on the fibre stresses and a significant effect on matrix strains at high level of applied strain. The highest reduction of matrix plastic strain of approximately 89 % was found when an interphase thickness of 0.6 μm was included in the model.

In the fragmentation test, failure in a short fibre composite is thought to be governed by the development of micro-voids involving a slow crack growth. The RT void growth model was used to investigate failure for this composite system. A uniform void size in the matrix material was assumed at the initial stage. Based on the RT void growth model, the void growth rate depends on the hydrostatic stress and the von Mises stress fields ahead of the crack tip. The initiation of a matrix crack was predicted when the failure envelope, derived from eq.3.4, and the angular variation of

plastic strain just touch. This condition indicates the location containing critical voids, which implies a fracture location. The matrix crack was predicted to initiate at the semi-cone angle of 18° and at an applied strain of 0.3 % by this criterion.

Matrix viscoplasticity was found to have an effect on failure in a long fibre composite. When fibre fracture takes place, the increase in the strain rate near the fracture location reduces the matrix ductility. This makes catastrophic failure involving rapid crack-growth in the matrix material, more likely. The semi-cone angle of a matrix crack was predicted to be about twice the value for a short fibre system. It was also found that the fibre stress profiles are characteristic of the matrix crack geometries. It has been found that the viscoplastic model has more available strain energy than that in the elasto-plastic model. This is because the strain energy dissipated by plasticity in the viscoplastic model is apparently less than that in elasto-plastic model.

When an individual fibre fractures in a multi-fibre composite, the stress redistribution near the fracture location may induce failure of the neighbouring intact fibres. The inter-fibre spacing is an important factor in determining the effect of the stress redistribution, and whether or not a domino effect of fibre fracture will occur. The presence of a matrix crack was found to increase the PAL by approximately 75 % and gives better agreement for the fibre stress profiles with LRS results. However, it was found to have less effect on the SAFs in the hexagonal array models compared to those in the planar array models.

9.2 Future Research

Since this research project was based on the available experimental data provided by ICE/HT-FORTH [59], the recent LRS work at ICE/HT-FORTH will be used as a basis for suggested future work in FE analysis of failure in composites.

9.2.1 Interphase study

As the mechanical properties of the interphase are varying through its thickness, it was difficult to use FE analysis to create a realistic model for the micromechanics of composites. The development of a special element, which can model mechanical properties varying through the thickness of an element, is the way to improve the FE model for a micromechanical analysis of composites. Since the interphase is classified as a viscoelastic material [115], it may play an important role in the dynamics of the event. Performing dynamic FE analysis would be a further improvement for this research.

9.2.2 Micromechanics of failure in short fibre composites

A study of failure in a short fibre composite under compression would be the extension of the work in Chapter 3. Since micro-voids close under compressive loading and fibre buckling occurs in this case, the search for a suitable failure criterion and a critical fibre length is waiting to be investigated. The available LRS results for a short fibre reinforced epoxy composite under compressive loading have been accomplished by Vlattas *et al.* [116]. A study of failure in a short fibre composite under fatigue loading is one of interesting topics to be investigated.

As mentioned in section 3.1 concerning the shear strain reversal in a short fibre composite, matrix cracking is likely to occur under fatigue loading. The LRS results for this case are available by Koimtzoglou *et al.* [11].

9.2.3 Micromechanics of failure in long fibre composites

In order to investigate the effect of fibre recoil on matrix cracking, the implementation of a crack propagation simulation in a fully dynamic FE analysis needs to be developed. As mentioned in section 5.4.4, the calculated strain rates in a quasi-static elasto-viscoplastic FE analysis are exaggerated. An adaptive mesh with a moving crack tip is required in order to predict the direction of crack initiation during each simulation step. The micromechanical FE analysis of a long fibre composite under fatigue loading is waiting to be investigated. The LRS results performed at ICE/HT by Koimtzoglou *et al.* [117] are now available to be used to validate the FE analysis.

9.2.4 Micromechanical analysis of multi-fibre composites

A micromechanical FE analysis of cross-ply composites would be a further development of the work described in Chapters 7 and 8. Matrix cracking was also found in the cross-ply composites, as reported by several authors [43-45]. The LRS results at ICE/HT have been accomplished by Arjyal *et al.* [118-119]. Three-dimensional FE analysis can be performed using those available LRS results to investigate the stress transfer characteristics and failure mechanisms in the cross-ply composites.

Appendix A

Laser Raman Spectroscopy (LRS)

The principle of this technique is based on the strain sensitivity of the Raman vibration modes of crystalline fibres and is a direct consequence of the change in the bond stiffness with the bond extension or contraction. The procedure of stress/strain measurement involves the suitable calibration curves in the air, which relates the atomic frequencies of fibres to the applied values of stress or strain. Thus, the Raman wavenumbers of the embedded fibres in a composite can be converted by means of the calibration curves to values of stress or strain.

The LRS results used in this work were measured by a novel remote laser Raman microprobe, developed by Galiotis, Paipetis and Vlattas [10]. The main feature of the new probe is the use of fibre-optic cable to send and receive laser. The advantage of using fibre-optic cable is that operation of the microprobe in horizontal, vertical and multi-angle directions are permitted (see Fig. 1. 2 (a), (b)). A miniature CCD camera on the back of the microprobe allows simultaneously operation of both the Raman and optical microscope.

In the experimental set-up, the composite specimen is placed in the mechanical tester and the laser power of about 1 mW, is used for a Raman probe (see Fig. A. 1), and focused to a submicrometre-sized spot on the specimen. The collected Raman light was delivered through the optical fibre to a SPEX 1000M single monochromator.

The Raman signal was collected by a Wright Instrument CCD and stored in a PC-compatible computer.

LRS has some limitations in measurement. The resolution of LRS is limited within a measurement window of approximately 1 μm. LRS is unable to measure the stress in internal fibre of the hexagonal array composites, as described in Chapter 8, due to the reflection of Raman waves by surrounding fibre. Since the accuracy of LRS is based on the optical resolution, therefore it produces noise in the measurement. There is a limit on the frequency for dynamic loading conditions as a result of focusing limitations in LRS.

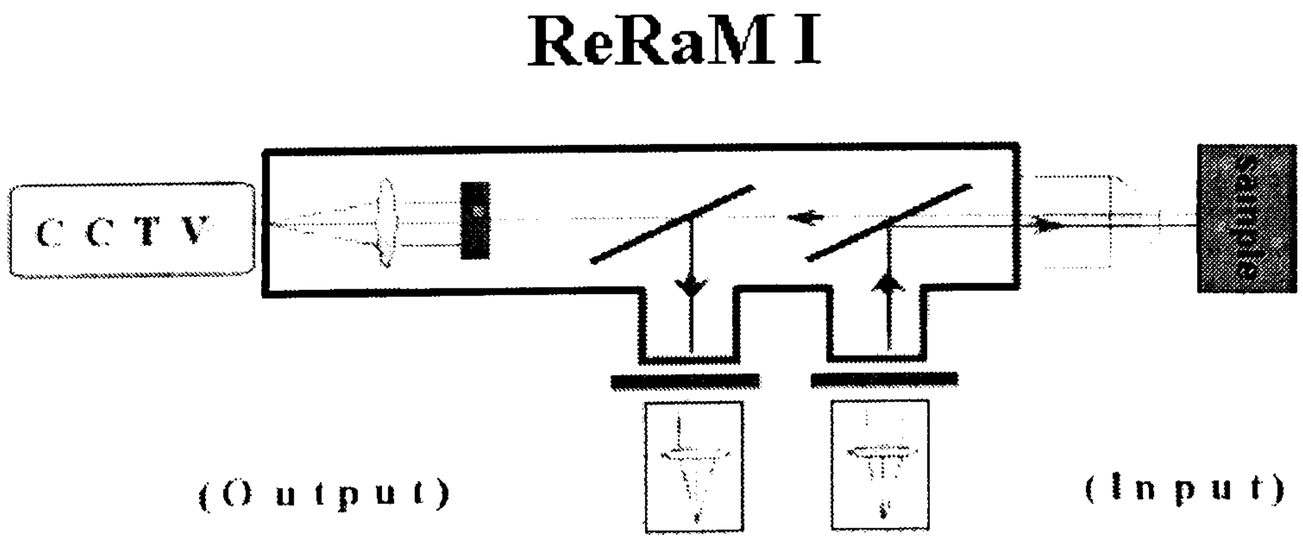

Figure A. 1 Remote Raman probe set-up

Appendix B

Mechanical Properties of Epoxy Matrix MY750/HY951 (from manufacturer)

Resin type	MY750/HY951	
Minimum storage life (months)	resin	12
	hardener	12
Vapour pressure mm Hg	resin	1 (180°C)
	hardener	<0.01 25°C
Initial viscosity of the mixture, cP	20-25°C	3500-4500
	40 °C	700-750
Minimum curing time, h	25 °C	24-36
	40 °C	10-15
	60 °C	2-3

Mechanical and physical properties	MY750/HY951
Tensile strength (Kg/mm^2)	4-6
Compressive strength (Kg/mm^2)	12-13
Flexural strength (Kg/mm^2)	8-12
Impact strength ($Kg\ cm/\ cm^2$)	6-10
Specific gravity ($g/\ cm^3$)	1.15-1.20
Coefficient of linear thermal expansion 10^{-4} / °C	65-75
Modulus of elasticity ($Kg\ /mm^2$)	300-350
Martens heat distortion temp. (°C)	50-60
Decomposition temp. (°C)	270-280

```
**********************
** INPLONG.INP  **
**********************
*PREPRINT, ECHO=NO, MODEL=NO
********************
** MODEL GEOMETRY *
********************
**
*NODE, NSET=ALLNODE
 1,   3.300000,   0.0000000,    0.0000000
 2,   3.450000,   0.0000000,    0.0000000
       .
       .
*ELEMENT, TYPE=CAX8     , ELSET=S1
    1    1    2    4    3   63   65   66   64
    2    3    4    6    5   66   68   69   67
       .
       .
*************************
** MATERIAL DEFINITIONS *
*************************
*MATERIAL, NAME=FBR
*DENSITY
  1.000000    ,
*ELASTIC, TYPE=ENGINEERING CONSTANTS
0.020, 0.392, 0.020, 0.030, 0.270, 0.030, 0.012, 0.008
0.012
*EXPANSION, TYPE=ORTHO
2.5E-05, -0.250E-06, 2.5E-05
*MATERIAL, NAME=MTRX
*DENSITY
  1.000000    ,
*ELASTIC, TYPE=ISO
 260E-05   , 0.36, 0.000
*EXPANSION, TYPE=ISO
5.8E-05
*PLASTIC
120E-07, 0.0
250E-07, 0.0035
310E-07, 0.0116
*MATERIAL, NAME=IPH1
*DENSITY
  1.000000,
*ELASTIC, TYPE=ISO
 0.19144    ,0.360,    0.000
*EXPANSION, ZERO = 0.0000000
 0.0000000,   0.0000000
*MATERIAL, NAME=IPH2
*DENSITY
  1.000000    ,
*ELASTIC, TYPE=ISO
 0.0366277    ,0.360,    0.000
*EXPANSION, ZERO=0.0000000
 0.0000000, 0.0000000
*MATERIAL, NAME=IPH3
*DENSITY
  1.000000    ,
*ELASTIC, TYPE=ISO
 768.7E-05    ,0.360,    0.000
*EXPANSION, ZERO=0.0000000
 0.0000000,     0.0000000
*MATERIAL, NAME=IPH4
*DENSITY
```

```
  1.000000    ,
*ELASTIC, TYPE=ISO
 295.88E-05    ,0.360,    0.000
*EXPANSION, ZERO=     0.0000000
 0.0000000,     0.0000000
**************************
** KINEMATIC CONSTRAINTS *
**************************
*NSET, NSET=L32
 5238 6774 5286 6870 5334 6966 5382 7062 5430 7158 5478 7254 5526 7350 5574
7446
 5622 7542 5670 7638 5718 7734 5766 7830 5814 7926 5862 8022 5910 8118 5958
8214
 6006 8310 6054 8406 6102 8502 6150 8598 6198 8694 6246 8790 6294 8886 6342
8982
 6390 9078 6438 9174 6486 9270 6534 9366 6582 9462 6630 9558 6678
*NSET, NSET=L43
 667810157100 61
*NSET, NSET=L53
100611066110565
*NSET, NSET=L63
105651116511069
*NSET, NSET=L73
110691166911573
*NSET, NSET=FBEND
115731418913709141881370814187137071418613706141851 3705
*NSET, NSET=DIST
   1    2   63  154  185  246  277  338  369  430  431  432  433  434  585  586
 587  588  589  890  891  892  893  894  895  896  897  898  899  900  901  902
 903  904  905  906  907  908  909  910  911
**********************************
** Temperature Drop, ΔT=50°C  **
**********************************
*STEP, INC=200
*STATIC
0.1, 1.0, 0
*TEMPERATURE
ALLNODE, -50
*BOUNDARY
 FBEND ,     2,    2
*BOUNDARY
L32     ,    2,    2
*BOUNDARY
L43     ,    2,    2
*BOUNDARY
L53     ,    2,    2
*BOUNDARY
L63     ,    2,    2
*BOUNDARY
L73     ,    2,    2
*NODE FILE, FREQUENCY=201
U
*EL FILE, POSITION=AVERAGED AT NODES, FREQUENCY=201
S,E, ENER
*EL FILE, POSITION=INTEGRATION POINTS, FREQUENCY=201
S
*EL FILE, POSITION=INTEGRATION POINTS, FREQUENCY=201
COORD
*EL FILE, POSITION=INTEGRATION POINTS, FREQUENCY=201
E
*END STEP
```

```
**************************
** Applied Strain 1.3 % **
**************************
*STEP, INC=200
*STATIC
0.1, 1.0, 0
*BOUNDARY, OP=MOD
 DIST    ,    2,    2, -3.9
*BOUNDARY, OP=MOD
 FBEND   ,    2,    2
*BOUNDARY, OP=MOD
L32      ,    2,    2
*BOUNDARY, OP=MOD
L43      ,    2,    2
*BOUNDARY, OP=MOD
L53      ,    2,    2
*BOUNDARY, OP=MOD
L63      ,    2,    2
*BOUNDARY, OP=MOD
L73      ,    2,    2
*NODE FILE, FREQUENCY=201
U
*EL FILE, POSITION=AVERAGED AT NODES, FREQUENCY=201
S,E, ENER, PE
*EL FILE, POSITION=INTEGRATION POINTS, FREQUENCY=201
S
*EL FILE, POSITION=INTEGRATION POINTS, FREQUENCY=201
COORD
*EL FILE, POSITION=INTEGRATION POINTS, FREQUENCY=201
E
*END STEP
**************************
** Fibre Fracture       **
**************************
*STEP, INC=200
*STATIC
0.1, 1.0, 0
*BOUNDARY, OP=NEW
 DIST    ,    2,    2, -3.9
*BOUNDARY, OP=NEW
L32      ,    2,    2
*BOUNDARY, OP=NEW
L43      ,    2,    2
*BOUNDARY, OP=NEW
L53      ,    2,    2
*BOUNDARY, OP=NEW
L63      ,    2,    2
*BOUNDARY, OP=NEW
L73      ,    2,    2
**************************
** RESULTS OUTPUT CONTROL *
**************************
*NODE FILE, FREQUENCY=201
U
*EL FILE, POSITION=AVERAGED AT NODES, FREQUENCY=201
S,E, ENER, PE
*EL FILE, POSITION=INTEGRATION POINTS, FREQUENCY=201
S
*EL FILE, POSITION=INTEGRATION POINTS, FREQUENCY=201
COORD
*EL FILE, POSITION=INTEGRATION POINTS, FREQUENCY=201
E, PE
*END STEP
```

```
*******************
** INPSHRT.INP  **
*******************
** MATERIAL DEFINITIONS
*MATERIAL, NAME=FIB
*DENSITY
  1.000000    ,
*ELASTIC, TYPE=ENGINEERING CONSTANTS
0.020, 0.392, 0.020, 0.030, 0.270, 0.030, 0.012, 0.008
0.012
*EXPANSION, TYPE=ORTHO
2.5E-05, -0.250E-06, 2.5E-05
*MATERIAL, NAME=MTRX
*DENSITY
  1.000000    ,
*ELASTIC, TYPE=ISO
 260E-05  , 0.36, 0.000
*EXPANSION, TYPE=ISO
5.8E-05
*PLASTIC
120E-07, 0.0
250E-07, 0.0035
310E-07, 0.0116
*MATERIAL, NAME=INT1
*DENSITY
  1.000000    ,
*ELASTIC, TYPE=ISO
 0.19144    ,0.360    ,    0.000
*EXPANSION, ZERO=     0.0000000
 0.0000000,     0.0000000
*MATERIAL, NAME=INT2
*DENSITY
 1.000000    ,
*ELASTIC, TYPE=ISO
 0.0366277    ,0.360    ,    0.000
*EXPANSION, ZERO=0.0000000
 0.0000000,     0.0000000
*MATERIAL, NAME=INT3
*DENSITY
  1.000000    ,
*ELASTIC, TYPE=ISO
 768.7E-05    ,0.360    ,    0.000
*EXPANSION, ZERO=0.0000000
 0.0000000,     0.0000000
*MATERIAL, NAME=INT4
*DENSITY
  1.000000    ,
*ELASTIC, TYPE=ISO
 295.88E-05    ,0.300    ,    0.000
*EXPANSION, ZERO=0.0000000
 0.0000000,     0.0000000
** KINEMATIC CONSTRAINTS
*NSET, NSET=DIST
  850  860  870  880  890  900  910  920  930  940  950  970  990 1010
1030 1050
 1070 1090 1110 1130 1150 1170 1180 1190 1210 1630 1631 1632 1633 1634
1635 1636
```

```
 1637 1638 1639 1640 1641 1642 1643 1644 1645 1646 1647 1648 1649 1650
1651 1652
 1653 1654 1655 1656 1657 1658 1659 1660 1661 1662 1663 1664 1665 1666
1667 1668
 1669 2470 2471 2472 2473 2474 2475 2476 2477 2478 2479 2480 2481 2482
2483 2484
 2485 2486 2487 2488 2489 2490 2491 2492 2493 2494 2495 2496 2497 2498
2499 2500
 2501 2502 2503 2504 2505 2506 2507 2508 2509
*NSET, NSET=FIXED
155081550915510155111551215919159201592115922276322808228532289822943
2
298823033
230782312323168232132330323393234832357323663237532384323933240232411
32
438224383
243842438524747247482474924750258752592025965260552722527270273152740
52
857528620
286652875529565296102970029701297022970329704297052970629707297082970
92
971029711
297122971329714297152971629717297182971929720
*****************************
** Temperature Drop, ΔT=50°C **
*****************************
*STEP, INC=200
*STATIC
0.1, 1.0, 0
*TEMPERATURE
ALLNODE, -50
*BOUNDARY
FIXED   ,    2,    2
*NODE FILE, FREQUENCY=201
U
*EL FILE, POSITION=AVERAGED AT NODES, FREQUENCY=201
S,E, ENER
*END STEP
*************************
** Applied Strain 0.4 % **
*************************
*STEP, INC=200
*STATIC
0.1, 1.0, 0
*BOUNDARY, OP=MOD
 DIST    ,    2,    2, -1.1976
*BOUNDARY, OP=MOD
FIXED   ,    2,    2
*****************************
** RESULTS OUTPUT CONTROL *
*****************************
*NODE FILE, FREQUENCY=201
U
*EL FILE, POSITION=AVERAGED AT NODES, FREQUENCY=201
S,E, ENER, PE
*END STEP
*****************************
```

** **VOIDSHRT.INP** **

```
      .
      .
**********************************************
** Define Contact Elements at the Fibre End Face **
**********************************************
*NSET, NSET=TOP
3098, 3153, 3099, 3154, 3100, 3155, 3101, 3156, 3102,
3157, 2278, 2333, 2279, 2334, 2280, 2335, 2281, 2336,
2202, 2282, 2756, 2708, 2759, 2709, 2760, 2710, 2761,
2711, 2762, 2712, 2938, 2918, 2639, 2919, 3000, 2978,
3001, 2979, 4124, 4094, 4104, 3870, 3890, 11956,
*ELSET, ELSET=LOWER
1385, 1386, 1387, 1388, 1389, 1390, 1391, 1392, 1393,
1394, 1395, 1396, 1397, 1398, 1399, 1400, 1401, 1402,
1403, 1404, 1405
*SURFACE DEFINITION, NAME=LOWER, TRIM=YES
LOWER
*CONTACT NODE SET, NAME=TOP
TOP
*CONTACT PAIR, INTERACTION=PAIR1, ADJUST=0.001
TOP, LOWER
*SURFACE INTERACTION, NAME=PAIR1
**************************
** MATERIAL DEFINITIONS *
**************************
*MATERIAL, NAME=FBR
*DENSITY
  1.000000    ,
*ELASTIC, TYPE=ENGINEERING CONSTANTS
0.020, 0.392, 0.020, 0.030, 0.270, 0.030, 0.012, 0.008
0.012
*EXPANSION, TYPE=ORTHO
2.5E-05, -0.250E-06, 2.5E-05
*MATERIAL, NAME=MTX
*DENSITY
  1.000000    ,
*ELASTIC, TYPE=ISO
 260E-05  , 0.34, 0.000
*PLASTIC
408.40E-07, 0.0
457.70E-07, 0.003958
490.74E-07, 0.0057675
514.15E-07, 0.008764
540.57E-07, 0.020776
549.85E-07, 0.029835
552.70E-07, 0.034920
553.00E-07, 0.042693
*EXPANSION, TYPE=ISO
5.8E-05
**************************
** KINEMATIC CONSTRAINTS *
**************************
*NSET, NSET=L256
 4217 4233 4218 4234 4219
*BOUNDARY
L256    ,    2,    2
```

```
*NSET, NSET=L1560
 9423 9429 4219
*BOUNDARY
L1560    ,     2,     2
*NSET, NSET=L1562
 9432 9438 9423
*BOUNDARY
L1562    ,     2,     2
*NSET, NSET=L1564
 9447 9465 9446 9464 9445 9463 9432
*BOUNDARY
L1564    ,     2,     2
*NSET, NSET=L1566
 9468 9474 9447
*BOUNDARY
L1566    ,     2,     2
*NSET, NSET=L1568
 9483 9501 9482 9500 9481 9499 9468
*BOUNDARY
L1568    ,     2,     2
*****************************
** Temperature Drop, ΔT=50°C **
*****************************
*STEP, INC=200
*STATIC
0.1, 1.0, 0
*CONTROLS, PARAMETERS=FIELD, FIELD=DISPLACEMENT
0.01, 0.1 , , ,
*TEMPERATURE
ALLNODE, -50
*END STEP
*************************
** Applied Strain 0.15% *
*************************
*STEP, INC=200
*STATIC
0.1, 1.0, 0
*PRINT, PLASTICITY=YES
*NSET, NSET=DISP
10698, 10699, 10700, 10701, 10702, 10703, 10704, 10705, 10706,
10707, 10708, 10808, 10809, 10810, 10811, 10812, 10813, 10814,
10815, 10816, 10817, 11018, 11019, 11020, 11021, 11022, 11023,
11024, 11025, 11026, 11027, 11118, 11119, 11120, 11121, 11122,
11123, 11124, 11125, 11126, 11127, 11318, 11319, 11320, 11321,
11322, 11368, 11369, 11370, 11371, 11372, 11468, 11478, 11498,
11508, 11528, 11538, 11558, 11559, 11560, 11588, 11589, 11590,
11648, 11658, 11678, 11679, 11680, 11708, 11709, 11710
*BOUNDARY
DISP     ,    2,    2,   .450000
*BOUNDARY
L256     ,     2,     2
*BOUNDARY
L1560    ,     2,     2
*BOUNDARY
L1562    ,     2,     2
*BOUNDARY
L1564    ,     2,     2
```

```
*BOUNDARY
L1566   ,     2,     2
*BOUNDARY
L1568   ,     2,     2
**************************
** RESULTS OUTPUT CONTROL *
**************************
*FILE FORMAT, ASCII
*NODE FILE, FREQUENCY=200
U
*NODE PRINT, FREQUENCY=200
U
*EL FILE, POSITION=AVERAGED AT NODES, FREQUENCY=200
S,E
*EL FILE, POSITION=INTEGRATION POINTS, FREQUENCY=200
S
*EL FILE, POSITION=INTEGRATION POINTS, FREQUENCY=200
COORD
*EL FILE, POSITION=AVERAGED AT NODES,  FREQUENCY=200
PE
*EL FILE, POSITION=INTEGRATION POINTS, FREQUENCY=200
E
*EL PRINT, POSITION=AVERAGED AT NODES,  FREQUENCY=200
S, E
*EL PRINT, POSITION=AVERAGED AT NODES,  FREQUENCY=200
PE
*EL PRINT, POSITION=NODES,  FREQUENCY=200
S, E
*EL PRINT, POSITION=INTEGRATION POINTS, FREQUENCY=200
E
*END STEP
**
*****************************************************
```

```
** VISCOSNE.INP **
************************
** MATERIAL DEFINITIONS *
************************
*MATERIAL, NAME=FIB
*DENSITY
  1.000000    ,
*ELASTIC, TYPE=ENGINEERING CONSTANTS
0.020, 0.392, 0.020, 0.030, 0.270, 0.030, 0.012, 0.008
0.012
*EXPANSION, TYPE=ORTHO
2.5E-05, -0.250E-06, 2.5E-05
*MATERIAL, NAME=MTX
*DENSITY
  1.000000    ,
*ELASTIC, TYPE=ISO
 243.5E-05  , 0.34, 0.000
*PLASTIC, RATE=0
408.40E-07, 0.0
457.70E-07, 0.003958
490.74E-07, 0.0057675
514.15E-07, 0.008764
540.57E-07, 0.020776
549.85E-07, 0.029835
*PLASTIC, RATE=0.01
470E-07, 0.0
549.35E-07, 0.001192
603.97E-07, 0.003496
621.38E-07, 0.004948
647E-07, 0.009874
654E-07, 0.016744
*PLASTIC, RATE=0.025
470E-07, 0.0
598E-07, 0.002732
659.13E-07, 0.007134
689.94E-07, 0.011703
694.3E-07, 0.015483
*PLASTIC, RATE=0.2
600E-07, 0.0
689E-07, 0.002707
732.84E-07, 0.005347
764.07E-07, 0.008587
768.5E-07, 0.01226
*PLASTIC, RATE=0.4
604.2E-07, 0.0
714.47E-07, 0.002081
774E-07, 0.008107
780E-07, 0.01226
*PLASTIC,RATE=1.2
604.2E-07, 0.0
702.06E-07, 0.0008
748E-07, 0.004161
779E-07, 0.00742
787E-07, 0.0121
*EXPANSION, TYPE=ISO
5.8E-05
*NSET, NSET=TOP
```

```
11, 22, 33, 44,  55,  66, 87, 108, 129, 150,
171,1931,1939,1966,1968,1991,
1992, 2000, 2002, 2003, 2004, 2005, 2009, 2010, 2011, 5498, 5500, 5509,
5510,
5511, 5515, 5516, 5517, 5570, 5571, 5572, 5573, 5574, 5625, 5626, 5627,
5628,
5629, 5870, 5871, 5872, 5873,5914, 5915, 5916, 5917, 6110, 6111, 6112,
6113,
6114, 6165, 6166, 6167, 6168, 6169, 6410, 6411, 6432, 6433, 6530, 6531,
6552,
6553, 6650, 6651, 6672, 6673, 6774, 6775, 283,  284,  285,  286,  287,
288,
295,  296,  297,  298,  299,  311,  312,  313,  314,  319,  320,  321,
322,
331,  332,  333,  334,  335,  341,  342,  343,  344,  345,  356,  357,
360,
361,  366,  367,  370,  371, 6774, 6786, 6787, 6788, 6789, 6804
*BOUNDARY
TOP     ,    2,    2
******************************
** Temperature Drop, ΔT=50°C **
******************************
*STEP, INC=100
*STATIC
 20, 1000.0, 0.0
*CONTROLS, PARAMETERS=FIELD, FIELD=DISPLACEMENT
0.01, 0.1 , , ,
*TEMPERATURE
ALLNODE, -50
*NODE FILE, FREQUENCY=0
*EL FILE, POSITION=AVERAGED AT NODE, FREQUENCY=0
*EL PRINT,FREQUENCY=0
*END STEP
**************************
** Applied strain =1.3% **
**************************
*STEP, INC=100
*STATIC
10, 1000, 0
*NSET, NSET=DISP
 265  266  267  281  282 5419 5425 5428 5434 5441 5442 5443 5459 5460
5461 5464
 5470 5477 5478 5479 5495 5496 5497
*BOUNDARY
DISP    ,   2,   2, -4.5
** compensate with the displacement from temperature drop **
*NSET, NSET=TOP
11, 22, 33, 44,  55,  66, 87, 108, 129, 150,
171,1931,1939,1966,1968,1991,
1992, 2000, 2002, 2003, 2004, 2005, 2009, 2010, 2011, 5498, 5500, 5509,
5510,
5511, 5515, 5516, 5517, 5570, 5571, 5572, 5573, 5574, 5625, 5626, 5627,
5628,
5629, 5870, 5871, 5872, 5873,5914, 5915, 5916, 5917, 6110, 6111, 6112,
6113,
6114, 6165, 6166, 6167, 6168, 6169, 6410, 6411, 6432, 6433, 6530, 6531,
6552,
```

```
6553, 6650, 6651, 6672, 6673, 6774, 6775, 283,  284,  285,  286,  287,
288,
295,  296,  297,  298,  299,  311,  312,  313,  314,  319,  320,  321,
322,
331,  332,  333,  334,  335,  341,  342,  343,  344,  345,  356,  357,
360,
361,  366,  367,  370,  371, 6774, 6786, 6787, 6788, 6789, 6804
*BOUNDARY
TOP     ,    2,    2
*NODE FILE, FREQUENCY=1000
U
*EL FILE, POSITION=AVERAGED AT NODE, FREQUENCY=1000
ENER
*ENERGY FILE, FREQUENCY=1000
*END STEP
**********
** FIBRE FRACTURE *
**********
*STEP, INC=100
*STATIC
1E-4, 1.666E-3, 0
*NSET, NSET=TOP2
11, 22, 33, 44,  55,  66, 87, 108, 129, 150,
171,1931,1939,1966,1968,1991,
1992, 2000, 2002, 2003, 2004, 2005, 2009, 2010, 2011, 5498, 5500, 5509,
5510,
5511, 5515, 5516, 5517, 5570, 5571, 5572, 5573, 5574, 5625, 5626, 5627,
5628,
5629, 5870, 5871, 5872, 5873,5914, 5915, 5916, 5917, 6110, 6111, 6112,
6113,
6114, 6165, 6166, 6167, 6168, 6169, 6410, 6411, 6432, 6433, 6530, 6531,
6552,
6553, 6650, 6651, 6672, 6673, 6774, 6775
*BOUNDARY, OP=NEW
TOP2    ,    2,    2
*NSET, NSET=DISP
 265  266  267  281  282 5419 5425 5428 5434 5441 5442 5443 5459 5460
5461 5464
 5470 5477 5478 5479 5495 5496 5497
*BOUNDARY, OP=NEW
DISP    ,   2,   2, -4.5
**********
** RESULTS OUTPUT CONTROL *
**********
*FILE FORMAT, ASCII
*NODE FILE, FREQUENCY=1
U
*EL FILE, POSITION=AVERAGED AT NODE, FREQUENCY=2
S,E, ENER, ER
*EL FILE, POSITION=AVERAGED AT NODE,  FREQUENCY=2
PE
*ENERGY FILE, FREQUENCY=2
*END STEP
```

```
** CRKPROPG.INP **
************************
** MATERIAL DEFINITIONS *
************************
*MATERIAL, NAME=FB
*DENSITY
  1.000000    ,
*ELASTIC, TYPE=ENGINEERING CONSTANTS
0.020, 0.392, 0.020, 0.030, 0.270, 0.030, 0.012, 0.008
0.012
*EXPANSION, TYPE=ORTHO
2.5E-05, -0.250E-06, 2.5E-05
*MATERIAL, NAME=MTX
*DENSITY
  1.000000    ,
*ELASTIC, TYPE=ISO
 243.5E-05  , 0.34, 0.000
*PLASTIC, RATE=0
408.40E-07, 0.0
457.70E-07, 0.003958
490.74E-07, 0.0057675
514.15E-07, 0.008764
540.57E-07, 0.020776
549.85E-07, 0.029835
*PLASTIC, RATE=0.01
470.00E-07, 0.0
549.35E-07, 0.001192
603.97E-07, 0.003496
621.38E-07, 0.004948
647.00E-07, 0.009874
654.00E-07, 0.016744
*PLASTIC, RATE=0.025
470.00E-07, 0.0
598.00E-07, 0.002732
659.13E-07, 0.007134
689.94E-07, 0.011703
694.30E-07, 0.015483
*PLASTIC, RATE=0.2
600.00E-07, 0.0
689.00E-07, 0.002707
732.84E-07, 0.005347
764.07E-07, 0.008587
768.5E-07, 0.01226
*PLASTIC, RATE=0.4
604.20E-07, 0.0
714.47E-07, 0.002081
774.00E-07, 0.008107
780.00E-07, 0.01226
*PLASTIC,RATE=1.2
604.20E-07, 0.0
702.06E-07, 0.0008
748.00E-07, 0.004161
779.00E-07, 0.00742
787.00E-07, 0.0121
*EXPANSION, TYPE=ISO
5.8E-05
```

```
**********************************
** THERMAL LOADING, DT= 50 C **
**********************************
*STEP, INC=100
*STATIC
 2, 200, 0.0
*CONTROLS, PARAMETERS=FIELD, FIELD=DISPLACEMENT
0.01, 0.1 , , ,
*TEMPERATURE
ALLNODE, -50
*NSET, NSET=MEND1
   81  82  83  84  85  86  87  88  89  90  91  92  93  94  95
   96  97  98  99 100 101 102 103 104 105 106 107 108 109 110
*BOUNDARY
MEND1, 2, 2
*NSET, NSET=FEND
  3383 3424 3465 3506,799
*BOUNDARY
FEND, 2, 2
*NSET, NSET=END
 2413 2443 2473 2503 2533 2563 2593 2623 2653 2683 2713 2743 2773 2803
 2833 2863 2893 2923 2953 2983 3013 3043 3073 3103 3133 3163 3193 3223
 3253 3283 3313 3607 3637 3667 3697
*BOUNDARY
END, 2, 2
*NODE FILE, FREQUENCY=10
U
*EL FILE, POSITION=AVERAGED AT NODE, FREQUENCY=10
S, E, ENER
*ENERGY PRINT, ELSET=PHY1, FREQUENCY=201
*ENERGY PRINT, ELSET=PHY2, FREQUENCY=201
*ENERGY FILE
*EL FILE, POSITION=AVERAGED AT NODE, FREQUENCY=10
PE
*END STEP
**************************
** Applied strain =1.3% **
**************************
*STEP, INC=100
*STATIC
1, 200, 0
*BOUNDARY
END, 2, 2, -4.5
*BOUNDARY
 MEND1, 2, 2
*BOUNDARY
FEND, 2, 2
*FILE FORMAT, ASCII
*NODE FILE, FREQUENCY=10
U
*EL FILE, POSITION=AVERAGED AT NODE, FREQUENCY=10
S, E, ENER
*ENERGY PRINT, ELSET=PHY1, FREQUENCY=201
*ENERGY PRINT, ELSET=PHY2, FREQUENCY=201
*ENERGY FILE
*EL FILE, POSITION=AVERAGED AT NODE, FREQUENCY=10
PE
```

```
*END STEP
**********************
** CRACK PROPAGATION  **
**********************
*STEP, INC=200
*STATIC
1E-4, 8.33E-3, 0.0
*MODEL CHANGE, TYPE=CONTACT PAIR, REMOVE
 UPPER2, LOWER2
*BOUNDARY, OP=NEW
 MEND1,    2,    2
*NSET, NSET=DISP
 2422 2452 2482 2512 2542 2572 2602 2632 2662 2692 2722 2752 2782 2812
 2842 2872 2902 2932 2962 2992 3022 3052 3082 3112 3142 3172 3202 3232
 3262 3292 3322 3616 3646 3676 3706
*BOUNDARY, OP=NEW
END,   2,   2, -4.5
**************************
** RESULTS OUTPUT CONTROL *
**************************
**
*NODE FILE, FREQUENCY=10
U
*EL FILE, POSITION=AVERAGED AT NODE, FREQUENCY=10
S,E, ENER
*ENERGY PRINT, ELSET=PHY1, FREQUENCY=201
*ENERGY PRINT, ELSET=PHY2, FREQUENCY=201
*ENERGY FILE
*EL FILE, POSITION=AVERAGED AT NODE,  FREQUENCY=10
PE
*END STEP
**************************************************************************
```

REFERENCES

1. Giffith, A. A. (1920) The phenomena of rupture and flow in solids, *Phil. Trans. Royal Soc.*, **221A**, 163-198.
2. Cox, H. L. (1952) The elasticity and strength of paper and other fibrous materials, *Br. J. Appl. Phy.* , **3**, 72-79.
3. Kelly, A., and Tyson, W.R. (1965) Tensile properties of fibre reinforced metals: copper/tungsten and copper/molybdenum, *J. Mech. Phy. Solid.* , **13**, 329-350.
4. Rosen, B. W. (1965) Mechanics of composite strengthening, Fibre composite Material, American Society for metal, Metal Park, OH, **Chapter 3**, 37-75.
5. McGarry, F. J. (1968) Crack propagation in fibre reinforced plastic composites, Fundamental Aspects of Fibre Reinforced Plastic Composites, *Interscience*, New York.
6. Owen M.J., Dukes, R., and Smith, T. R. (1968) Fatigue and failure mechanisms in GRP with special reference to random reinforcements. *SPI, 23rd Annual Technical Conference*, Washington, D.C., Febuary 1968, **Section 14-A**.
7. Broutman, L. J. and Sahu S. (1969) Progressive damage of a glass reinforced plastic during fatigue. *SPI, 24th Annual Technical Conference, Washington, D.C., February 1969*, **Section 11-D.**
8. Gibson, R. F. (1994) Principles of composite material mechanics. *McGraw-Hill*, New York.
9. Hull D. and Clyne, T.W. (1996) An introduction to composite materials, **2nd ed.**, *Cambridge University Press*, Cambridge.

10. C. Galiotis, V. Chohan, A. Paipetis and C. Vlattas. (1996) Interfacial measurements in single and multi-fibre momposites using the technique of laser Raman spectroscopy. *ASTM-STP 1290*, Spragg, J. C. and Drzal, L. T., (ed.) American Society for Testing and Materials, 19-33.

11. Koimtzoglou C., Kostopoulos, V., and Galiotis, C. (2001) Micromechanics of reinforcement and damage initiation in carbon fibre/epoxy composites under fatigue loading. *Composites Part A*, **32**, 457-471.

12. Marston C. and Galiotis C. (1998) On the failure of unidirectional carbon-epoxy composites, Part I: The effect of fibre sizing upon filament fracture and damage evolution. *J. Mat. Sci.*, **33**, 5311-5325.

13. Sirivedin, S., Fenner, D. N., Nath, R. B., and Galiotis C. (2000) Matrix crack propagation criteria for model short carbon fibre-epoxy composites. *Comp. Sci. Tech.*, **60**, 2835-2847.

14. Tang, C.Y., Peng, L.H., Li, C. C., Shen, W., and Tsui, C. P. (2001) Experimental study on stable growth of crack and craze damage in HIPS under tension at room temperature. *Polymer Testing*, **20**, 241-251.

15. Weibull, W. (1951) A statistical distribution function of wide applicability, *J. Appl. Mech.*, **18**, 293-305.

16. Plueddeman, E. P. (1974) Mechanisms of adhesion through silane coupling agents, *Composite Materials*, **6**, Plueddeman (ed.), Academic Press, New York, 174-216.

17. Tong, J., Guild, F. J., Ogin, S. L., and Smith, P.A. (1997) On matrix crack growth in quasi-isotropic laminates Part II: Finite element analysis, *Comp. Sci. Tech.*, **57**, 1537-1545.

18. Nath, R. B., Fenner, D.N., and Galiotis C. (1996) Elasto-plastic finite element modelling of interfacial failure in model Kevlar 49 fibre-epoxy composites, *Composites Part A*, **27A**, 821-832.

19. Mullin, J., Berry, J.M., and Gatti, A. (1968) Some fundamental fracture mechanisms applicable to advanced filament reinforced composites, *J. Comp. Mat.* , **2**, 82-103.

20. Busschen, A. ten, and Selvadurai, A. P. S. (1995) Mechanics of the segmentation of an embedded fibre, Part I: Experimental investigations, *J. Appl. Mech.*, **62**, 87-97.

21. Selvadurai, A. P.S., Busschen, A. ten, and Ernst, L. J. (1991) Batman-cracks: Observations and numerical simulation, *Proc. 13 Can. Congr. Appl. Mech. CANCAM' 91*, Winnipeg, Canada, 382-383.

22. Chamis, C. C. (1974) Mechanics of load transfer at the interface, *Interfaces in Polymer Matrix Composites*, **6**, Broutman, L. J. and Crock, R. H. (ed.), Academic Press, New York, 31-77.

23. Dekkers, M.E.J. (1985) The deformation behaviour of glass bead filled glassy polymers, *Ph.D. Thesis*, Tech. Univ. Eindhoven, The Netherlands.

24. Sancaktar, E. (1991) Non-linear viscoelastic behaviour of the fibre-matrix interface, Theory and Experiment, *Proc. Euromech Colloquium*, **269**, Vautrin A. (ed.), St. Etienne, France.

25. Song, D.Y., Takeda, N., Shioya, T., and Nakata, K. (1996) Approximate analysis of the stress state near the fibre ends of short fibre-reinforced composites and the consequent microfracture mechanisms, *Composites Part A*, **27A**, 357-364.

26. Baillie, C. and Buxton, A. (1998) A quantitative study of matrix crack propagation in the fragmentation test, *Composites Part A*, **29A**, 1091-1097.

27. Paipetis, A. and Galiotis, C. (1996) Effect of fibre sizing on the stress transfer efficiency in carbon/epoxy model composites, *Composites Part A*, **27A**, 755-767.

28. Paipetis, A. and Galiotis, C. (1997) A study of the stress-transfer characteristics in model composites as a function of material processing, fibre sizing and temperature of the environment, *Comp. Sci. Tech.*, **57**, 827-838.

29. Piggott, M. R. (1987) Debonding and friction at fibre-polymer interface. Part I : Criteria for failure and sliding. *Comp. Sci. Tech.*, **30**, 295-306.

30. Piggott, M. R. (1992) Interface properties and their influence of fibre-reinforced polymers, *Composite Applications: The role of matrix, fibre, and interface*, Vigo, T. L., and Kinzig, B. J. (ed.), VCH Publishers, New Orlean, **Chapter 9**, 221-265.

31. Hutchinson, J. W. and Jensen, H. M. (1990) Models for fibre debonding and pullout in brittle composites with friction, *Mech. Mater.*, **9**, 139-163.

32. Kim, J. K., and Mai, Y. W. (1996) Modelling of stress transfer across the fibre-matrix interface, *Numerical Analysis and Modelling of Composite Materia*l, Bull, J. W. (ed.), Blackie Academic & Professional, London, **Chapter 10**, 287-326.

33. Paipetis A., Galiotis, C. Liu, Y. C., and Nairn, J. A. (1999) Stress transfer from the matrix to the fibre in a fragmentation test: Raman experiments and analytical modelling, *J. Comp. Mat.* , **33**, 377-339.

34. Nath R B, Fenner D N, Galiotis C. (1996) Finite element modelling of interfacial failure in model carbon fibre-epoxy composites, *J Mat Sci*, **31**, 2879-2883.

35. Galiotis, C., Fenner, D. N., Nath, R. B., and Sirivedin, S. Meeting record at Queen Mary & Westfield College, University of London, on 30th,September,1998. *unpublished.*

36. Nath R B, (1998) Finite element analysis of interfacial failure in fibre-reinforced composites, *Ph.D. Thesis*, King's College, University of London, UK.

37. Curtin W.A. (2000) Dimensionality and size effects on the strength of fibre-reinforced composites, *Comp. Sci. Tech.*, **60**, 543-551.

38. Liu, H. –Y., Mai, Y. –W., Ye, L. and Zhou, L. –M. (1997) Stress transfer in the fibre fragmentation test: Part III Effect of matrix cracking and interface debonding, *J. Mat. Sci*, **32**, 633-641.

39. Detassis, M., Frydman, E., Vrieling, D., Zhou, X. F., Wagner, H. D., and Nairn, J. A. (1996) Interface toughness in fibre composites by the fragmentation test, *Composites Part A*, **27A**, 769-773.

40. Jacobs, E., and Verpoest, I. (1998) Finite element modelling of damage development during longitudinal tensile loading of coated fibre composites, *Composites Part A*, **29A**, 1007-1012.

41. Zhou, L. M., Kim, J. K. and Mai, Y. W. (1992) Interfacial debonding and fibre pull-out stresses, Part II A new model based on the fracture mechanics approach, *J. Mat. Sci.*, **27**, 3155-3166.

42. Zhou, X. –F., Nairn, J. A., and Wagner, H. D. (1999) Fibre-matrix adhesion from the single-fibre composite test: Nucleation of interfacial debonding, *Composites Part A*, 1387-1400.

43. Tong J., Guild, F. J., Ogin, S. L., and Smith, P. A. (1997) On matrix crack growth in quasi-isotropic laminates, Part I: Experimental investigation, *Comp. Sci. Tech.*, **57**, 1527-1535.

44. Ogin, S. L., Smith, P.A., and Beaumont, P. W. R. (1985) Matrix cracking and stiffness reduction during the fatigue of [0/90] GFRP laminates, *Comp. Sci. Tech.*, **22**, 23-31.

45. Heslehurst, R. B. (1996) Analysis and modelling of damage and repair of composite materials in aerospace, *Numerical Analysis and Modelling of Composite Materia*l, Bull, J. W. (ed.), Blackie Academic & Professional, London, **Chapter 2**, 27-59.

46. Laws, N. and Dvorak, G. J. (1988) Progressive transverse cracking in composite laminates, *J. Comp. Mat.* , **22**, 900-916.

47. Tsai, C. –L., Daniel, I. M. and Lee, J. –W. (1990) Progressive matrix cracking of crossply composite laminates under biaxial loading, in Microcracking-induced Damage in Composites, Dvorak, G. J. and Lagoudas, D. C.(ed.) *Proc. of ASME 1990 Winter annual meeting*, AMD-Vol. 111, MD-Vol. 22, American Soc. Of Mecchanical Engineers, New York, 9-18.

48. Lou, Y.C., and Schapery, R. A. (1971) Viscoelastic characterisation of a non-linear fibre –reinforced plastic, *J. Comp. Mat*, **5**, 208-234.

49. Wang, C., Sun, C. T., and Gates, T. S. (1996) Elastic/viscoplastic behaviour of fibre-reinforced thermoplastic composites, *J. Reinf. Plas. Comp.* , **15**, 360-377.

50. Zaoutsos, S. P., Papanicolaou, G. C., and Cardon, A. H. (1998) On the non-linear viscoelastic behaviour of polymer-matrix composites, *Comp. Sci. Tech.*, **58**, 883-889.

51. Gao, Z. J., and Xiang, X. Y. (1999) A variational approach to analysing laminates with cracks and viscoplasticity: The model and its validation, *J. Comp. Mat.* , **33**, 443-479.

52. Caruso, J. J., and Chamis, C. C. (1986) Assessment of simplified composite micromechanics using three-dimensional finite element analysis, *J. Comp. Tech. Res.*, **8**, 77-83.

53. Hedgepeth, J. M., and van Dyke, P. (1967) Local stress concentrations in imperfect filamentry composite materials, *J. Comp. Mat.* , **1**, 294-309.

54. Wagner, H. D., and Eitan, A. (1993) Stress concentration factors in two-dimensional composites: Effects of material and geometrical parameters, *Comp. Sci. Tech.*, **46**, 353-362.

55. Wagner, H. D., Amer, M. S., and Schadler, L. S. (1996) Fibre interactions in two-dimensional composites by Raman spectroscopy. *J. Mat. Sci.*, **31**, 1165-1173.

56. Chohan, V., and Galiotis, C. (1997) Effects of interface, volume fraction and geometry on stress redistribution in polymer composites under tension, *Comp. Sci. Tech.*, **57**, 1089-1101.

57. Van den Heuvel, P. W. J., Wubbolts, M. K., Young, R. J., and Peijs, T. (1998) Failure phenomena in two-dimensional multi-fibre model composites, Part V: A finite element study, *Composites Part A*, **29A**, 1121-1135.

58. Lane, R., Hayes, S. A., and Jones, F. R. (2001) Fibre/matrix stress transfer through a discrete interphase, Part II: High volume fraction systems, *Comp. Sci. Tech.*, **61**, 565-578.

59. ICE/HT–FORTH, Institute of Chemical Engineering and High Temperature Processes –Foundation for Research and Technology – Hellas, Patras, Greece.

60. Garton, A., Wang, S., and Stevenson W. T. K. (1992) Chemical effects at carbon-polymer interfaces, *Composite Applications: The role of matrix, fibre, and interface*, Vigo, T. L., and Kinzig, B. J. (ed.), VCH Publishers, New Orlean, **Chapter 11**, 277-291.

61. Crasto A., Own S-H., Subramanian R. V. (1986) Interphase modification in carbon-fibre composites via electrodeposition, *Composite Interfaces*, Elsevier Science Publishing, 133-147.

62. Theocaris, P.S. (1984) On the evaluation of adhesion between phases in fibre composites, *Colloid & Polymer Sci.*, **262**, 929-938.

63. Theocaris, P.S., Sideridis, E. P., and Papanicolaou, G. C. (1985) The elastic longitudinal modulus and Poisson's ratio of fibre composites, *J. Rein. Plas. and Comp.*, **4**, 397-418.

64. Theocaris, P. S., and Phillippidis, T. P. (1985) Theoretical evaluation of the extent of mesophase in particulate and fibrous composites, *J. Rein. Plas. and Comp.*, **4**, 173-185.

65. Jasiuk, I., and Kouider, M. W. (1993) The effect of an inhomogeneous interphase on the elastic constants of transversely isotropic composites, *Mechanics of Materials*, **15**, 53-63.

66. Ishida, H. (1984) A review of recent progress in the studies of molecular and microstructure of coupling agents and their functions in composites, coating and adhesive joints, *Polymer Composites*, **5**, 101-123.

67. Peacock, J. A., B. Fife, E. Nield and Crick, R. A. (1986) Examination of the morphology of aromatic polymer composite (APC-2) using an etching technique, *Proceedings of the first International Conference on Composite Interfaces*, 299-306.

68. Daadbin, A., Gamble, A. J., and Sumner, N. D. (1992) The effect of the interphase and material properties on load transfer in fibre composites, *Composites*, **23**, 210-214.

69. King, T. R., Blackketter, D. M. , Walrath, D. E., and Adams, D. F. (1992) Micromechanics prediction of the shear strength of carbon fibre/epoxy matrix composites : The influence of the matrix and interface strengths, *J. Comp. Mat.*, **26**, 559-573.

70. Mikata, Y. (1994) Stress fields in a continuous fibre composite with a variable interphase under thermo-mechanical loadings, *J. Eng. Mat. Tech.*, **116**, 367-377.

71. Daoust, J., Vu-Khanh, T., Ahlstrom, C. and Gèrard, J. F. (1993) A finite element model of the fragmentation test for the case of a coated fibre, *Comp. Sci. Tech.*, **48**, 143-149.

72. Jacobs, E., and Verpoest, I. (1998) Finite element modelling of damage development during longitudinal tensile loading of coated fibre composites, *Composites Part A*, **29A**, 1007-1012.

73. Di Anselmo, A., Accorsi, M. L., and DiBenedetto, A. T. (1992) The effect of an interphase on the stress and energy distribution in the embedded single fibre test, *Comp. Sci. Tech.*, **44**, 215-225.

74. Ho H., and Drzal L. T. (1995) Non-linear numerical study of the single-fibre fragmentation test, Part I: Test mechanics, *Comp. Eng.*, **5,**1231-1244.

75. Ho H., and Drzal L. T. (1995) Non-linear numerical study of the single-fibre fragmentation test, Part II: A parametric study, *Comp. Eng.*, **5,**1245-1259.

76. Nath, R. B., Fenner, D. N., and Galiotis, C. (2000) The progressional approach to interfacial failure in carbon reinforced composite: elasto-plastic finite element modelling of interface cracks, *Composites Part A,* **31A**, 929-943.

77. Selvadurai A. P. S., and Busschen, A. ten. (1995) Mechanics of a fragmentation test involving an embedded fiber, Part II: Computational modeling and comparisons. *J. Appl. Mech.*, **62**, 98-107.

78. Erdogan, F., and Sih, G. C. (1963) On the crack extension in plates under plane loading and transverse shear, *ASME J. Basic. Eng.*, **85**, 519-525.

79. Sih, G. C. (1974) Strain-energy-density factor applied to mixed mode crack problems, *Int. J. Fract.* , **10**, 305-321.

80. Chang, K. J. (1981) On the maximum strain criterion -A new approach to the angled crack problem, *Eng. Fract. Mech*, **14**, 107-124.

81. Rice, J. R. (1968) A path independent integral and the approximate analysis of strain concentration by notches and cracks, *J. Appl. Mech.*, **35**, 379-386.

82. He M Y, Hutchinson J W. (1989) Kinking of crack out of an interface, *J. Appl. Mech.*, **56**, 270-278.

83. Hayashi K, Nemat-Nasser S. (1981) Energy-release rate and crack kinking under combined loading, *J. Appl Mech.*, **48,** 520-524.

84. Liebowitz H, Lee D, Subramonian N. (1981) Criteria for predicting crack entension angle and path in plane crack problems. *Proc. Inte.r Conf. Analytical and Experimental Fracture Mechanics*, Mirabile, Italy.

85. Murakami Y. (1981) Prediction of crack propagation path (numerical analyses and experiments). *Proc. Inter. Conf. Analytical and Experimental Fracture Mechanics*, Mirabile, Italy.

86. Cherepanov G P. (1962) The stress state in a heterogeneous plate with slits (in Russian), Izvestiga AN SSSR, OTN, Mekhan. i Mashin (ed.),**1**, 131-137.

87. England A H. (1965) A crack between dissimilar media, *J. Appl. Mech.*, **32**, 400-402.

88. Hutchinson, J.W., (1990) Mixed mode fracture mechanics of interfaces, Metal-Ceramic Interfaces, Ruhle M, Evans A G, Ashby M F ,Hirth J P, (ed.), New York: Pergamon Press.

89. Rice J R, Sih G C. (1965) Plane problems of cracks in dissimilar media, *J. Appl. Mech.*, **32**, 418-423.

90. McCrum N G, Buckley C P, Bucknall C B. (1990) Principles of Polymer Engineering, Oxford: Oxford University Press.

91. Rice J R, Tracey D M. (1969) On the ductile enlargement of voids in triaxial stress fields, *J. Mech. Phys. Solids*, **17**, 201-217.

92. McClintock F A. (1968) A criterion of ductile fracture by the growth of holes, *J. Appl. Mech.*, **35**, 363-71.

93. Ritchie R O, Thomson A W. (1985) On macroscopic and microscopic analyses for crack initiation and crack growth toughness in ductile alloys. *Metall Trans*, **16A,** 233-248.

94. McMeeking R M. (1977) Finite deformation analysis of crack-tip opening in elastic plastic materials and implications for fracture, *J. Mech. Phys. Solids*, **25**, 357-381.

95. Johnson W, Mellor P B. (1983) Engineering Plasticity, 2nd ed., Ellis Horwood Limited,

96. O'Dowd N P. (1998) Advanced Fracture Mechanics: Lectures on Fundamentals of Elastic and Elastic-Plastic Fracture. Imperial College of Science Technology and Medicine, University of London, UK.

97. Harlin G, Willis J R. (1988) The influence of crack size on ductile-brittle transition. *Proc. Royal. Soc. London*, **A415**, 197-226.

98. Hanxing Z, Changchun L, Guangxia L. (1991) The critical void growth and crack initiation condition in the crack tip zone of 20g steel, *Eng. Fract. Mech*, **38**, 175-183.

99. Barsoum R S. (1977) Triangular quarter-point element as elastic and perfectly-plastic crack tip elements, *Int. J. Num. Meth. Eng.*, **11**, 85-98.

100. ABAQUS 5.6 (1997) User and Theory Manuals, Hibbitt, Karlson & Sorensen Inc, USA.

101. ABAQUS's lecture note (1996) Fracture Mechanics, Hibbitt, Karlson & Sorensen Inc., USA.

102. Courtney, T. H. (2000) Mechanical Behaviour of Materials, McGraw-Hill International Editions, Material Science/Metallurgy Series, Boston, USA.

103. Dowling, N. E. (1993) Mechanical behaviour of materials: Engineering methods for deformation, fracture, and fatigue, Prentice Hall international edition, New Jersey, USA.

104. Anderson, T. L. (1991) Fracture Mechanics: Fundamental and applications, CRC Press Inc., Boston, USA.

105. Tong J., Guild, F. J., Ogin S. L., and Smith P.A. (1997) On matrix crack growth in quasi-isotropic laminates: Part II finite element analysis, *Comp. Sci. Tech.*, **57**, 1537-1545.

106. Sih, G. C. (1991) Mechanics of Fracture Initiation and Propagation: Surface and volume energy density applied as failure criterion, Kluwer Academic Publishers, London, UK.

107. Sih G. C., Chao C.K., Hwu Y.J., and Hsu C.T. (1990) Springback in cold metal forming of AOO-H steel. *Theor. Appl. Fract. Mech.*, **14,** 81-99

108. Detassis M., Frydman E., Vrieling D., Zhou X. –F., Wagner H. D., and Nairn J. A. (1996) Interface toughness in fibre composites by the fragmentation test, *Composites Part A*, **27A**, 769-773.

109. Drzal, L. T., and Madhukar, M. J. (1993) Fiber-Matrix Adhesion and Its Relationship to Composite Mechanical Properties, *J. Matr. Sci.*, **28**, 569-610.

110. Fiedler, B., Klisch, A. and Schulte, K. (1998) Stress Concentrations in Multiple Fibre Model Composites, *Composites Part A*; **29A**: 1013-1019.

111. Sastry A. M., Phoenix S. L., and Schwartz C. (1993) Analysis of interfacial failure in a composite microbundle pull-out experiment, *Comp. Sci. Tech.*, **48**,237-251.

112. Eischen J. W., and Torquato S. (1993) Determining elastic behaviour of composites by the boundary-element method, *J. Appl. Physics*, **74**, 159-170.

113. Choi H. S., and Achenbach J.D. (1995) Stress states at neighbouring fibres induced by single-fibre interphase defects, *Int. J. Solids and Struct.*, **32**, 1555-1570.

114. FEMGV, Femsys Limited, Leicester, UK

115. Fisher, F. T., and Brinson, L. C. (2001) Viscoelastic interphase in polymer-matrix composites: Theoretical models and finite-element analysis, *Comp. Sci. Tech.*, **61**, 731-748.

116. Vlattas, C., and Galiotis, C. (1991) Monitoring the Behaviour of Polymer Fibres under Axial Compression, *Polymer*, **32**, 1788-1793.

117. Koimtzoglou, C., Kostopoulos, V., Galiotis, C., and Paipetis, S. A. (1998) Monitor the Stress Transfer Characteristics in Composites under Static and Dynamic Loading Conditions, ECCM-8, Science, Technologies and Applications, Crivelli-Visconti, I. (ed.), *Woodhead Publ. Ltd.*, Cambridge, **3**, 281-283.

118. Arjyal, B. P., Galiotis, C., Ogin, S. L., and Whattingham, R. D. (1998) Residual strain and Young's modulus determination in cross-ply composites using an embedded aramid fibre strain sensor, *Composites Part A*, **29A**, 1363-1369.

119. Arjyal, B. P., Galiotis, C., Ogin, S. L., and Whattingham, R. D. (1998) Monitoring local strains in cracked cross-ply composites using an embedded aramid fibre strain sensor, *J. Mat. Sci.*, **33**, 2745-2750.

ELSEVIER

Composites Science and Technology 60 (2000) 2835–2847

COMPOSITES SCIENCE AND TECHNOLOGY

www.elsevier.com/locate/compscitech

Matrix crack propagation criteria for model short-carbon fibre/epoxy composites

S. Sirivedin [a], D.N. Fenner [a,*], R.B. Nath [b], C. Galiotis [c]

[a] *Department of Mechanical Engineering, King's College, University of London, Strand, London, WC2R 2LS, UK*
[b] *Birkbeck College, University of London, Malet Street, London, WC1E 7HX, UK*
[c] *Institute of Chemical Engineering & High Temperature Processes, Foundation for Research & Technology-Hellas, Patras, Greece*

Received 4 April 2000; received in revised form 23 June 2000; accepted 1 August 2000

Abstract

Linear elastic and elasto-plastic finite-element analyses have been used to investigate the initiation of a conical-shaped matrix crack from the end of a single sized carbon short-fibre embedded in an epoxy matrix subjected to tensile loading. A maximum hoop-strain criterion and the modified Rice and Tracey micro-void nucleation, growth, and coalescence model are used to predict the crack angle. In the later case the applied strain at failure is also predicted. When the effects of the thermal residual stresses induced during the fabrication process are included, the predicted cone angle of the crack decreases from 23 to 18°, according to the maximum hoop-strain criterion. By using the Rice and Tracey model a cone angle of 16° was predicted, with or without the inclusion of thermal residual stresses, whereas the failure strain of the composite was shown to increase from 0.14 to 0.3% when the thermal stresses were included.

Keywords: Conical crack; Carbon-fibre/epoxy composite; Matrix cracking; Short fibre; Void growth; Ductile fracture; Sizing

1. Introduction

As the tensile loading on a model short-carbon-fibre/epoxy composite is increased most of the load is transferred via the matrix to the fibre. Interfacial shear stresses are induced at the fibre/matrix interface as a result of the difference between the material properties of the matrix and fibre. Eventually these stresses reach a critical value, the interfacial shear strength, beyond which point one or more of the following mechanisms of interfacial failure [1] are observed experimentally:

- *Mode α:* localised matrix yielding at the intact interface in the vicinity of the stress concentration associated with the fibre end corner. This is accompanied by debonding of the fibre end and the formation of a penny-shaped interface crack [see Fig. 1(a)].
- *Mode β:* in the case of a relatively weak fibre/matrix interface, a cylindrical interface crack subsequently propagates from the debonded fibre end [see Fig.1(b)]. Unlike the fibre end penny-shaped crack this crack remains closed as tensile loading on the composite increases, and load transfer across its contacting faces is maintained by a mechanism of frictional stress transfer.
- *Mode γ:* in the case of a strong interface a conical matrix crack subsequently propagates from the debonded fibre end [see Fig. 1(c)] at an angle θ_c to the fibre axis. This matrix crack opens with increasing applied load, thereby suppressing load transfer across the crack faces.

In practice, the interfacial bond strength is increased by treating the fibres with a size. In a sized system there is an increased likelihood of matrix crack Mode γ, as opposed to an interface crack Mode β, forming part of the progressive failure mechanism of the composite. A Mode γ matrix crack initiated at a fibre end during loading of the composite has been observed in a composite consisting of single sized short carbon fibres embedded in an epoxy matrix system [2–4], in a boron-fibre/epoxy system [5,6] and in a glass-fibre/polyester system [7]. Finite-element (FE) and boundary-element analyses have been used to

* Corresponding author. Tel.: +44-20-7848-2256; fax: +44-20-7848-2932.
E-mail address: david.fenner@kcl.ac.uk (D.N. Fenner).

0266-3538/00/$ - see front matter
PII: S0266-3538(00)00167-6

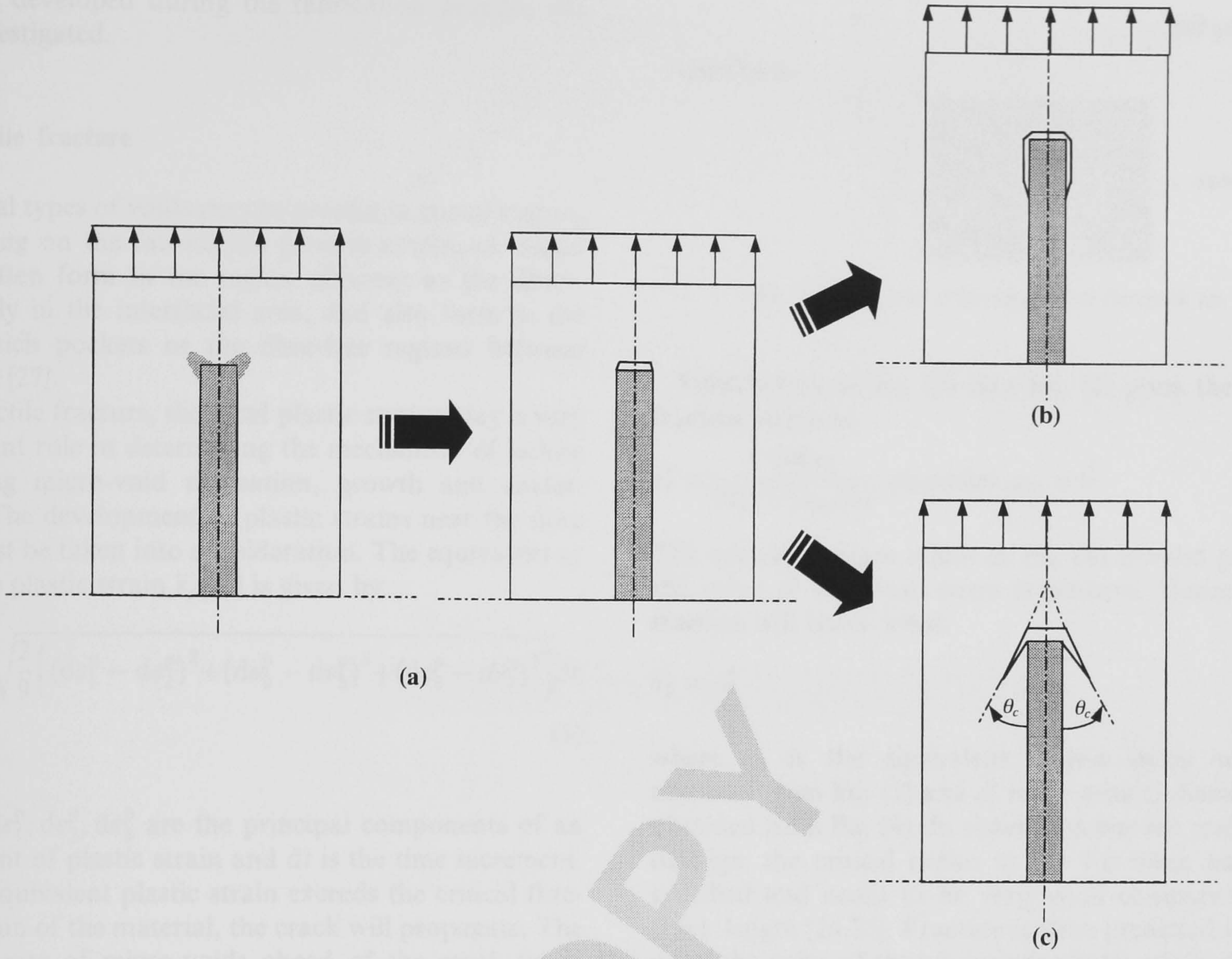

Fig. 1. Failure mechanisms: (a) Mode α; (b) Mode β; (c) Mode γ.

investigate this phenomenon [1,8]. In each case the angle of the conical crack used in the model was adjusted to give the best correlation between the predicted and experimentally measured fibre stresses. No attempt was made to predict a priori the angle of the conical matrix crack.

A number of criteria have been proposed for the general crack kinking problem, involving brittle fracture of a homogeneous material. These include the maximum normal stress and the maximum hoop stress criteria [9], the maximum elastic strain energy release rate criterion [10], the minimum strain energy density criterion [11] and the maximum strain criterion [12]. In the case of elasto-plastic fracture Rice's J integral [13] is often employed, but is unsuitable for the present system because of the presence of unloading.

For bi-material elastic systems several authors [14–21] have made theoretical and numerical predictions of crack propagation paths. These approaches are not appropriate for the current task of predicting the direction of a conical matrix crack due to the existence of matrix plasticity. Epoxy resin exhibits some ductility [22] and therefore it is reasonable to assume conditions of ductile fracture at the matrix crack tip. One possible approach is to apply a maximum hoop strain criterion to the results obtained using elasto-plastic FE analysis.

At the micro-mechanical level the mechanism of ductile fracture includes micro-void nucleation, growth, and coalescence. A model [23] that contains a single spherical void in a perfectly plastic von Mises material was developed by Rice and Tracey (RT). In this model, the void growth rate depends exponentially on the ratio of the mean stress to the von Mises stress. The assumption is that fracture occurs when the ratio between the void size and the void spacing exceeds a critical value. The critical fracture strain ϵ_f^* can be obtained from this model which has been modified and used as a fracture criterion by McClintock [24], Ritchie et al. [25], and McMeeking [26].

In this work, the local stress and strain fields around the corner of a debonded fibre end in a short-carbon-fibre/epoxy composite, obtained using elastic and elasto-plastic FE analyses, are compared. Predictions for the direction of propagation of a Mode γ crack, based on the maximum hoop strain criterion and the RT void-growth criterion, are compared. Using the latter criterion the applied strain at failure for the composite is also predicted. The effects of thermal residual

stresses, developed during the fabrication process, are also investigated.

2. Ductile fracture

Several types of voids may be present in epoxy matrix, depending on the fabrication process employed. Small voids often form in the region adjacent to the fibres, especially in the interfacial area, and also form in the matrix-rich pockets or the fibre-free regions between laminae [27].

In ductile fracture, the local plastic strains play a very important role in determining the mechanism of failure involving micro-void nucleation, growth and coalescence. The development of plastic strains near the fibre end must be taken into consideration. The equivalent or effective plastic strain $\bar{\varepsilon}_p$[28] is given by:

$$\bar{\varepsilon}_{\mathrm{p}} = \int_0^t \sqrt{\frac{2}{9}\left[(\mathrm{d}\varepsilon_1^{\mathrm{p}} - \mathrm{d}\varepsilon_2^{\mathrm{p}})^2 + (\mathrm{d}\varepsilon_2^{\mathrm{p}} - \mathrm{d}\varepsilon_3^{\mathrm{p}})^2 + (\mathrm{d}\varepsilon_3^{\mathrm{p}} - d\varepsilon_1^{\mathrm{p}})^2\right]}\,\mathrm{d}t \tag{1}$$

where $\mathrm{d}\varepsilon_1^{\mathrm{p}}, \mathrm{d}\varepsilon_2^{\mathrm{p}}, \mathrm{d}\varepsilon_3^{\mathrm{p}}$ are the principal components of an increment of plastic strain and $\mathrm{d}t$ is the time increment. If this equivalent plastic strain exceeds the critical fracture strain of the material, the crack will propagate. The growth rate of micro-voids ahead of the crack tip is sensitive to the mean stress in this region. If the mean stress is negative, void closure leads to an increase in the effective fracture strength of the material. Using the approach of Rice and Tracey [23] the critical fracture strain in a triaxial stress field ahead of the crack tip can be expressed as:

$$\varepsilon_{\mathrm{f}}^* = \frac{\ln\left(\frac{d_{\mathrm{p}}}{D_{\mathrm{p}}}\right)}{0.283\exp(1.5\sigma_{\mathrm{m}}/\bar{\sigma})} \tag{2}$$

where d_{p} is the critical void spacing, D_{p} is the critical void size, σ_{m} is the mean stress and $\bar{\sigma}$ is the von Mises stress. The micro-voids ahead of the crack tip within the epoxy matrix nucleate, grow and coalesce due to the high mean stresses induced near the fibre corner (see Fig. 2). The crack propagates when the plastic strain in the ligaments between voids reaches a critical value. In practice, the critical void size and void spacing are difficult parameters to measure and in order to evaluate their ratio, reference is made to the tensile test. If failure occurs in the tensile test, where $\bar{\sigma} = \sigma$ and $\sigma_{\mathrm{m}} = \sigma/3$, when $\epsilon_{\mathrm{f}}^* = \epsilon_{\mathrm{ft}}$ [29] the ratio of the critical void spacing to void size in Eq. (2) is then given by:

$$\ln\left(\frac{d_{\mathrm{p}}}{D_{\mathrm{p}}}\right) = 0.283\varepsilon_{\mathrm{ft}}\exp(0.5) \tag{3}$$

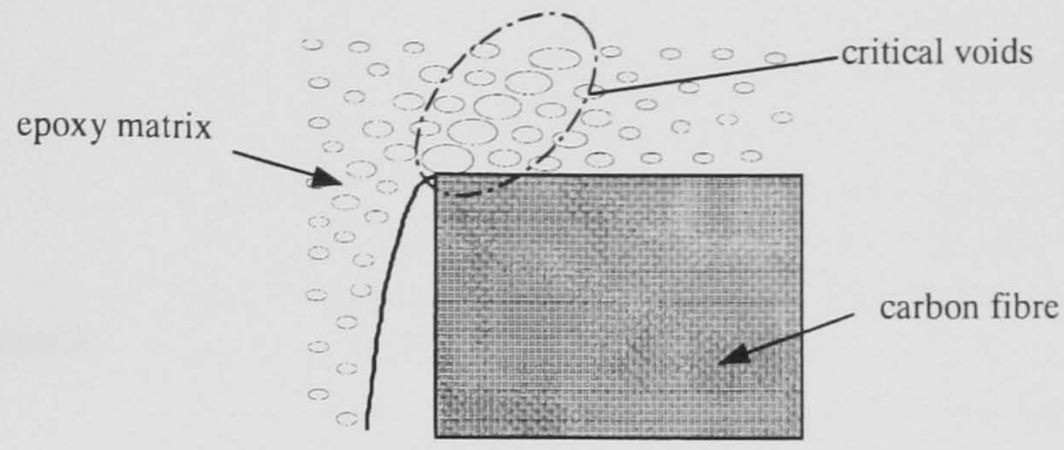

Fig. 2. Micro-void concentration at the crack tip.

Substitution of Eq. (3) into Eq. (2) gives the critical fracture strain as

$$\varepsilon_{\mathrm{f}}^* = \frac{1.648\varepsilon_{\mathrm{ft}}}{\exp(1.5\sigma_{\mathrm{m}}/\bar{\sigma})} \quad \text{provided } \sigma_{\mathrm{m}} > 0 \tag{4}$$

The critical fracture strain in Eq. (4) is valid provided the value of the mean stress is positive. Hence ductile fracture will occur when:

$$\bar{\varepsilon}_{\mathrm{p}} = \varepsilon_{\mathrm{f}}^* \tag{5}$$

where $\bar{\varepsilon}_{\mathrm{p}}$ is the equivalent plastic strain which is obtained from Eq. (1) and $\varepsilon_{\mathrm{f}}^*$ is the critical plastic strain obtained from Eq. (4). In order to define the scale of the damage, the critical radius in the FE mesh has to be specified and needs to be very small compared to the crack length [24,25]. Fracture is then predicted to occur when the value of the equivalent plastic strain ahead of the crack tip reaches the value of the critical plastic strain at the same point. This criterion has been employed by Ritchie et al. [25], Harlin et al. [30] and Hanxing et al. [31].

3. FE model

A FE study of the conical-shaped matrix crack in a model carbon fibre/epoxy composite system was performed by Nath et al. [1]. Linear-elastic FE analysis with a pre-defined matrix crack propagation path was used and the results obtained for the fibre stress were correlated with experimental measurements obtained by Paipetis et al. [2,3]. The angle of the conical crack in the FE model which gave the best correlation between the predicted and experimentally measured fibre stresses was found to be $\theta_{\mathrm{c}} = 20°$.

In the current work, a penny-shaped crack resulting from fibre-end debonding is assumed to exist. Contact elements were defined between the fibre-end face and the matrix to enable load transfer to occur across the crack faces during crack closure. In the FE model, the outer matrix radius R_{m}, matrix length l_{m}, fibre radius R_{f} and the fibre length l_{f} are 50, 300, 3.25 and 260μm, respectively (see Fig. 3) and the mesh consists of 3865 axisymmetric eight-node elements [see Fig. 4(a)]. A

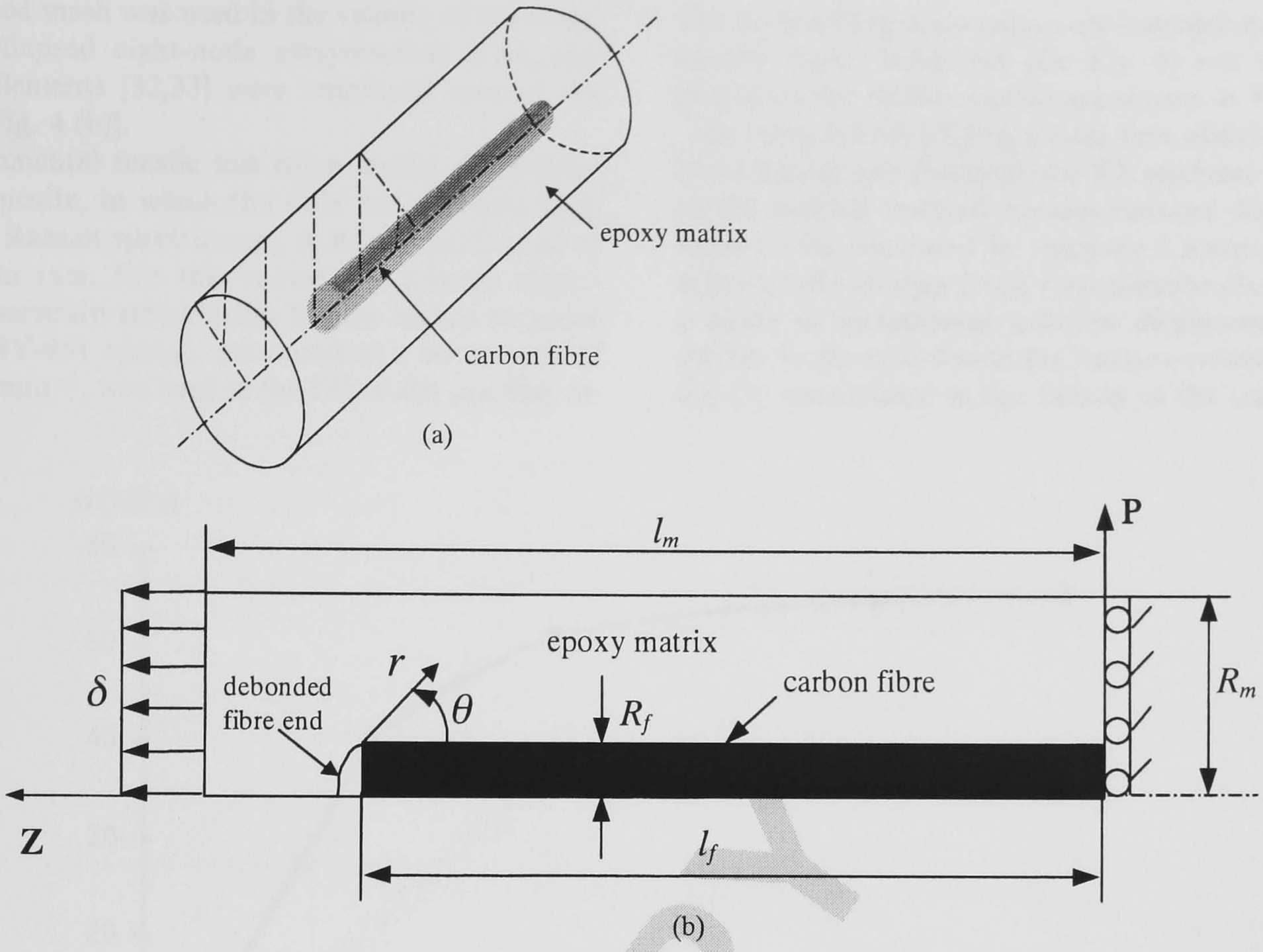

Fig. 3. (a) Carbon-fibre/epoxy composite specimen; (b) axisymmetric FE model.

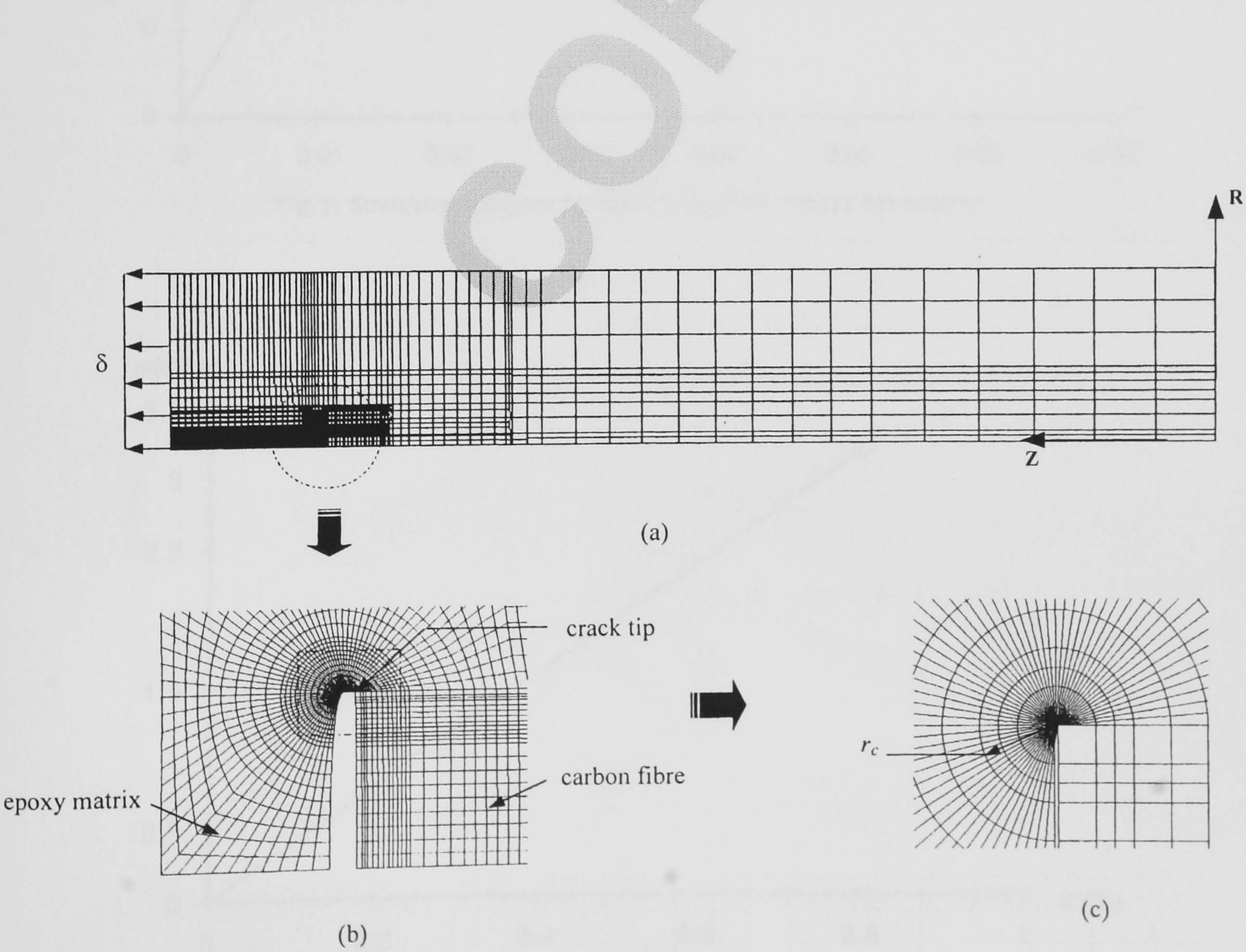

Fig. 4. (a) Axisymmetric FE mesh; (b) detail of FE mesh around the fibre end; (c) detail of a critical radius, r_c.

highly refined mesh was used in the vicinity of the crack tip and collapsed eight-node axisymmetric triangular crack tip elements [32,33] were employed around the crack tip [Fig. 4 (b)].

The incremental tensile test for a model short-fibre/epoxy composite, in which the fibre stress is measured using laser Raman spectroscopy (LRS), is performed at a low strain rate. For this reason the relaxed elasto-plastic stress/strain relationship for the matrix material (MY-750/HY-951 epoxy), measured at a strain rate of 0.25×10^{-2} min^{-1}, was used in the FE model (see Fig. 5). The carbon fibre is a transversely isotropic material with linearly elastic behaviour (see Fig. 6) and the material properties for both materials are shown in Table 1.

By using ABAQUS [33] results were obtained for both linear elastic and elasto-plastic FE analyses. The effects of the thermal residual stresses induced during manufacture were simulated by applying a temperature drop in the initial load step. In the case of elasto-plastic analysis, a series of incremental uniform displacements δ was applied to the model until the fracture criterion given by Eq. (5) was satisfied in the vicinity of the crack tip.

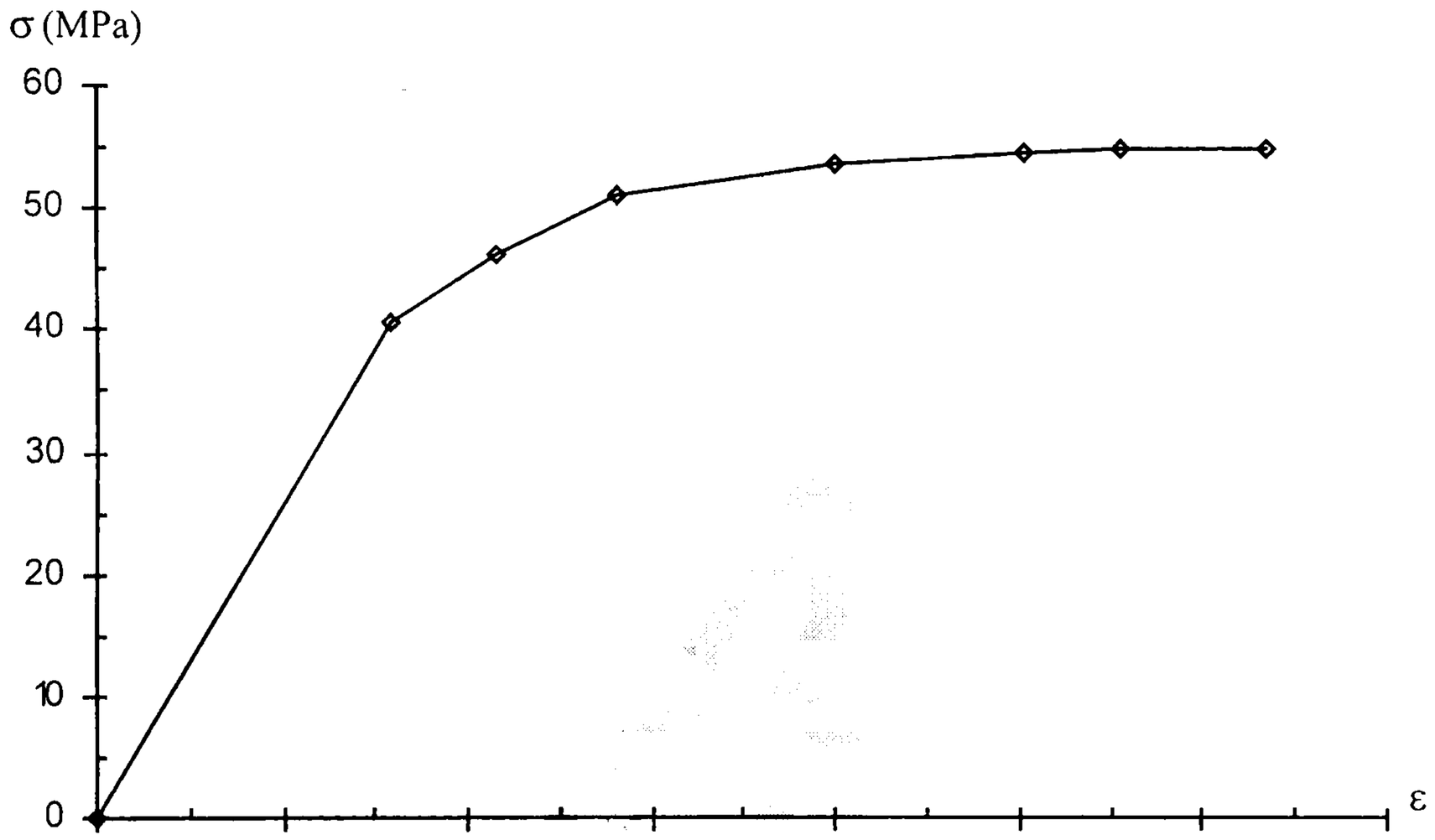

Fig. 5. Stress/strain diagram for epoxy matrix MY-750/HY-951 at 20°C.

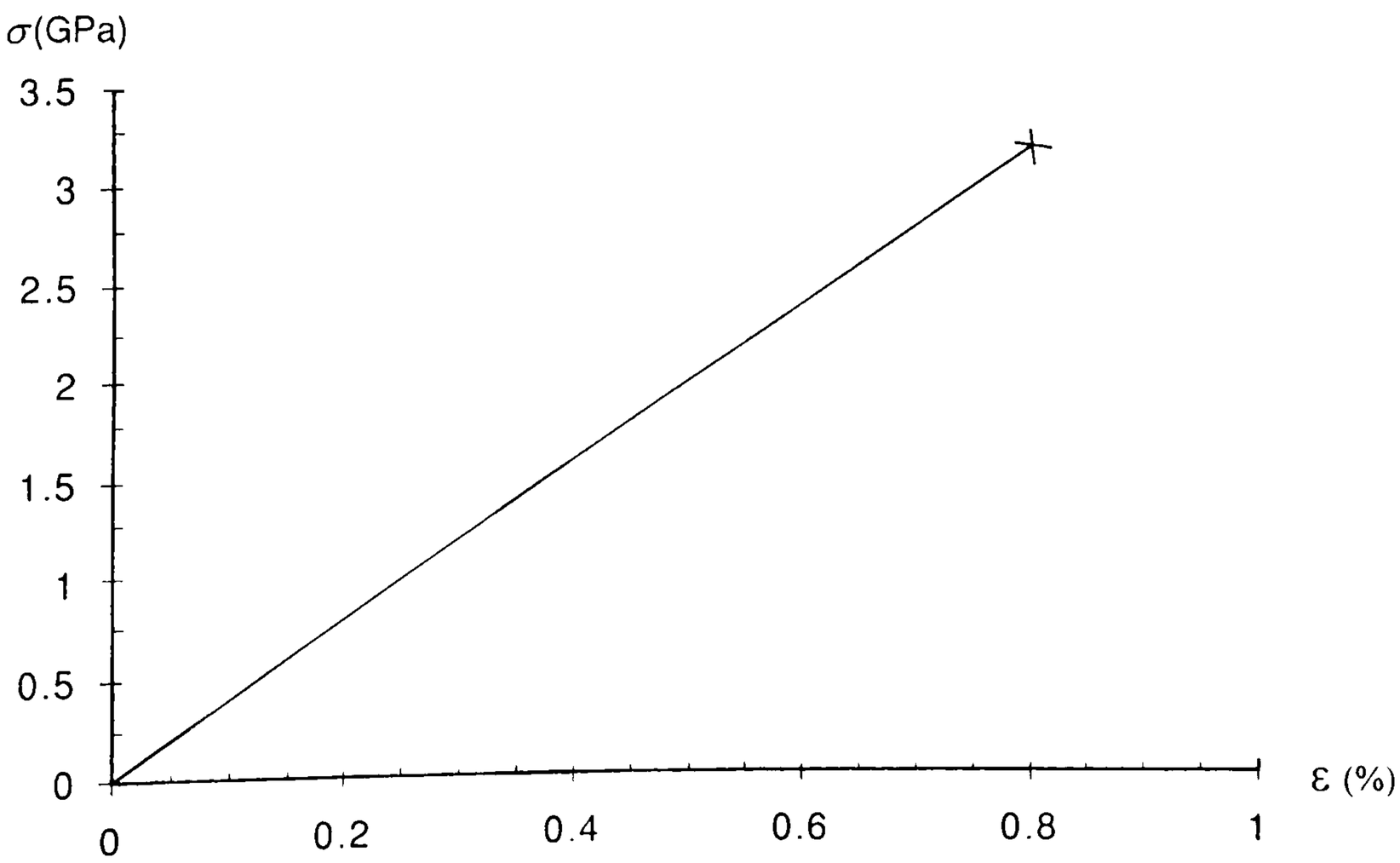

Fig. 6. Stress strain diagram for carbon fibre.

4. Results and discussion

4.1. No thermal residual stresses

The stress and strain components in the FE model, obtained in terms of a global cylindrical co-ordinate system, were converted to components for a local polar co-ordinate system (r,θ) which has its origin at the debonded fibre end crack tip (see Fig. 3). In order to evaluate the critical crack-propagation conditions, a critical radius from the crack tip, r_c, equal to 0.2 μm was chosen which is about 32 times smaller than the crack length. The critical radius corresponds to the third ring of nodes around the crack tip thereby avoiding the inaccuracies associated with the collapsed crack-tip elements within the first ring [see Fig. 4(c)]. The angular variation of the stress and strain components at a critical radius $r_c = 0.2$ μm for an applied strain of 0.14%, obtained using linear elastic FE analysis, are shown in Figs. 7 and 8, respectively. The corresponding results obtained using elasto-plastic FE analysis are shown in Figs. 9 and 10.

By comparing the stress results in Figs. 7 and 9 it can be seen that for the elasto-plastic results the shear stress $\sigma_{r\theta}$ in the plastic zone near the interface is reduced to about half the value obtained from linear-elastic analysis. The radial stress σ_{rr} increases from a negative to positive value and has a maximum value at about $\theta = 140°$ which is only about half the maximum value obtained using linear-elastic analysis. The hoop stress $\sigma_{\theta\theta}$, which is likely to play an important role in opening the crack, has its maximum value at about $\theta = 77°$ for both analyses. The maximum hoop stress predicted using elasto-plastic analysis is somewhat lower than the value obtained using linear-elastic analysis as a result of the plastic behaviour of the matrix. The shear strain $\epsilon_{r\theta}$ near the interface obtained using elasto-plastic analysis (see Fig. 10) is about 6 times greater than the value obtained using linear-elastic analysis (see Fig. 8). The other strain components are also higher and have their

Table 1
Material properties of carbon fibre and epoxy matrix

Material properties	Carbon fibre	Matrix MY-750/HY-951 (relaxed properties)
Axial tensile modulus (GPa)	392	2.6
Transverse modulus (GPa)	20	2.6
Axial tensile strength (GPa)	3.2 (fracture)	41×10^{-3} (yield)
Axial fracture strain (%)	0.8	6.13
Transverse Poisson's ratio $\nu_{R\theta}$	0.27	0.34
Poisson's ratio in R–Z direction, ν_{RZ}	0.03	0.34
Axial coefficient of thermal expansion (K^{-1})	-25×10^{-6}	58×10^{-6}
Transverse coefficient of thermal expansion (K^{-1})	25×10^{-6}	58×10^{-6}

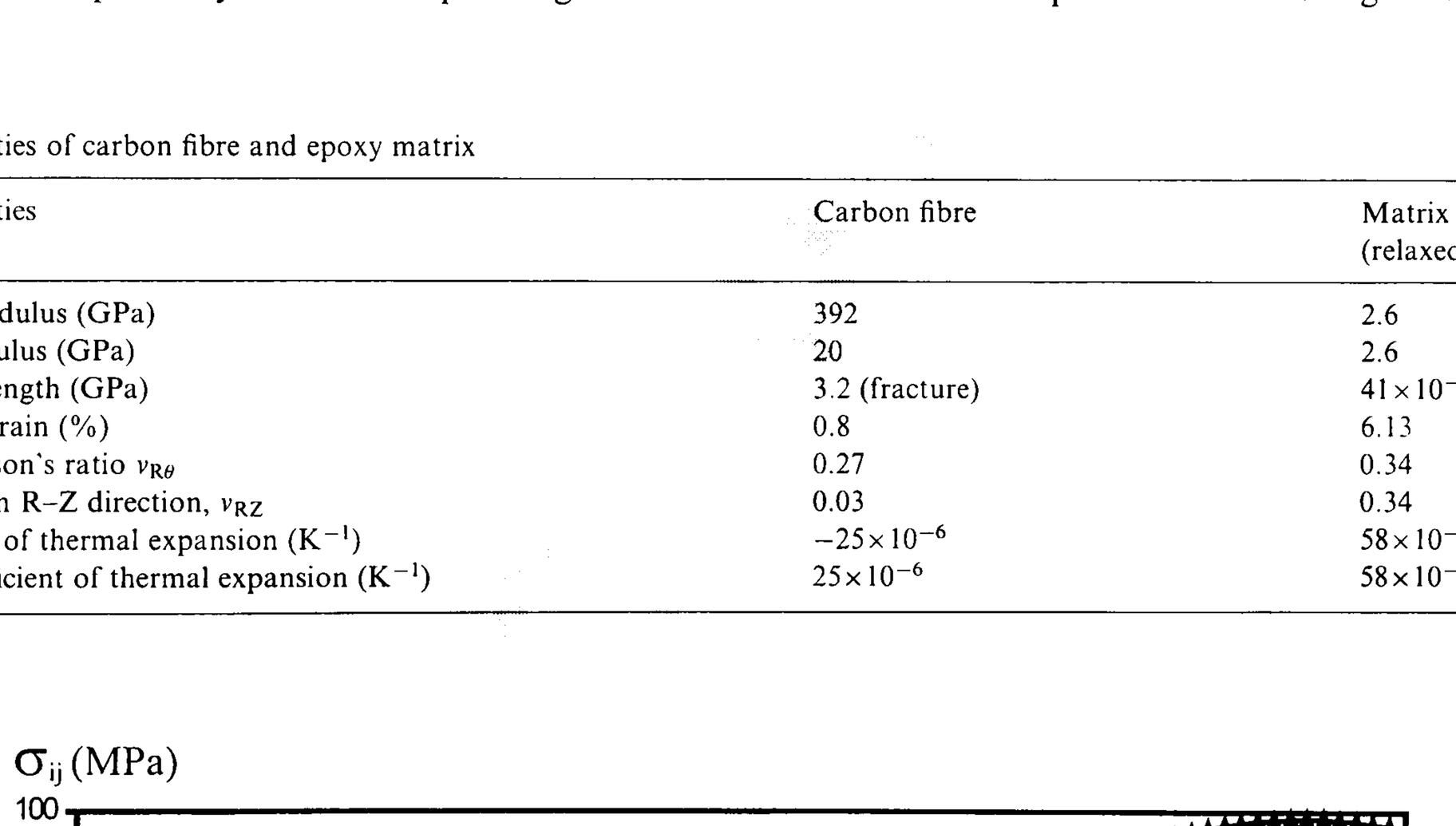

Fig. 7. Angular variation of stresses, obtained from linear-elastic FE analysis, $\epsilon_{appl.} = 0.14\%$.

turning points at about $\theta = 20°$, which is about half the angle calculated using linear-elastic analysis. To determine the mode of fracture, the elasto-plastic results were compared with the experimental results [3]. The interfacial shear strain obtained from linear-elastic FE analysis is about 2 times higher than the value calculated using elasto-plastic FE analysis (see Figs. 7 and 9). The crack may therefore prefer to propagate into the matrix rather than along the fibre/matrix interface for a sized system.

The maximum hoop-stress criterion predicts a crack angle which is much higher than that suggested by Nath et al. [1] and is, in any case, inappropriate for ductile fracture. The maximum hoop-strain criterion predicts a crack angle of about 23°.

To use the RT void-growth model to predict fracture, the envelope of the critical fracture strain can be obtained from Eq. (4) by computing the local values at every nodal point at the critical radius. The curve representing the angular variation of the equivalent plastic strain is then compared with the curve for the angular variation of the critical fracture strains for every incremental load case. The failure criterion is satisfied when the two curves just touch, as shown in Fig. 11. It

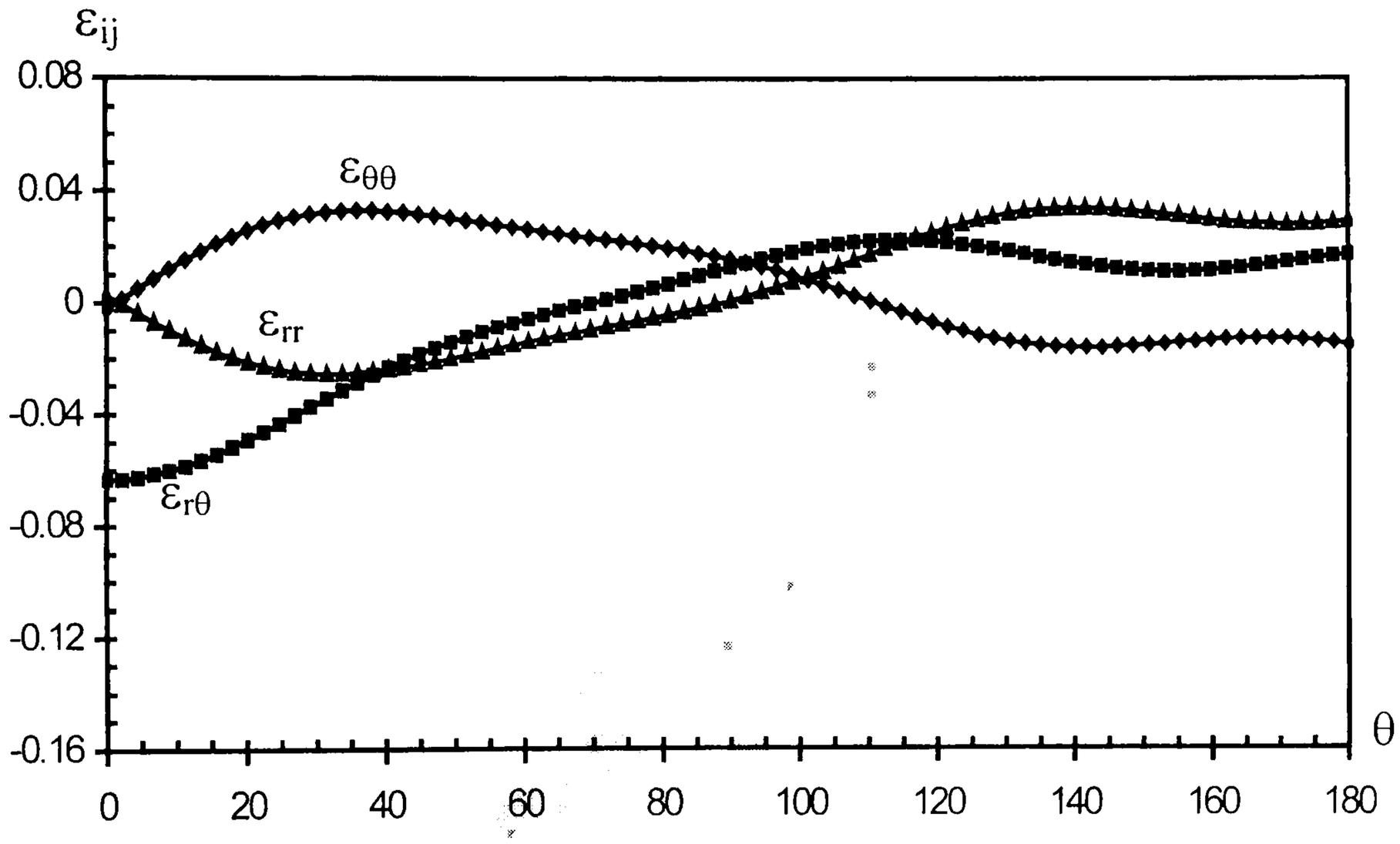

Fig. 8. Angular variation of strains, obtained from linear-elastic FE analysis, $\epsilon_{appl.} = 0.14\%$.

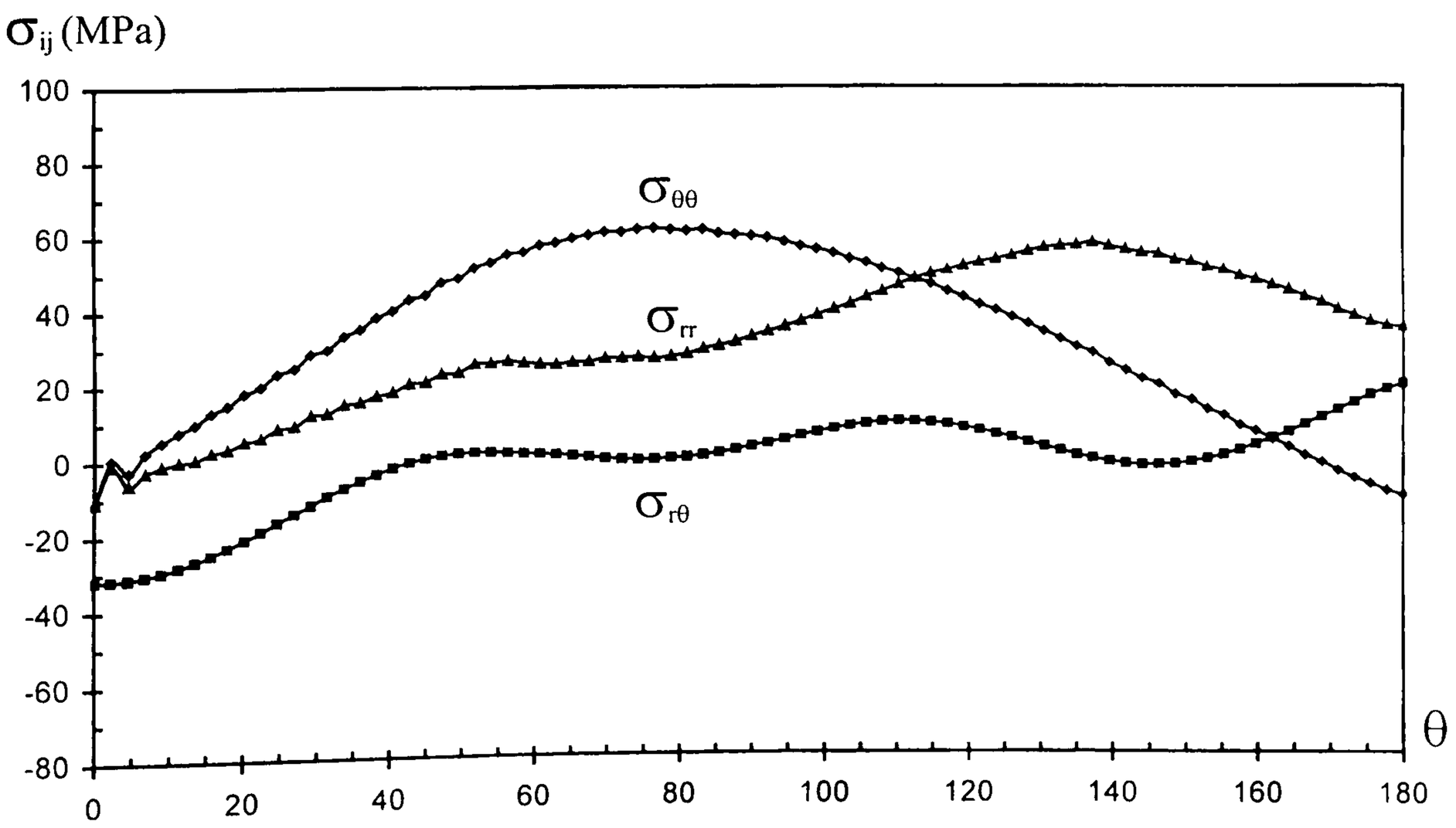

Fig. 9. Angular variation of stresses, obtained from elasto-plastic FE analysis, $\epsilon_{appl.} = 0.14\%$.

was found that the critical crack propagation conditions were satisfied at $\theta = 16°$, on the critical radius $r_c = 0.2$ μm, when the applied strain on the composite reaches 0.14%. The matrix crack angles predicted by the maximum hoop-strain criterion are slightly higher than the RT void-growth model but only the latter is capable of predicting the applied strain at failure.

4.2. Effect of thermal residual stress

Fabrication of the composite specimen induces thermal residual stresses. During fabrication, the matrix is initially a viscous fluid, which subsequently cools and crystallises. As a consequence of the coefficient of thermal expansion mismatch between the fibre and matrix materials, the larger contraction of the matrix puts the fibre into compression and also induces localised yielding at the fibre end [35]. In the elasto-plastic FE model used to investigate the effect of thermal stresses, it is assumed that the fibre end is initially bonded. A series of uniform temperature drops ΔT in the range 30–50°C (see Fig. 12) are applied to the FE models in order to obtain the values of the maximum residual fibre stress to compare with the experimental results [2,3]. The

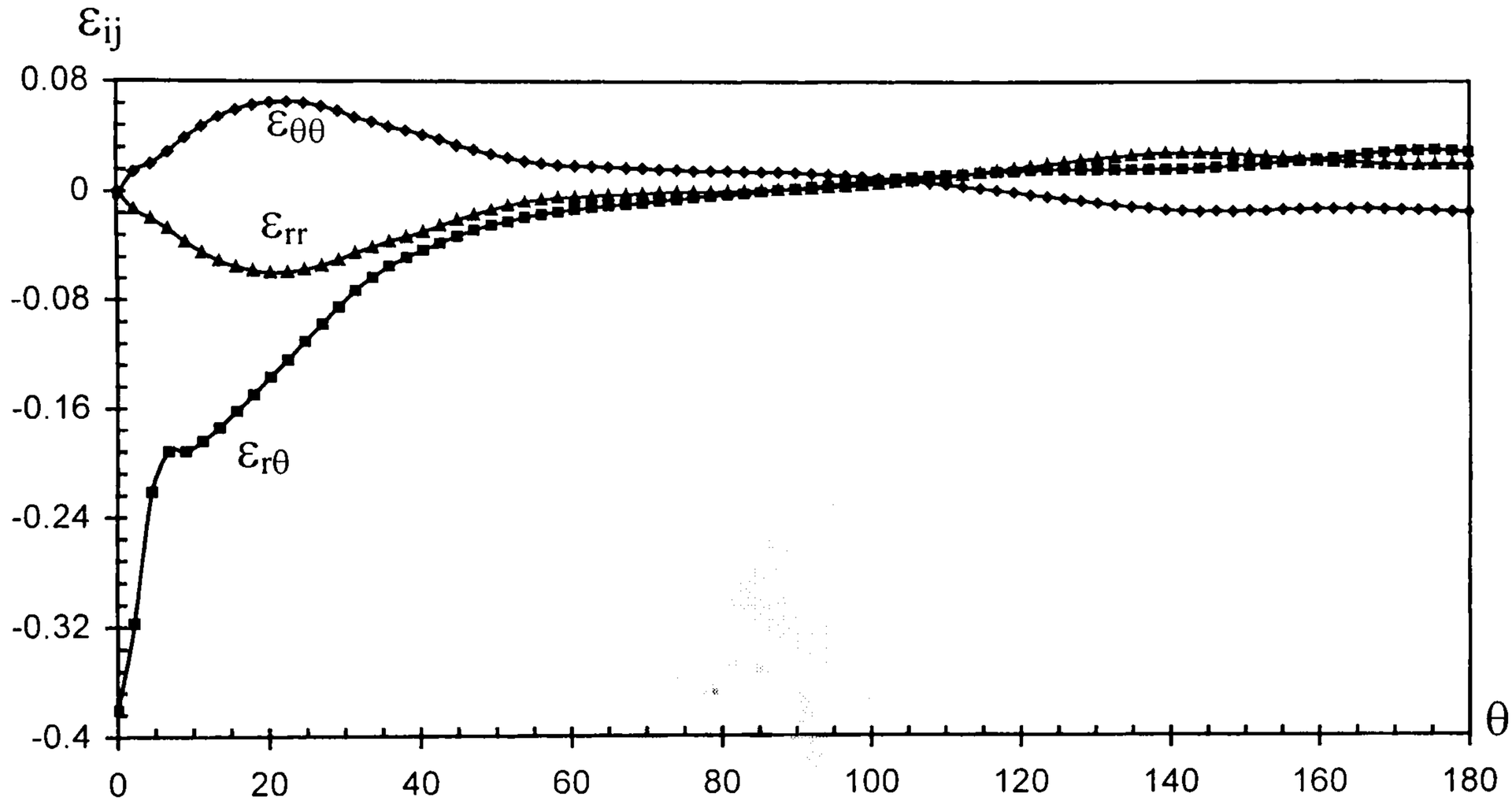

Fig. 10. Angular variation of strains, obtained from elasto-plastic FE analysis, $\epsilon_{appl.} = 0.14\%$.

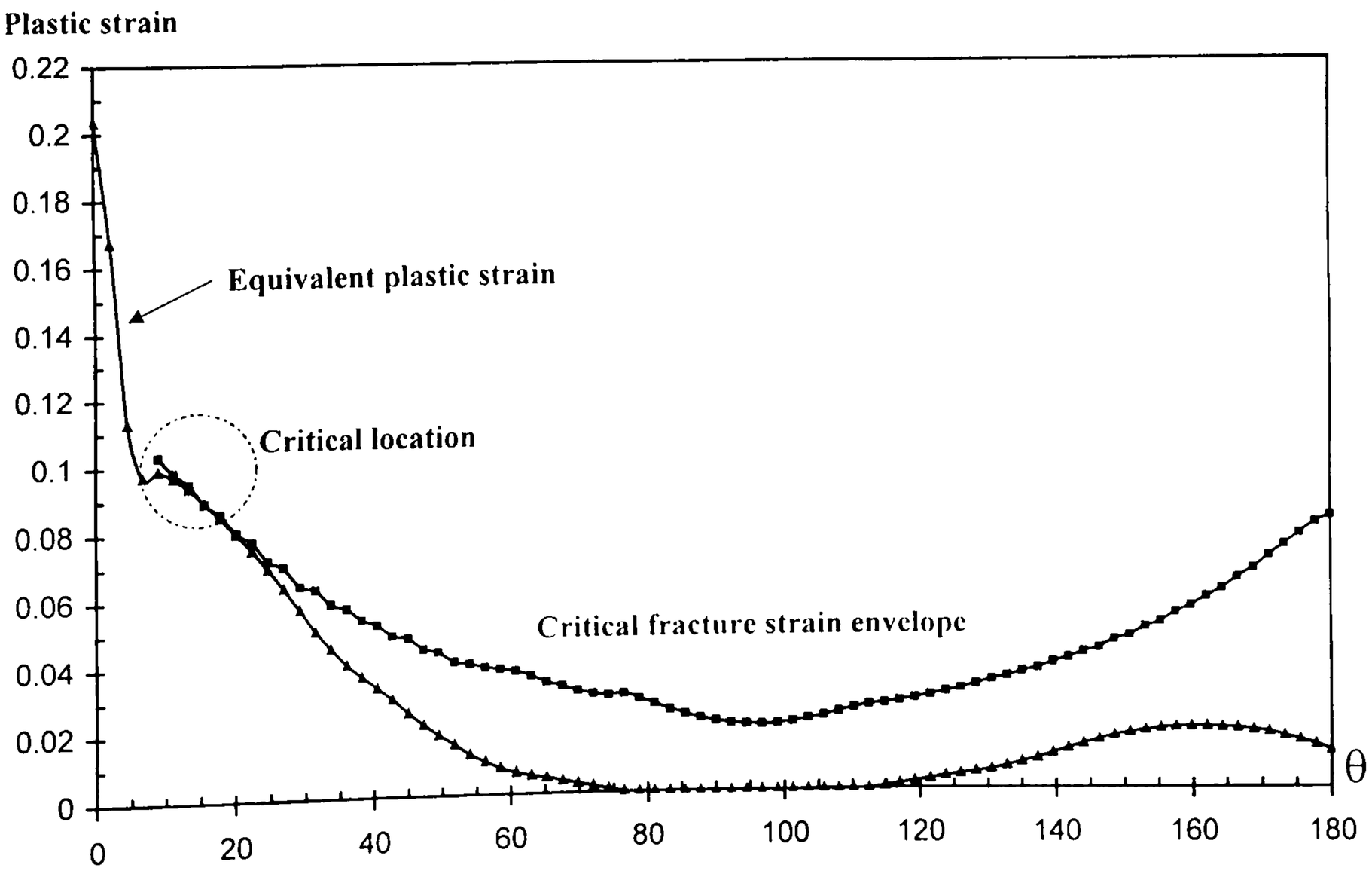

Fig. 11. Crack initiation condition ar $r_{c=0.2}$ μm with $\epsilon_{appl.} = 0.14\%$.

maximum residual fibre stress obtained for a 50°C temperature drop is predicted to be −0.78 MPa which agrees well with the experimentally measured value −0.75 MPa [2,3]. The angular variation of thermal stress and strain components around the fibre corner for $\Delta T = -50$°C are shown in Figs. 13 and 14, respectively. At this stage, the hoop stress $\sigma_{\theta\theta}$ is negative as a result of the contraction of the matrix around the stiffer fibre.

In reality, there is some relieving of the residual stresses in the matrix material during cooling [35]. The hoop strain $\epsilon_{\theta\theta}$ at the fibre corner near the interface is negative and could not lead to crack initiation in the matrix since the micro-voids would be closed. In uniaxial compression, the matrix material exhibits a higher ductility than in tension.

4.3. Combined effect of thermal and mechanical loading

The thermal residual stresses and strains as a consequence of fabrication are believed to affect the overall strength of the composite. As the matrix cools during fabrication of the composite it contracts around the

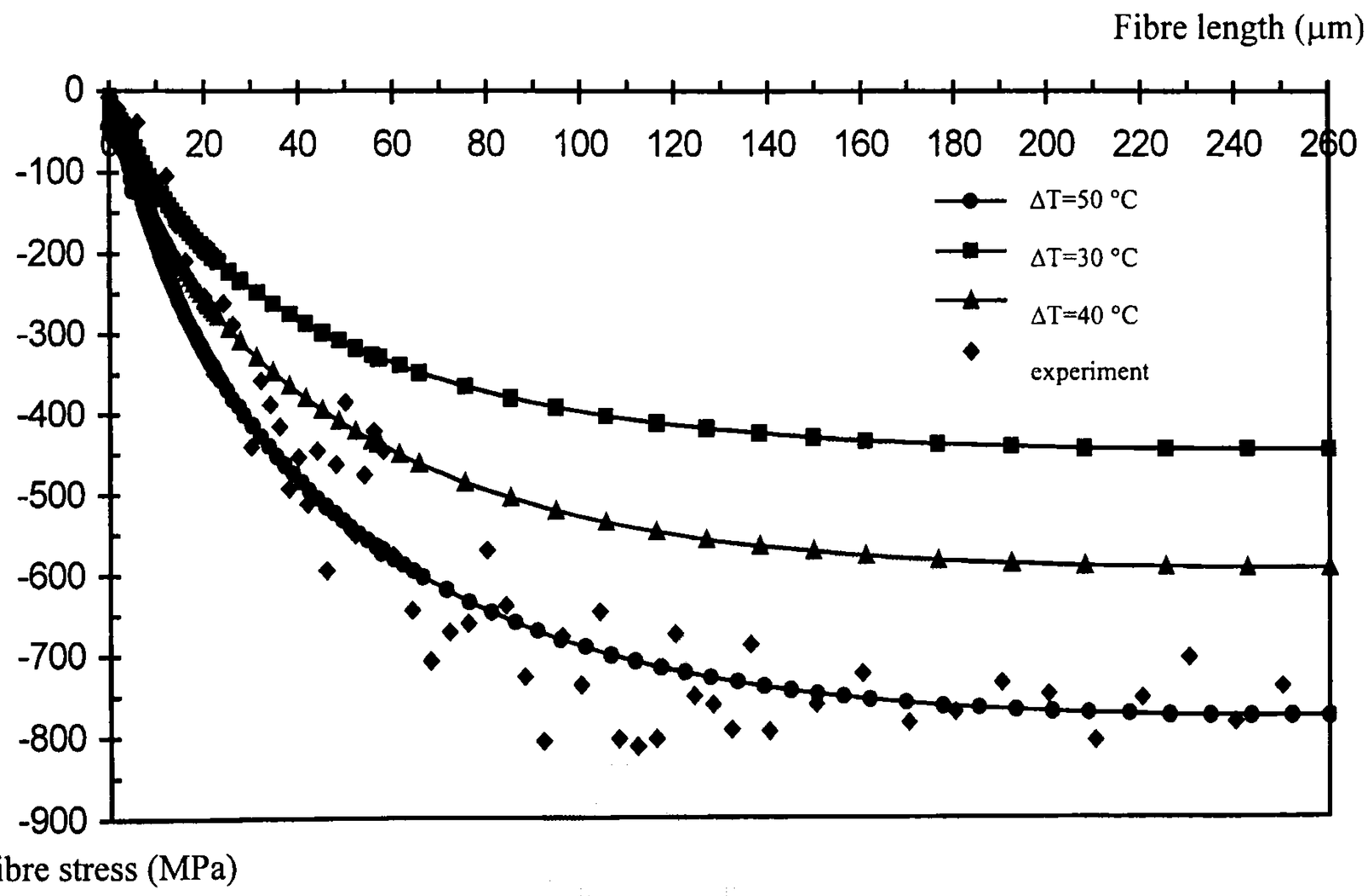

Fig. 12. Axial variation of fibres stress for elasto-plastic analysis with various of temperatures drops ΔT.

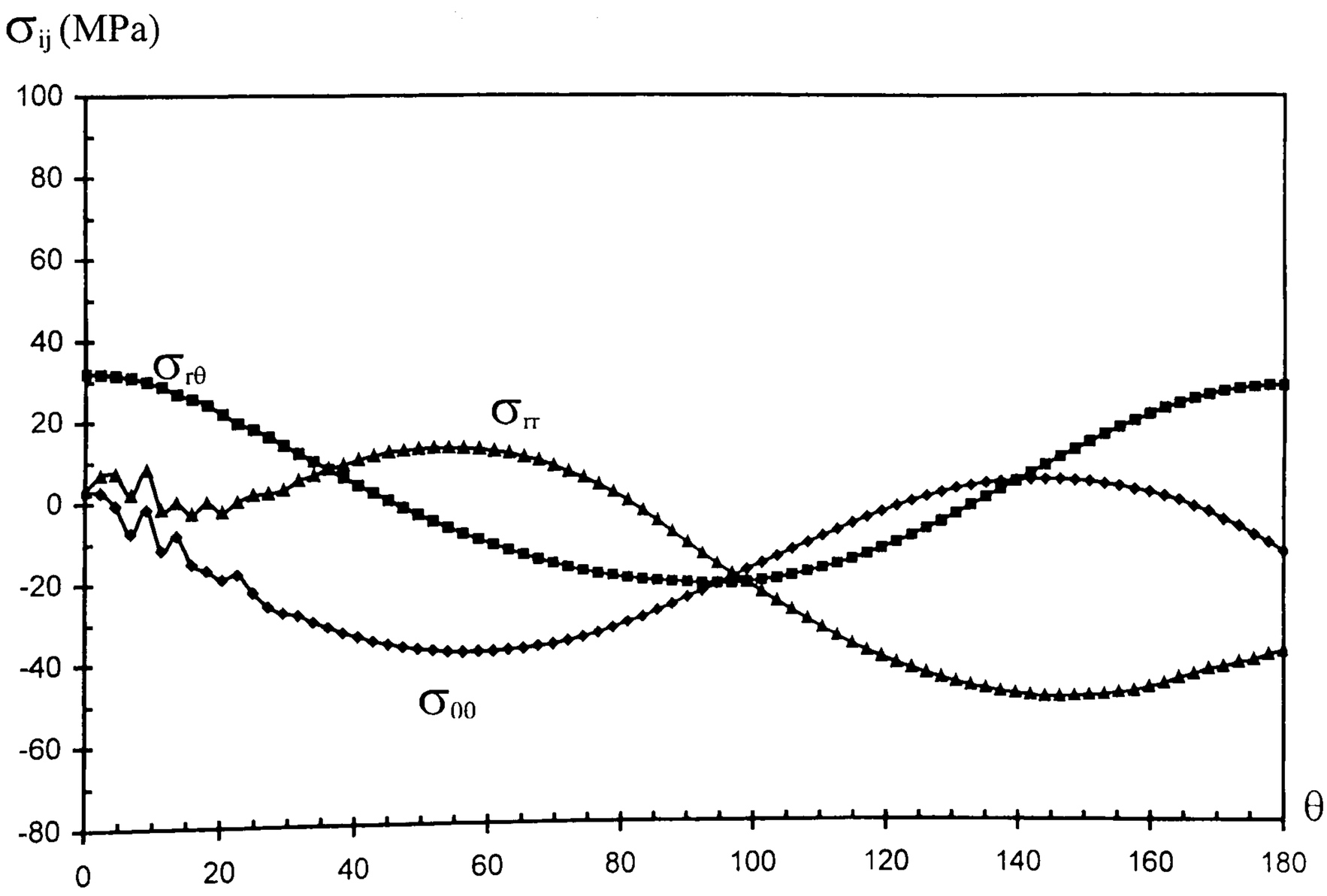

Fig. 13. Angular variation of stresses under thermal load, obtained from elasto-plastic under thermal load, $\Delta T = 50$ C.

fibre end, leading to compression in this region. The initial condition is now that the mean stress in the matrix in this region is compressive. When a uniform displacement is subsequently applied to the composite the mean stress becomes tensile. The angular variation of stress and strain around the fibre end corner are shown in Figs. 15 and 16, respectively. At an applied strain of 0.3%, a maximum fibre stress of 300 MPa was found to occur at the midpoint of the fibre and a maximum interfacial shear stress of about 22 MPa was found to occur at the fibre end. These values agree well with experimental results [2,3].

The maximum hoop strain criterion predicts the angle of the crack propagation to be about 18°. The equivalent plastic strain calculated by ABAQUS is now accumulating from a state of compression. The RT void-growth

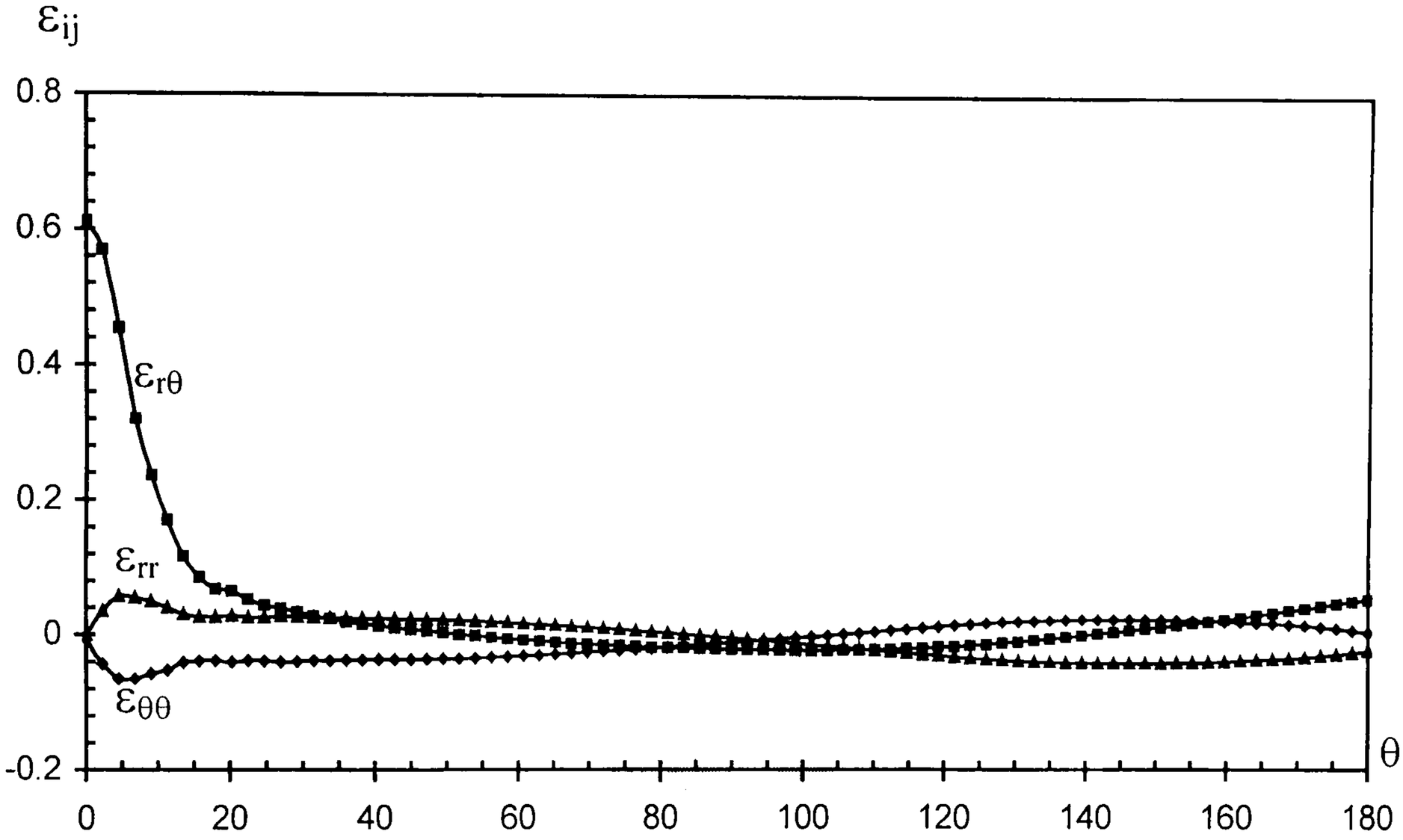

Fig. 14. Angular variation of strains obtained from elasto-plastic analysis under thermal load for $\Delta T = 50$ C.

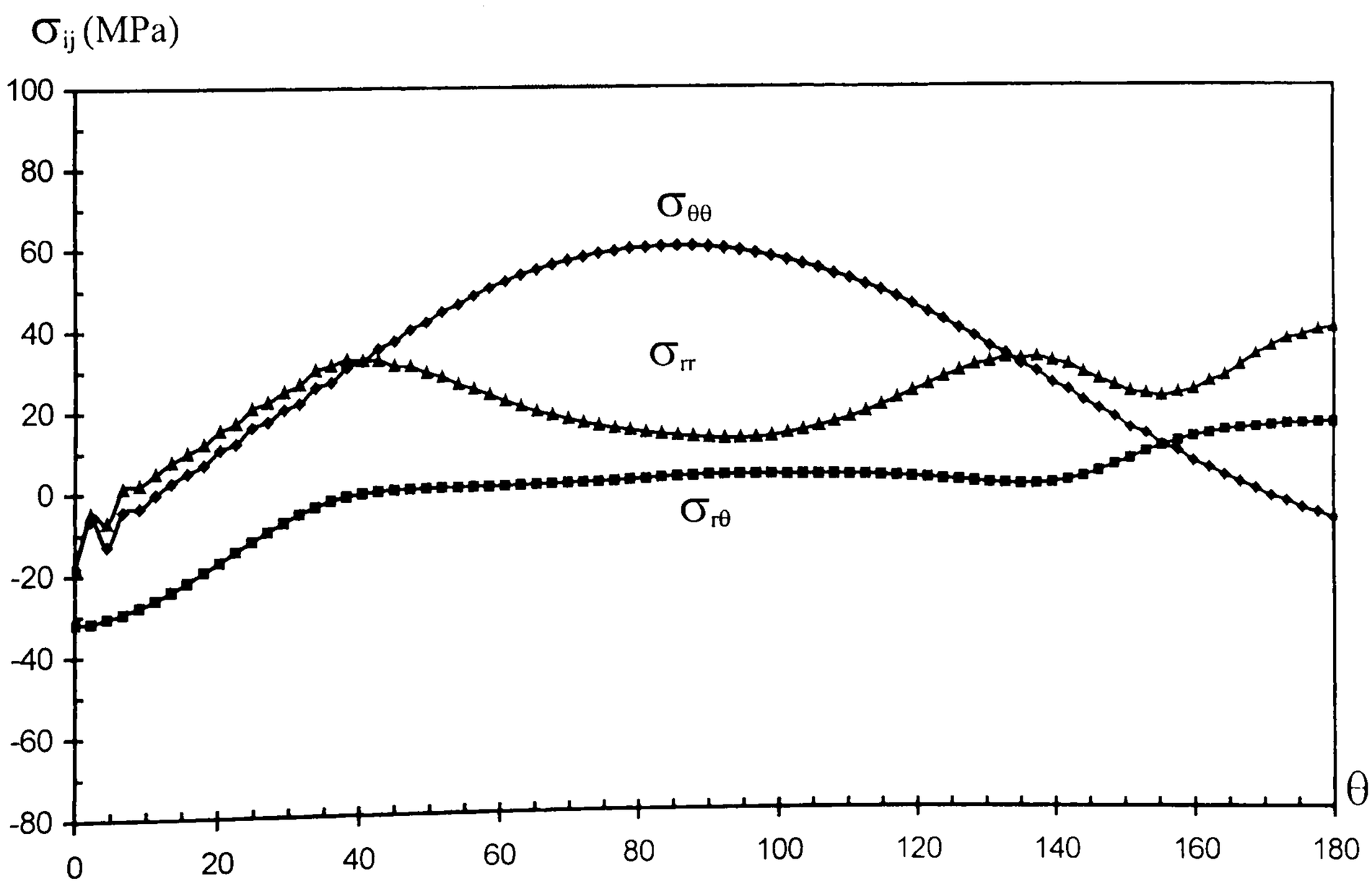

Fig. 15. Angular variation of stresses under thermal and mechanical load, obtained from elasto-plastic FE analysis, for $\varepsilon_{appl.} = 0.3\%$.

model, which is based an increasing void size and a decreasing void spacing, does not take the compressive plastic strains into account. The equivalent plastic-strain magnitude, which is a current positive measure of equivalent plastic strain, was used to determine failure in the matrix material. The definition of the plastic-strain magnitude is a scalar product of the two plastic strain tensors ϵ_{pl} [34]. It was found that the critical crack-propagation conditions were satisfied at $\theta = 16^{\circ}$, when the applied strain on the composite reached 0.3% (see Fig. 17).

The axially elongated shape of the plastic zone for the critical condition is shown in Fig. 18. When the applied strain was increased beyond 0.3% the plastic zone was

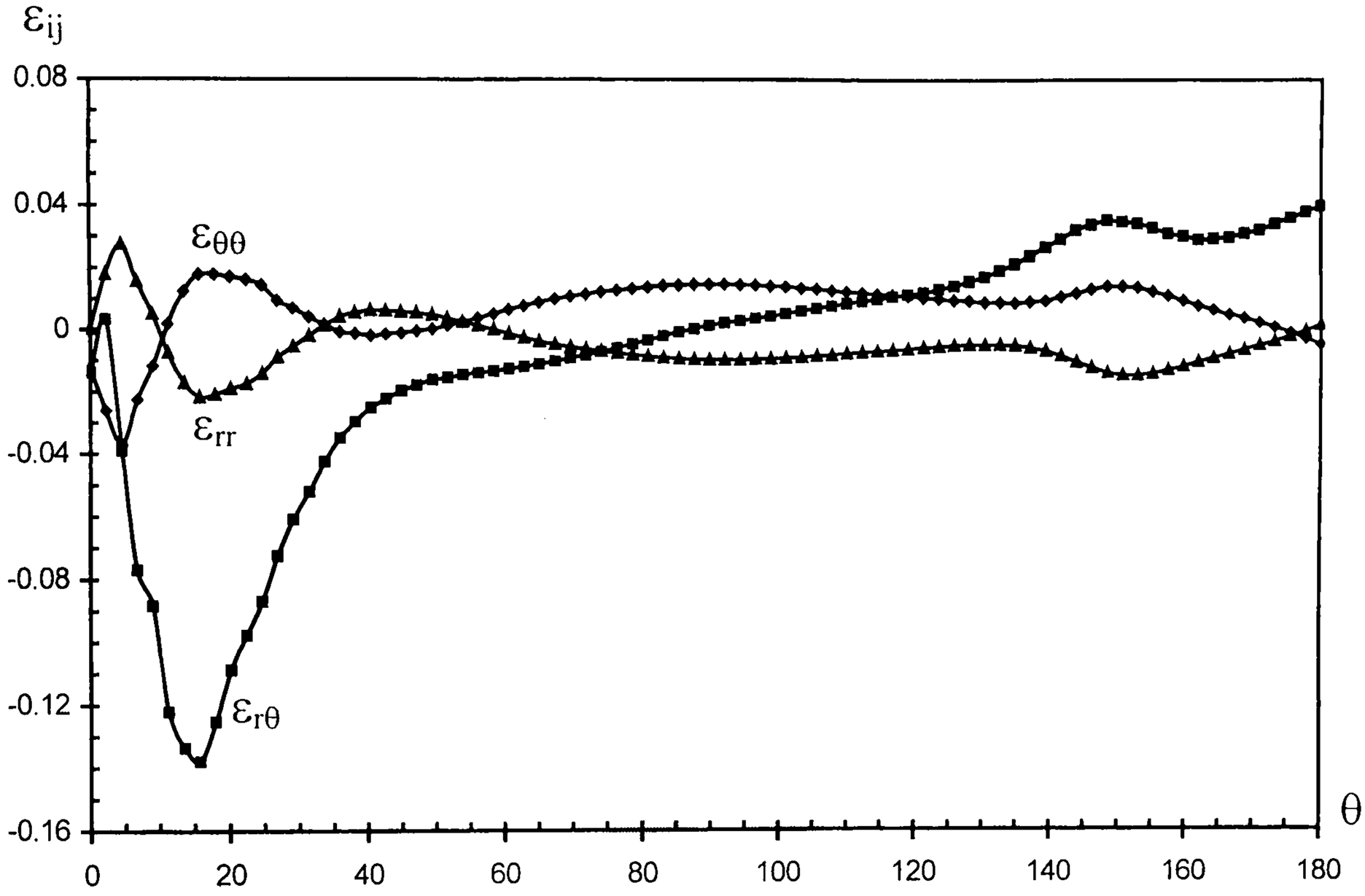

Fig. 16. Angular variation of strains under thermal and mechanical load, obtained from elasto-plastic FE analysis, for $\epsilon_{appl.} = 0.3\%$.

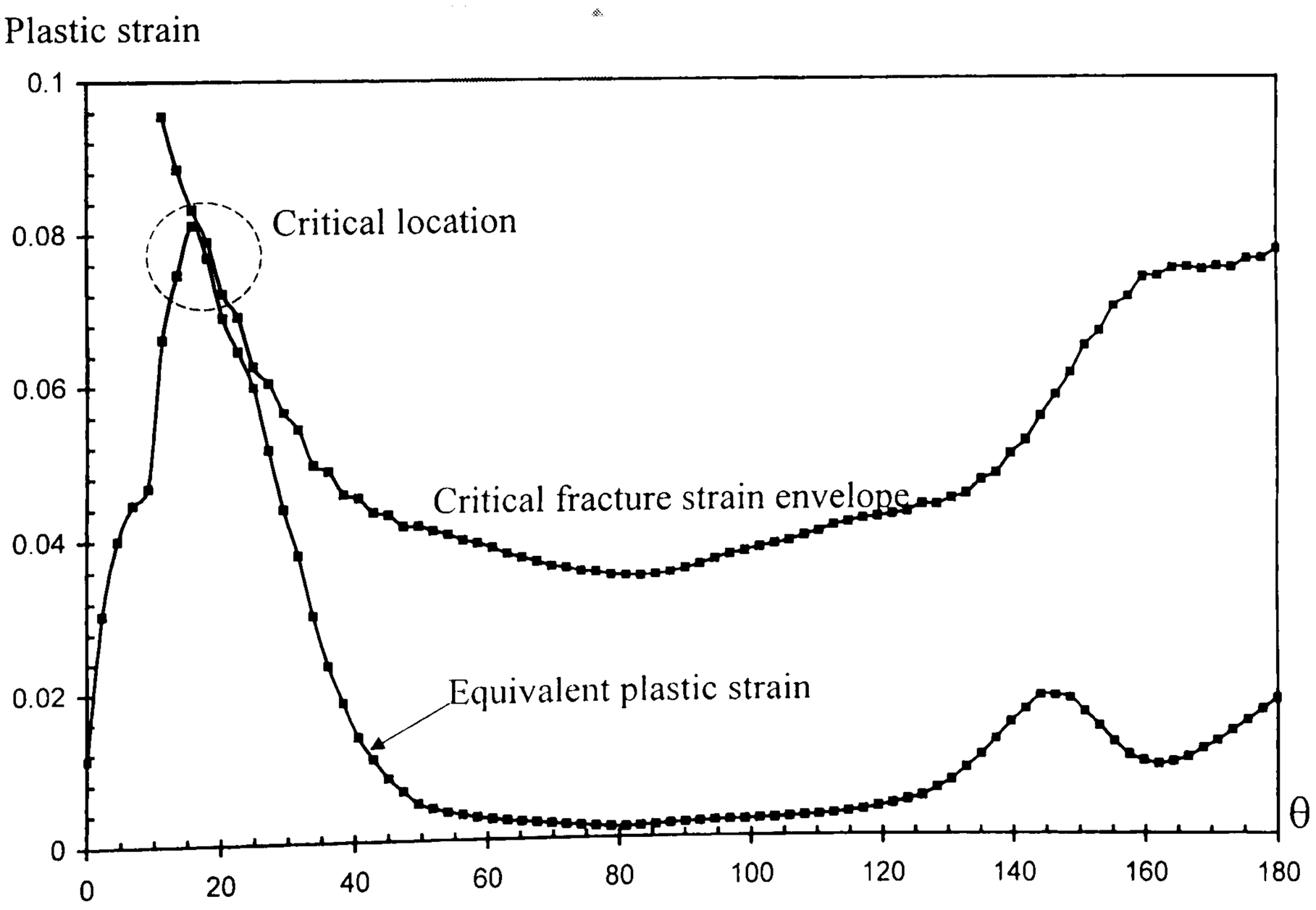

Fig. 17. Crack-initiation condition at $r_c = 0.2$ μm under thermal and mechanical loading with $\epsilon_{appl.} = 0.3\%$.

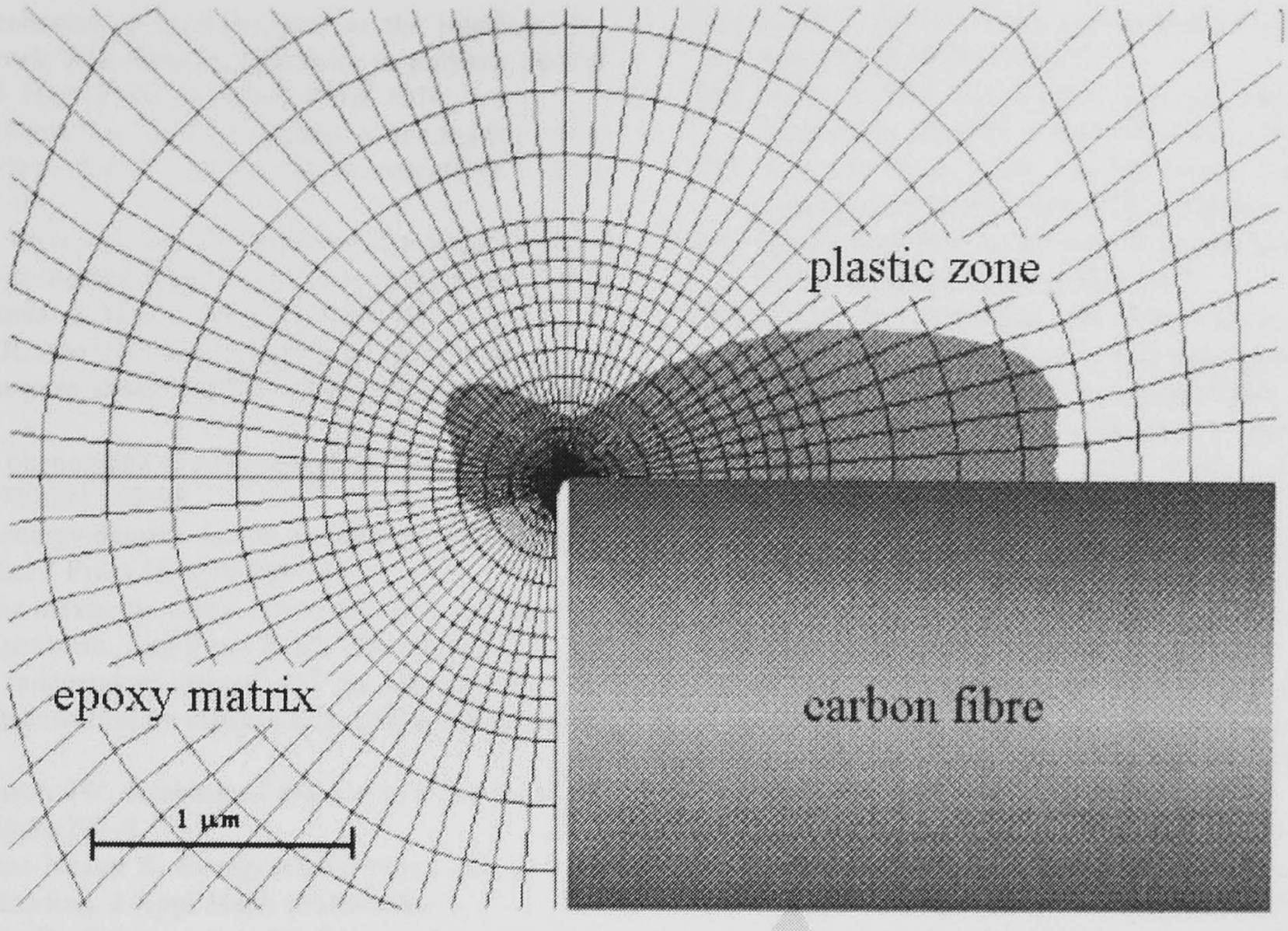

Fig. 18. Extent of plastic zone for combined thermal and mechanical loading, $\epsilon_{appl.} = 0.3\%$.

observed to grow further in the axial direction with little change in the radial direction.

5. Conclusions

Fracture criteria have been employed to predict the matrix crack angle using the results obtained from FE analysis. The maximum hoop-stress criterion did not give a realistic result and is not appropriate for ductile fracture. The maximum hoop strain criterion, applied to the results obtained using elasto-plastic FE analysis, predicts a crack angle close to that predicted using the RT micro-void growth model but is incapable of predicting the applied strain on the composite at failure.

The fracture criterion that seems to be most appropriate for this type of system is the RT micro-void growth model which takes account of the effects of void nucleation, growth, and coalescence. Although at the macroscopic level the effect of voids can be ignored, ignoring this effect at the micro-mechanical level results in erroneous predictions of composite strength. Crack propagation conditions at a critical radius are satisfied when the curve for the variation of the equivalent plastic strain around the crack tip touches the critical fracture-strain envelope. The applied failure strain obtained by experiment is a little higher than the applied failure strain calculated by the RT void-growth model, probably probably a result of the assumption of fibre end debonding in the FE model.

Thermal residual stresses and strains have a very strong influence on the failure mechanism at the fibre/matrix interface and on the critical applied strain. The presence of a strong interphase will prevent the interface from debonding. The inclusion of thermal residual stresses causes the location of the maximum equivalent plastic strain adjacent to the fibre/matrix interface to change from 0 to 16°, and as a result of shear strain reversal [36] the applied strain on the composite at failure is predicted to increase from 0.14 to 0.3%.

Acknowledgements

The first author would like to thank Dr. N.P. O'Dowd for useful discussions and suggestions during the course of this work.

References

[1] Nath RB, Fenner DN, Galiotis C. Finite element modelling of interfacial failure in model carbon fibre-epoxy composites. J Mat Sci 1996;31:2879–83.
[2] Paipetis A, Galiotis C. A study of the stress-transfer characteristics in model composites as a function of material processing, fibre sizing and temperature of the environment. Comp Sci Tech 1997;57:827–38.
[3] Paipetis A, Galiotis C. Effect of fibre sizing on the stress transfer efficiency in carbon/epoxy model composites. Composites Part A 1996;27A:755–67.
[4] Sancaktar E. Nonlinear viscoelastic behaviour of the fibre–matrix interface, theory and experiment. Proc Euromech Colloquium 269, St. Etienne, France, 1991.
[5] Mullin JV, Berry JM, Gatti A. Some fundamental fracture mechanisms applicable to advanced filament reinforced composites. J Comp Mat 1968;2:82–103.

[6] Chamis CC. Mechanics of load transfer at the interface. In: Broutman IJ, Crock RH, editors. Interfaces in polymer matrix composites, vol 6. New York: Academic Press, 1974.
[7] Selvadurai APS, Busschen Aten. Mechanics of the segmentation of an embedded fiber, Part I: experimental investigations. J Appl Mech 1995;62:87–97.
[8] Selvadurai APS, Busschen Aten. Mechanics of a fragmentation test involving an embedded fiber, Part II: computational modeling and comparisons.. J Appl Mech 1995;62:98–107.
[9] Erdogan F, Sih GC. On the crack extension in plates under plane loading and transverse shear. ASME J Basic Eng 1963;85:519–25.
[10] Griffith AA. The phenomena of rupture and flow in solids. Philos Trans Series A 1920;221:163–98.
[11] Sih GC. Strain-energy-density factor applied to mixed mode crack problems. Int J Fract 1974;10:305–21.
[12] Chang KJ. On the maximum strain criterion-a new approach to the angled crack problem. Eng Fract Mech 1981;14:107–24.
[13] Rice JR. A path independent integral and the approximate analysis of strain concentration by notches and cracks. J Appl Mech 1968;35:379–86.
[14] He MY, Hutchinson JW. Kinking of crack out of an interface. J Appl Mech 1989;56:270–8.
[15] Hayashi K, Nemat-Nasser S, Energy-release rate crack kinking under combined loading. J Appl Mech 1981;48:520–4.
[16] Liebowitz H, Lee D, Subramonian N. Criteria for predicting crack entension angle and path in plane crack problems. In: Proc Inter Conf Analytical and Experimental Fracture Mechanics, Mirabile, Italy; 1981.
[17] Murakami Y. Prediction of crack propagation path (numerical analyses and experiments). In:Proc Inter Conf Analytical and Experimental Fracture Mechanics, Mirabile, Italy, 1981.
[18] Cherepanov GP. The stress state in a heterogeneous plate with slits. Izvestiga AN SSSR, OTN, Mekhan. i Mashin 1962;1:131–7(in Russian).
[19] England AH. A crack between dissimilar media. J Appl Mech 1965;32:400–2.
[20] Hutchinson JW. Mixed mode fracture mechanics of interfaces. In: Ruhle M, Evans AG, Ashby MF, Hirth JP, editors. Metal-ceramic interfaces. New York: Pergamon Press, 1990.
[21] Rice JR, Sih GC. Plane problems of cracks in dissimilar media. J Appl Mech 1965;32:418–23.
[22] McCrum NG, Buckley CP, Bucknall CB. Principles of polymer engineering. Oxford: Oxford University Press, 1990.
[23] Rice JR, Tracey DM. On the ductile enlargement of voids in triaxial stress fields. J Mech Phys Solids 1969;17:201–17.
[24] McClintock FA. A criterion of ductile fracture by the growth of holes. J Appl Mech 1968;35:363–71.
[25] Ritchie RO, Thomson AW. On macroscopic and microscopic analyses for crack initiation and crack growth toughness in ductile alloys. Metall Trans 1985;16A:233–48.
[26] McMeeking RM, Finite deformation analysis of crack-tip opening in elastic plastic materials implicationsforfracture. J Mech Phys Solids 1977;25:357–81.
[27] Hull D, Clyne TW. An introduction to composite materials. 2nd ed. Cambridge: Cambridge University Press, 1996.
[28] Johnson W, Mellor PB. Engineering plasticity, 2nd ed. Ellis Horwood Limited, 1983.
[29] O'Dowd NP. Advanced fracture mechanics: lectures on fundamentals of elastic and elastic–plastic fracture. University of London, UK: Imperial College of Science Technology and Medicine, 1998.
[30] Harlin G, Willis JR. The influence of crack size on ductile–brittle transition. Proc Royal Soc London 1988;A415:197–226.
[31] Hanxing Z, Changchun L, Guangxia L. The critical void growth and crack initiation condition in the crack tip zone of 20g steel. Eng Fract Mech 1991;38:175–83.
[32] Barsoum RS. Triangular quarter-point element as elastic and perfectly-plastic crack tip elements. Int J Num Meth Eng 1977;11:85–98.
[33] ABAQUS 5.6. User and theory manuals. USA: Hibbitt-Karlson & Sorensen Inc, 1997.
[34] Nath RB, Finite element analysis of interfacial failure in fibre-reinforced composites. PhD thesis, Department of Mechanical Engineering, King's College, University of London, 1998.
[35] Ho H, Drzal LT. Non-linear numerical study of the single-fibre fragmentation test. Part I: test mechanics Comp Eng 1995;5:1231–44.
[36] Nath RB, Fenner DN, Galiotis C. Elasto-plastic finite element modelling of interfacial failure in model Kevlar 49 fibre–epoxy composites. Composites Part A 1996;27A:821–32.